Role of Cyclin-Dependent Kinase 9 in the zebrafish embryonic heart

Gianfranco Matrone

Doctor of Philosophy

The University of Edinburgh

2013

DECLARATION

I declare that the research described within this thesis is my own work and that this thesis was composed by myself unless otherwise stated.
Neither this thesis nor any part thereof has been submitted for any other degree or professional qualification.

Gianfranco Matrone

ABSTRACT

ROLE OF CYCLIN-DEPENDENT KINASE 9 IN THE ZEBRAFISH EMBRYONIC HEART

Cardiac hypertrophy leading to heart failure remains a leading cause of morbidity and mortality in the 21st century despite major therapeutic advances. Improved understanding of novel molecular and cellular processes contributing to cardiac hypertrophy therefore continues to be important. Cyclin-dependent Kinase 9 (CDK9), part of a family of proteins controlling cell cycle and growth, has emerged as one such potential candidate over the last 5 years.

CDK9 is the catalytic subunit of the CDK9/CyclinT complex and acts by phosphorylating the carboxy-terminal domain of RNA polymerase II. Hypertrophic signals, such as Endothelin-1 (ET-1) and phenylephrine, have been shown to cause CDK9 activation leading to a hypertrophic response in cultured mouse cardiomyocytes associated with reactivation of the foetal gene program. CDK9 also forms a complex with GATA4 to play a role in differentiation of mouse ES cells into cardiomyocytes. These findings suggest a specific role for CDK9 in controlling growth and differentiation of cardiomyocytes and merits further study in models where cardiomyocyte differentiation and proliferation are key contributors. In contrast to mammals, zebrafish retain a high cardiomyocyte proliferative capacity throughout their life span and can readily repair following injury.

I have examined the role of CDK9 on global and cardiac development in the zebrafish embryo. I have also assessed the impact of CDK9 manipulation on response to ventricle injury using a laser-induced injury model developed and validated as part of my thesis.

My findings confirm that normal growth of the embryonic ventricle is associated with a rapid increase in cardiomyocyte number, that was of 50% in the period 96-120 hpf, accompanied by increasing chamber trabeculation. This is also characterized by an increase in the gene expression of most of cardiac development relevant transcription factors, *i.e.* GATA4, 5 and 6, and MEF2c.

The significant reduced cardiovascular function (14% of Ejection Fraction compared

to 20% in controls) at 2 h post laser injury in the zebrafish embryonic heart promptly recovers at 24 hour post-laser, accompanied by acceleration of cardiomyocyte proliferation, that increased of 49% in injured ventricles compared to 20% in controls in the period 2-24 h post-laser.

Pharmacological and genetic inhibition of CDK9 activity also significantly reduced cardiac growth, cardiomyocyte number, ventricle function and impairs functional recovery following laser injury. Conversely, genetic inhibition of LARP7, a CDK9 repressor, resulted in increased cardiomyocyte number and was associated with full functional and cellular recovery following laser-injury.

In conclusion, I have provided evidence, in the zebrafish embryonic heart, that CDK9 plays an important role in cardiac growth and development and impacts significantly on cardiomyocyte proliferation. I have also shown that CDK9 manipulation significantly affects cellular and functional recovery following laser-induced injury. Further studies are required to further define the role of CDK9 and LARP7 in the heart and develop therapeutic strategies using this pathway that could contribute to cellular repair mechanisms in the adult mammalian heart.

DEDICATION

In memory of my Parents

Pasquale and Giuseppina

"Macte nova virtute, puer, sic itur ad astra"

Virgil (Aeneid, IX, 641)

ACKNOWLEDGEMENTS

At the end of this PhD I feel to be better as scientist and as man. I am lucky to have received high quality mentoring and supervision throughout my PhD. For this I am very grateful to Drs Martin Denvir and Carl Tucker for their constant support, encouragement and patience.

I am very thankful to Prof. John Mullins for admitting me to the University of Edinburgh PhD Programme at the Queen's Medical Research Institute and for his precious support throughout.

I am particularly grateful to my colleague Kathryn Wilson for help with Q-PCR analysis and Inter-observer Variation analysis and Jonathan Taylor for help assembling the synchronized laser system. A thanks goes to Dr Matt Sharp, Adrian Thomson, James Baily and Sharron Vass for their excellent technical assistance. For kindly gifting transgenic strain, I owe gratitude to Prof. Calum MacRae for the cmlc2:EGFP line, Dr. Steve Renshaw for GATA1:DsRed line and Dr. Tim Chico for flk1:EGFP line. I also would like to thank David Lyons and Sari Penning for her valued input during thesis committee meetings.

Thank you to all lab members, past and present, that have been great to both work and socialize with. Last but not least, thank you to my fiancée Giovanna and my Family for always being there and supporting me.

Abstracts, Oral Presentations, Publications, Awards and Scientific Public Engagement

Journal Articles

- Laser-targeted ablation of the zebrafish embryonic ventricle: a novel model of cardiac injury and repair. G Matrone, JM Taylor, KS Wilson, J Baily, GD Love, JM Girkin, JJ Mullins, CS Tucker, MA Denvir. Under revision at IJC.
- Cyclin dependent kinase 9 modulates cardiomyocyte proliferation in the zebrafish heart. G Matrone, KS Wilson, J Baily, JJ Mullins, CS Tucker, MA Denvir. In preparation.
- Histological, cellular and molecular changes are associated with systolic and diastolic function during heart development in the zebrafish. G Matrone, KS Wilson, J Baily, JJ Mullins, CS Tucker, MA Denvir. In preparation.

Abstracts

- Matrone G, Wilson KS, Tucker CS, Mullins JJ, Denvir MA. Modulation of cyclin-dependent kinase 9 impacts on cardiomyocyte proliferation in the developing zebrafish heart. Keytone Symposium "New Frontiers in Cardiovascular Genetics Beyond GWAS", Tahoe City, California, 13-18 January 2013.
- Matrone G, Tucker CS, Mullins JJ, Denvir MA. Cyclin-dependent kinase 9 inhibition impacts on cardiomyocyte proliferation in the developing zebrafish heart. *Eur Heart J, 33(Suppl 1)2012:pp1041*.
- Matrone G, Wilson KS, Mullins JJ, Tucker CS, Denvir MA. Role of Cyclin-Dependent Kinase 9 in cardiac injury-recovery in the zebrafish embryo. Conference Frontiers in Cardiac and Vascular Regeneration, International Centre for Genetic Engineering and Biotechnology - Trieste 2012. Selected oral communication.
- Matrone G, Tucker CS, Mullins JJ, Denvir MA. Cyclin Dependent Kinase 9 inhibition impairs cardiomyocyte proliferation in the zebrafish embryo.

Scottish Cardiovascular Forum, Dundee, February 2012.

- Matrone G, Tucker CS, Hamilton-Smith KM, Mullins JJ, Denvir MA. Laser injury to embryonic zebrafish heart ventricle: a new model of cardiac damage. *Proc Physiol Soc 23 (2011).* Selected oral communication.
- Matrone G, Wilson KS, Tucker CS, Mullins JJ, Denvir MA. Quantification of cardiomyocyte proliferation during early development and following heart laser injury in zebrafish embryo. The 7th European Zebrafish Meeting, EICC, Edinburgh, July 2011.
- Matrone G, Wilson KS, Tucker CS, Mullins JJ, Denvir MA. Effect of CDK9 Inhibitor Flavopiridol on Cardiomyocyte Proliferation in the Zebrafish Embryo. The 7th European Zebrafish Meeting, EICC, Edinburgh, July 2011.
- Matrone G, Hamilton-Smith KM, Tucker CS, Mullins JJ, Denvir MA. Laser myocardial injury–recovery model in the zebrafish embryo. Scottish Society for Experimental Medicine, QMRI, Edinburgh, 8th May 2011.
- Matrone G, Wilson KS, Tucker CS, Mullins JJ, Denvir MA. Quantification of cardiomyocyte proliferation during early development and following heart laser injury in zebrafish embryo. *Proc Physiol Soc 19 (2010).* Selected oral communication.

Awards

- March 2013 - Awarded EdZeb Bursary (£450) for the Zebrafish Meeting 2013, Barcelona, Spain
- January 2013 - Awarded Physiological Society Travel Grant (£500) for the Keytone Symposium New Frontiers in Cardiovascular Genetics Beyond GWAS, Tahoe City, Nevada, USA
- October 2012 - Awarded Keystone Symposia Scholarship ($1200) for the Keytone Symposium New Frontiers in Cardiovascular Genetics Beyond GWAS, Tahoe City, Nevada, USA

- June 2011 - Runner-up Student Poster Prize at the CVS Annual Symposium
- June 2011 – Shortlisted image in "The Mending Broken Heart" selection from the British Heart Foundation Image Competition
- May 2011 - Awarded Physiological Society Travel Grant (£450) for the Physiological Society Main Meeting, Oxford, UK
- May 2010 - Awarded Physiological Society Travel Grant (£340) for Physiological Society Main Meeting in Manchester, UK

Public engagement

- Performer at the Bright Club Comedy as part of the Edinburgh International Science Festivals 2012.
- Demonstrator: "Heart Health" exhibit for Discover Science, Edinburgh Science Festival, Edinburgh, April 2010 and April 2011.
- Demonstrator: "Stem Cells for Blood Transfusion?" exhibit, Royal Society's Summer Science Exhibit, London, June 2010
- Student representative of Health & Safety Committee at the BHF Centre for Cardiovascular Science, Queen's Medical Research Institute, University of Edinburgh, academic years 2010-2012.

TABLE OF CONTENT

LIST OF FIGURES

LIST OF TABLES

ABBREVIATIONS

7SK	7SK small nuclear RNA
Aa	amino acid
ADA	atrial diastolic area
ALPM	anterior lateral plate mesoderm
Amhc	atrial myosin heavy chain
ATP	adenosine-5'-triphosphate
AV	atriovantricular
BA	bulbus arteriosus
Brd4	bromodomain Protein 4
BrdU	5-Bromo-2′-deoxyuridine
Bpm	beat per minute
Cdc	cell division cycle
CDK	cyclin-dependent kinase
CKI	CDK-inhibitors
CLP-1	cardiac lineage protein-1 (CLP-1)
CMLC2	cardiac myosin light chain 2
CTD	carboxy-terminal domain
CVBF	cardinal vein blood flow
DAB	3,3'-Diaminobenzidine
DISF	DRB-Induced Stimulating Factor
DMSO	dimethyl Sulfoxide
DNA	deoxyribonucleic acid
Dpf	days post fertilisation
DRB	5,6-dichloro-l-b-D-ribofuranosylbenzimidazole
EF	ejection fraction
EM	embryo medium
ES	embryonic stem
FGF	fibroblast growth factor

FPS	frame per second
HEXIM	hexamethylene bisacetamide-induced protein
HIV	human immunodeficiency virus
HR	heart rate
IHD	ischaemic heart disease
miR-1	microRNA-1
MO	morpholino
MO-CDK9splice	morpholino-CDK9 splice-site blocking
MO-CDK9mism	morpholino-CDK9mismatch
MO-CDK9transl	morpholino-CDK9 translation blocking
NELF	negative elongation factor
OC	outer curvature
ON	overnight
PBS-Tx	PBS+Triton-X100 0.1%
PFA	paraformaldehyde
PHH3	phosphoHistone H3
pRb	proteins of retinoblastoma
PTEFb	positive-transcription elongation Factor b
PVCn	proliferating ventricle cardiomyocyte number
Q-PCR	quantitative polymerase chain reaction
RNA	ribonucleic acid
RNAP	RNA polymerase
RT	room temperature
snRNP	small nuclear ribonucleoprotein
TAK	Tat-associated kinase
TF	transcription factors
TUNEL	Terminal dUTP Nick End-Labeling
TVCn	total ventricle cardiomyocyte number
VDA	ventricle diastolic area
VMHC	ventricle myosin heavy chain

Chapter 1
Introduction

1.1 General Introduction

Gene expression is a fundamental mechanism of the life; through its tight regulation, all organisms control their biological processes (Sims et al., 2004).

In all Metazoans genetic studies have shown that the genes coding for proteins remain constant (Mattick, 2011), despite the very different complexity of the organisms. The human genome, in fact, encodes approximately 20,000 genes, about the same number as the simple nematode *Caenorhabiditis elegans* (Stein *et al*., 2003) or the corn (Candela and Hake, 2008) and less than the zebrafish, that possess more than 26,000 protein-coding genes (ENCODE project) (Howe *et al*., 2013). In addition, human genes are encoded in about only 1% of the genome, with the other 99% containing complex instructions that direct the intricate turning on and off of gene transcription (Clamp *et al*., 2007) (Pennisi, 2012). This suggests that specific regulatory mechanisms must program progressively more complex organisms (Rokas, 2008).

Spatio-temporal tuning of gene expression patterns underpins cell-type specificity in multicellular organisms and probably underlies many disease processes. Indeed, many cellular processes are known to control gene expression.

In eukaryotes, the RNA transcription is the main stage where gene regulation occurs. Transcription consists of a series of distinct and consecutive phases: pre-initiation, promoter clearance and initiation, elongation and termination. In a transcription pre-initiation phase, several transcription factors (TF) precisely position RNAP II at the level of the start site. Transcription factor TFIIH remodels the pre-initiation complex and produces an open complex where the DNA template is aligned in the active site of RNAP II. This switch on the RNAP II that start to pair nucleotides with the correspondent DNA template.

Initiation of RNA synthesis is preceded by the promoter escape, the process in which *RNAP* II leaves behind the burden of several TFs, essential in the previous step (promoter clearance and initiation). As observed in a range of genes, the RNAP II continues for about 40 nucleotides along the DNA before stopping. This phase,

called Promoter proximal pausing of RNAP II, mainly depends on the activity of two negative elongation factors, DRB-induced stimulating factor (DISF) and the negative elongation factor (NELF). This regulatory mechanism could be essential to assess that the RNAP II is properly positioned for productive elongation (Wada *et al.*, 1998; Yamaguchi *et al.*, 1999). In their presence, RNAP II only forms short aborted transcripts. The intervention of the Positive Transcription Elongation Factor b (P-TEFb) is critical for releasing the pausing and promoting a mature elongation complex. Finally, in the termination phase of the RNA synthesis, the pre-mRNA is released. The P-TEFb complex, composed of Cyclin Dependent Kinase 9 and cyclins, will be discussed in more details in section 1.3.

Another key role in the gene regulation is represented by dynamic changes, also called epigenetic mechanisms, of chromatin. These are characterized by modifications of histones, *i.e.* methylation, phosphorylation, acetylation and ubiquitination (Jenuwein and Allis, 2001; Strahl and Allis, 2000).

1.2. Cyclin-dependent kinases

Cell division and differentiation are tightly controlled processes, particularly in multicellular organisms that need a precise coordination of multiple cell types in different tissues (Malumbres, 2011). First studies of cell division mechanisms date back to the genetic screens in yeast (Hartwell, 1974; Nurse, 1975; Nurse, 2000) when several cell division cycle (Cdc) genes were recognized as key players throughout the cell cycle (Malumbres, 2011; Malumbres and Barbacid, 2009). The number of cell-cycle regulator elements has increased considerably during evolution. Most original yeast Cdc genes are highly conserved throughout evolution, although these individual genes have then formed gene families in Higher Vertebrate, reflecting the high diversity of cell types. Among the regulators of the cell cycle progression, there are the cyclin-dependent kinases (CDKs) that also retain a critical role in human disease (Malumbres, 2007).

The CDKs are serine/threonine kinases, *i.e.* they phosphorylate the hydroxyl group in the amino acids serine or threonine within the proteins. They are essential for life

via their ubiquitous phosphorylation reactions (Morgan, 1995). Most of CDKs require binding partners called cyclins that serve as regulatory subunits. Some CDKs can be activated by several types of cyclins, whereas others only associate with one specific cyclin.

So far, 20 CDKs are known and, despite the high level of sequence and structural homology between them, each CDK seems to be involved in different cellular processes (Gopinathan *et al.*, 2011), mainly cell cycle and RNA transcription.

1.2.1 Cyclin dependent kinases: Role in the Regulation of the Cell Cycle and Transcription

Some CDK–cyclin complexes are directly involved in driving the cell cycle. Among these, CDK1 is involved in the mitosis, CDK2, CDK4 and CDK6 are interphasic and are associated with ten cyclins of type A-, B-, D- and E (Malumbres and Barbacid, 2007; Malumbres *et al.*, 2008). Other CDK members moderately implicated in the regulation of the cell cycle are CDK3, partnering with cyclin C that acts during interphase (Ren and Rollins, 2004) and CDK5, involved in neuronal cell cycle arrest and differentiation (Zhang *et al.*, 2008). CDK7, associated with cyclin H, can fulfil a role either in cell cycle, by phosphorylating and so activating CDKs, mainly CDK1 and CDK2 (Larochelle et al., 2007), or during transcription (see below). It has been hypothesized that this dual role of CDK7 may promote the coupling of these two processes during cell cycle progression (Loyer *et al.*, 2005).

A number of CDK family members, in particular CDK7, CDK8 and CDK9, have been shown to be mainly involved in transcriptional regulation and mRNA processing (Meijer and Raymond, 2003; Prelich, 2002; Vermeulen *et al.*, 2003). These enzymes are evolutionarily conserved from yeast to mammals, and all three are components of different protein complexes. CDK7 (called Kin28 in yeast) is a part of the transcription factor TFIIH (Orphanides *et al.*, 1996). CDK7/cyclin H complexes are implicated in the initiation phase of transcription, *i.e.* in the clearance of the promoter and then in the progression of transcription following phosphorylation of the Ser5 in the C-terminal domain of the large subunit of RNA polymerase II

(Fisher, 2005; Rodriguez *et al.*, 2000; Orphanides and Reinberg, 2002).

CDK8 associates with cyclin C in the Srb/Mediator complex (Akoulitchev *et al.*, 2000) and functions in transcriptional events prior to elongation (Cho *et al.*, 1998). Recently, CDK8 has been shown to induce colon cancer by a gene amplification mechanism (Firestein *et al.*, 2008).

The third kinase, CDK9, is part of P-TEFb complex (Zhu *et al.*, 1997) and, as the main subject of this thesis, will be discussed in more details in the following chapters and sections.

CDK10 and CDK11 also display their roles in regulating transcription and the G2/M phase of transition in the cell cycle (Malumbres and Barbacid, 2005). CDK12 and CDK13, in association with L-type cyclins, regulate alternative splicing (Chen *et al.*, 2006; Chen *et al.*, 2007). CDK14 to CDK18 play specific functions in the control of diverse cellular processes, although the relevance of these kinases is mostly unknown (Gopinathan *et al.*, 2011; Malumbres, 2011). Because of the importance of the CDKs in many cellular processes, they require a tight regulation. Members of the Ink4 and Cip/Kip family are among the most important endogenous CDK inhibitors (CKIs) (Sherr and Roberts, 1995).

1.3 Cyclin-dependent kinase 9

Among all the CDKs, CDK9 has been shown to be an important regulatory molecule that could act as a linking node of several diseases, HIV and cardiac hypertrophy, just to mention a few (Krystof *et al.*, 2010). Its structure, biological function, and especially its involvement in cardiac development, growth and function are discussed in detail in the following sections. Separate sections are devoted to CDK9 molecular inhibitors and their pharmacological modulation.

1.3.1 CDK9: Molecular structure and isoforms

Following a screening aimed to isolating factors involved in the mammalian cell cycle, Grana et al., (Grana *et al.*, 1994) isolated from the human cDNA library and characterized a CDC2-related protein kinase with a characteristic motif Pro-Ile-Thr-

Ala-Leu-Arg-Glu, called later CDK9. Since then, many new findings have increased our knowledge of this new factor. It is known that cyclin T or K is the binding partner (Peng *et al.*, 1998; Zhu *et al.*, 1997; Wei *et al.*, 1998). Human CDK9 gene maps to chromosome 9q34.1 (Bullrich *et al.*, 1995) and is composed of six introns and controlled by a TATA-less housekeeping promoter (Liu and Rice, 2000). Molecular structure of CDK9 protein includes a kinase fold comprising N- and C-terminal lobes (Baumli *et al.*, 2008) and a T loop structure for the access of the ATP substrate (Morgan, 1995; Pavletich, 1999). Two isoforms of 42kDa ($CDK9_{42}$) and 55kDa ($CDK9_{55}$) are known, under control of two different promoters in the CDK9 gene (Marshall and Grana, 2006). The transcript codes for $CDK9_{42}$ protein contains 372aa and is regulated by a GC-rich and lacking of TATA element promoter located at nucleotides -352 to -1. While $CDK9_{55}$ originates from a promoter located upstream of the $CDK9_{42}$ promoter start codon , *i.e.*, with the $CDK9_{55}$ ATG codon located at -351 (Liu and Herrmann, 2005; Shore *et al.*, 2003). This generates a 13 kDa amino-terminal extension that contains 117aa, in frame with the 42kDa protein (Shore *et al.*, 2005; Shore *et al.*, 2003).

1.3.2 CDK9: Differential expression and distribution

Although CDK9 is ubiquitous, the two isoforms distribute differentially in tissues and cell compartments. In mice, $CDK9_{42}$ predominate in spleen, thymus and testis, whereas $CDK9_{55}$ is predominantly expressed in lung, liver and brain (Shore *et al.*, 2005; Shore *et al.*, 2003). The cellular relative abundance of one or the other isoform is associated with specific developmental stage and cell commitment (Kohoutek, 2009). In human primary undifferentiated monocytes, $CDK9_{42}$ is the predominant isoform, changing to $CDK9_{55}$ upon induced differentiation of monocytes into macrophages (Liu and Herrmann, 2005). Whereas human macrophages stimulated with LPS or infected with the human immunodeficiency virus type 1 reverse the ratio in favor of $CDK9_{42}$ (Shore *et al.*, 2003). Rat hepatocytes (in adaptation to culture) express mainly $CDK9_{55}$, however $CDK9_{42}$ expression in primary cell cultures becomes higher than $CDK9_{55}$ expression (Shore *et al.*, 2005). Moreover,

$CDK9_{55}$ seems to be essentially found in the cell nucleus (Shore *et al.*, 2003) whereas $CDK9_{42}$ is present in the both cell compartments, nucleus and cytoplasm (Falco *et al.*, 2002). CDK9 isoforms differential expression is also clear in the human cervical carcinoma HeLa cell line and mouse NIH-3T3 fibroblasts where $CDK9_{42}$ is preferentially expressed (Shore *et al.*, 2003). Furthermore, in various tissues, particularly in the hematopoietic system (Liu and Herrmann, 2005), muscle (Giacinti *et al.*, 2006; Simone and Giordano, 2007) and adipogenesis (Iankova *et al.*, 2006) $CDK9_{55}$ seems to be implicated in the regulation of cell differentiation. These findings also indicate that the CDK9 isoforms are differentially regulated in a cell type specific fashion and in a signal-dependent manner. The pattern of CDK9 isoform expression in the heart is not published in any species.

1.3.3 CDK9 as part of the P-TEFb complex

In 1997, Zhu and colleagues first isolated from Drosophila a complex of CDK9 with a cyclin T1 (Zhu *et al.*, 1997). Nowadays, we know that two different CDK9 isoforms can bind four possible cyclin subunits (Cyclin T1/T2(a,b)/K) (Fu *et al.*, 1999; Peng *et al.*, 1998; Zhou *et al.*, 2006), forming a heterodimer that is the core element of the P-TEFb complex. Cyclin T1 and T2 are the most entailed in the P-TEFb complex and contain two cyclin box folds, each including five helices (H), and short N-terminal (HN) and C-terminal (HC) helices (Baumli *et al.*, 2008). CyclinT and CDK9 bind through the cyclin H3, H4 and H5 helices and the CDK alpha C helix and beta 4 strand and, partially, through their N-terminal domains (Baumli *et al.*, 2008; Wang and Fischer, 2008).

The P-TEFb complex is found in the cells in 2 mutually exclusive forms (Zhou *et al.*, 2006). The CDK9/Cyclin complex, the transcriptionally active fraction of the P-TEFb complex, is typically associated with the transcription factor NF-kB (Barboric *et al.*, 2001; Wei *et al.*, 1998) and/or the coactivator of transcription bromodomain protein 4 (Brd4) (Jang *et al.*, 2005; Yang *et al.*, 2005). However, a transcriptionally inactive complex, with lower kinase activity (7SK small nuclear RiboNucleoProtein (snRNP)) also contains P-TEFb, hexamethylene bisacetamide-induced protein (HEXIM) 1

and/or HEXIM2 (Barboric *et al.*, 2005; Yik *et al.*, 2003), the noncoding 7SK small nuclear RNA (Michels *et al.*, 2003; Nguyen *et al.*, 2001; Yang *et al.*, 2001) and the La-related protein 7 (LARP7) (He *et al.*, 2008; Markert *et al.*, 2008). 7SK acts as a molecular scaffold, which links HEXIM1 and 2 and LARP7 directly, promoting the repression of the CDK9 in the P-TEFb complex.

The dynamic sharing of P-TEFb between the complexes represents a functional balance that can be perturbed. In fact, HIV-1 Tat increases the active form of the P-TEFb and triggers viral transcription by commandeering it from 7SK snRNP (Barboric *et al.*, 2007). In particular, the P-TEFb complex (also called TAK) is targeted by the Tat protein, a specific HIV transactivator (Price, 2000; Rice and Herrmann, 2003) which, following interaction with the cyclin T1, recruits the kinase complex. TAK/P-TEFb complex phosphorylates the CTD and this activates transcription elongation from the HIV genome.

1.3.4 CDK9: activation and regulation

CDK9 activity is regulated by reversible multiple modifications. For instance, CDK9 contains a T loop structure (aa 168–197) which undergoes phosphorylation on Thr186 thus triggering major conformational change, creating the catalytic pocket for the ATP binding (Cho *et al.*, 2010; Li *et al.*, 2005). This ATP binding promotes the correct position of the kinase for substrate recognition of the Serine/Threonine-Proline motif (Baumli *et al.*, 2008) in the Carboxy-terminal domain (CTD) of the RNAPII. Although full activation of P-TEFb requires phosphorylation on CDK9/Thr186 residue, there are other sites in CDK9, Thr29/362/363 and Ser175/347, prone to be phosphorylated and affecting CDK9 activities.

For example, phosphorylation of Ser175 promotes the interaction P-TEFb - Brd4, and autophosphorylation at Thr29 reduces CDK9 activity. Other CDK9 modifications, such as acetylation at Lys44/48, modulate P-TEFb activity. Post-translational modifications, including phosphorylation, ubiquitination, and acetylation, pertain also to other players of the P-TEFb complex that can regulate the P-TEFb activity (Cho *et al.*, 2010). These complex regulatory mechanisms of P-TEFb

reflect an intricate interplay between modifications of chromatin, RNAPII and the regulation of transcription elongation (Cho *et al.*, 2010).

1.3.5 CDK9: effects on the transcription

RNAP II possesses an extra C-terminal domain (CTD) on its largest subunit, Rpb1 (Buratowski, 2009), which is responsible for many of the activities of this enzyme. However, the most important is probably the role of the CTD for different proteins involved in transcription, mRNA processing, and histone modifications (Buratowski, 2009). The CTD sequence contains multiple repeats of the heptamer Tyr1-Ser2-Pro3-Thr4-Ser5- Pro6-Ser7, or YSPTSPS according to the nomenclature of Marshall (Marshall *et al.*, 1996). In the CTD heptad sequence, Serines (Ser) 2, 5 and 7 can be dynamically phosphorylated. Once activated, CDK9 typically phosphorylates Ser2 in the heptamer, allowing the elongation transcriptional activity. Phosphorylation of Ser5 and, as more recently shown, Ser7 phosphorylation occurs during transcription initiation by TFIIH (Akhtar *et al.*, 2009) (Glover-Cutter *et al.*, 2009). CDK9 also phosphorylates DSIF (Peterlin and Price, 2006) and NELF (Yamada *et al.*, 2006), which release these inhibiting factors and promote transcription elongation.

The CDK9/PTEFb complex has been also associated with co-transcriptional histone modification in a CTD dependent and independent manner (Pirngruber *et al.*, 2009a). Indeed, the P-TEFb complex leads to monoubiquitination of histone H2B and trimethylation of histone H3 (Pirngruber *et al.*, 2009b), and also acetylation and phosphorylation (Li *et al.*, 2009) in the nucleosomes that normally would prevent the path of the elongating RNAPII. In addition, CDK9 seems to be involved in DNA repair and mRNA processing (Bres *et al.*, 2008; Liu and Olson, 2010; Romano and Giordano, 2008).

1.3.6 CDK9: role in the heart

Hypertrophy is characterized by global increases in mRNA and protein synthesis. The P-TEFb complex, a key driver for transcription, is clearly associated with

cardiac hypertrophy (Sano *et al.*, 2002). Sano and colleagues demonstrated that CDK9 activity was increased in cardiac hypertrophy in mammals, in-vitro and in-vivo. In addition, CDK9 activity was not affected by variations in CDK9 or cyclin T levels, but was derepressed by the dissociation of 7SK small nuclear RNA (7SK RNA), an endogenous inhibitor of the CDK9 (Nguyen *et al.*, 2001; Yang *et al.*, 2001). Subsequently, it has been reported that HEXIM1 was the main CDK9 inhibitor, which relies on the support of 7SK molecule (Michels *et al.*, 2004; Yik *et al.*, 2003). Human HEXIM1 is the homologue of the cardiac line age protein-1 (CLP-1) in mouse (Huang *et al.*, 2002). CLP-1 knockout mice die during fetal development and exhibit all the genetic and physical hallmarks of cardiac hypertrophy (Huang *et al.*, 2004). Furthermore, the dissociation of CLP-1 from P-TEFb in cardiomyocytes occurs following hypertrophic stimuli (Espinoza-Derout *et al.*, 2007). Furthermore, the muscle-specific microRNA-1 (miR-1), which normally keeps CDK9 derepressed at the transcriptional level (Sayed *et al.*, 2007), was downregulated at a very early stage, following cardiac hypertrophy induced in a mouse model of aortic constriction–induced hypertrophy. CDK9 has also been shown to regulate cell-cycle and is involved in cardiomyocytes differentiation from mice embryonic stem cells (Kaichi *et al.*, 2011).

1.4 CDK9 as a therapeutic target in human diseases

So far, several CDKs inhibitor compounds have been developed with a range of selectivity for CDK9: Flavopiridol, (Caracciolo *et al.*, 2012) Roscovitine (Berberich *et al.*, 2011), DRB (Baumli *et al.*, 2010), SNS-032 (Chen *et al.*, 2009b) and AT7515 (Santo *et al.*, 2010). Flavopiridol and Roscovitine are the best-known CDK9 inhibitors tested in clinical trials as anticancer (Canduri *et al.*, 2008). Both compounds have been shown to inhibit several CDKs, although Roscovitine mainly inhibits CDK2, 5, 7 and 9 while Flavopiridol has shown preference for CDK9 (Ki <3 nmol/L compared with Ki values of 40 to 70 nmol/L for cell-cycle CDKs (Chao and Price, 2001)). As the activity of the P-TEFb complex, as a transcription factor is required for the

expression of most genes, completely blocking CDK9 activity does not appear at first glance an ideal targeted therapeutic strategy. However, a partial inhibition of CDK9 activity might be beneficial in the treatment of those human diseases characterized by abnormal growth, such as cancer and pathological cardiac hypertrophy, or infectious organism replication, such as HIV, in which CDK9 has been suggested as a key player (Romano and Giordano, 2008) (Wang and Fischer, 2008). These have led to an intensive investigation for novel CDK9 inhibitors for therapeutic applications (Krystof and Uldrijan, 2010; Nemeth *et al.*, 2011). It is the high rate of conservation among members of the CDK family that makes it challenging to generate selective CDK9 inhibitors (Krystof *et al.*, 2010; Wang and Fischer, 2008). Nevertheless, the structural comparison of catalytic domains of these enzymes have shown small differences in the architecture of the ATP binding site and this could be the key tool in developing CDK-specific inhibitors (Eswaran and Knapp, 2010).

Besides the implications in pathologic cellular processes, CDK9 and P-TEFb activity appears to be ubiquitously expressed, whilst also being highly expressed in terminally differentiated cells and tissues (Bagella *et al.*, 1998), *i.e.* neurons, myocytes and lymphocytes (Marshall and Grana, 2006). This suggests a role in specialized cellular functions. Furthermore, CDK9 is specifically targeted by cytokines including tumour necrosis factor (MacLachlan *et al.*, 1998) and interleukin-6 (De Falco and Giordano, 2002), suggesting a regulatory role in the inflammation, immune responses, cell differentiation, growth and survival. Therefore, targeting CDK9 could represent a suitable therapeutic strategy (Krystof *et al.*, 2012). CDK9 seems to be implicated in several pathological conditions, including cancer, heart failure, viral infections, neurological disorders, inflammation and diabetes (Malumbres *et al.*, 2008; Weinmann and Metternich, 2005).

In the subsequent sections I report the main medical areas in which CDK9 and the P-TEFb complex is actually under intense observation for possible clinical implications.

1.4.1 The role of CDK9 in Oncology

For proliferative disorder therapies, the development of anticancer agents targeting the cell cycle, represents a viable strategy (Wang and Fischer, 2008). Indeed, CDKs modulation in cancer has gathered great interest (Boyer and Cheng, 2008; Malumbres and Barbacid, 2005; Malumbres and Barbacid, 2007). Deregulation of CDK9 pathways may be involved in the origin and maintenance of transformed cell phenotype (Bellan *et al.*, 2004; Gan *et al.*, 2003). CDK9-related pathway imbalance has been reported in several human tumors: neuroblastoma and lymphomas (Bettayeb *et al.*, 2007; Fu *et al.*, 1999), primary neuroectodermal tumor (De Falco and Giordano, 2002), rhabdomyosarcoma (Simone and Giordano, 2007) and prostate cancer (Lee *et al.*, 2001).

1.4.2 The role of CDK9 in Virology

P-TEFb complex is at the centre of a surge in pharmaceutical interests regarding several antiviral therapies. It has been reported the recruitment of the P-TEFb in the B-cell cancer-associated Epstein-Barr virus (Bark-Jones *et al.*, 2006), T-lymphotropic virus type 1 by the transcriptional activator Tax (Zhou *et al.*, 2006) and Human Immunodeficiency Viruses (HIV) (Stevens *et al.*, 2006). The replication of HIV in human cells requires the P-TEFb complex, which acts as Tat-associated kinase (TAK) and promotes the replication of the viral genome. Without TAK, the transcription of HIV would stop within the first 60 nucleotides (Kao *et al.*, 1987).Several studies have reported novel approaches to target CDK9/cyclin T1, including antiretroviral drugs and/or gene therapy, in order to suppress HIV replication (O'Keeffe *et al.*, 2000; Foskett *et al.*, 2001; Bellan *et al.*, 2004).

1.4.3 The role of CDK9 in Heart Failure

Heart failure is a common cardiovascular disease where the heart has impaired contractile reserve resulting in an inability to pump sufficient blood to meet the metabolic demands of the body (Kaye and Krum, 2007;Lips et al., 2003). The primary causes of heart failure in developed nations include ischemic heart disease

and hypertension (McMurray and Pfeffer, 2005; Latronico *et al.*, 2008). The adult mammalian heart responds to injury and stress with inflammation, fibrosis and scar formation and has a very limited regenerative capacity of cardiomyocytes (Bergmann *et al.*, 2009; Quaini *et al.*, 2002). Surviving cardiomyocytes attempt to adapt to workload by undergoing compensatory hypertrophy that culminates in progressive pump failure.

CDK9 has been shown to play a role in response to cardiac hypertrophy in the mammalian heart (Sano *et al.*, 2002; Sano *et al.*, 2004) but little is known about its role in the progress from compensatory hypertrophy to heart failure. The possibility that it could play a role in cardiomyocyte proliferation is hinted at by evidence suggesting that the CDK9$_{55}$ isoform is involved in the regeneration of skeletal myocytes in mammals (Giacinti *et al.*, 2008). In addition, CDK9 activity also appears to induce muscle-specific transcription and tissue repair through CTD hyperphosphorylation (Sleep *et al.*, 2010). Further elucidation of CDK9-related mechanisms in cardiomyocytes is therefore a key issue and could be critical for designing new strategies for prevention and treatment of cardiac hypertrophy and subsequent heart failure.

Although CDK9 has been much studied, elucidation of its plethora of functions is far from complete. For example, few data are reported on its role on cardiomyocyte proliferation in vitro and in vivo, either in the adulthood or in the embryonic life (see Section 1.3.6) (Sano *et al.*, 2002; Sano and Schneider, 2003; Sano and Schneider, 2004). In particular, there is very limited data on CDK9 in the zebrafish (Kohoutek, 2009), an organism that is increasingly recognized as an important vertebrate model to study heart development, disorders and regeneration (Santoriello and Zon, 2012).

1.5. Zebrafish: Model of medical research

The zebrafish has distinct advantages as a model organism for cardiac diseases and is ideally suited to explore fundamental molecular pathways such as those associated with CDK9.

1.5.1. A fascinating new vertebrate model

The use of the zebrafish as a model for studying the genetics and development was proposed by George Streisinger, that characterized many aspects of this vertebrate, including morphology and functional features of the zebrafish embryo and developed husbandry as well as genetic techniques. His pioneering work laid the foundation for future developments, see (Grunwald and Eisen, 2002) and http://www.neuro.uoregon.edu/k12/george_streisinger.html.

In 1984, Christiane Nüsslein-Volhard that was involved in molecular studies on Drosophila, after reading a paper by George Streisinger on zebrafish (Streisinger *et al.*, 1981), compelled her to try the application of her Drosophila results on zebrafish, to understand the genetics of higher vertebrate development. She had unexpected success, establishing the first zebrafish colonies in her laboratory in 1986. In 1995, Nüsslein-Volhard was awarded the Nobel Prize for Physiology or Medicine for her work on the development of Drosophila (Raju, 2000). Many people believe that this award was the real catalyst for zebrafish model use in preference to other fish species, such as Medaka and Fugu with a century of history in genetics (Furutani-Seiki and Wittbrodt, 2004). In 1996, many research groups published their work, in a special issue of Development journal (Nusslein-Volhard, 2012) describing 1500 zebrafish mutants providing the first large-scale screen using zebrafish as a model. This clearly demonstrated the strength of this model system for forward genetic screens (http://dev.biologists.org/content/123/1.toc).

1.5.2 Advantages of the zebrafish as a model organism

The zebrafish model is an ideal model for studying vertebrate development and human diseases (Ackermann and Paw, 2003). Females produce 100-200 offspring per week, embryos develop rapidly ex-utero and are transparent during their early life, which allows the visualization of developmental processes. As Streisinger and colleagues showed, gynogenesis can be used in zebrafish to produce genetically uniform and homozygous diploid offspring that carry out two sets of maternally

inherited chromosomes (Streisinger *et al.*, 1981). One of the advantages of genetically uniform line is that they can be used in different labs and results obtained are not corrupted by the variance in genetic background. In addition, large-scale forward-genetic screens following mutagen treatment have permitted to identify mutations affecting organogenesis (Langenau and Zon, 2005).

In addition, zebrafish is ideal for toxicological and chemical studies as it can easily take up chemicals from their water environment. Moreover, one of the most important tools is the antisense morpholino technology, which is unique for the rapid assessment of gene function in living zebrafish. Pros and cons of this specific technique will be discussed in Section 1.5.3. For a more comprehensive description of the zebrafish model, see the reviews (Lieschke and Currie, 2007; Shin and Fishman, 2002).

1.5.3 Genetic Intervention: Morpholino antisense gene knock-down technology

Morpholino (MO) antisense technology is an approach for blocking gene expression in-vivo and so to investigate gene function, particularly in zebrafish. Morpholino antisense oligonucleotide are short chains of about 25 elements, synthetically produced, very similar to those of the RNA and DNA but with a morpholino ring in place of the ribose ring (Eisen and Smith, 2008). Morpholino acts through an RNAase-H–independent mechanism by inhibiting translational initiation (Summerton and Weller, 1997) or by hindering the proper splicing of RNA (Draper *et al.*, 2001).

The first approach, where the MO is designed against the initiation codon of the target mRNA, is particularly attractive when the intron-exon structure of the target gene to inhibit is unknown. This was successfully used in zebrafish for the first time by Nasevicius and Ekker (Nasevicius and Ekker, 2000). With this method, however, it could be difficult to assess the efficacy of the effective gene knock-down when an antibody to estimate protein levels is not available (Eisen and Smith, 2008). Whereas the pre-mRNA splicing-inhibiting approach has the advantage that one can quantify

the efficacy of the MO by Q-PCR analysis (Draper *et al*., 2001). Moreover, such an approach does not affect maternal transcripts that would be normally translated in the embryo. It is therefore necessary that both approaches are used to corroborate data obtained from each approach.

MOs provide advantages over other antisense oligonucleotides including resistance to nucleases, that means more stability, and the absence of a negatively charged backbone that reduce non-specific interaction with other cell parts and, as a consequence, the toxicity (Corey and Abrams, 2001).

However, as with each technique, morpholino technology also present lacks that must be addressed to avoid misleading results. Firstly, one must guarantee that all eggs are injected with the same amount of morpholino. Although the use of calibrated needles can reasonably facilitate this delivery, a uniform MO diffusion into the embryo is more difficult to achieve. A skilled experimenter, however, should be able to inject a high percentage of eggs with the MO into the targeted site, *i.e.* below the cell mass into the zone of cytoplasmic streaming. Then, MOs lissaminated or biotinylated at the 3' or 5' end of the oligo allows the visualization of the oligo into the cells under fluorescence.

1.5.3.1 Controls MO

One matter of concern in relation to use of MO technology is the possibility that the MOs designed to block our gene of interest could also affect one or more other genes. This would produce off-target effects, meaning that phenotypic features observed following the injection of the MO are in part or completely caused by other genes being knockdown. Therefore, appropriate controls must be included in the study that would help the operator to assess whether the observed phenotype is genuinely a consequence of the loss of function of the gene under investigation. One control is represented by the injection of a MO mismatch oligo that should differ from the MO specific sequence by at least 4 out of 25 nucleotides in order to not interfere with translation of the target mRNA (Rana *et al.*, 2006).

One of the effects of the MOs is the activation of p53 by an unknown mechanism

(Robu *et al.*, 2007). As p53 is a protein involved in cell cycle arrest and apoptosis, the morpholino could produce non-specific phenotypic effects derived from the p53-induced apoptosis. Therefore, another control consists in the co-injection of the morpholino targeted specific with an anti-p53 Morpholino to suppress the P53-activation related phenotypic effects.

1.5.3.2 Rescue MO

Another problem is that the phenotype observed is not caused by the loss of a specific transcript but, rather, may result from the toxic effect of the morpholino itself.

One strategy used to provide evidence for the specificity of a morpholino is the reversion of the phenotypic effects by co-injecting the morpholino targeted-specific with an mRNA coding for the protein that the Morpholino is designed to knock down. This control, called 'rescue', requires an mRNA with a modified 5'-UTR (Untranslated Region), so that it cannot be targeted by the Morpholino (Malaga-Trillo *et al.*, 2009) but still retains the correct coding region encoding the protein of interest. The return of the embryo to wild-type phenotype, following the replacement of the protein knocked down by the morpholino, is an evidence of morpholino specificity (Bill *et al.*, 2009).

Moreover, considering that the penetrance of each MOs is different, the rescue experiment requires the injection of different volume of mRNA and comparison of embryos from the same batch that have been injected with MO alone or with MO plus mRNA (Heasman, 2002).

When all these controls are performed, the experimenter have a certain level of confidence in the specificity of the MO and the validity of the results.

1.5.4 Zebrafish embryo as a model of cardiac disease

The zebrafish heart represents an ideal model to study many aspects of cardiac disorders (Bakkers, 2011). Zebrafish heart development has been well characterized (Tu and Chi, 2012; Liu and Stainier, 2012; Yelon *et al.*, 2002; Staudt and Stainier,

2012) since early publications on this topic (Stainier and Fishman, 1992; Stainier *et al.*, 1993). Despite having only two chambers, it retains many of the structural traits and developmental complexity of an Amniote's heart, including a three-layer ventricular wall (epicardium, myocardium and endocardium) from three days post fertilization (Serluca, 2008) and it appears to have first and second heart fields (Hami *et al.*, 2011), although the second heart field may represent an early haemopoietic lineage (Peterkin *et al.*, 2009).

The zebrafish embryonic heart is particularly suited to studying aspects of cardiomyocyte proliferation for a number of important reasons. Firstly, the embryonic heart in the early stages is composed of only a few hundred cardiomyocytes (Bostrom *et al.*, 2010; Targoff *et al.*, 2008) and this facilitates accurate and reproducible studies assessing total cardiomyocyte number and changes with growth. In addition, transgenic technology using fluorescent proteins (Burns *et al.*, 2005; Detrich, 2008) can be targeted to developing cardiomyocytes, which allows the ready visualization of in-vivo development and function of these cells (Choi *et al.*, 2013).

The small size of these embryos permits exchange of gases by passive diffusion, allowing their survival and reasonably normal development for several days even in the complete absence of blood circulation (Chen *et al.*, 1997). This permits the phenotypic analysis of embryos with severe or lethal cardiovascular mutations and defects (Isogai *et al.*, 2001; Weaver, 2011) which would have been extremely difficult to assess in higher vertebrates, such as avian or mammalian embryos that cannot live in absence of a functional cardiovascular system (Stainier, 2001).

1.5.5 Assessment of cardiac function

Several methods have been proposed to assess cardiac function in the zebrafish and each of them present pros and cons.

Doppler echocardiography has been used to measure cardiac performance in the adult zebrafish (Ho *et al.*, 2002). However, the zebrafish embryo heart is too small to be properly analysed with the instruments that this technique adopts.

A method more suitable for embryos assumes that the zebrafish ventricle can be represented by a three-dimensional figure such as a prolate spheroid (Hou and Burggren, 1995; Shin *et al.*, 2010). The related standard formula for the volume employs long and short-axis ventricular planes.

Whereas the Simpson's method, also called method of discs, assumes that ventricular volume is the sum of the volumes of individual discs into which the ventricle can be sliced (Coucelo and Joaquim, 2000). In the clinical setting, ventricle ejection fraction is defined as the fractional volume of blood ejected by the left ventricle during each cardiac cycle (Dorosz *et al.*, 2012) and it is traditionally assessed echocardiographically with the method of discs (Folland *et al.*, 1979). However, this method is subject to errors due to foreshortening, poor endocardial definition, narrow echocardiographic windows, and assumptions about LV shape. Moreover, by the effect of the propagation of uncertainties, the error committed in the calculation of a volume will be higher when compared to an area-based formula. Nevertheless, this is the method that several authors use in the zebrafish embryo (Antkiewicz *et al.*, 2006; Kim *et al.*, 2007).

In this thesis, the Fractional Area Change of the Ventricle, that here we simply called Ejection Fraction (EF), was used to assess cardiac performance in the zebrafish embryo. This method has been preferred and adopted in this thesis because it was practical and highly reproducible and has been already used in previous experiments with the zebrafish embryo in our Institute (KM Hamilton-Smith, PhD thesis). It is important to note that these data served not to assess the absolute cardiac performance but exclusively to compare control with treated groups of embryo. A similar method has been previously used in the zebrafish embryo (Shu *et al.*, 2003), although the authors used ventricle long-axis length instead of the area. The fractional area change has been used in human (Royse and Royse, 2000), mainly for research purposes, for quantifying changes in the short-axis image of the left ventricle (Domanski *et al.*, 1992). The fractional area change is assessed by manual planimetry of the area circumscribed by the endocardium at end-diastole (EDA) and end-systole (ESA) and is calculated according to the

formula: Fractional area change = (EDA - ESA) ÷ EDA

The method has been validated in one study which compared radionuclide blood pool imaging with transesophageal echocardiography area ejection fraction (Urbanowicz *et al.*, 1990).

1.6. Early cardiac development in vertebrates

The heart is reported to be one of the first organ to form and function during vertebrate embryogenesis (Serluca, 2008). According to the most accepted theory on the cardiac origin, the embryonic heart can be considered as a spontaneously contracting blood vessel, formed by an inner endothelial (endocardial) layer and an outer muscular (myocardial) layer (Stainier, 2001). Studies on cardiac development in many animal model systems both vertebrate, including the zebrafish, and invertebrate, have increased our comprehension of heart formation (Bishopric, 2005; Moorman and Christoffels, 2003). Below details a chronological description of early cardiac development, up to 48 hpf, with cellular and molecular events involved in cardiac cell differentiation and tissue morphogenesis in the zebrafish (Stainier, 2001).

Myocardial cells are derivatives of the Anterior Lateral Plate Mesoderm (ALPM), which emerges from the primitive streak during gastrulation (Buckingham *et al.*, 2005). The ALPM has two recognizable pools of myocardial progenitor cells: atrial and ventricular (Stainier *et al.*, 1993), with the atrial cells located more ventrally (Keegan *et al.*, 2004). Cardiogenic differentiation requires the homeobox-containing transcription factor NKX2.5, a highly conserved myocardial expression pattern (Lints *et al.*, 1993; Targoff *et al.*, 2008). Mutant analysis in zebrafish has shown that Bmp2b and Nodal signalling promote NKX2.5 expression and cardiogenic differentiation by inducing GATA5 (Reiter *et al.*, 2001; Schlange *et al.*, 2000; Schultheiss *et al.*, 1997). While GATA5 seems to be required for the initiation of NKX2.5 expression, Fgf8 is essential to its maintenance (Reifers *et al.*, 2000; Reiter *et al.*, 1999) and is also required for cardiogenic differentiation. Reduced total myocardial tissue in the Hands off/Hand2 mutant has also indicated that this basic

helix-loop-helix transcription factor plays an important role in cardiogenic proliferation and ventricular chamber formation (Yelon *et al.*, 2000).

At the 12-somite stage (15 hpf), an increasing expression of sarcomeric myosin light chain polypeptide 7 (myl7, also called cmlc2) genes is detectable in the ALPM (Yelon *et al.*, 1999; de Pater *et al.*, 2009). At this stage, myocardial cells migrate medially expressing ventricle myosin heavy chain (vmhc) giving rise to ventricular cardiomyocytes. Myocardial cells also migrate laterally and express atrial myosin heavy chain (amhc), slightly later than the expression of vmhc, giving rise to atrial cardiomyocytes (Berdougo *et al.*, 2003). During this stage, and up to 25-somite stage (22hpf), the myocardial tissue expands mainly into a more lateral (atrial) region in a process called venous pole differentiation. This latter process requires Islet1 (Marques *et al.*, 2008) and Bmp signaling (Cai *et al.*, 2003). Once cardiac precursors have settled onto the midline, at 17-19hpf, they merge posteriorly to form a horseshoe-shaped structure (Stainier *et al.*, 1993; Yelon *et al.*, 1999). Anterior cells then converge medially and bind to form a cone. Initially dorso-ventrally orientated, this cone turns by 90 degrees to finally settle on the anteroposterior axis. The apex of the cone, containing ventricular cells, will give rise the arterial pole of the heart, while the base of the cone, containing atrial cells and located on the left of the midline, will give rise to the venous one (Wang *et al.*, 1998). There are a number of key factors involved in the process of morphogenesis including hyaluronic acid (Smith *et al.*, 2008), which is a glycosaminoglycan of the extracellular matrix produced by hyaluronan synthase 2, Nodal (Bisgrove *et al.*, 1999; Feldman *et al.*, 1998) and Bmp (Schlange *et al.*, 2000; Nguyen *et al.*, 1998) growth factors.

At 24 hpf, the heart tube is fully formed and new cardiomyocytes arise at the arterial pole in a mechanism that resembles the second heart field described in Amniotes (Kelly and Buckingham, 2002). In this process, FGF signaling is essential, as shown in ace/fgf8 zebrafish mutants affecting the ventricle size (de Pater *et al.*, 2009; Schultheiss *et al.*, 1997). These pathways are only part of a complex network of spatial and temporally restricted factors that orchestrate cardiac differentiation.

At this stage cardiomyocytes also start to express late differentiation genes

including sarcomeric markers such as troponin T, tropomyosin and myosin. Transcription factors Fau/gata5 (Reiter *et al.*, 1999) and han/hand2 (Yelon *et al.*, 2000) are involved in this process as their mutants show reduced amount of these proteins. Mef2c, gata4, gata6 (Black and Diego, 1999) and TBX5 (Begemann and Ingham, 2000; Bruneau *et al.*, 1999) also start to be expressed in cardiomyocytes at this stage, although their role in terminal cardiomyocyte differentiation remains to be clarified (Ruvinsky *et al.*, 2000).

By 36 hpf, the heart tube bows towards the right side of the embryonic midline, forming the ventricle, while the future atrium remains in the mid line. This process is promoted by molecular pathways, such as Nodal (Bisgrove *et al.*, 1999; Yan *et al.*, 1999; Yost, 1999). Subsequently, a looping of the heart tube occurs, mainly by rotation of the venous pole, forming a S-shaped organ with two chambers, the ventricle and atrium. Molecular factors, such as natriuretic peptide A, and intra-cavity haemodynamic pressure induce chamber ballooning, with the formation of an outer and inner curvature of the chambers (Christoffels *et al.*, 2004).

In fish the heart persists as a single ventricle and single atrium separate by a valve. The venous pole forms a sinus venosus and the outflow tract is a thick walled single vessel called the bulbous arteriosus. At 48 hpf, therefore, the zebrafish heart has formed into four clearly defined structures arranged sequentially as sinus venosus, atrium, ventricle, and bulbus arteriosus (Hu *et al.*, 2000). At this stage the atrial myocardium is typically one cell thick while the ventricle has at least two cell layers. Then, the endocardium lines the heart, with a thin layer of cardiac jelly that keeps it separated from the myocardium. At this early stage, no valves separating the segments are present yet. By 72 hpf the AV valve begins to form between the atrium and ventricle arising from the AV cushions. Thereafter, the heart will be lined with epicardium and enveloped in the pericardium, associated with pericardial muscles running in antero-posterior direction (Hu *et al.*, 2000). By 5 days post-fertilization (dpf), the ventricular myocardial layer is formed by two to three cells thick with an extensive trabeculae network inside while the inner atrium remains smooth with only one-to-two-cell layers. In the meanwhile, the atrioventricular and the ventricle-

bulbus arteriosus form two-cusps valves, with mesenchymal, cushion-like leaflets (Hu *et al.*, 2000).

Later steps in heart formation in higher vertebrates including mammals, birds and frogs are differentiation of a specialized conduction system, septation of cardiac chambers and of the outflow tract. These complex developmental processes are ensured by proliferation, migration and architectural organization of cardiomyocyte as well as endocardial and epicardial cells (Brand, 2003; Moorman and Christoffels, 2003; Staudt and Stainier, 2012).

1.7. Cardiomyocyte proliferation: hyperplasia versus hypertrophy

1.7.1 During cardiac development

During embryogenesis, proliferation of cardiomyocytes is the main source for the heart growth. Cardiomyocytes proliferate along the heart tube walls, that are initially very thin, and within the atrioventricular septum. In particular, the outer surface of the heart, called the compact region (Chen *et al.*, 2009a), retains the cardiomyocytes highest proliferative rate. The epicardium, the thin layer of cells enveloping the heart, provide mitogenic signals source that stimulate proliferation of cardiomyocytes within the compact zone (Pennisi *et al.*, 2003). Among the epicardial-derived critical regulator of cardiac growth there is the retinoic acid and relative receptors (Guadix *et al.*, 2011). Newly formed cardiomyocytes thicken the ventricular wall and organize fingerlike projections along the inner ventricle surface giving rise to trabeculae, structures that increase force generation and oxygen and nutrient exchange. The endocardium, the specialized endothelial layer of the heart, also provide fundamental growth signals for embryonic cardiomyocytes, such as the peptide of the neuregulin family and their related tyrosine kinase receptors (Zhao et al. 1998). The intense cardiomyocyte proliferative activity observed during the embryonic heart growth, is accompanied by intracardiac flow forces that play a fundamental epigenetic function in shaping the early heart (Hove *et al.*, 2003), also

promoting the ballooning of the outer curvature of the ventricle (Christoffels *et al.*, 2000).

1.7.2. Transition from the fetal to the adult life

While cardiomyocytes divide extensively and rapidly during fetal life they lose the proliferative capacity shortly after birth in rodents. However, Porrello and colleagues (Porrello *et al.*, 2011) have shown that neonatal mouse cardiomyocyte not only continue to proliferate for up to one week after birth, they also conserve the capacity to regenerate the cardiac apex following surgical resection. This finding has re-energized the search for mechanisms that underpin cell cycle arrest in the mammalian heart with the intention of pursuing key molecular targets that might induce mature mammalian cardiomyocytes to re-enter the cell cycle.

In humans, cardiomyocyte proliferative capacity is lost at few months after birth when they withdraw from the cell cycle and remain in G0 stage apparently indefinitely (Poolman and Brooks, 1998; Busk and Hinrichsen, 2003; Engel, 2005; Bicknell *et al.*, 2007). In addition, cell cycle appears closely coupled to accumulation of cell mass during development, in order to maintain consistency of cell size (Neufeld and Edgar, 1998). In most species, this hyperplastic-to-hypertrophic transition is characterized by changes in degree of ploidy and number of nuclei as cardiomyocytes undergo additional DNA replication followed by cytokinesis and/or karyokinesis (Li *et al.*, 1996; Li *et al.*, 1998). For example, mammalian fetal cardiomyocytes, including human have a single nucleus with a diploid genome (2n). While adult human cardiomyocytes are mostly mononucleated and tetraploid (4n) and adult mice cardiomyocytes are mainly binucleated and diploid (2n) (Laflamme and Murry, 2011). Indeed, several reports have shown a gradual decrease in the incorporation of radiolabeled thymidine soon after birth, coincident with the formation of binucleated cardiomyocytes in mice (Soonpaa *et al.*, 1996; Clubb and Bishop, 1984). This process is associated with an evident increase in myofibril density and development of mature intercalated discs (Pasumarthi and Field, 2002).

1.7.3. During adulthood

In contrast to the early neonate, terminally differentiated mammalian cardiomyocytes show only a hypertrophic response to mitogenic stimuli (Bicknell *et al.*, 2003; Capasso *et al.*, 1992).

The cardiac hypertrophy in the adult heart can be physiological, as that observed in response to exercise, and pathological, as observed in response to excess of stress, including myocardial infarction, pressure overload, contractile dysfunction and hypertension. Hypertrophy can culminate to dilated cardiomyopathy, characterized by cardiomyocyte loss due, at least partially, by the activation of apoptotic pathways (Kang and Izumo, 2003). This second inauspicious form of cardiac hypertrophy is promoted by abnormalities in cardiomyocyte calcium homeostasis (Frey *et al.*, 2000).

There is a well recognized link between mammalian cardiomyocyte hypertrophy and proliferation which involves a complex web of interconnected signaling pathways, including JAK, PLC, JNK, ERK, Calcineurin, STAT, RAS, MEF2 (Heineke and Molkentin, 2006). In addition to the increase in RNA and protein, hypertrophy results in transcriptional reprogramming that closely resemble the 'fetal' gene program that drives hyperplasia in the developing fetus (Olson, 2004; Olson and Schneider, 2003).

It is hypothesized that cardiomyocyte hypertrophy, without hyperplasia, in mammals might be the result of a fundamental block in karyokinesis and cytokinesis, by which the adult cardiomyocyte is unable to disassemble sarcomeres, uncouple from neighbouring cells and divide (Ahuja *et al.*, 2007).

1.7.4 Mammals versus Zebrafish

Adult mammalian cardiomyocytes ability to re-enter the cell cycle and proliferate is very limited in comparison with lower vertebrates, including fish (Martin-Puig *et al.*, 2012). The underlying molecular mechanisms permitting proliferation in lower vertebrates are not well known and represent a potentially important therapeutic target for a range of cardiac disorders where cardiomyocyte loss plays a major role.

A relevant difference between mammalians and zebrafish might be that in the latter, cardiomyocytes do not undergo acytokinetic mitosis. In fact the majority of cardiomyocytes in adult zebrafish continue to have a single nucleus and a diploid genome (2n) and show significant proliferative ability (Wills *et al*., 2008).

Therefore, a key place to start to understand mammalian cardiomyocyte proliferation is during in-utero growth and development of the heart and in the perinatal period, studying the processes that underlie cardiomyocyte exit from the cell cycle. This may help us understand the mechanism responsible for definitive arrest of cell cycle in adult cardiomyocytes. Interestingly, Becker et al. (Becker *et al.*, 2011) created and analysed a zebrafish embryo reporting a mutation in the troponin (tnnt2) gene, that cause hypertrophic cardiomyopathy (HCM) in mammals. Although the gene expression pattern and sarcomeric organization were similar to those observed in humans and mouse models with HCM, these morphants exhibited a hyperplastic, rather than hypertrophic, myocardial response.

Ultimately, a detailed understanding of the pathways and processes involved in cardiomyocyte differentiation, migration and growth may help to harness cardiomyocyte proliferation as a therapy for human diseases associated with significant cardiomyocyte loss.

Cell cycle promoters, such as CDKs, cyclins, and proto-oncogenes are markedly expressed in embryonic hearts, corresponding to high cardiomyocyte cell cycle activity, while their expression is lower in the adult heart. In general, negative cell cycle regulatory genes are upregulated, such as CDKs inhibitors, in adult hearts, where cardiomyocyte cell cycle activity is extremely low (Pasumarthi and Field, 2002). These key observations provide a clear rationale for exploration of the fundamental pathways associated with CDK9 in the heart and support the need for further elucidation in relevant animal models.

Thus, although there is little evidence the zebrafish embryo or adult fish actually shows cardiomyocyte hypertrophy, it does appear to demonstrate a hyperplastic response when other species would demonstrate hypertrophy. Therefore, I have used the zebrafish embryo as an accessible model in order to evaluate its potential

for examining the upstream aspects of hyperplastic pathways.

1.8. Response to Injury in the adult heart

In the mammalian (Xu and Baldini, 2007) and fish heart (Brand, 2003) there is a common set of genes that drive growth and development of the embryonic heart. This gene program is also activated in the adult mammalian heart following injury or haemodynamic stress as demonstrated in the mouse, rat and rabbit heart (Heineke and Molkentin, 2006; Alexander and Bruneau, 2010). Many of these genes also appear to be activated in cardiomyocytes in response to resection of the ventricle apex in the zebrafish (Lien *et al.*, 2012) (Mercola *et al.*, 2011). While this process has been studied in a variety of mammalian animal models less is known about the related processes in the adult human heart.

1.8.1 Response to Heart Injury in Mammals

The commonest cause of heart injury in developed countries is ischaemic heart disease (IHD), either as a consequence of acute myocardial infarction or through chronic ischaemic damage (Levy *et al.*, 2002). The World Health Organization states that, in 2008, 30% of all global deaths were associated with cardiovascular disease (WHO, 2011). In addition to acquired disease such as IHD, the impact of an ageing population with degenerative cardiac disease associated with hypertension or valvular heart disease also create an important contribution to cardiomyocyte dysfunction and loss (Lips *et al.*, 2003; Berenji *et al.*, 2005; Haider *et al.*, 1998). Following such stimuli, the human heart typically responds with cardiomyocyte hypertrophy combined with hyperplasia of non-cardiomyocyte cell populations in the heart including fibroblasts (Heineke and Molkentin, 2006).

Cardiac hypertrophy, characterized by an increased cardiomyocyte size, enhanced protein synthesis and re-organization of the sarcomere (Frey and Olson, 2003), is acknowledged as an adaptive physiological response intended to preserve cardiac function in the face of increasing haemodynamic stress. It normalizes wall tension and is necessary in the short term to allow the animal to adapt to the initiating

stressful stimulus (Heineke and Molkentin, 2006). However, prolonged stimulus to cardiac hypertrophy can result in an abnormal cellular response within the myocardium typified by interstitial fibrosis, a switch to less efficient myosin types and abnormal calcium handling (Aoki *et al.*, 2000). These features result in so called adverse remodelling of the ventricle and in addition to contractile dysfunction leading to congestive cardiac failure it can also significantly increase the risk of arrhythmia and sudden death. Apoptosis is also a feature of cardiac hypertrophy particularly when associated with congestive heart failure (Velez Rueda *et al.*, 2012). Unlike other organs in the body, such as the liver, the heart does not appear to possess a mechanism to replace cardiomyocytes. However, more recently new evidence has emerged that the adult mammalian heart does indeed contain a very small population of progenitor cells capable to differentiate into cardiomyocytes (Rubart and Field, 2006). These cells might play a role in the replacement of lost cardiomyocytes although do not appear to be activated in injured cells replacement process (Wills *et al.*, 2008).

Currently, many laboratories and institutions around the world are focused on the transplantation of various types of progenitor cells into infarcted hearts to achieve a myocardial tissue renewal. To date most of these studies suggest that, while there may be improvements in cardiac function, there is little evidence in both human and mouse models that progenitors fully engraft and mature into active cardiomyocytes (Dragneva *et al.*, 2013; Chen *et al.*, 2013; Kearns-Jonker *et al.*, 2012; Buccini *et al.*, 2012; Menasche, 2011). There is evidence however that they may increase angiogenesis, leading many to believe that transplanted progenitors release a variety of growth factors that contribute to the response to injury by stimulating growth and repair of non-cardiomyocyte derived cells (Iwasaki *et al.*, 2011; Wang *et al.*, 2010; Foubert *et al.*, 2008).

1.8.2 Models of Heart Injury in Mammals

A variety of mechanisms are present in all organisms for dealing with tissue damage resulting from injury or disease. Mammals can regenerate liver and

pancreas, can partially repair injury of peripheral nerves or skeletal muscle, but retain poor regenerative ability of other organs (Alcon *et al.*, 2012).

Following transmural Myocardial Infarction (MI) in rats and human the typical response to injury is inflammation and ventricular remodeling with fibrotic tissue formation at the site of MI and around of this (Anversa *et al.*, 1993; Weber *et al.*, 1989). Reparative fibrosis appearing within and around the MI region is essential to safeguard the structural integrity of infarcted tissue, although interstitial fibrosis in non-infarcted myocardium alters tissue stiffness and lead to diastolic ventricular dysfunction (Sun and Weber, 2000). Cryoinjury, has been reported to as an alternative model to coronary artery ligation in adult mice (van den Bos *et al.*, 2005) and was tried previously in the clinical setting as an ablative technique for the treatment of arrhythmias (Gallagher *et al.*, 1977).

1.8.3 Models of Heart Injury in Lower Vertebrates

There are no well-described models of infarction or other cardiac injuries in lower vertebrates. Surgical removal of ventricle apex in salamanders (newt) and zebrafish (approximately 20% ventricle apex resection) has provided a reproducible and reliable model of cardiac regeneration (Poss *et al.*, 2002). However, this resection model is probably only feasible in a low-pressure heart such as that found in lower vertebrate species and in the early post-natal time period in mice, but not in a high-pressure system typical of adult mammals where acute bleeding from the resection site results in rapid death. In addition, the apex resection model is less comparable with clinically relevant models of heart injury in mammals such as coronary artery ligation which result in acute necrosis followed by formation of a fibrous scar (Abarbanell *et al.*, 2010). Recently, the cryoinjury model in the adult zebrafish heart has partially addressed this issue, since the damaged tissue is maintained in situ (Gonzalez-Rosa and Mercader, 2012; Schnabel *et al.*, 2011). Following cryoinjury, the adult zebrafish heart demonstrates features of regeneration including cardiomyocyte proliferation. However, this cryoinjury model, as with other injury-recovery models in the adult, requires up to 4 months for complete repair of the

heart. Therefore, a model of heart injury and recovery which shortens the time of response and repair and which can be readily assessed functionally would be a desirable experimental tool.

1.9. Heart regeneration mechanisms

1.9.1. Mammalian regeneration

During the 20th century it was accepted that heart is essentially a post-mitotic organ and cardiac growth in the adult was attributed exclusively to cardiomyocyte hypertrophy (Karsner *et al.*, 1925; Macmahon, 1937) (Linzbach, 1960; Zak, 1974). However, since the 1990s, evidence of cardiomyocytes proliferation in adult human hearts started to appear (Quaini *et al.*, 1994; Kajstura *et al.*, 1994; Beltrami *et al.*, 2001). Quaini and co-workers demonstrated the presence of proliferating cell nuclear antigen, a marker of the G1-S cell cycle phases, in adult human hearts with ischemic and dilated cardiomyopathy. Evidence of metaphasic chromosomes together with cytokinesis was also demonstrated in normal myocardium and in ischemic and dilated cardiomyopathy and in myocardial infarction suffering patients (Kajstura *et al.*, 1994; Beltrami *et al.*, 2001). Considerable disagreement remains on the frequency of these cellular events in normal and diseased myocardium.

The measured rate of cell division is affected by the methods used to detect DNA synthesis and count cardiomyocytes (Soonpaa *et al.*, 1996). In normal adult rats it has been reported a percentage of synthesizing DNA cardiomyocytes in a range from 0.005%-3.15%, that decreases at 0.0004%-0.04%, in mice. In adult mammals injured hearts these percentages are even more variable, ranging from 0.0006%-43.6% in rats and 0.0055%-0.5% in mice (Soonpaa *et al.*, 1996). Indeed, adult cardiomyocytes rarely appear to re-enter the cell cycle and proliferate (Pasumarthi and Field, 2002), which could certainly explain the low cardiac regenerative capacity of the mammalian heart.

However, the presence of active DNA synthesis, even if low, gives rise to the expectation that proliferation of adult cardiomyocytes could be therapeutically

stimulated. In particular, some reports have shown that adult mammalian cardiomyocytes can proliferate in culture after treatment with Fgf1 concomitant with p38MAP kinase inhibition (Engel, 2005). Other studies have demonstrated the presence of putative progenitor cells within the hearts of adult mammals, suggesting that the heart has the potential for homeostatic or regenerative renewal (Beltrami *et al.*, 2003; Laugwitz *et al.*, 2005; Moretti *et al.*, 2006). Why such progenitor cell populations are not able to repair cardiac muscle in response to injury and, most importantly, how to trigger this ability, is not yet clear. The mechanisms involved in the cardiac regenerative process in other species are being carefully examined to assess whether these could be harnessed or reactivated in mammals. The zebrafish has emerged as a useful and interesting model for this purpose.

1.9.2 Zebrafish heart regeneration

While adult mammals display poor regenerative ability, lower vertebrates, such as salamanders and fish, can regenerate most of the organs following significant injury or loss of tissue. In the zebrafish resection of up to 20% of the ventricle apex results in complete regeneration within 60 days (Poss *et al.*, 2002). Zebrafish heart regeneration proceeds through injury-induced proliferation of cardiomyocytes capable to divide and proliferate postnatally (Nag *et al.*, 1979; Matz *et al.*, 1998; Raya *et al.*, 2003; Poss *et al.*, 2002). BrdU labelling studies have shown BrdU-positive cardiomyocytes along the leading edge of the regenerating heart. Lepilina et al. (Lepilina *et al.*, 2006) suggested that regenerating myocardium rises and matures from undifferentiated cardiomyocytes progenitor cells of epicardial origin. In contrast, two recent genetic fate-mapping studies (Jopling *et al.*, 2010; Kikuchi *et al.*, 2010) unambiguously demonstrated that pre-existing committed cardiomyocytes are instead the main source in the cardiac regeneration in the zebrafish model.

Although cellular mechanisms involved in the cardiac regeneration have recently started to be unraveled, there is yet a strong need to explore new candidate molecular pathways that might be involved in the cardiomyocyte response to stress and injury in order to better understand the potential mechanisms that underpin

hypertrophy and hyperplasia in the heart. As discussed extensively above, one emerging molecule involved in the response to hypertrophy in adult mammalian myocardium is CDK9 (Sano *et al.*, 2002), which is known to play a key role in cell proliferation in a number of settings.

1.10 Hypothesis and Aims

1.10.1 Hypothesis

CDK9 plays a key role in proliferation of cardiomyocytes during normal development and following heart injury.

1.10.2 Aims

- What is the normal pattern of cardiomyocyte growth during development in the zebrafish and how does this relate to function?
- What is the role of CDK9 on cardiac growth and function during normal development?
- What are the effects of heart laser injury during development of the normal zebrafish heart?
- What is the impact of CDK9 modulation on the response to laser injury in the zebrafish embryonic heart?

Chapter 2
Materials and Methods

2.1 Zebrafish, A(SP)Act 1986 and Ethical Review

All animal experiments described in this study were performed in accordance with the UK Home Office (Scientific Procedures) Act 1986 (online resource http://www.legislation.gov.uk/ukpga/1986/14/contents) and were approved by the ethical review committee.

Zebrafish embryo and larva are protected by the Act from the time at which they become capable of independent feeding, which in the zebrafish is accepted to be at 5 dpf. Life stages before this time are considered to be not sufficiently aware that they will suffer or otherwise have poor welfare when a procedure is carried out on them (online source www.nc3rs.org.uk).

2.2 Husbandry, Breeding and Egg collections

Zebrafish husbandry, embryo collection, dechorionation (section 2.11.1) and maintenance were performed according to accepted standard operating procedures (Westerfield, 2000; Nüsslein-Volhard, 2002).

Zebrafish were maintained in the QMRI (BRR) Zebrafish Facility at the Queen's Medical Research Institute, The University of Edinburgh, at a temperature of 28.5°C on a 14h light/10h dark cycle and staged as described by (Kimmel *et al.*, 1995). Fish were kept in egg water, containing a weak solution (0.33%) of methylene blue (King British, Lincolnshire, UK) (100μL in 3L of system water, in order to inhibit fungal growth), until they underwent spontaneous dechorionation (2-3 dpf) and were then allowed to develop in embryo medium. Details of the chemical constituents of solutions can be found at http://zfin.org/zf_info/zfbook/cont.html#cont10.

2.3 Zebrafish lines

In order to optimize visualization of the heart and other organs, the transgenic line expressing Green Fluorescent Protein (GFP) under the control of the cardiomyosin light chain 2 promoter (cmlc2:EGFP; (Burns *et al.*, 2005)) was used (figure 2.1). The golden mutant (Lamason *et al.*, 2005), characterized by delayed and reduced melanin pigmentation, was used on early experiments to improve heart

visualization under microscopy at 3 days post fertilization (dpf). Similarly, to visualize vascular structures, including the endocardium, the transgenic line expressing GFP under the control of flk1/vegfr2 (flk1:EGFP; (Jin *et al.*, 2005)) promoters were used. To discern embryonic cardiomyocytes from red blood cells, the GATA1:dsRed line (Gray *et al.*, 2007) was crossed with cmlc2:GFP to obtain double GFP/dsRED positive embryos.

2.4 Anaesthesia and Euthanasia

Buffered Tricaine (MS222, Ethyl 3-aminobenzoate methanesulfonate salt; Sigma-Aldrich Company Ltd., Dorset, UK) 20μM was used to anaesthetize embryos from 1 to 5dpf. Depth of anaesthesia was assessed by ataxia and loss of response to stimuli. Tricaine 1mM MS222 was used to euthanize embryos, in accordance with the UK Home Office Schedule 1 methodology. Detailed solution chemistry for buffered MS222 solution can be found at http://zfin.org/zf_info/zfbook/chapt10.html#wptohtml63.

2.5 Microscopy

A number of different microscopy techniques were used to optimize imaging for various aspects of this thesis.

2.5.1 Mounting technique for imaging

Whole fixed embryos were mounted on microscope cavity slides (Hawksley, Sussex, UK) in a drop of glycerol 100%, covered with a coverslip and sealed with transparent nail varnish. Isolated zebrafish embryonic hearts (see section 2.8) were mounted as above, but using flat instead of cavity slides.

2.5.2 Stereomicroscopy and Fluorescence

Dissecting stereomicroscopes, Leica Fluo MZ16 (Leica Microsystems Ltd., Buck, UK), installed in the QMRI (BRR) Zebrafish Facility, which provided both white and fluorescent light, were used for microsurgical embryo heart dissection and daily

A

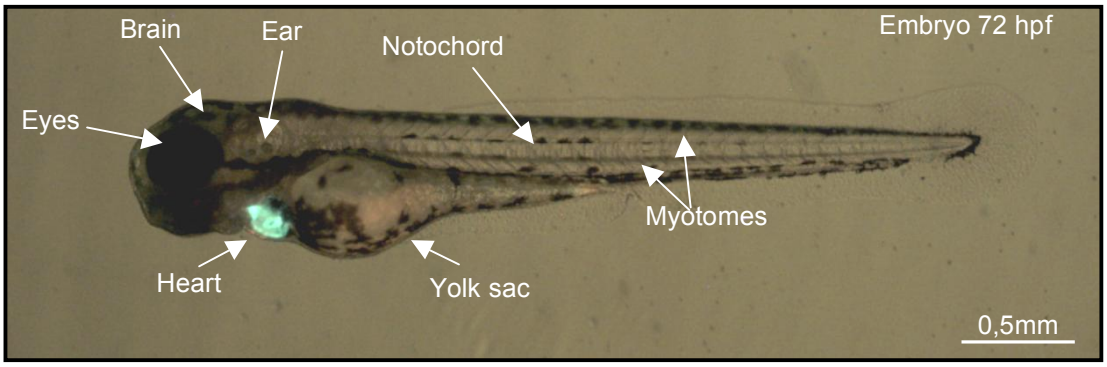

B

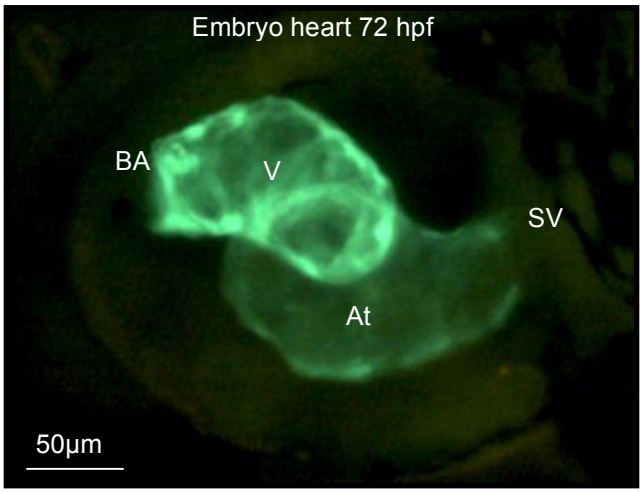

Figure 2.1 - Transgenic cardiac myosin light chain (cmlc)2:EGFP zebrafish embryo. A. The embryo, here shown at age 72 hpf has a length of about 3mm at this stage. Its transparency, in conjunction with utilization of fluorescent technology to mark organ or tissue specific signaling proteins or cellular entities, allows for powerful imaging of organ development. In this transgenic line expressing Green Fluorescent Protein (GFP) under the control of the cardiac specific cardiomyosin light chain 2 promoter, the heart is green (B). Key: V- ventricle; At- atrium, BA – Bulbus arteriosus, SV – Sinus Venosus

checks of embryo survival and gross phenotype. Images were captured with a camera Leica DFC300FX (Leica Microsystems Ltd., Buck, UK) mounted on the microscope and connected to a computer using Leica Application Suite software (LAS V3.8).

2.5.3 Compound microscopy and Fluorescence

For accurate organ observation, live embryos in embryo medium were visualized under a compound fluorescence microscope Axioskop II MOT Plus (Carl Zeiss Ltd., Cambridge, UK) with a X40 dipper objective lens. To evaluate cardiac function (see section 2.6) video-images were captured by a black and white digital video camera IonOptix CCD100 MyoCam^{tm} (IonOptix Ltd., Ireland) or a colour camera JVC TK-C1481BEG (JVC, Long Beach, CA, USA) both at 30 frames per second mounted on top and linked to a computer provided with Pinnacle Studio software (www.pinnaclesys.com). Photographs of embryos were adjusted for brightness and contrast in ImageJ software (National Institute of Health, USA) and/or Microsoft Power Point and identical adjustments were made for active treatment groups and controls.

2.5.4 Confocal microscopy

Confocal microscope Leica SP5 (Leica Microsystems Ltd., Buck, UK) was used to collect high-resolution Z-stack images of whole zebrafish embryos or isolated zebrafish heart ventricles. Argon laser, set at 30% power, was used to excite GFP at 488nm excitation wavelength. Ultraviolet laser, set at 15% power, was used for DAPI at 408 nm excitation wavelength. Neon laser 555, set at 50% power, was used for Alexa Fluor at 555 nm excitation wavelength. Z-stack images were captured at a rate of 1 image/3μm of tissue) by a LAS AF software (Leica Microsystems Ltd., Buck, UK). Objective 10X was used to pinpoint isolated hearts onto the slide, while 40X and 63X oil objectives were used for high-resolution visualization of the organ.

2.6 Evaluation of Cardiac Function

2.6.1 Video image capture in living zebrafish embryos

Tg(cmlc2:EGFP) zebrafish embryos (1 to 5dpf) were placed, one at a time, in a 35mm Petri dish and supplied with anaesthetic buffered MS222 20μM in embryo medium. This dose of anaesthetic was shown to have minimal impact on the beating hearts while the room temperature in which all the experiments were conducted significantly reduce physiologic heart rate and the general cardiac function (Denvir *et al.*, 2008). The plate was positioned under a Zeiss fluorescence microscope Axioskop II MOT Plus (Carl Zeiss Ltd., Cambridge, UK) (see section 2.3.2), provided of a HAL100 halogen illuminator, with a 40X water dipper objective. Video images were captured with the video camera (30 frame per second, fpm) mounted on the microscope linked to a computer using video-capture software (Pinnacle Studio, www.pinnaclesys.com). Videos of beating hearts, for measuring ejection fraction and heart rate, were captured under fluorescence light by selecting the blue (488nm) filter to excite GFP, while videos of the posterior cardinal vein to assess blood flow velocity were captured under white light.

2.6.2 Analysis of Ejection Fraction

Video images were analysed using the freeware software program ImageJ; this is a public domain image processing software tool developed at the National Institute of Health and was adopted for its relative ease of use to assess cardiac function. For the purposes of cardiac function analysis, diastole and systole were defined as the largest and smallest outlined area of the ventricle as visualized under fluorescent light (see figure 2.2). The atrium was excluded from the region of analysis by adjusting the intensity of the video image using a pre-amplifier linked to the video camera. The bulbus arteriosus was excluded from the region of analysis at the time of analysis of the image.

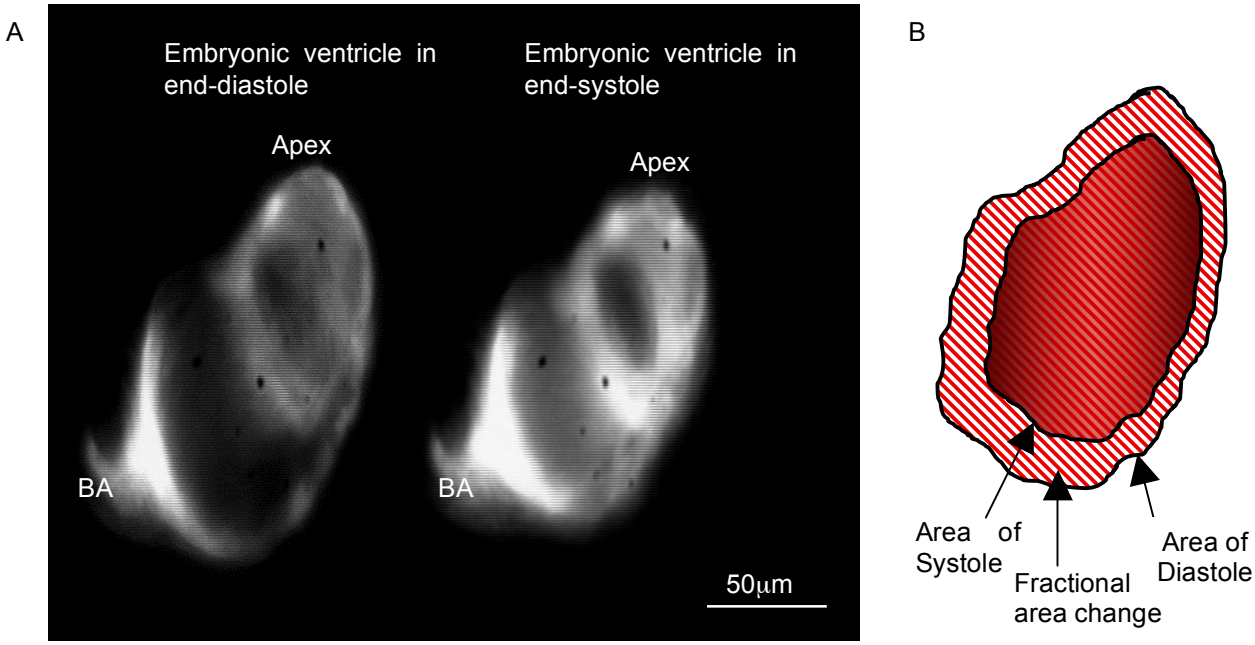

Figure 2.2 - Assessment of Ejection Fraction in the zebrafish embryonic heart. A. Black and white images, captured under fluorescence microscopy, of zebrafish embryo heart ventricle in end-diastole (left image) and end-systole (right image) in the same cardiac cycle, selected from a video of a cmlc2:EGFP zebrafish embryonic heart (72 hpf). B. Schematic representation showing the ventricular area in end-systole (dark red stripes) subtracted from the area in end-diastole (light red stripes) for calculating the Area Fractional shortening, in this context called Ejection Fraction. BA=bulbus arteriosus.

Fractional area change of the ventricle, that here we call ejection fraction (EF) was calculated using the following formula: EF= ((EDA - ESA)) ÷ EDA) x 100

Where EDA is the End-Diastolic area and ESA is the End-Systolic area.

Results of Ejection Fraction refer to the mean of three cardiac cycles. Intra- and inter-observer variation was assessed by Bland-Altman method for comparing paired measurements (see Statistic section 2.15). Data for area of the ventricle in end-diastole is also presented as a measure of ventricle size during normal development and following laser injury measured in tg(cmlc2:EGFP) embryos. These data provide an assessment of the growth in heart size during development and the loss of GFP positive cells following laser.

2.6.3 Heart Rate

Heart rate (HR) was determined by examining ventricle beating in the same video captured as above (see Section 2.6.1). The number of heartbeat were counted for all the duration of the video, that was at least 10 sec. HR was then expressed as beat per minute (bpm).

2.6.4 Cardinal vein blood velocity

Blood velocity was estimated in the posterior cardinal vein (Isogai *et al.*, 2001; Rider *et al.*, 2012) by assessing frame by frame motion of single blood cells determined from video images captured as described in section 2.6.1 in the zebrafish tail at the level of the cloaca (see figure 2.3). Four erythrocytes per fish (at least 4 embryos per group) over 10 frames at video frame-rate of 30 frames per second (fps) were analyzed using ImageJ to determine mean blood cell velocity ($\mu m \cdot s^{-1}$).

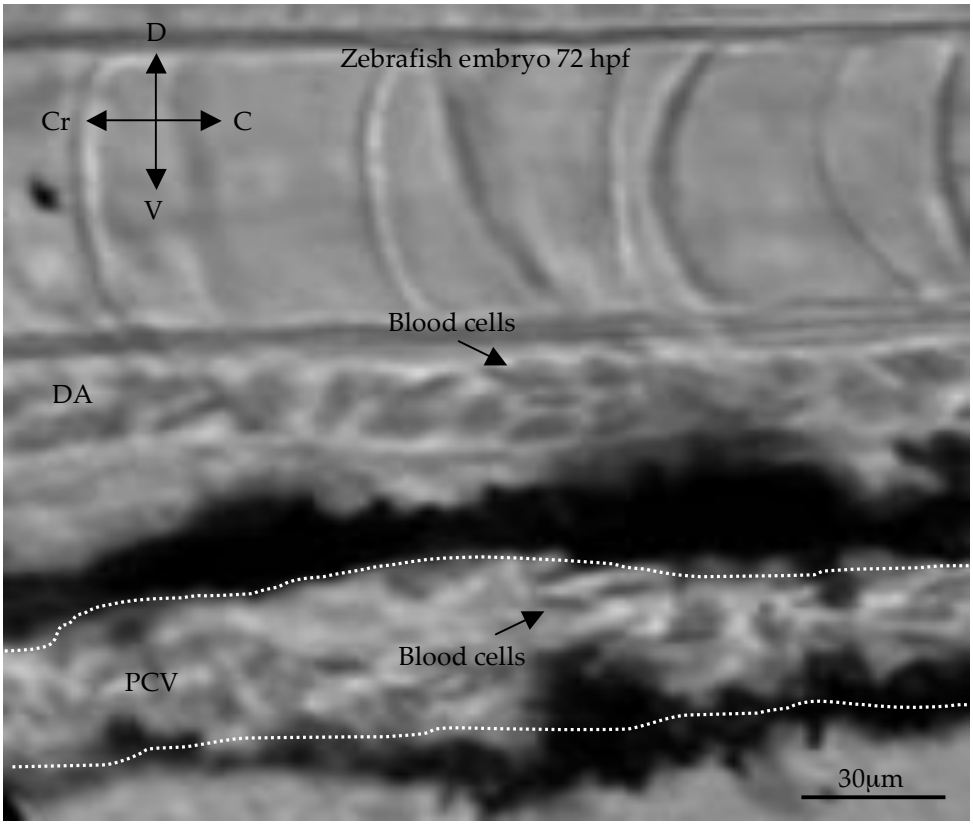

Figure 2.3 - Analysis of cardinal vein blood velocity in the zebrafish embryo. From a video (at 30 fps) captured in the zebrafish embryo tail at the level of the cloaca, the path of single blood cells was followed over 10 consecutive frames in the posterior cardinal vein. Video frames were analyzed using ImageJ, previously calibrated with a slide graticule of 1mm length. Blood cell velocity corresponded to the distance from the first to the tenth frame and was expressed as $\mu m \cdot s^{-1}$. Key: DA – Dorsal aorta, PCV – Posterior Cardinal Vein, Cr – Cranial, C – Caudal, D – Dorsal, V – Ventral.

2.7 Laser Injury Model

Utilization of a laser in the biomedical field is not new. However, the technique described here of a highly selective and focused injury to the rapidly beating zebrafish embryonic ventricle using a laser offers unique advantages compared to previous use in the same model (Gray *et al.*, 2007; Yalcin *et al.*, 2010). For this purpose, two different types of laser system were explored.

2.7.1 PALM Microbeam

The PALM MicroBeam (Carl Zeiss PALM® MicroLaser Technologies, Cambridge, UK) system includes two main parts: the visual core and the PALM laser. The visual core includes an inverted microscope with associated software and a camera for brightfield and fluorescence imaging. The PALM laser includes a diode pumped Q-switched solid state laser (CryLaser FTSS 355-50), with a beam diameter of 450 ± 150μm, peak power > 70 kW at 1 - 100 Hz and pulse width ≤ 1.0 ns. The laser is controlled by commercially provided software (PALMRobo software, Carl Zeiss, Cambridge, UK). In order to check functionality and efficacy of the laser beam, each embryo was placed on its flank on a membrane slide (fig. 2.4 A and C). The membrane slide 1.0 PET (Zeiss PALM® MicroLaser Technologies), see figure 2.4 B, is a regular 1mm thick glass slide covered by a 1.35μm thick polyethylene naphthalate film, which is highly absorptive in the UV-A range, facilitating the laser injury. Once exposed to the laser beam, the membrane slide shows a 20-30μm diameter burn as a result (fig. 2.4 B).

Preliminary experiments were performed to set laser parameters: energy and focal width. The determined and final chosen values were: Focus 80, Energy 60 (both in a scale 1-100, arbitrary units of the manufacturer), taking into consideration the amount of damage caused, either in the ventricle or in other structures, and the survival of the embryo.

At 48 hpf the developing heart tube loops to create a single atrium and single ventricle in a process that can occur in a right or left-handed fashion.

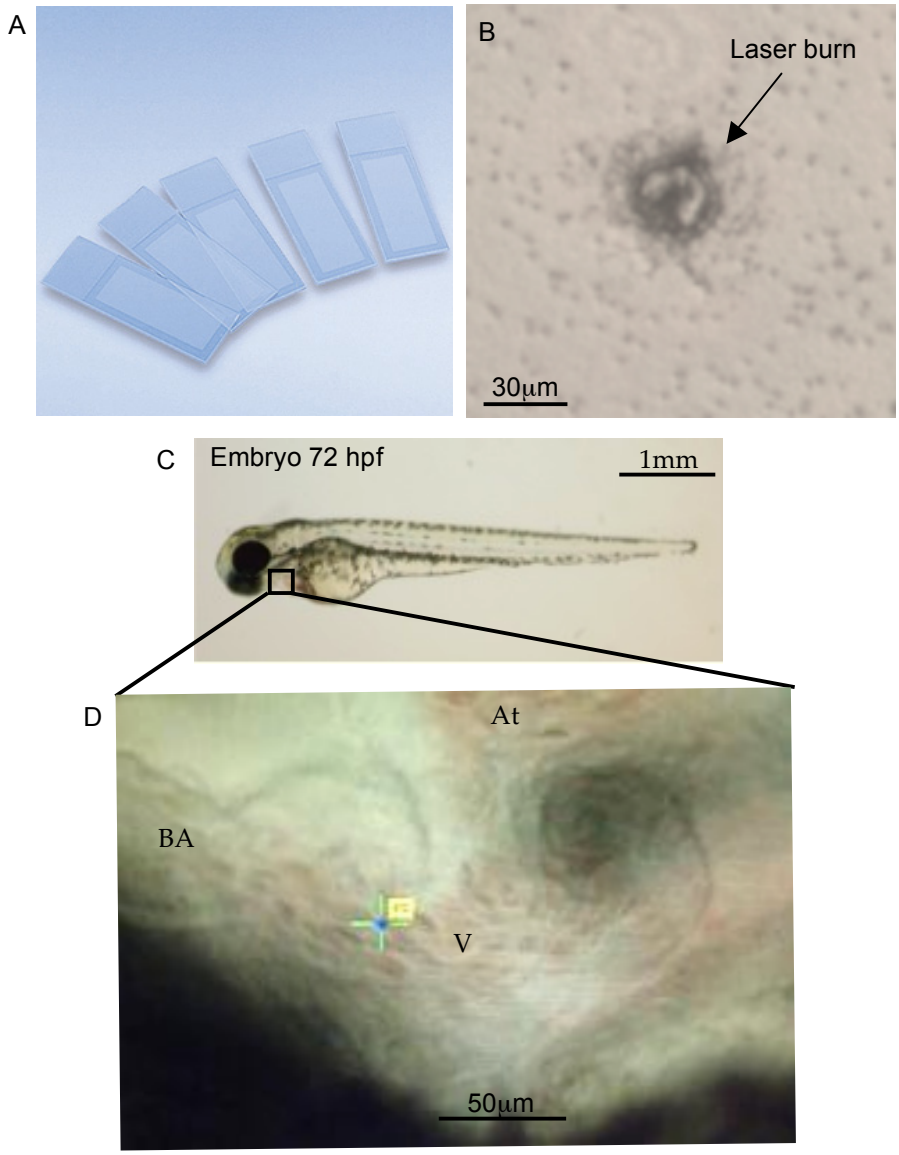

Figure 2.4 - Laser injury protocol using the Zeiss PALM® Laser. A. Membrane slides 1.0 PET (image from https://www.micro-shop.zeiss.com) were used in our laser injury protocol in order to check the efficiency of the laser beam before the start of each experiment. Following laser beam delivery on the slide film, this shows typically a 20-30µm diameter burn (B). C. Zebrafish embryos at age 72 hpf were laid on their left side on the membrane slide and a single laser beam was delivered in the mid-ventricle (image D, obtained using an objective 20X) in correspondence of the blue spot in the green cross of the PALM system. (BA= bulbus arteriosus; V=ventricle; At= atrium).

Predominantly in the zebrafish this occurs as a right-handed rotational event leaving the ventricle predominantly positioned to the right of the midline in a ventral location and the atrium lying towards the midline in a more dorsal position (Hu et al., 2001). Therefore, to ensure a clear view of the ventricle, embryos were ideally laid on their left side to provide the best view of the beating ventricle. Laser pulses were administered to the tail of the embryo as controls in some experiments.

2.7.2 XYClone laser ablator and Optical Gating System

One of the limits of any laser technique is the difficulty in delivering the laser beam to a specific area of the rapidly beating zebrafish embryo heart or to deliver multiple laser shots to a given area. With the zebrafish lying on its side on a glass slide, the atrium and ventricle images are commonly overlapping, making it difficult to injure the ventricle without damaging the atrium or atrioventricular (AV) cushions. By using a micro-probe it is possible to re-position embryos into a more optimal position allowing a non-overlapping view of the ventricle. In addition to the time involved in performing this task, the manual handling of the embryo can induce stress and can occasionally result in some damage to the embryo.

2.7.2.1 XYClone laser ablator

To overcome the problems mentioned above, we developed a unique custom-built Optical Gating System (see Section 2.7.2.2) linked to an Infrared Laser Ablator XYClone (Hamilton-Thorne Inc., Maryland, USA), figure 2.5. This system allowed synchronization between the laser pulse and the cardiac cycle. We compared the effects of this laser on ventricle damage with the synchronization system on and off. Embryos were placed under the microscope as for the PALM Laser (section 2.7.1). The infrared laser objective combines a Class 1 Laser (Infrared Solid State Diode 1450 nm; 300mW @ focus) with custom designed 20X objective. Images captured by a standard digital video camera (ProSilica GS650, Lambda Photometrics Ltd., Hertfordshire, UK) mounted on an inverted microscope (Carl Zeiss Ltd., Cambridge, UK) are displayed on a monitor as a live video image of the sample.

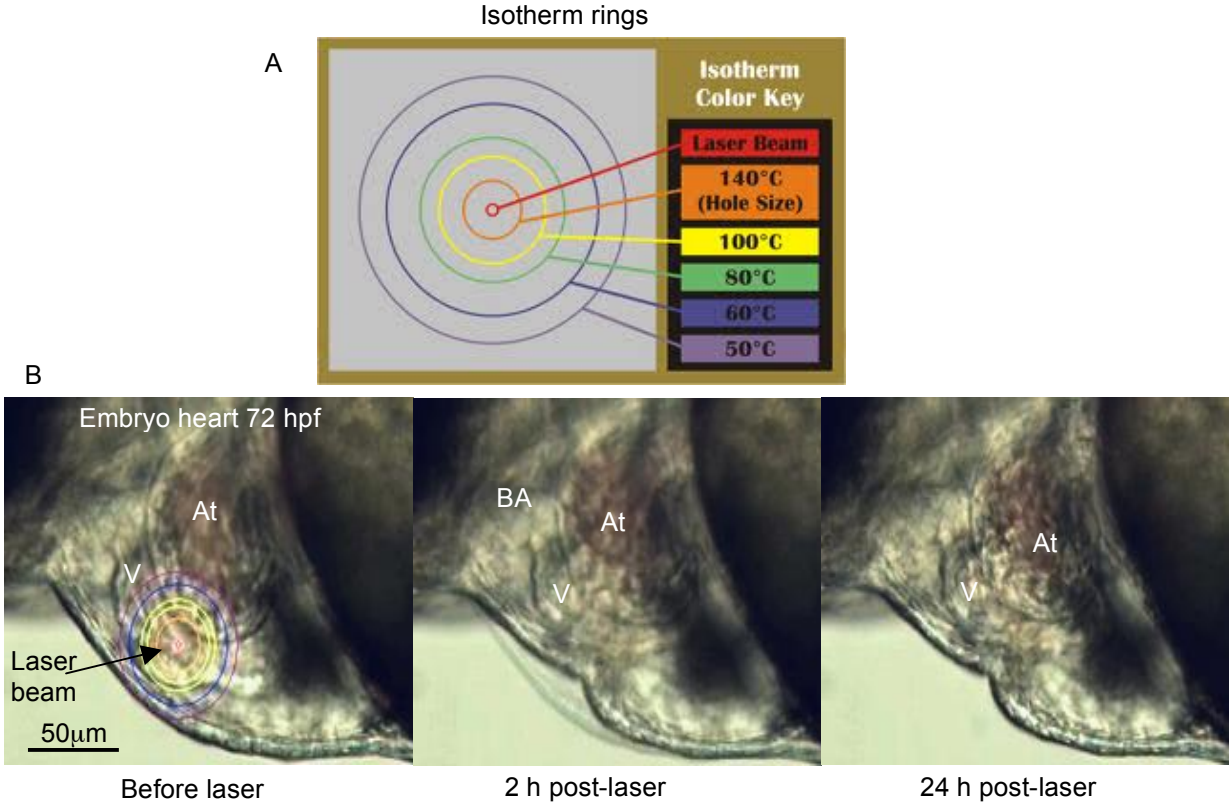

Figure 2.5 – Laser injury of the zebrafish embryonic heart (aged 72 hpf) using Infrared Laser Ablator XYClone (Hamilton-Thorne). A. Isotherm Rings is a tool included in the software associated with the XYClone laser ablator, that provide the user with information related to the temperature reached in the injured tissue area and also help prevent potential harmful effects during the injury (Image from www.hamiltonthorne.com). B. Sequence of images selected from a video captured with a video camera associated with the microscope showing a typical event of cardiac laser injury, before laser and then at 2 and 24 hour post-laser. BA – Bulbus arteriosus, V - Ventricle; At - Atrium.

The XYClone software provided an overlay of isotherm rings, six concentric circles with different colours that indicate the peak temperature reached at that radius of the circle when the laser is fired at its current power (figure 2.5 A). A built-in collimated red indicator beam target (RED-I) indicated the position of the laser beam in the field of view. A great advantage of using the RED-I, over the PALM microbeam system, is that you can fire the laser while looking through the eyepieces of the microscope. An example of laser injury in the zebrafish embryonic ventricle is reported in figure 2.5 B.

2.7.2.2 Optical Gating System

The Optical Gating System allows high-precision real-time image to an arbitrary position in the cycle of the zebrafish embryo beating heart (Taylor *et al.*, 2011). This system was developed by Jonathan Taylor and colleagues at the Durham University and was adapted from Dr. Taylor in our Institute to permit synchronous firing of the laser while I developed the method of achieving localized injury in the zebrafish embryonic heart using laser.

Images captured by the video camera (ProSilica GS650, Lambda Photometrics Ltd., Hertfordshire, UK) are analyzed by custom real-time image analysis software with custom timing hardware to trigger a signal for the laser to fire. The user selects the point in the cardiac cycle that the laser should be fired from a sequence of presented images representing one full heart cycle. The software then analyzes subsequent image frames, as they are received from the camera, calculating the precise time at which the heart will next be in the selected position. The laser is electrically triggered at the moment the heart is next in this position. Video and still images are used to verify that the correct region was injured by the laser pulse. The laser pulse was delivered during mechanical diastole, which we defined as the video image with the ventricle at its largest size.

This novel approach also permitted the assessment of multiple laser pulses on the heart ventricle. The multi-laser protocol involved the delivery of 1 to 5 laser pulses to the mid-region of the ventricle at 1 minute intervals during ventricular diastole.

This multi-laser approach could be achieved without creating significant injury to nearby cardiac structures using the Optical Gating System. In addition, the Optical Gating System permitted precise targeting of the laser to specific intra-cardiac structures such as the atrioventricular (AV) cushions, bulbus arteriosus and different regions of the atrium and ventricle. To assess whether there were regional differences in the response to injury the ventricle was divided arbitrarily into 3 regions (basal (B), mid (M) and apical (A)) and the effects of a single laser pulse to each of these regions on heart rate and function was assessed.

2.8 Isolation of zebrafish embryonic hearts

Embryonic hearts were extracted by two methods.

2.8.1. Surgical extraction of single embryo hearts

To preserve the integrity, morphology and structure, plus allow full penetration of antibodies during immunohistochemistry, embryonic hearts were removed by microdissection (figure 2.6 A).

Tg(cmlc2:EGFP) zebrafish embryos were collected in 1.5ml eppendorf tubes in 500μL of embryo medium (EM) and euthanized by anesthetic overdose of tricaine, as detailed in Section 2.4. Embryos were washed twice in physiological buffer solution (PBS)+Triton-X100 (Sigma-Aldrich Company Ltd., Dorset, UK) 0.1% (PBS-Tx) and fixed in paraformaldehyde (PFA) (Sigma-Aldrich Company Ltd., Dorset, UK) 4% diluted in PBS-Tx overnight (ON) at 4°C or 3h at room temperature (RT), *i.e.* 22°C.

Following fixation, samples were then washed in PBS and placed in a Petri dish coated by a layer of agar 2%. By gentle movements of fine forceps (Dumont #5), pericardial sac was carefully opened and cmlc2:EGFP hearts were exposed (figure 2.6 A). Hearts were manually extracted under fluorescence light and placed in pre-chilled PBS for immediate immunohistochemistry or stored in methanol 100% for later histological analysis as required. Surgical extraction of embryonic hearts is the method of election when few embryos per experimental group are available.

2.8.2 Mechanical-agitation method for extraction of zebrafish embryo hearts

Molecular studies, such as protein or nucleic acid analysis, require a certain amount of biological samples according to the sensitivity of the instrument used. To harvest larger numbers of embryonic hearts, a mechanical-agitation extraction method was adopted using a previously published technique (Burns and MacRae, 2006); this approach permits the collection and aggregation of up to 200-300 embryonic hearts (figure 2.6 B). To facilitate and aid the tracking of isolated hearts, cmlc2:EGFP embryos were used. This technique exploits the capacity of fluid forces in a medium repeatedly drawn into and expelled from a needle and syringe to rupture embryonic yolk membranes and extract, among other tissues, intact hearts.

Prior to disruption, embryos were anaesthetized, transferred to a 1.5-mL microfuge tube (Eppendorf UK Limited, Stevenage, UK), washed three times with embryo disruption medium (EDM) and resuspended in 1.25 mL of fresh EDM. EDM contained Gibco Leibovitz's L-15 Medium (Life Technologies Ltd, Paisley, UK) and 10% fetal bovine serum (Life Technologies Ltd, Paisley, UK). The 2mL microfuge tube, a 19-gauge needle and a 5mL syringe were manipulated by hand. Approximately 1mL EDM containing embryos was drawn into the needle and syringe and immediately expelled back into the microfuge tube 25 times at a rate of 3 seconds per syringe motion. Fragmented embryos were applied to a 100μm nylon mesh (Cell strainer, Becton and Dickinson, Oxford, UK), figure 2.6 B, and the flow-through was collected in a 35mm Petri dish. The microfuge tube, needle, syringe, and mesh were washed with additional media that was added to the flow-through. The flow-through was subsequently applied to a 40μM nylon mesh (Cell strainer, Becton and Dickinson, Oxford, UK,). The Petri dish that collected the 100μm flow-through was rinsed with additional media that was applied to the 40μM mesh. The 40μM mesh was inverted, and the retained material was washed off with EDM into a clean 35mm Petri dish. Intact GFP positive ventricles, many of them still beating and many of them with the atrium still attached, were identified under fluorescent

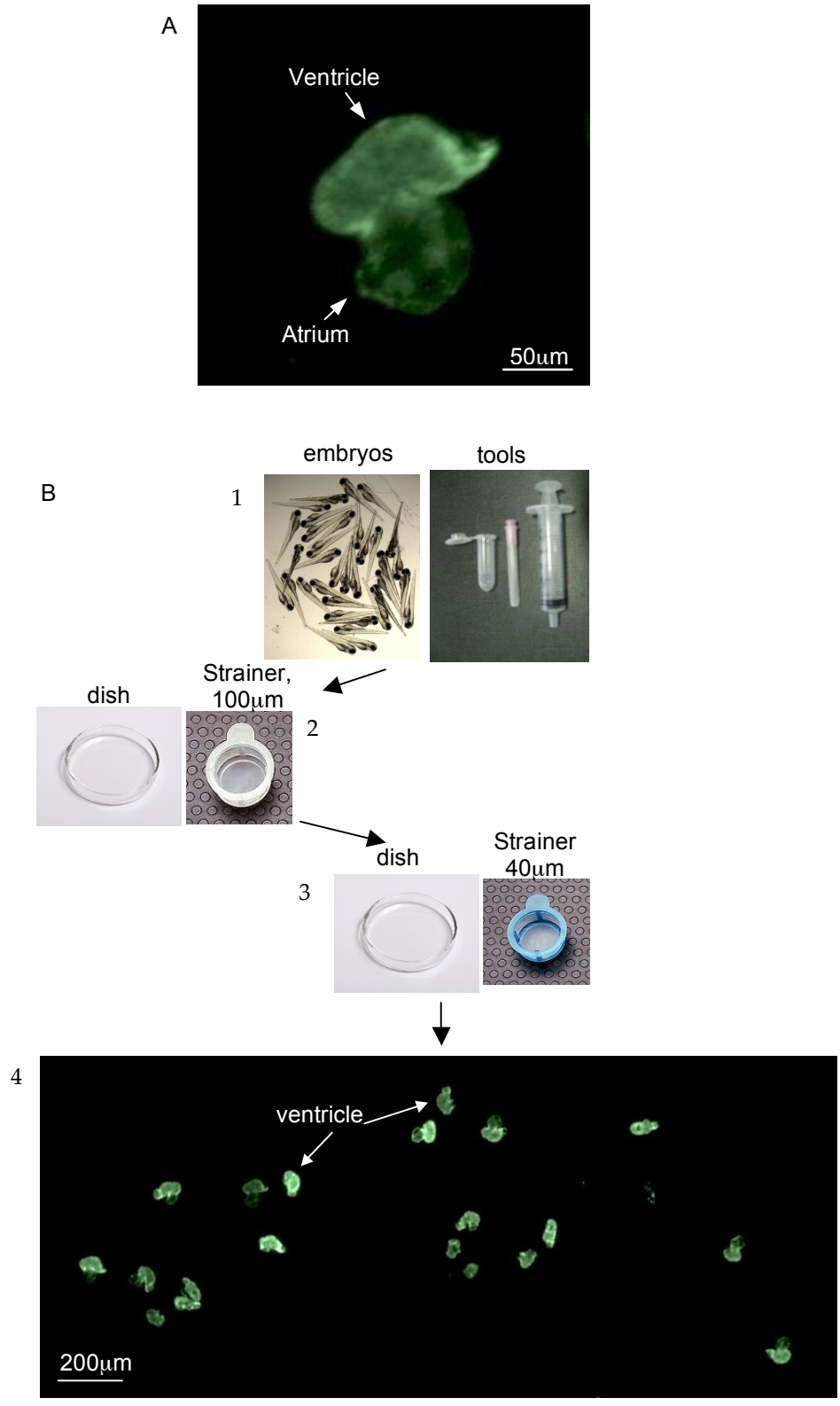

Figure 2.6 - Techniques for isolation of zebrafish embryonic hearts. A. For immunohistochemical staining purpose, cmlc2:EGFP heart (in this image at 96 hpf) were fixated in PFA 4% and then microdissected singularly, suspended in PBS, under a fluorescent microscope. This approach preserves the integrity of the heart morphology and structure. B. Mechanical agitation method was used for high throughput hearts extraction needed, *e.g.*, to obtain a proper RNA yield to perform PCR analysis: 1) embryos in EDM are drawn and expelled several times into and from a syringe in a microfuge, then 2) the liquid was applied to a 100μm nylon mesh (image from http://www.bdbiosciences.com) in a Petri dish to elute hearts, 3) the eluted was then applied to a 40μm nylon mesh (image from http://www.bdbiosciences.com) to separate debris from the hearts. Retained material was washed off from the strainer into a clean dish and 4) GFP positive hearts were collected by a p100 pipette.

light and collected selectively with a p100 micropipette under transmitted light. Approximately 10 ventricles were collected each time the micropipette was filled, see figure 2.6 B).

To minimize contamination by non-cardiac tissues, the hearts were subsequently expelled into a 35mm Petri dish containing fresh EDM and retrieved selectively a second time before being accumulated in a microfuge tube on ice. Hearts were pelleted, the media was decanted, and the preparations were frozen in a dry ice/ethanol bath prior to storage at -80°C.

2.9 Immunohistochemistry

2.9.1 BrdU labelling

BrdU (5-Bromo-2'-deoxyuridine) labelling (figure 2.7) was performed as described in Laguerre et al. (Laguerre *et al.*, 2005) and modified as follows. Live embryos, aged 1-5 dpf, were placed in a 90mm diameter Petri dish and incubated in BrdU (Sigma-Aldrich Ltd., Dorset, UK) 10 mM in embryo medium with 15% DMSO (Sigma-Aldrich Ltd., Dorset, UK) for 20 min, on a surface of ice; thermal shock allows BrdU penetration within the embryo. The Petri dish with embryos was then removed from the ice, embryos were then rinsed twice with fresh EM previously warmed at 28.5°C and allowed to recover in the incubator at 28.5°C for 1 hour. Embryos were then euthanised in tricaine and fixated overnight in PFA 4%. Embryos were rinsed three times in PBS-Tx, this represents the holding solution that will be used for washing or incubation of applied substances.

To aid antibody penetration within the tissues, embryos were digested with Proteinase K (Sigma-Aldrich Ltd., Dorset, UK) 10μM for 20min at RT. Embryos were rinsed several times in PBS-Tx and re-fixed for 30min in PFA 4% and rinsed twice in PBS. Embryos were then washed twice with HCl 2N and incubated at RT in the same solution for 1 hour. They were rinsed three times in PBS and incubated for 1-2 hours in bovine serum albumin (BSA) (Sigma-Aldrich Ltd., Dorset, UK) 3% blocking solution at RT or overnight (ON) at 4°C while gently shaking.

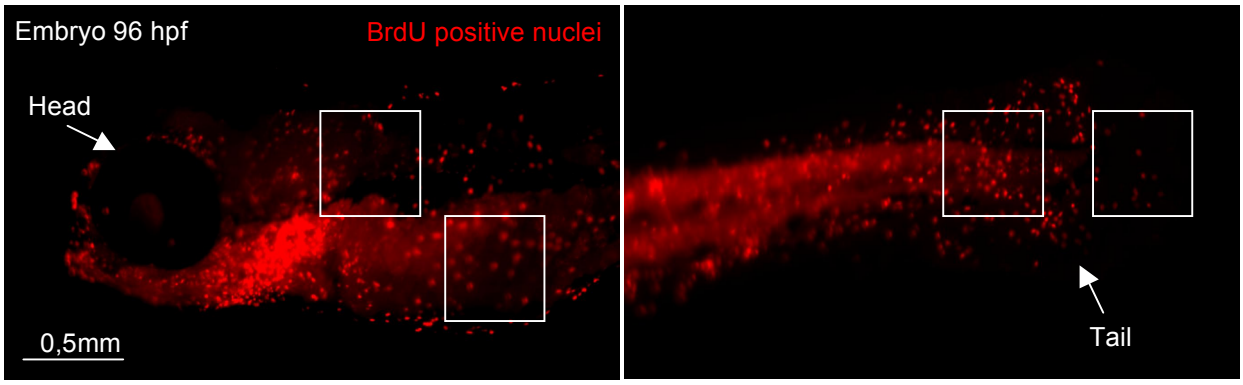

Figure 2.7. BrdU staining on whole mount zebrafish embryo. Two images captured under fluorescence microscopy corresponding to the cranial (right) and caudal (left) ends of the embryo, here at age 96 hpf. Red spots following immunostaining are BrdU positive nuclei and correspond to cell undergoing DNA replication. BrdU analysis using ImageJ software was assessed by counting red spots in the region of interest delimited by white squares and corresponding to an area of 10,000 μm^2.

Embryos were then incubated for 2h in anti-BrdU (1:100 rat; Abcam, Cambridge, MA, USA) at RT or ON at 4°C.

After rinsing several times, embryos were incubated for 2h with anti-mouse TRITC (1:500) in the dark. Embryos were washed twice in fresh PBS and then mounted on chambered slides (Microscope cavity slides 2 cell, Hawksley, Sussex, UK) with ProLong® Gold antifade reagent (Invitrogen, Paisley, UK) as a medium. Embryos were then examined on a fluorescence microscope Zeiss Axioskop II MOT Plus (Carl Zeiss Ltd., Cambridge, UK) using a 40X objective and images captured for later analysis. BrdU positive nuclei were counted in at least 5 embryos per group (figure 2.7). The sampling strategy employed for image capture involved randomly selecting two fields from embryo body length. Images were downloaded to a computer for image analysis with ImageJ software. For each image collected, a region of interest of 10,000 μm^2 was used within the image to count BrdU positive nuclei (figure 2.7).

2.9.2 Staining of Cardiomyocyte nuclei

PhosphoHistone H3 (PHH3) staining was performed to observe mitosis while DAPI labelling was used to count the total number of ventricle positive nuclei in isolated hearts. Zebrafish cardiomyocytes are mononucleated, therefore each PHH3- or DAPI-positive nucleus was considered one cardiomyocyte.

cmlc2:EGFP/GATA1:dsRed crossed line was used to confirm that only cardiomyocyte nuclei (GFP positive) were counted and not red blood cell nuclei (dsRed positive). Hereafter, we refer to the total number of DAPI positive nuclei in isolated embryonic hearts as total ventricle cardiomyocytes number (TVCn) and PHH3 positive nuclei as proliferating ventricle cardiomyocytes number (PVCn). Samples were initially prepared by microdissecting and removing the hearts from embryos, as detailed in section 2.8.1.

2.9.2.1 PhosphoHistone H3 (PHH3) staining

Isolated hearts were washed in PBS-Tx and, to help antibody penetration within the

ventricle, were incubated in 10μg/mL Proteinase K for 10 mins at RT, then washed again in PBS-Tx. Hearts were fixed again in PFA 4% for 20 mins at RT, washed in PBS-Tx and blocked in BSA 5% diluted in PBS-Tx O.N. at 4°C. Heart ventricles were incubated in anti PhosphoHistone H3 (rabbit, 1:200 in PBS-Tx + BSA2%; Millipore, MA, USA) for 3h at RT, washed in PBS-Tx and incubated in Alexa Fluor anti-rabbit 1:500 (Life Technologies Ltd, Paisley, UK) for 2 h at RT. Samples were then washed three times in PBS, before mounting (see section 2.5.1).

2.9.2.2 DAPI

Isolated hearts were washed in PBS-Tx and incubated in DAPI (Sigma-Aldrich Ltd., Dorset, UK) 1:1000 (stock 1mg/mL) for 30 mins at RT, then washed 30 mins in PBS, before mounting (see section 2.5.1).

2.9.2.3 Counting Total and Mitotic Cardiomyocyte numbers

Cardiomyocytes were counted using ImageJ software; DAPI labeled nuclei in the whole ventricle (figure 2.8) were counted by marking them with a tag while moving progressively through the z-stack of images, thus ensuring individual nuclei are not counted twice. The same type of analysis was repeated for PHH3 positive nuclei in the whole ventricle, this will provide the PVCn. Intra- and inter-observer variation was assessed by Bland-Altman method for comparing paired measurements (see Statistic section 2.15).

2.9.3 Histopathology: Haematoxylin & Eosin staining

Haematoxylin & Eosin (H&E) staining was used to examine histological features of cells and organs (Sabaliauskas *et al.*, 2006). After fixation in 4% PFA for 3h at RT or ON at 4°C, specimens were dehydrated through an ascending ethanol series (from 25% - 100% in five steps) and embedded in paraffin in a transverse or sagittal orientation. Serial 5μm sections including the heart and some of up and downstream tissue were cut on a microtome and stained with H&E, according to standard protocols (Sabaliauskas *et al.*, 2006).

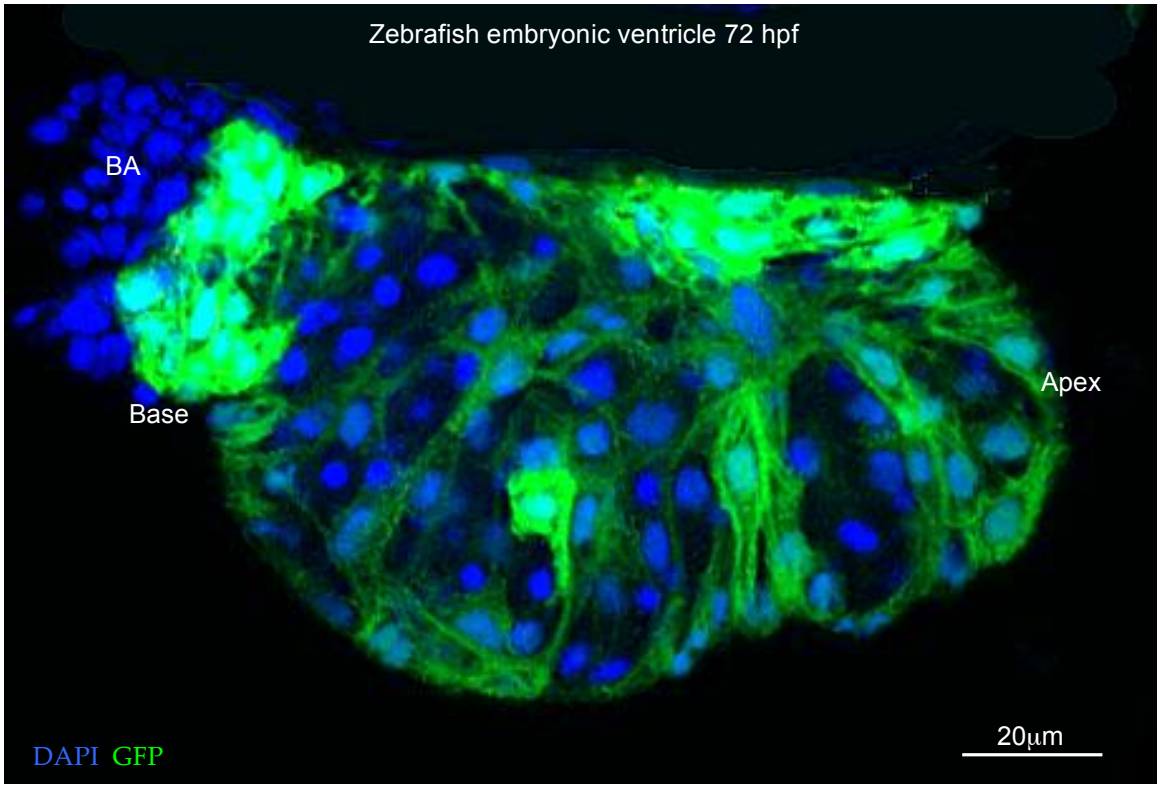

Figure 2.8 – Isolated zebrafish embryonic heart ventricle to assess cardiomyocyte number. Confocal imaging of a microdissected cmlc2:EGFP zebrafish heart ventricle at 72 hpf, stained with DAPI (blue). This dye labels all ventricular cells, however only DAPI positive nuclei overlapping GFP (green) signal were counting as cardiomyocyte nuclei. Cardiomyocytes were counted using ImageJ software and were counted by marking DAPI and GFP positive cells with a tag while moving progressively through the z-stack of images, thus ensuring individual nuclei are not counted twice. BA= bulbus arteriosus

H&E is a general histological stain for cell nuclei (haematoxylin, coloured blue) and other structures (cytoplasm, collagen and muscle fibers) stained with eosin and therefore coloured red. Sections were observed under compound microscope setting 20X or 40X objective and images were captured by a microscope linked standard colour camera.

A qualitative analysis of typical cytomorphological alterations of apoptotic cells (cell shrinkage, eosinophilic dense cytoplasm, pyknotic nuclei, karyorrhexis) was performed on zebrafish embryos by H&E stained tissue sections (see section 2.9.3), visible under light compound microscopy.

For H & E staining of zebrafish embryos at several developmental stages, see online reference source: http://zfatlas.psu.edu/progress.php

2.10 Apoptotis assessment

2.10.1 Whole-mount Terminal dUTP Nick End-Labeling (TUNEL) assay

The TUNEL method is used to assay the endonuclease cleavage products by enzymatically end-labeling the DNA strand breaks (Kressel and Groscurth, 1994; Ito and Otsuki, 1998). Apoptotic cell death in whole-mount zebrafish was detected according to a modification of the ApopTag rhodamine In Situ Apoptosis Detection kit (Chemicon, CA, USA) protocol. Embryos were fixed overnight in PFA 4% at 4°C. Embryos were washed in PBS and the pericardial sac was opened and the heart exposed to help penetration of chemicals and antibodies within the heart. Then, embryos were permeabilized with proteinase K (10μg/ml) followed by two further washes in PBS. They were then fixed again in PFA 4%, then placed in prechilled ethanol:acetic acid (2:1) at -20°C, washed 3 times in PBS-Tween 0.1% before incubation in equilibration buffer and further steps as recommended by the manufacturer (http://www.millipore.com). Images of TUNEL assay staining (figure 2.9 A) were quantified by counting positive staining puncta in the whole heart from Z-stack confocal images using ImageJ.

Zebrafish embryo 72 hpf

A

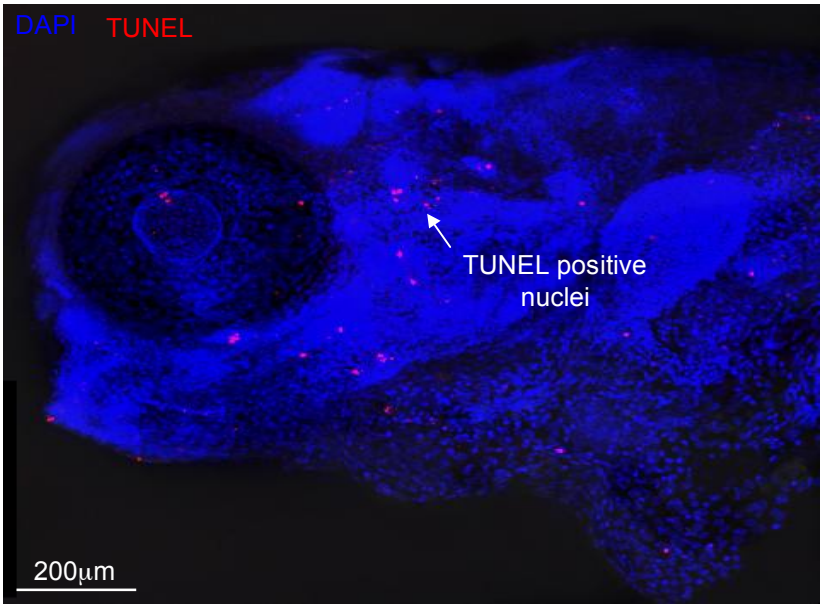

B

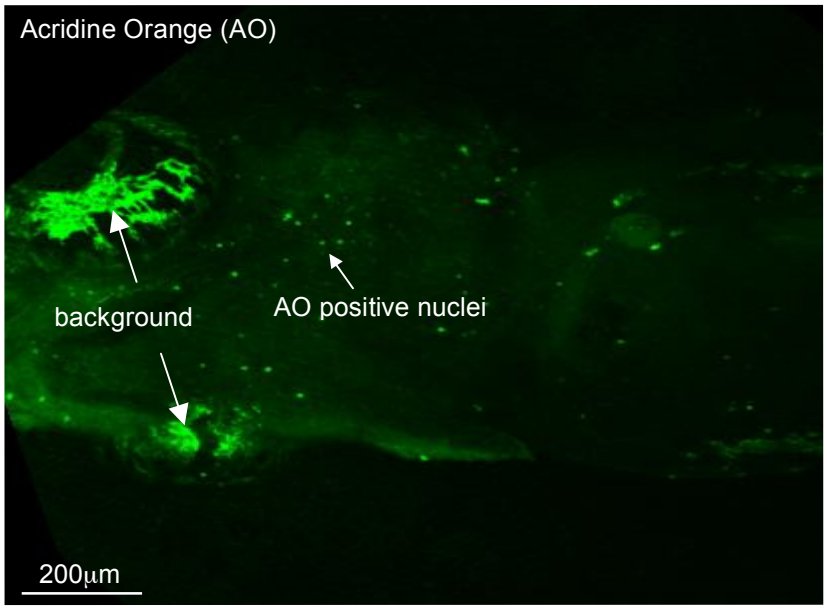

Figure 2.9 – Apoptosis assays in the zebrafish. Two methods were used to assess apoptosis in the whole-mount embryo. Image A shows Terminal dUTP Nick End-Labeling (TUNEL) staining in a Wik (wild type) zebrafish embryo 72hpf, counterstained with DAPI. Red spots represent TUNEL positive nuclei labelling apoptotic bodies. Image B shows Acridine Orange (AO) vital dye assay in the zebrafish embryo 72 hpf. Green puncta represent AO positive nuclei.

2.10.2 Acridine orange

One of the most commonly used techniques to assess apoptosis utilizes the vital dye Acridine Orange (AO) (Sigma-Aldrich Ltd., Dorset, UK), a nucleic acid intercalating dye that emits green fluorescence when bound to dsDNA and selectively stains apoptotic rather than necrotic cells (Abrams, 1993; Furutani, 1996), figure 2.9 B. AO stock solution is prepared at 1mg/ml in milliQ water and stored at -20C, and light protected. Dechorionated embryos were incubated in AO 2.5μg/ml in embryo medium for 30 mins followed by 3 times washes of 10 mins each with embryo medium. Tricaine 20μM was added to the medium to anesthetize embryos, according to section 2.4. Embryos were mounted on a chambered glass slide (Hawksley, Sussex, UK) in a drop of embryo medium and sealed with coverslip (see section 2.5.1). Slides were wrapped in aluminium foil to prevent bleaching.

Fluorescent or confocal microscope (GFP filter set: excitation 473, emission 520) were used to observe green fluorescence of AO in the whole embryo and the heart; each group includes ≥ 10 embryos for each experiment, AO labeled puncta were counted as apoptotic bodies (figure 2.9 B).

2.11 Protein analysis

2.11.1 Dechorionating & deyolking of embryos

Embryos were surgically removed from their chorions, when present at the time of the experiment, using fine forceps. Yolks of embryos below 72 hpf were removed by mechanical agitation, (see Section 2.9.2) while in older embryos, where yolk is more difficult to separate, this was detached surgically by forceps (Dumont #5).

Deyolked embryos were transferred into fresh, cooled PBS solution and rinsed twice. At this point, embryos can be processed before loading on a gel or frozen in liquid nitrogen and stored at -70°C, after transferring to an eppendorf tube 1.5mL and removing as much liquid as possible.

2.11.2 Samples Protein Extraction

Samples in a 1.5mL eppendorf tube were microfuged for 1-2 minutes and supernatant was removed. About 100-150 μL RIPA Lysis Buffer (Millipore, MA, USA), previously diluted in deionized water from a stock 10X, were added and homogenized with a microfuge pestle for 30 s and then sonicated for 30 s at 5-8 μW, until embryo sample is no longer visible. Samples were kept in ice for 30 mins, then were briefly vortexed and then microfuged 1-2 mins at full speed (13,000 rpm). Supernatant was collected and then placed in a new 1.5mL tube and pellet was discarded. Samples were stored at -20°C.

2.11.3 Bradford Protein Assay

The protein concentrations of zebrafish embryos homogenates were determined colorimetrically using a Bio-Rad protein assay kit (Bio-Rad, Hemel Hempstead, UK) and the Bradford method of detection (Bradford, 1976). Protein concentration was measured before loading on a gel. Protein assay dye reagent was diluted in deionized water (1:5, freshly prepared) as well as a series of bovine serum albumin protein standards (concentration range 0.125 – 2 mg/ml, stored at 4°C) prepared in deionized water. Water was used as the Blank sample. The assay was performed in triplicate by adding Bio-Rad diluted dye (200 μl) to the protein sample and protein standards (5 μl each). The dilutions of unknown proteins were prepared on the basis of an initial assessment of the colour change upon mixing the protein and the diluted dye. The assay was performed at RT. The plate was shaken to mix and allowed to stand for 15 mins. UV absorbance was measured (595 nm) on a UV/visible spectrophotometer (Shimadzu, Milton Keynes, UK) and protein concentrations of samples were calculated (expressed as mg/ml) from the standard curve, allowing for the dilution factor.

2.11.4 Preparation of gel samples

Samples were taken out from -20°C and thawed on ice. An appropriate amount of protein sample containing 20μg of total protein was taken in a fresh eppendorf tube

and immediately added with 4µl of 4X laemmli buffer (for 1X, 2% SDS, 50mM Tris, 0.01% bromophenol blue, 10% glycerol) and deionised water to make a final volume of 16µl. Samples were mixed and heated at 95°C for 5 mins.

2.11.5 Gel electrophoresis

Samples were separated by electrophoresis on a NuPAGE® Novex® 4-12% Bis-Tris Gel 1.0 mm thick (Life Technologies Ltd, Paisley, UK). The gel, stored at 4°C, was fitted with gel tank (Bio-Rad Laboratories, Hercules, CA, USA) and immersed in NuPAGE® MOPS SDS Running Buffer 20X (Life Technologies Ltd, Paisley, UK), previously diluted in deionised water. The gel comb was removed and the wells were flushed out thoroughly with buffer. The wells were loaded with the samples by using gel loader tips (Eppendorf, UK). A 5µl of Novex® Sharp Pre-stained Protein Standard (Life Technologies Ltd, Paisley, UK) was also loaded in the two outer wells to identify the molecular weight of bands. Gels were run at a voltage 100 V for 30 mins and then at 150 V for another 60 mins.

2.11.6 Gel transfer

Gels were transferred to nitrocellulose membranes Protran (Sigma-Aldrich Ltd., Dorset, UK) using the Electrophoretic Transfer Cell (Biorad Laboratories, Hercules, CA, USA). A gel sandwich was prepared within the cassette consisting of fiber pad, blotting paper (both from Bio-Rad Laboratories, Hercules, CA, USA), gel, nitrocellulose membrane, filter paper and fiber pad. The gel sandwich cassette was placed within the transfer module and tank, which was then filled with Towbin transfer buffer (TRIS 0.025 M, Glycine 0.192 M, pH 8.6 ± 0.1). The transfer was run at 100 V and 300 mA for about 3 h at 4 °C. Nitrocellulose was then stained in Red Ponceau (Sigma-Aldrich Ltd., Dorset, UK) for 5 mins and then washed in water to check the presence of protein, while the remaining gel was stained in Comassie Blue R-250 0.5% (Bio-Rad Laboratories, Hercules, CA, USA) for 1 h followed by several wash in decoloration solution to assess that a good transfer occurred.

2.11.7 Immunoblotting

After transfer, nitrocellulose membrane was blocked with 20 ml of 5% dried skimmed milk (Marvel Premier Brands Ltd., Lincolnshire, UK) in TBS Tween (20mM Tris-Cl [0.2 M Tris-Cl, pH 7.6], 137mM Sodium Chloride, 0.1% Tween 20 [Polyoxyethylenesorbitan monolaurate, BDH, Poole, UK]) on a platform shaker for 1 hour at RT. Then the membrane was washed 3 times (5 mins each) with PBS-Tween 0,1% and then incubated in primary antibody at a concentration according to antibody manufacturer (usually 1:500 - 1:1000) in Bovine Serum Albumin (Sigma-Aldrich Ltd., Dorset, UK) 3% overnight at 4°C. The membrane was washed 3 times inn PBS-Tween 0,1% prior to incubation with a secondary antibody, linked to the horse radish peroxydase, at a concentration of 1:10000 in dried skimmed milk 5% for 1 hour. A final series of washes was performed as above, before the blot was developed.

2.11.8 Chemiluminescent detection

Nitrocellulose membrane was exposed for 1 min to the Enhanced Chemiluminescence solution (ECL; Amersham, UK) following the manufacturer's instructions. Excess ECL substrate from the membrane was removed by touching the edge of the membrane to a piece of tissue paper. Then the membrane was placed down on a film layer, previously disposed inside a film cassette. The bubbles were carefully removed from the membrane that was then covered with another film layer, fixed on the cassette with tape and exposed to a photographic film (BioMax XAR Film Kodak, Sigma-Aldrich Ltd., Dorset, UK) for an adequate exposure time. The film was developed and immunoreactivity (band density) was quantified by densitometry (online source: http://rsbweb.nih.gov/ij/docs/user-guide.pdf) using ImageJ.

2.12 Gene expression analysis

2.12.1 RNA extraction from whole zebrafish embryos

RNA extraction and reverse transcription were performed by using Qiagen RNeasy mini kit (Qiagen, West Sussex, UK). Embryos were placed in an eppendorf tube 1.5mL, euthanised with tricaine overdose (see section 2.4) and stored in RNAlater (Life Technologies Ltd, Paisley, UK) or, for immediate RNA extraction, placed directly in buffer RLT 600µL. Each eppendorf tube was added with two small metallic bead, previously autoclaved and wiped with RNase Zap (Life Technologies Ltd, Paisley, UK). Efficient disruption and homogenization was performed by milling for 45 s at 30 Hz (Mixer Mill 301 model, Retsch, Haan, Germany), taking care to keep the embryos homogenate cold at all times. Beads were removed and the samples were centrifuged at 13,000g, 3 mins, 4°C. The supernatant was placed in a new 2 mL eppendorf tube and the pellet discarded. Supernatant was added with an equal volume of 70% ethanol, mixed and placed in the RNeasy spin column subjected to centrifugation (12,000g, 30 s, 4°C). The eluate was discarded.

DNase treatment step followed to eliminate genomic DNA contamination. After wash with Buffer RW1 (350µl) and centrifugation for 15 s, 10 µl DNase I stock solution, previously diluted in 70 µl Buffer RDD, were added to the spin column and incubated 15 mins at RT. The column was then washed with Buffer RW1 (700µl) and Buffer RPE (500 µL). In each case, the eluate was discarded following centrifugation (12,000g, 15 s, 4ºC). Buffer RPE (500µl) was added to wash the membrane, followed by a further centrifugation step (12,000g, 2 mins, 4ºC). The spin column was then placed in a fresh 2 mL collecting tube and subjected to centrifugation (16,000g, 1 min, 4ºC) to eliminate any Buffer RPE carryover.

The spin column was then placed in a fresh 1.5 mL eppendorf, RNase-free water (30 µl) added and RNA eluted by centrifugation (12,000g, 1 min, 4°C). Eluted RNA was stored at -80°C.

2.12.2 RNA extraction from zebrafish embryonic hearts

For each sample, 300-500 hearts were extracted by Mechanical-agitation method (Section 2.8.2) from embryos previously prepared as in Section 2.11.1. RNA was isolated as described in Section 2.12.1.

2.12.3 Assessment of total RNA quantification and purity

RNA was quantified using a Nanodrop Spectrophotometer (Thermo Fisher, West Sussex, UK) in 1 μl of RNA sample. Concentration was determined by the absorbance at 260nm wavelength (A260), and the purity assessed by the ratio of RNA/DNA (A260/A280), which was deemed acceptable if between 1.9 and 2.1, and 260/230 (some contaminants, e.g. phenol, absorb at 230nm) > 2.2.

2.12.4 Assessment of total RNA quality

Quality of RNA was assessed by electrophoresis on agarose (Lonza, Berkshire, UK) gel (1% w/v in 0.5x TBE). Samples (2μl) were prepared by adding loading dye (Promega, WI, USA;) 1 in 5 diluted in distilled water. Sample were incubated at 85°C for 3 min to denature RNA before running on the gel (100V, 1hr) with a size marker (New England Biolabs, MA, USA). RNA integrity was assessed on basis of 18S and 28S ribosomal RNA (rRNA) bands. RNA integrity was deemed satisfactory if clear 28S and 18S rRNA bands were present without smearing, and if 28S rRNA band was approximately twice as intense as 18S rRNA band.

2.12.5 Reverse transcription

RNA was reverse transcribed in cDNA by using high capacity cDNA reverse transcription kit (Applied Biosystems, Warrington, UK).

For each sample, a volume containing 2 μg of RNA was pipetted in a 0.2mL microfuge, added with nuclease free water up to 10 μl and then another 10 μl of 2× RT master mix [Buffer 2 μl, dNTP Mix (100mM) 0.8 μl, Random Primers 2 μl, Multiscribe Reverse Transcriptase 1.0 μl, nuclease free water 4.2 μl] was added. Two

negative controls were prepared as above, one with water instead of RNA to identify any RNA contamination in reagents, the second without the reverse transcriptase enzyme in order to detect the presence of contamination by genomic DNA. Samples were incubated (25°C, 10 min; 37°C, 120min; 85°C, 5 min; 4°C, ∞) in a PCR machine, before being chilled to 4°C. The resultant cDNA was stored at -20°C.

2.12.6 Quantitative Real Time PCR (Q-PCR)

2.12.6.1 Introduction

Real-time or quantitative PCR (Q-PCR) permits quantification of starting amounts of DNA and cDNA templates and is based on the detection of fluorescent reporter molecule. The fluorescence arisen from these molecules is monitored throughout the Q-PCR process and increases as PCR product accumulates with each cycle of amplification. The Q-PCR technique employs two main chemistries: the DNA-binding dye SYBR Green I and TaqMan hydrolysis probes.

SYBR Green is a fluorescent DNA intercalating dye that binds all double–stranded DNA. The advantages of using this method are the simple assay design as only two primers are needed, ability to test multiple genes quickly without designing multiple probes, lower initial cost (probes cost more), and the ability to perform a melt-curve analysis to check the specificity of the amplification reaction.

Compared to the SYBR Green method, the probe based Q-PCR only detects the desired PCR product resulting in intrinsically increased specificity and sensitivity. Although fluorescent probes are quite expensive, they offer some advantages over DNA-binding dyes. One is their specificity for the target sequence, therefore non specific products are not measured. For this reason, this assay do not include melt curves analysis. Hydrolysis probe-based assay is the method adopted in our lab and was performed by Ms Kathryn Wilson.

2.12.6.2 Probe-based Q-PCR

Primers were designed to match probes within the Roche Universal Probe Library (https://www.roche-applied-science.com). Primers were diluted in TE buffer to give

a stock concentration of 100 μM. Any newly designed assay was validated by doing a standard curve. A good standard curve has a slope close to -3.3, low error, efficiency 1.7 – 2.1. For standard curve, with 9 data points, an aliquot of neat (undiluted) cDNA from all samples was mixed, and then diluted in the proportions 1/4, 1/8, 1/16, 1/32, 1/64, 1/128, 1/256, 1/512, 1/1024 and run in triplicate. Experimental cDNA samples were diluted 1/40 in RNase free water and, again, run in triplicate; by diluting 1/40 they should sit in the middle of the standard curve.

Diluted cDNA samples (2μl) or standard curve points were added to each well (of a 384 well plate), followed by Master Mix (8μl), consisting of the following components: Roche Master mix 5μl, Primer (forward and reverse) 0.1μl of each, Probe 0.1μl, Roche water 2.6μl. The plate was spun for 3 mins at 3,000rpm on a plate spinner and then placed in the Light Cycler 480.

Samples were heated for initial denaturation (95ºC, 5min), then underwent 50 cycles of PCR amplification, which consisted of denaturation (95ºC, 10 sec), annealing (60ºC, 30 sec) and elongation (72ºC, 1 sec). Upon completion of the PCR programme, samples were cooled (40ºC, 30 sec). For all the samples, amplification curves were plotted (y axis fluorescence, x axis cycle number). Triplicates were deemed acceptable if the standard deviation of crossing point (Cp) < 0.5 cycles. Relative quantitation was calculated using the delta CT method using Light Cycler software.

2.12.6.3 Normalisation of Q-PCR data

To enable quantitation of gene expression according to the amount of cDNA loaded, the data obtained from the Q-PCR were normalised according to housekeeping genes. These are generally constitutive genes which levels of expression are relatively constant in physiological conditions (Greer *et al*., 2010).

There are several housekeeping genes that are potentially employable and the choice depends on the type of experiment. In the zebrafish, authors have reported in different papers that elongation factor 1 alpha (ef1α) (McCurley and Callard, 2008), β-actin (Casadei *et al*., 2011) and 18S (Tang *et al*., 2007) are some of the most stable housekeeping genes during normal zebrafish development and in different

experimental conditions. I assessed the expression of these housekeeping genes between 24 and 120 hpf at 24 hours interval. In this experiments both ef1α (figure 2.10 A & B), in the whole embryo and in the zebrafish heart, and 18S (figure 2.10 C) in the whole embryo remained stable with no significant changes across 120 hours. In Chapter 3 all Q-PCR data are normalised to ef1α.

Housekeeping genes may vary depending on experimental conditions (Greer *et al.*, 2010). In our case, Ef1α varied following treatment with morpholino or flavopiridol (figure 2.11 A). For this reason we could not use this gene to normalize these data. Instead, β-actin was selected as this gene did not vary significantly in these experimental conditions (figure 2.11 B-C).

Data were shown graphically as fold change in gene expression compared to the housekeeping gene selected.

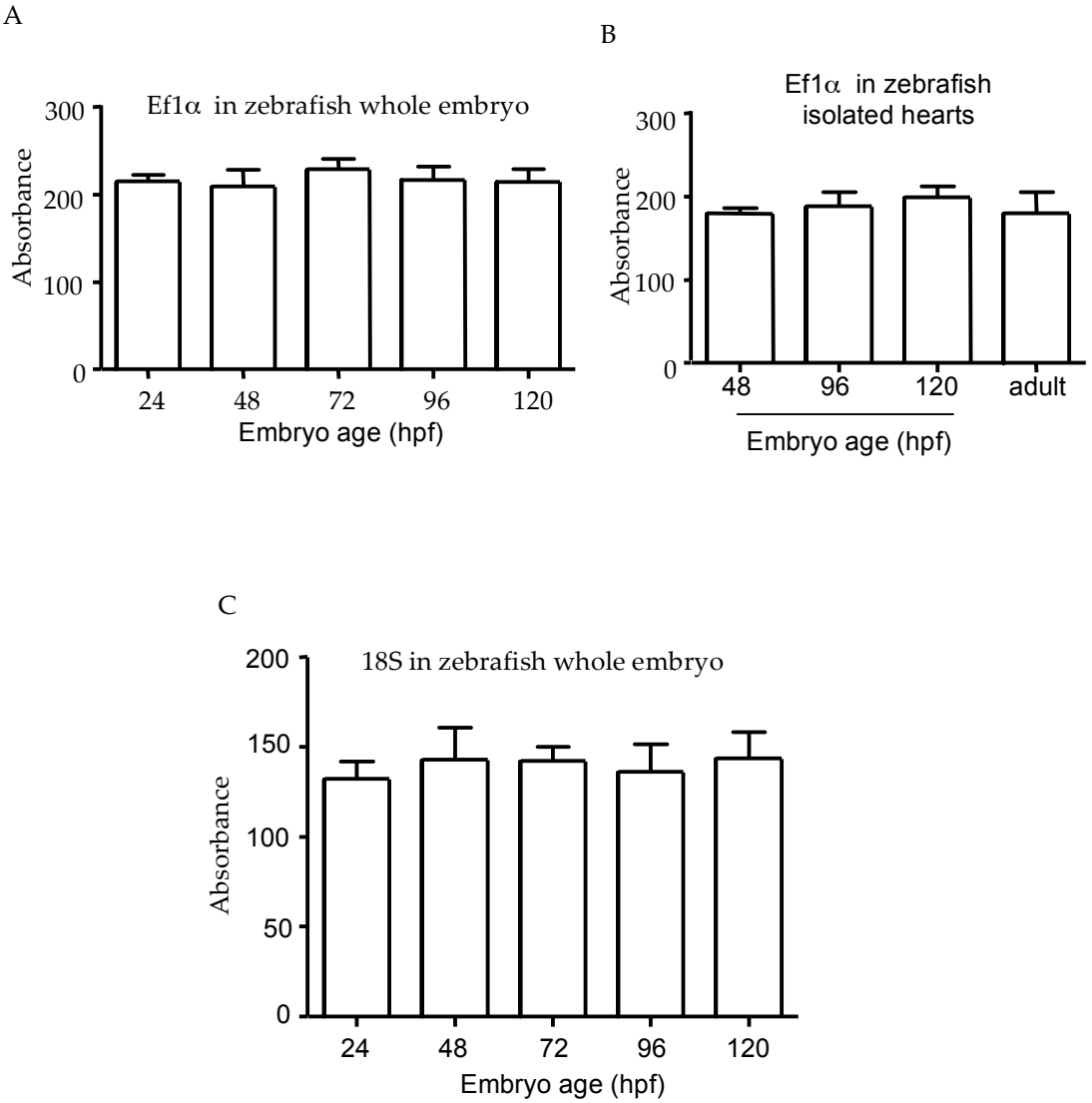

Figure 2.10 – Gene expression pattern of the Ef1α and 18S housekeeping genes during normal development in the zebrafish embryo. The Ef1α mRNA level, assessed (A**)** at 24, 48, 72, 96 and 120 hpf in the whole embryos and (B**)** at 48, 96, 120 hpf in isolated hearts and adult heart and was found to be stable. Ef1α was used to normalize mRNA level of genes of interest in time-course analysis. 18S mRNA level was also assessed (C**)** in the whole embryos and was found to be stable. Data were compared by one-way ANOVA, followed by Bonferroni's multiple comparison test. Each time-course was studied in 1 clutch of eggs, at least 10 embryos from the clutch were used to generate each time point. The data represents an average from studies in 3 clutches of eggs.

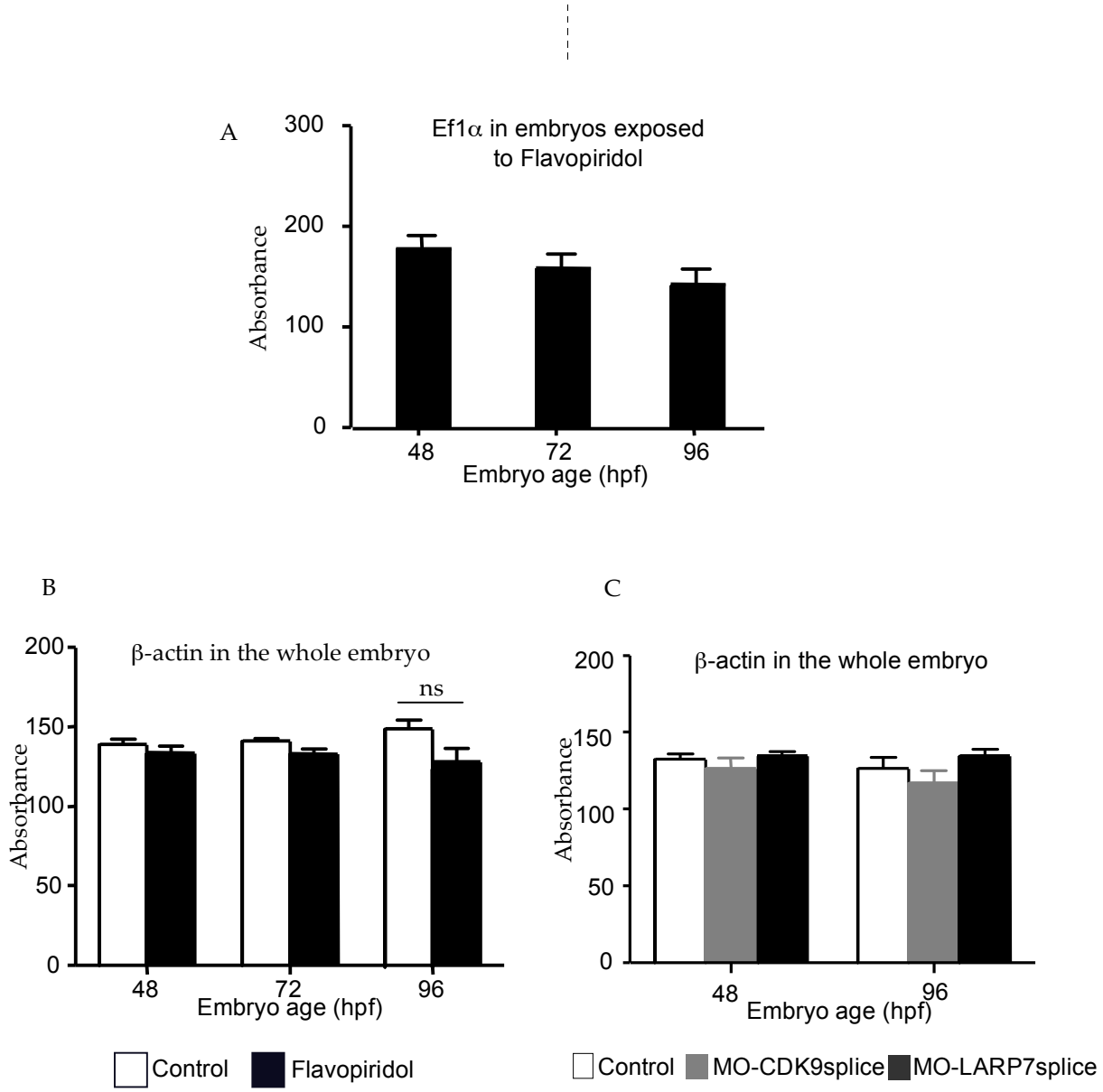

Figure 2.11 – Expression pattern of Ef1α and β-actin housekeeping genes in the zebrafish embryo following treatments. A**.** Ef1α was affected by flavopiridol during development at 48, 72 and 96 hpf, therefore it was not used to normalise Q-PCR data following flavopiridol and morpholino treatments. B-C. β-actin was not affected in the same conditions, therefore it was used to normalize mRNA level in experiments requiring exposure to flavopiridol **(**B), measured at 48, 72 and 96 hpf, or injection of morpholino (C)**,** measured at 48 and 96 hpf. Data were compared by two-way ANOVA followed by Bonferroni's multiple comparison test. Each time-course was studied in 1 clutch of eggs, at least 10 embryos from the clutch were used to generate each time point. The data represents an average from studies in 3 clutches of eggs. ns= non significant difference

2.13 Genetic knockdown by Morpholino oligonucleotides

2.13.1. Preparation of microinjection needles

The micropipettes used in the microinjection were freshly prepared and generated by pulling glass capillaries (GC100TF-10, Harvard Apparatus Ltd., Kent, UK) with the micropipette puller (PC-10 puller, NARISHIGE, Cambridge, UK), see manufacturer's instruction for full details. Pulling and clip temperature were 69°C and 75.9°C respectively. Before injection, the needle tips were carefully prepared to have a final tip of about 10 μm by using a surgical forcep (Dumont 5).

2.13.2 Morpholino design

Antisense morpholino (MO) to knockdown CDK9 and LARP7 expression in the zebrafish were designed with the help of the company Gene Tools (Oregon, USA; www.gene-tools.com) that synthetised all MOs.

I submitted to Gene Tools the target mRNA sequences for design and they suggested the best option. The translation blocking MO was designed to be complementary to sequence between the 5′ cap and about 25 bases 3′ of the AUG translation start site and inhibits progression of the initiation complex. The splice blocking MO targeted to the splice junction between exon 2 and intron 2 of the target pre-RNA, for both CDK9 and LARP7. A mismatch controls for the splice site morpholino was designed to serve as negative controls. All MOs were 3′-end labeled with Lissamine fluorochromes, a red fluorescent tag to monitor the distribution of MOs within the embryos. The MOs sequences used are listed in chapter 4.

2.13.3. Morpholino stock solution

Lyophilized morpholino, as it was delivered, was dissolved in deionized water to a stock concentration of 1 mM. Aliquotes of 10μL were prepared in 0.5mL eppendorf tube and stored at -20°C. Working concentration, specific for each morpholino, were

prepared by diluting in Danieau buffer (58mM NaCl, 0.7mM KCl, 0.4mM MgSO4, 0.6 mM Ca(NO3)2, 5.0 mM HEPES, pH 7.6).

2.13.4 Morpholino injection procedure

2.13.4.1 Calibration

The microinjection of fertilised eggs was performed at the 1-4 cell developmental stages using a Narishige IM300 Microinjector, to maximise morpholino penetration in all cells. Normally, an approximate injection pressure of 20 psi and a pulse duration of 3 millisecond were used. During the calibration procedure, a bolus of morpholino of about 0.1 mm of diameter was injected under the Leica Fluo MZ16 fluorescence microscope (Leica Microsystems Ltd., Buck, UK) into a drop of mineral oil previously placed on a 1 mm graticule with 0.01 mm divisions (figure 2.12 A). The amount of morpholino was calculated by the radius of the bolus and according to the formula of a sphere ($4/3 \bullet \pi \bullet r^3$). The same bolus, normally 0.5 nL, was injected into the yolk sac of each egg. The same micropipette used for the calibration and pressure settings was also used to inject eggs. Each new micropipette, either a broken replacement needle or change of injection solution, used required calibration.

2.13.4.2 Morpholino injection

A normal glass slide was placed in a 90 mm Petri dish, eggs were placed into the dish and, by using a plastic tip, positioned on a slide side. In order to reduce egg movements, excess of water was absorbed on a piece of tissue. Morpholino was injected into the egg just below the cell mass and into the area of cytoplasmic streaming so that the MO was carried up into the cell (figure 2.12 B-C). To increase the amount of morpholino injected, multiple boluses of morpholino were injected. As both the stock concentration and the molecular weight of the morpholino were known the final concentration of morpholino injected could be accurately determined.

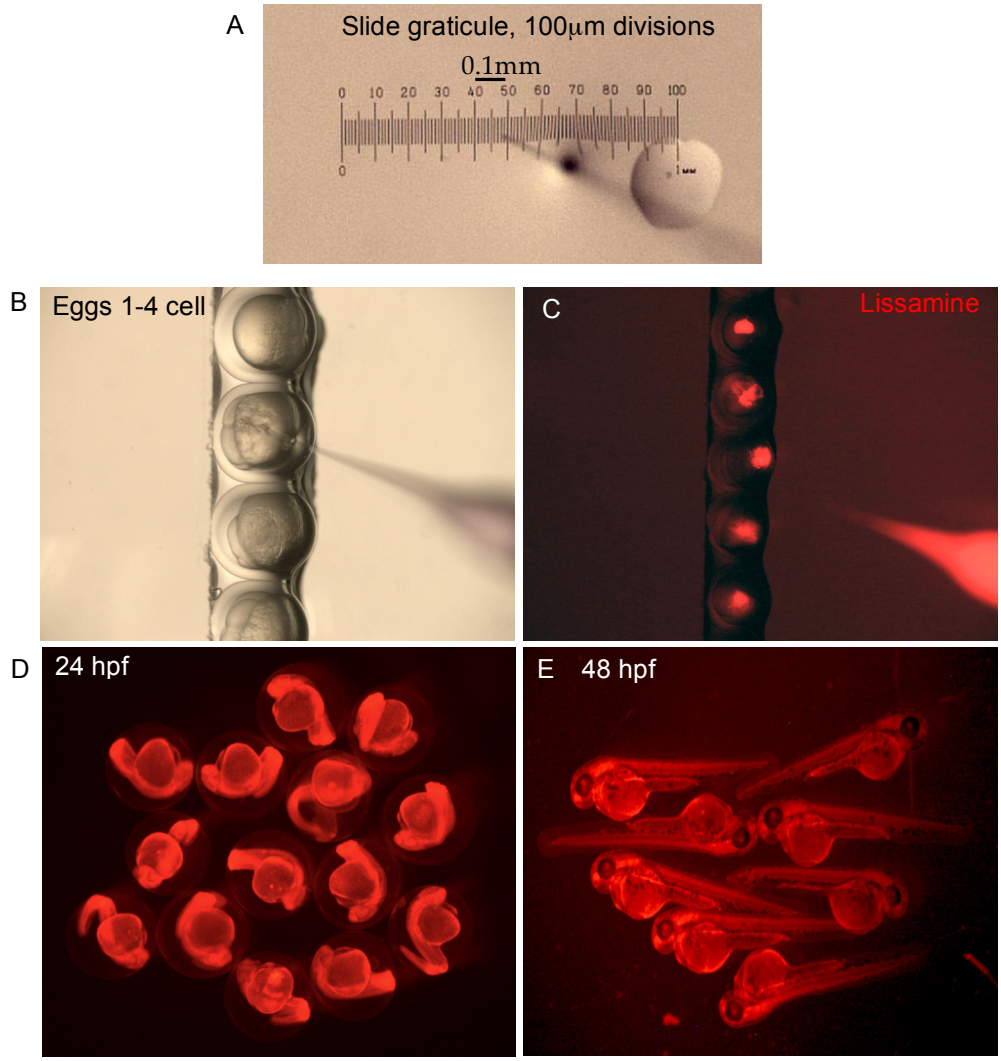

Figure 2.12 - Morpholino injection procedure. A. The amount of morpholino to inject into the eggs was previously calibrated on a slide graticule of 1mm, with 0.01mm divisions. B. Eggs at 1-4 cell stage were carefully placed in a 90mm Petri dish, at the flank of a glass slide and a bolus of 5 nL was injected in each egg. C. Successful injection was assessed under fluorescence microscope by the morpholino red tag lissamine. D-E Images of embryos captured at 24 and 48 hpf show the large diffusion of the morpholino in the whole body.

Embryos were screened at approximately 3 hours post injection to determine injection success and distribution of the morpholino within the embryo. Died or damaged embryos caused by the microinjection procedure were removed by 6 hpf. The diffusion of morpholino within the embryo 24-48 hpf is shown in figure 2.12 D-E).

2.13.5 Defining the whole-embryo and cardiac phenotype

Following flavopiridol exposure, embryo standard body length was measured as the distance from the snout to the caudal peduncle. This value is distinct from total body length, which is measured to the distal tip of the caudal fin. Total body length can be confounded by fin damage and is not recommended for staging purposes. Standard body length correlates well with all other measures of size (Parichy *et al.*, 2009) and is associated with overall embryonic development.

Following morpholino injection, zebrafish embryos survival and phenotype were examined every day from 1 up to 5 days post fertilisation (dpf). Whole embryo and cardiac phenotype were described on the basis of morphologic and functional characteristics. Embryo phenotype was based on the following parameters: Head size (Normal, smaller) and Body axis (normal (0-5%), curved (5-50%), curved (>50%)). Cardiac phenotype was based on the following parameters: Tail blood flow (normal, reduced, absent), Pericardial oedema (normal, mild, serious), Heart shape (normal, tubular, string), Heart rate, (normal (140-200bpm), low (60-140bpm), very low (0-60bpm)). All these experiments were performed by myself and each embryo was arbitrarily included in one of the above categories. At least 4 different experiments were performed. The percentage of embryos in each category above was calculated.

2.14 Preparation and optimization of pharmacological agents

2.14.1 Aphidicolin

Aphidicolin (Sigma) blocks cell proliferation by specifically inhibiting DNA Polymerase α (Sheaff *et al.*, 1991). In this study, aphidicolin was used to demonstrate the cardiac recovery following laser injury via proliferation of new cardiomyocytes (see Chapter 5). Preliminary optimization studies were performed (figure 2.13 and 2.14). All solutions of this drug were prepared from a stock solution of 15mM stored at -20°C.

In pilot experiments, the effects of aphidicolin were assessed across a range of concentrations (15μM - 150μM) dissolved in a range of concentrations of DMSO (1-4%). Long-term exposure to the drug was commenced at 24 hpf and up to 120 hpf. Embryo survival and gross phenotype (n=30 per group) were evaluated from 6 to 96 hour post-treatment. To assess DNA replication, BrdU staining on embryos (n=5 per group, see section 2.9.1) after 6, 24 and 48 hours of exposure was performed (figure 2.13 and 2.14). The optimal concentration of DMSO assessed in our pilot study was 1% (see figure 2.13) while the optimal concentration of drug appearing to inhibit cell cycle while ensuring optimal survival was found to be 30μM in DMSO 1%. Following 6h exposure to aphidicolin 30μM in DMSO 1%, embryo shape and survival did not show a difference when compared to controls, while BrdU labelling showed a 5% reduction of BrdU-positive nuclei (see figure 2.13 and 2.14). The 30μM aphidicolin, at 24h post-treatment, resulted in 20% embryos with a curly body, 99% survival and a reduction of 50% in BrdU-positive nuclei in the tail compared to controls. At 48h post-treatment, 25% embryos showed curly bodies, 96% survival, while BrdU analysis showed 73% reduction in the number of BrdU-positive nuclei.

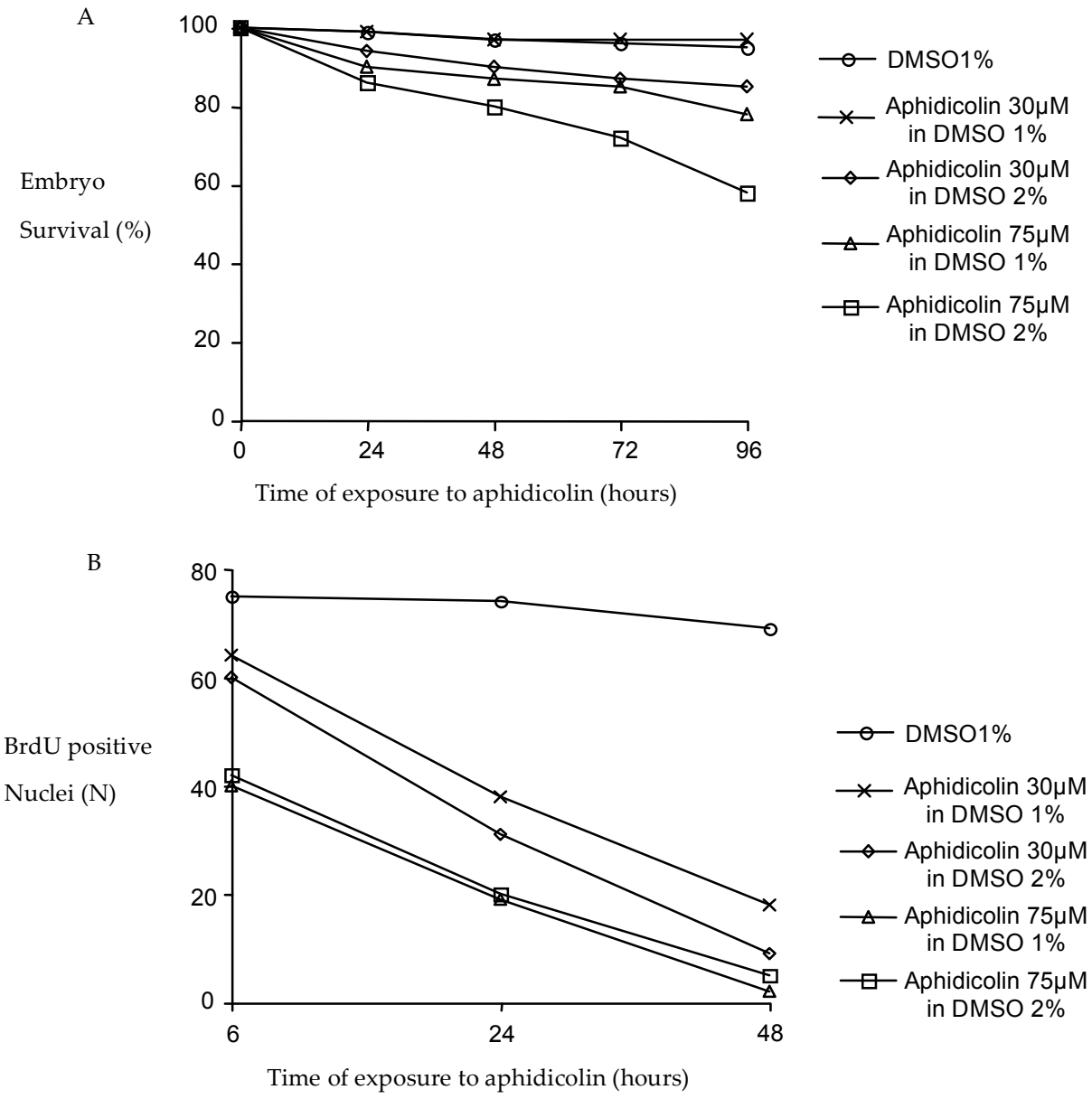

Figure 2.13 - Optimization of the pharmacological agent Aphidicolin. A. Curve of embryo survival following exposure to aphidicolin. Zebrafish embryos at 24hpf were exposed to several concentration of aphidicolin (here are shown 30 and 75 µM in DMSO 1 or 2%), surviving embryos were counted every 24 hours until 120hpf. B. Curve of cell proliferation, measured as BrdU positive nuclei, in zebrafish embryos following exposure to different dose of aphidicolin and DMSO, and assessed at 6, 24 and 48 hours after starting exposure to the drug.

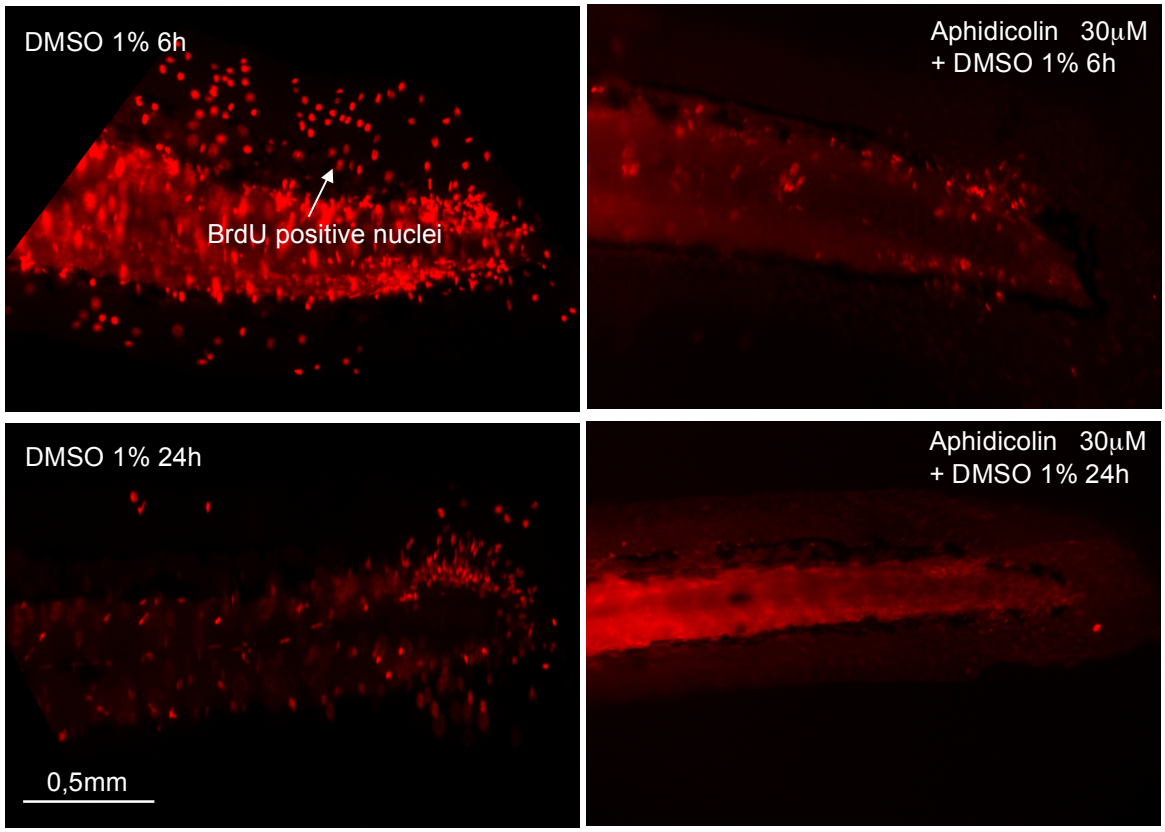

Figure 2.14 – Cell cycle inhibition by Aphidicolin 30 μM in the zebrafish embryo. Four representative fluorescent images of the zebrafish embryo tail exposed to Aphidicolin 30 μM, the concentration adopted in this thesis, at 6 and 24 after exposure to the drug, showing BrdU positive nuclei (red puncta). In order to select a suitable concentration of drug to use, embryos were previously exposed to different doses of Aphidicolin, in the range 15-150μM, and DMSO to favour the drug penetration. At 6, 24 and 48 hours after exposure to the drug, BrdU immunostaining was performed in the whole embryo to assess the effect of the Aphidicolin on cell proliferation.

2.14.2 Flavopiridol

Flavopiridol is a broad specificity CDK inhibitor with a distinct preference for CDK9 (Chao *et al.*, 2000). Flavopiridol (Sigma) was diluted in DMSO (Sigma), carrier solvent, at a stock concentration of 1mM. Bai et al., (Bai *et al.*, 2010) reported that at a concentration of 35μM in the bathing medium of zebrafish embryos for acute exposure, flavopiridol inhibits P-TEFb, while Seng et al. (Seng *et al.*, 2004) used 3μM to inhibit angiogenesis.

However, Flavopiridol at a concentration of 35μM was considered too high for long-term exposure, according to the purpose of this study that was to investigate the role of CDK9 either during normal development or following laser injury at 72hpf. Therefore, a dose ranging study was performed using flavopiridol at concentrations of 1μM - 5μM over 24-48 hours in embryos at 48-120 hpf (n=30 per group), figure 2.15. Initially, exposure to the Flavopiridol was started just after fertilization but this caused the death of 100% embryos 24 hpf. Therefore, the starting point was set at 24 hpf. Embryo survival, gross body and gross cardiac morphology were evaluated from 24 to 96 hours post treatment (*i.e.* from 48 to 120hpf) at several time points. Unlike aphidicolin study, no DMSO carrier was used because the exposure to the drug caused clear effects on the embryo survival and phenotype. Only phenotype data at 96 hour post treatment were recorded. The group exposed to flavopiridol 1μM showed 97% survival (figure 2.15), 9% of embryos showed curved body, 6% of embryos showed pericardial edema. Embryos exposed to Flavopiridol 3μM showed 88% survival, 28% curved body and 20% pericardial edema. Embryos exposed to flavopiridol 5μM reported 42% embryos survival, 80% of curved body and 68% pericardial edema. On the basis of these results, flavopiridol 3μM was adopted thereafter in these studies.

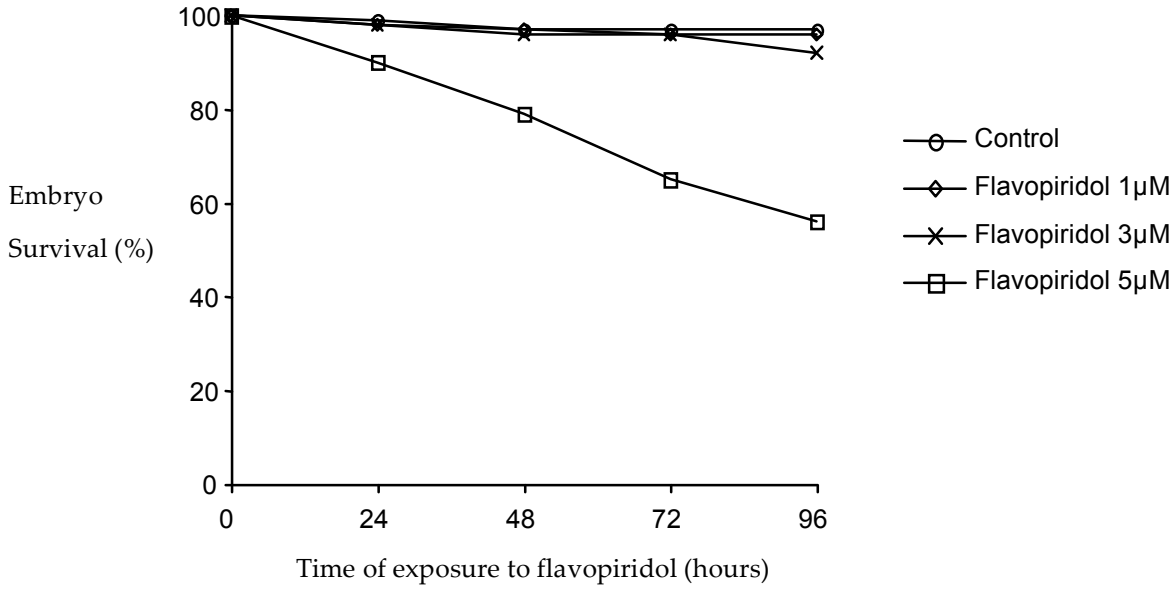

Figure 2.15 - Curve of embryo survival following exposure to flavopiridol. For the optimization of this pharmacological agent, different groups of zebrafish embryos were continuously exposed, from 24hpf up to 120 hpf, to a dose of flavopiridol 1, 3 or 5µM. Surviving embryos were counted every 24 hours until 120hpf. No DMSO carrier was used.

2.15 Data handling and Statistical Analysis

Data were presented as means ± standard error of the mean (SEM) and were graphed and analysed using GraphPad Prism (version 4.00) (GraphPad Software, San Diego, California, USA). D'Agostino and Pearson test was used to assess if values were sampled from a Gaussian distribution. This was the case in all our data, therefore parametric tests were used. For each data reported in this thesis, at least 3 experiments were performed, reported as 'n' in each graph unless stated, with embryos derived from different clutch of eggs. The number of embryos per experiment depends on the type of analysis and on the developmental stage considered: ≥5 embryos for cardiomyocyte counts, cardiovascular function or protein analysis, ≥10 for gene expression analysis. A P=0.05 the difference between means was considered to be statistically significant. Depending on the number of variables measured in each experiment, a one-way or a two-way ANOVA (Analysis of Variance) test were employed to compare means within and between groups. A repeated measures one- or two-way ANOVA was used when the same embryos were used at different time-points, for example to assess cardiovascular function. Bonferroni post-hoc test was used for comparing every pair of means. The Student's t-test was used when only two groups were included in the experiment, for example in Chapter 5 for comparison of the effect of the two laser systems used.

An assessment of intra and inter-observer variation of cardiomyocyte number was undertaken in a series of normal isolated cmcl2:EGFP hearts stained with DAPI. Intra-observer variation, my own variation, was done by repeating the cardiomyocyte count on two separate occasions with no knowledge of the measurement from the first round (figure 2.16). Inter-observer variation was done by comparing my measurement of cardiomyocyte number with that obtained by a colleague in the laboratory (KW). Assessment of inter and intra-observer variation in measurement of ejection fraction (figure 2.17) was undertaken in the same fashion. Data were analysed using a standard approach and presented as Bland-Altman (Bland and Altman, 1986) plots (figure 2.16 and 2.17). These analyses demonstrated that for the intra-observer variation the average of differences among

the two analysis was 3.2 for CMn and – 0,2 for ejection fraction, while for the inter-observer variation the average of differences among the two analysis was 1,75 for CMn and – 0,7 for ejection fraction.

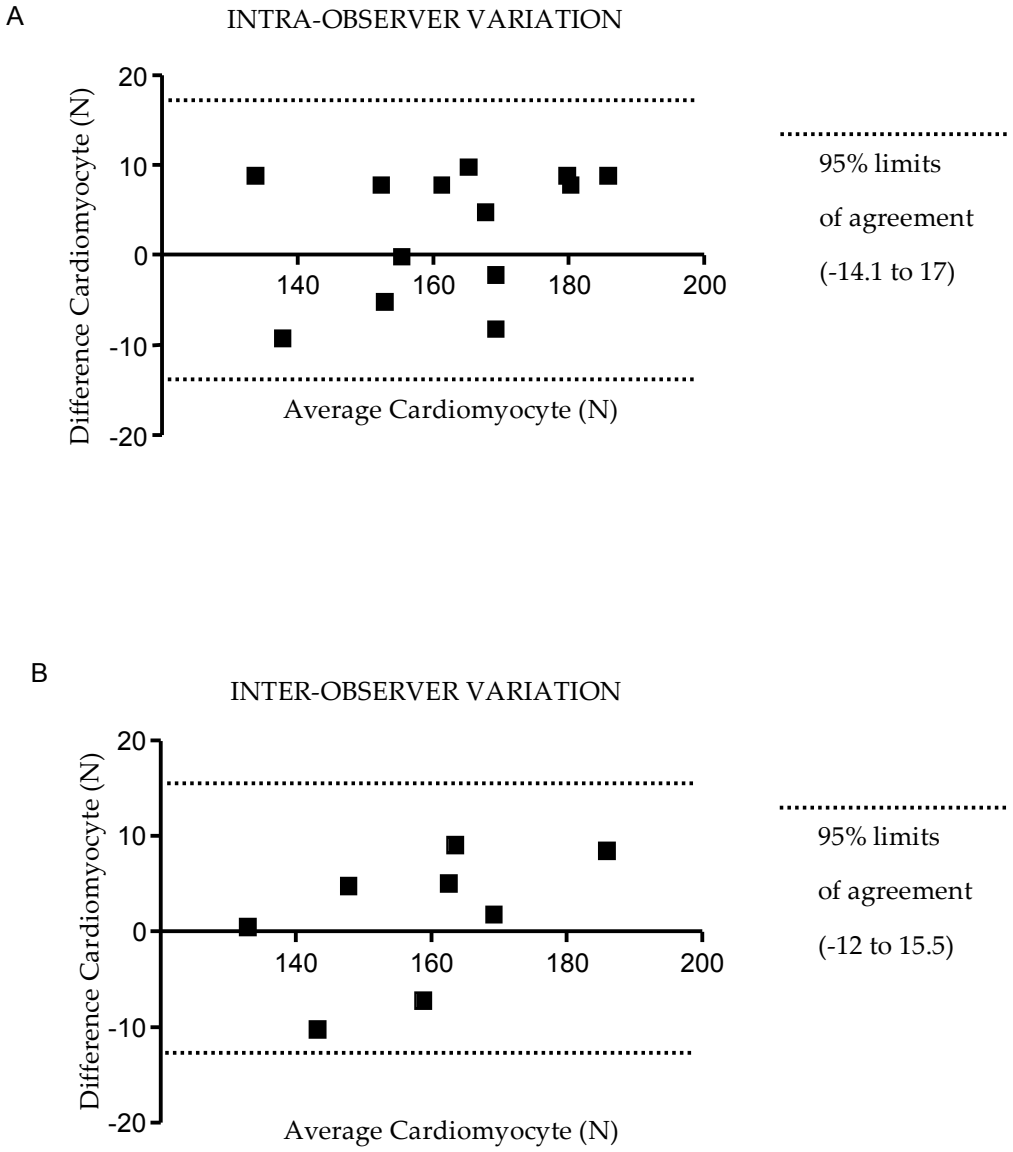

Figure 2.16 – Bland-Altman analysis for Total Ventricle Cardiomyocyte number (TVCn). This statistics was employed to assess Intra-observer (A) and Inter-observer (B) variation in counting cardiomyocyte with ImageJ. The difference between measures are plotted against the mean for the two analysis. The dotted line represents the 95% limits of agreement. TVCn was assessed twice in the same embryos (number of embryos=12).

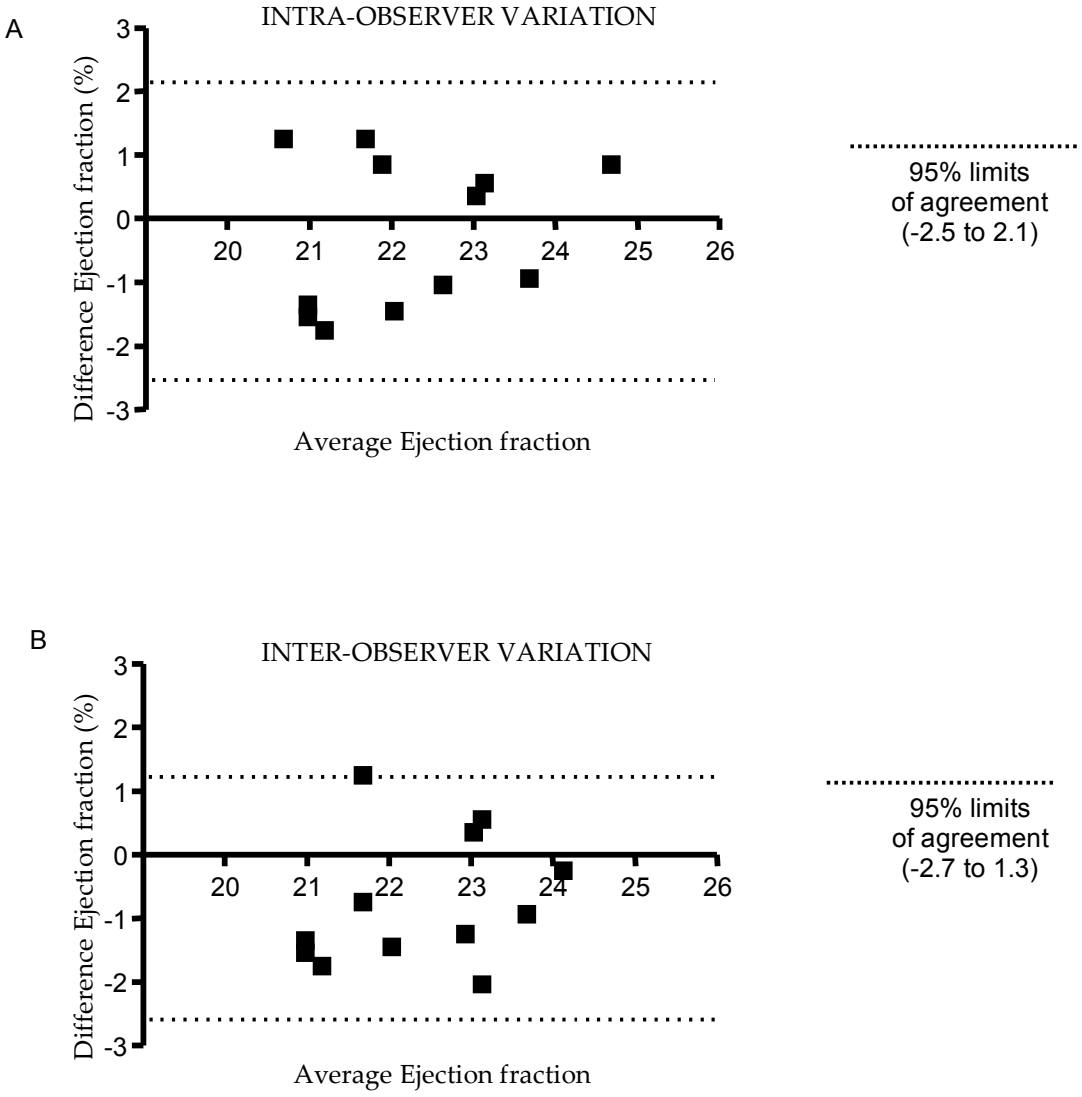

Figure 2.17 - Bland-Altman analysis for Ejection Fraction. This statistics was applied to assess Intra-observer (A) and Inter-observer (B) variation in the measurement of area with ImageJ. The difference between the measures are plotted against the mean for the two tests. The dotted line represents the 95% limits of agreement. Ejection Fraction was assessed twice in the same embryos (number of embryos=12).

Chapter 3
Zebrafish cardiac development

3.1 Introduction

In Vertebrates, cardiogenesis is a morphologically complex process that involves sequential heart primordia migration, folding, looping, septation and maturation to form the chambered heart. Fish and amphibian hearts are considered to be the ancestor of avian and mammalian hearts and have often been used as prototypes for studying cardiac development of these organisms (Moorman and Christoffels, 2003). Despite the evolutionary gap between fish and mammals, molecular data suggest that the essential regulatory elements of heart development are shared among vertebrates (Sheaff *et al.*, 1991; Moorman and Christoffels, 2003; Xavier-Neto *et al.*, 2007) and, in some cases, also with invertebrates (Perez-Pomares *et al.*, 2009). Common insights from the cardiac anatomy and physiology of many vertebrate groups are important to our overall understanding of cardiac development. According to the rules of Von Baer (VonBaer, 1828; Moorman and Christoffels, 2003), it is the embryonic rather than the adult heart that should be compared since the general features of a vertebrate group appear earlier in development than the adult specialized features.

In the last twenty years the zebrafish (Danio rerio) has emerged as a powerful model to study cardiac development. Forward genetic screens have identified many novel regulatory mechanisms with essential roles in cardiogenic specification and differentiation, migration of cardiac progenitor cells, heart tube morphogenesis, and cardiac function (Harvey, 2002).

The study of these characteristics in the zebrafish has helped improve our understanding of heart formation in mammals (Stainier and Fishman, 1992; Stainier *et al.*, 1993). Despite having only two chambers, the zebrafish heart retains many structural traits and developmental complexity of an Amniote's heart, including a three-layer ventricular wall (epicardium, myocardium and endocardium) from 3dpf (Serluca, 2008) and first and second heart fields (Hami *et al.*, 2011).

However, while early structural cardiac development up to 2dpf has been well studied there are few studies detailing the relationship between cardiomyocyte

proliferation, cardiac function and molecular markers of cardiac development. The zebrafish embryo provides an ideal model in which to study these issues.

Furthermore, since cardiomyocyte loss and contractile dysfunction are important cellular mechanisms in heart failure, there is obviously considerable interest in developing strategies to generate new cardiomyocytes. Improved understanding of cardiomyocyte growth and proliferation during embryogenesis might contribute to new approaches for treatment of degenerative adult cardiac disease, such as heart failure.

Aims of this chapter are:

- Characterise the normal growth pattern of cardiomyocytes in the zebrafish ventricle during the first 120 hours of development
- Characterize the changes in ventricle function and tail blood flow during the first 120 hours of development
- Characterize the pattern of gene expression of cardiac specific growth factors from whole embryos and in isolated embryonic hearts during the first 120 hours of development and in the adult heart
- Explore the relationship between these patterns

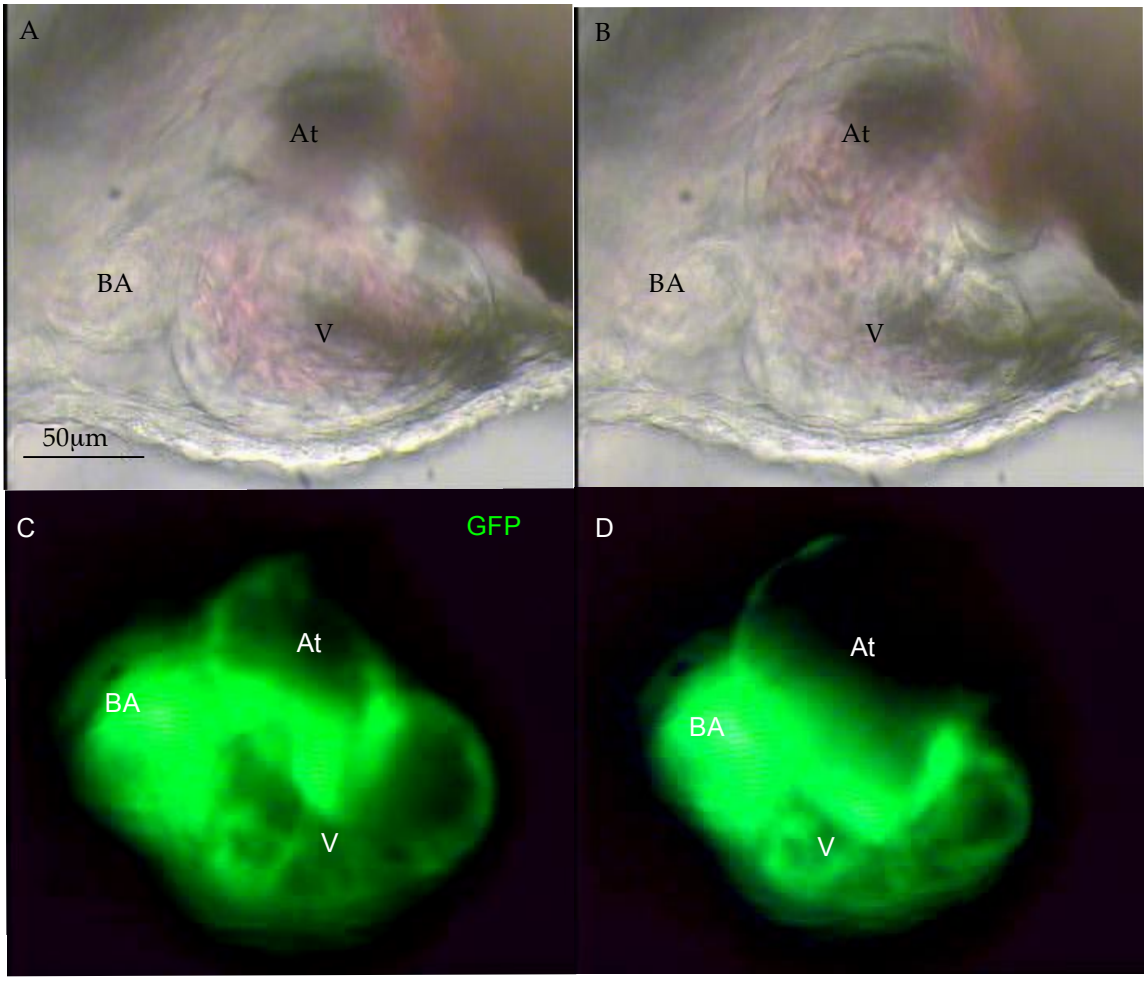

Figure 3.1 - cmlc2:EGFP zebrafish embryonic heart 72hpf. This still images of the same heart are part of two videos captured with a colour camera under white light (A-B) and fluorescence light (C-D). Images on the right and left side show the ventricle in end-diastole and end-systole, respectively. (V – ventricle, BA – bulbus arteriosus, At – atrium).

3.2 Materials and Methods

3.2.1 Zebrafish lines

Zebrafish transgenic cmlc2:EGFP embryos were used for all experiments, unless stated.

3.2.2 Ventricle structure and cardiomyocyte proliferation

Changes in ventricular structure and total ventricular cardiomyocyte number (TVCn) were assessed during developmental stages 48 (hatching period), 72, 96 and 120 hpf (early larva) by microdissecting embryonic hearts (Section 2.8.1), stained with DAPI (Section 2.9.2) and analysing under confocal microscope (Section 2.9.2.3). The whole ventricle structure was analysed by observing the GFP signal. In order to visualize also the shape of in-situ single cardiomyocytes, hearts analysed for ventricle structure were additionally stained with an antibody against DM-GRASP, a sarcolemmal integrin, called zn-5 (mouse; produced by Developmental Studies Hybridoma Bank) diluted 1:200 in PBS containing BSA 5%.

3.2.3 Cardiovascular function

Methods for cardiovascular function measurements have been detailed in section 2.6; these included ejection fraction (EF) and ventricular diastolic area (VDA) (section 2.6.2), heart rate (HR) (section 2.6.3), and cardinal vein blood velocity (CVBV) (section 2.6.4).

3.2.4 Gene expression analysis

Q-PCR technique, described in details in section 2.12, was used to assess the expression pattern in the period 24 to 120 hpf for a range of genes involved in the zebrafish development, including CDK9, LARP7, GATA4, 5 and 6, MEF2C, TBX5 and NKX2.5 (see Table 3.1 for primer sequences used). CDK9 and LARP7 analysis will be discussed in details in Chapter 4. The time-courses were performed in whole

embryos (section 2.12.1) and in isolated embryonic (section 2.12.2) and adult (6 month age) hearts. I examined a number of housekeeping genes to assess which remained most stable during the early period of development from 24 to 120 hpf (see figures 2.9 in Chapter 2 for all housekeeping genes). I subsequently chose the housekeeping gene EF1α to enable quantitation of gene expression according to the amount of cDNA loaded.

3.2.5 Protocol for assessment of cardiac function and growth

Embryos were grown in a stocking density of 40 embryo/90mm Petri dish in 30mL of embryo medium (EM). At 48hpf embryos were dechorionated, if not yet hatched, and placed singularly in a 2ml well in EM, replaced every day up to 120 hpf. Videos of embryonic hearts at 48, 72, 96 and 120hpf were captured and stored and single plane fractional area change of the ventricle was used as a surrogate marker of ejection fraction using ImageJ. At least 5 embryos from the same clutch were used for microdissection of hearts at 48, 72, 96 and 120hpf and following histochemistry for cardiomyocyte analysis.

3.2.6 Statistics

Details of statistical analysis are described in section 2.15. One-way ANOVA analysis was followed by Bonferroni'multiple comparison test to assess differences between mean at each time point.

Table 3.1 – Details of primers for real-time PCR for use with Roche Universal Probe Library (UPL). These include gene name with Pubmed accession number, Forward (F) and Reverse (R) primer sequences with related position on the gene, amplicon length and the number of the probe used.

Gene (Accession number)	Amplicon length (nucleotide)	Probe number	Primers sequence and position on the gene
CDK9 (NM 212591.1)	93	132	F: GGAGATCAAGAGGGTCATGC (474-493) R: ACATTGGCTGCTTTCATGTCT (546-566)
LARP7 (NM 199930.1)	76	65	F: CGCAAGAGCAAGCACAAA (674-691) R: AAGATTCCTGGCTTCCTTGG (730-749)
GATA4 (NM 131236.1148)	108	148	F: CCTGTGGACTCTACCATAAGATGA (641-664) R: GCTGACAGTTTGTGCAGGATAA (727-748)
GATA5 (NM 131235.2148)	82	148	F: GCGGCCTTTACCACAAGAT (1003-1021) R: GCTCGTCGTGATGTGCTTT (1066-1084)
GATA6 (NM 131557.1162)	125	162	F: CAGTCCTTCGTCAACACAGGT (1014-1034) R: ACGTCAAGCCTACATTGGTGT (1118-1138)
MEF2c (NM 131312.2)	77	44	F: GAAACACAGGAGGTCTGATGG (1067-1087) R: GTGGTTTCCGTACCCGTTT (1125–1143)
TBX5 (NM 130915.1)	71	2	F: CCACTGCATCAAGAGGAAAGT (1121-1141) R: CCACATACGGCTTCTTATAGGG (1170-1191)
NKX2.5 (NM 131421.1)	146	124	F: GGACAAAGGCAACAAAATCAA (317-337) R: CCTGACAAAACCCGATGTCT (443-462)

3.3 Results

3.3.1 Cardiac Growth

3.3.1.1 Ventricle Morphology

Analysis of ventricle structure showed a progressive increase in the ventricle trabeculation (figure 3.2). At 48 hpf, no trabecular formation was observed. These started to form at 72 hpf and increase at 96 hpf, while at 120 hpf a dramatic increase of trabeculae was observed (figure 3.2). Although the anti-DM-GRASP staining allowed visualization of a gross cardiomyocyte shape, a precise measurement of in-situ single cardiomyocyte area was not reliable.

3.3.1.2 Ventricle Cardiomyocyte Number

Total ventricle cardiomyocyte numbers (TVCn) during normal zebrafish heart development increased significantly by 30% between 48 and 72 hpf ($p<0.05$), 20% between 72 and 96 hpf ($p<0.01$) and 50% between 96 and 120 hpf ($p<0.001$) (figure 3.3).

3.3.1.3 Ventricle Diastolic Area

The size of the ventricle (ventricular diastolic area, VDA) (figure 3.4 A & B) increased between 48 to 72 hpf and increased significantly between 48 and 96 hpf ($p<0.05$), while it slightly decreased between 96 and 120 hpf.

3.3.2 Cardiac Function

3.3.2.1 Ejection Fraction

Cardiac function, assessed as ventricle fractional area change, had values in the range 22-24±2% (figure 3.4 A & C) between 48 to 120 hpf with no statistical significant changes over this developmental time period.

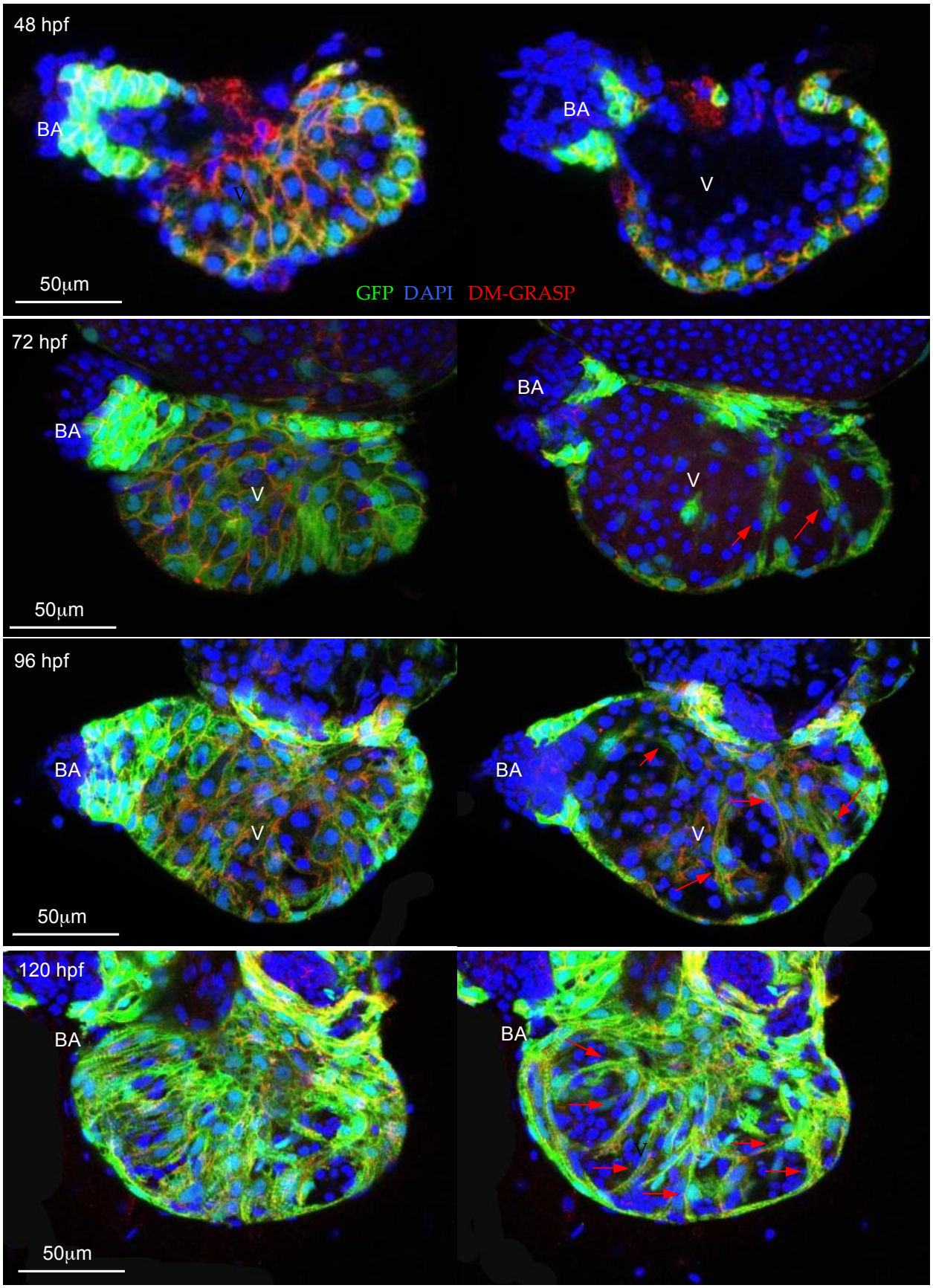

Figure 3.2 - Zebrafish embryo ventricle morphology. Confocal images of cmlc2:EGFP zebrafish embryo heart ventricle at different developmental stage (expressed in hour post-fertilization (hpf)), stained with anti-DM-GRASP (sarcolemmal integrin) in red, and counterstained with DAPI. Each time-point reports images of the same heart, of the ventricle surface (left side) and inside the ventricle (right side). Red arrows show trabecular formation inside the ventricle. Key: BA-bulbus arteriosus, At-atrium

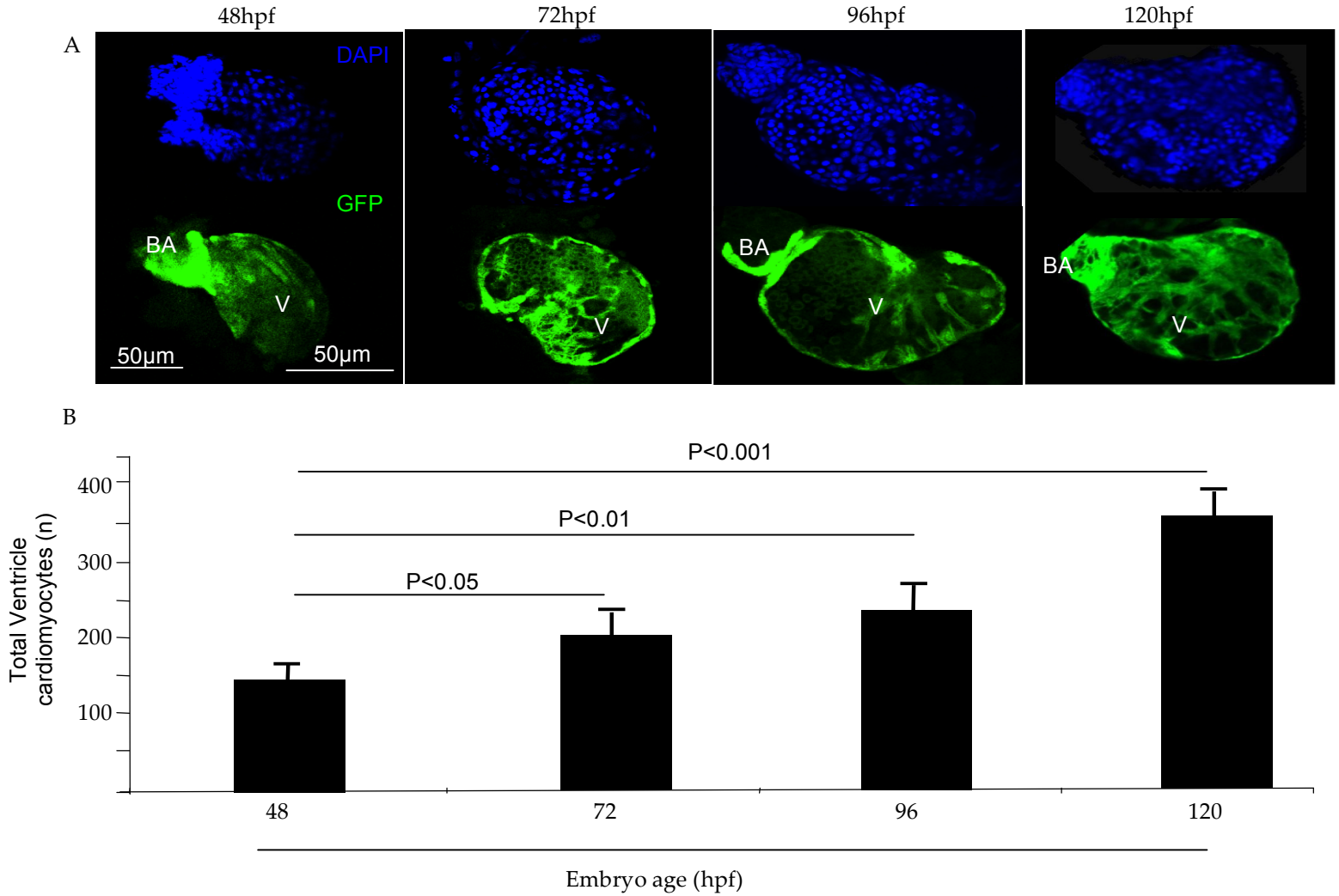

Figure 3.3 - Total ventricle cardiomyocyte number during normal development. A- images of cmlc2:GFP zebrafish embryo heart ventricles at several developmental age. At each time point, image captured under confocal microscopy show DAPI stained nuclei (upper panel), counted as single cardiomyocytes and the GFP background (lower panel). B- Diagram, showing the increase of total ventricle cardiomyocyte numbers over the time period, with an acceleration in the period 96-120 hpf. One-way ANOVA was employed to compare means, followed by Bonferroni's multiple comparison test. N=4 experiments were performed. In each experiment, embryo hearts derived from the same clutch of eggs.

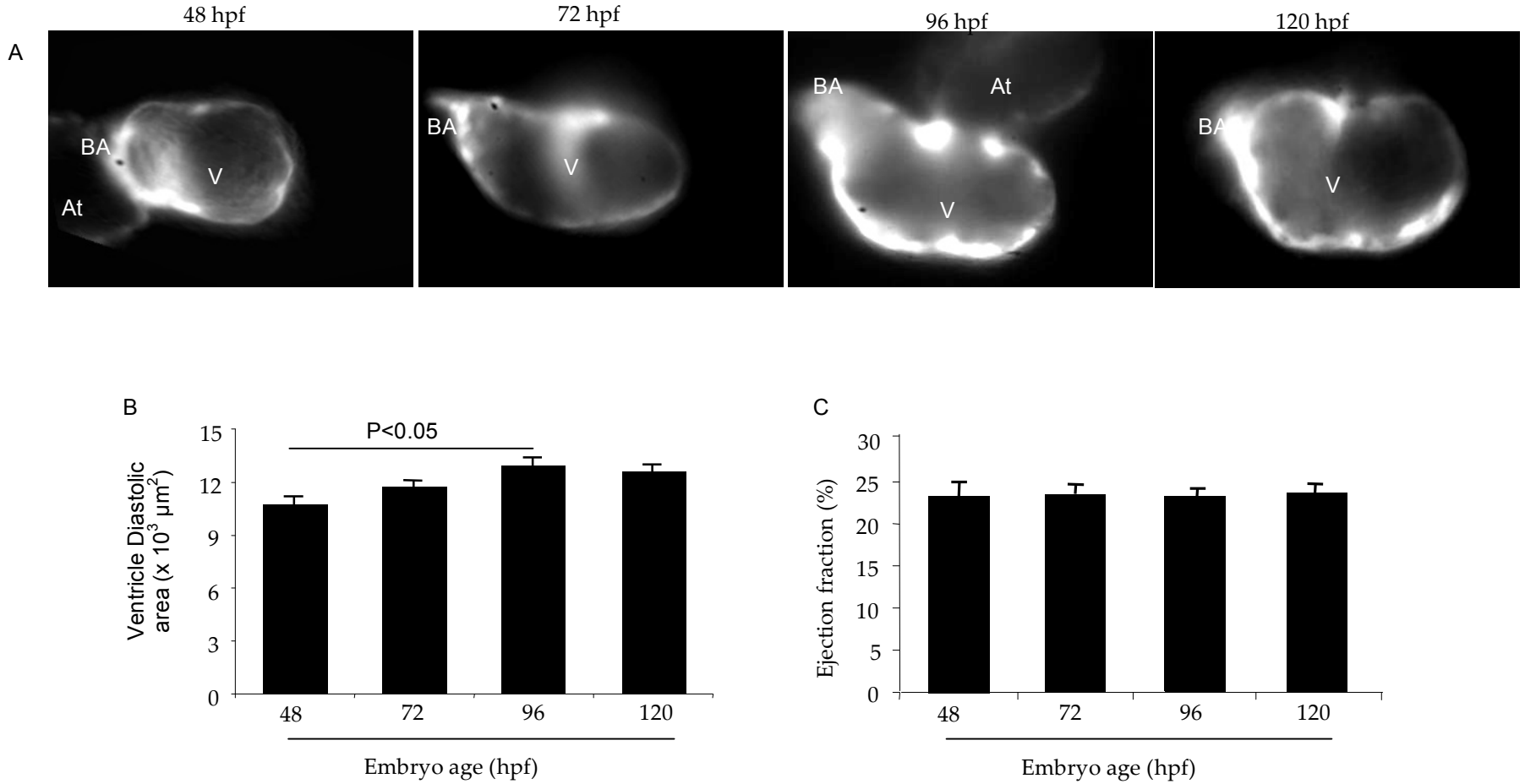

Figure 3.4 - Ventricle diastolic area (VDA) and Ejection fraction (EF) analysis in the zebrafish embryo. Analysis were repeated every day in the same embryos (tg(cmlc2:EGFP) line) from 48-120 hpf. A. Still images extracted from a video captured under fluorescence microscopy representing the cmlc2:GFP zebrafish embryo heart at the different developmental age. B. Diagrams showing variation in Ventricle diastolic area during the development, with a significant increase between 48 and 96 hpf. C. Diagrams showing variation in Ejection fraction during the development; there was no significant change between the different time point. A repeated measures one-way ANOVA was employed followed by Bonferroni's multiple comparison test, N=3 experiments. Key – BA=bulbus arteriosus, At=atrium, V=ventricle

3.3.2.2 Heart Rate

Heart rate showed a slight and progressive increase from 48 to 120 hpf (figure 3.5 A). One-way ANOVA test did not show significant differences among means at the different time points.

3.3.2.3 Posterior Cardinal Vein Blood Velocity

Erythrocyte velocity, measured in the zebrafish embryo posterior cardinal vein, increased significantly between 48 and 96 hpf ($p<0.05$) and 48 and 120 hpf ($p<0.01$) while it showed very similar values at 72 and 96 hpf. Then it slightly increased between 96 and 120 hpf (figure 3.5 B).

3.3.3 Gene expression

Transcription factors shown here (figure 3.6 and 3.7) were chosen on the basis of their importance in cardiac development of Vertebrates (Brand, 2003).

Among a number of housekeeping genes that I examined during normal development I found that the expression pattern of Ef1α housekeeping gene did not show variation between 24 and 120 hpf in the zebrafish embryo; therefore this was used as a control to normalize the level of other genes.

3.3.3.1 Gene expression in the developing Whole Embryo

GATA5 and MEF2c have the highest mRNA levels at 24 hpf (figure 3.6). GATA5 mRNA then decreased at 48 hpf and after this time point slightly increase up to 120 hpf, however with no statistical significant changes. MEF2c mRNA level increased at 48 hpf and then significantly decreased at 72 hpf ($P<0.05$) and then significantly increased up to 120 hpf ($P<0.05$). GATA4, after a decrease at 48 hpf, increased at 72 hpf and was then stable up to 120 hpf. GATA6 significantly increased up to 72 hpf $P<0.01$), when it showed the highest value, and then it significantly decreased up to 120 hpf ($P<0.01$) when we reported a value slightly higher than at 24 hpf (figure 3.6). NKX2.5 gene expression significantly increased between 48 and 96 hpf ($P<0.05$) and then slightly decreased at 120 hpf.

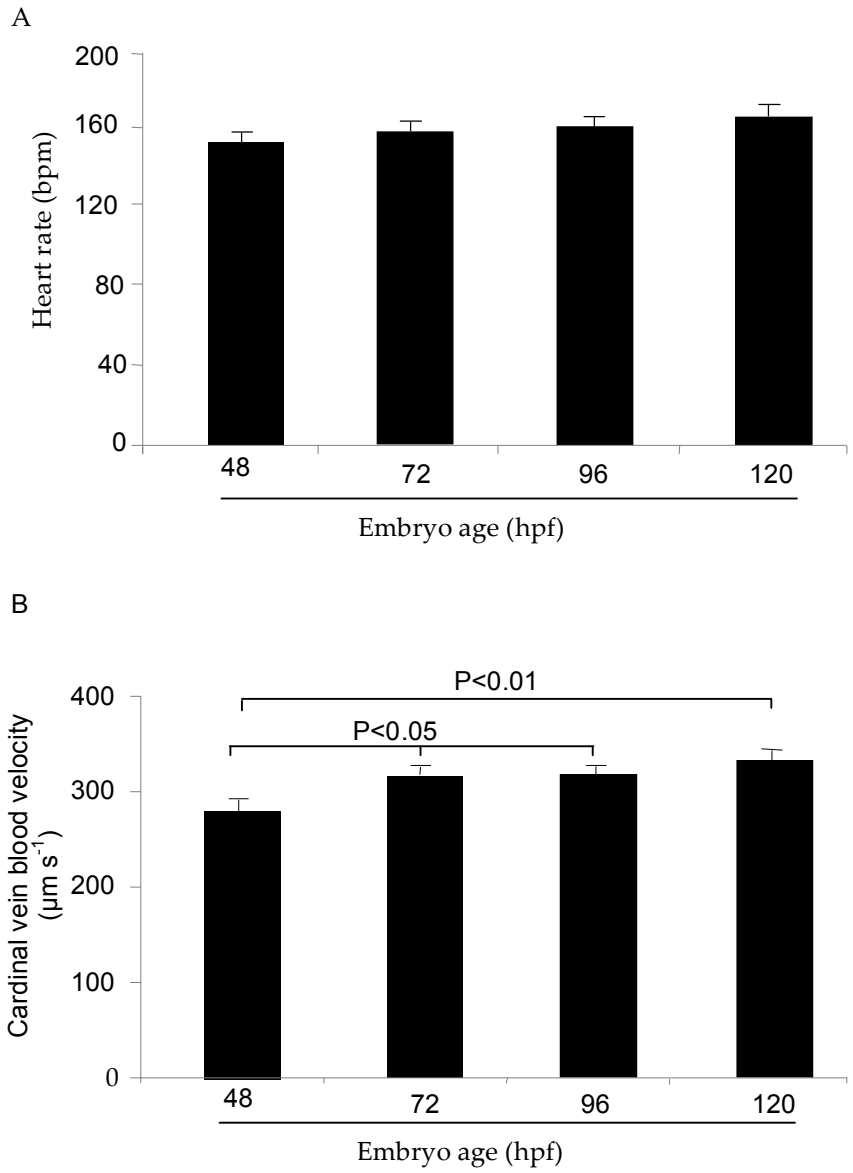

Figure 3.5 - Heart rate and cardinal vein blood velocity analysis in the zebrafish embryo. Analysis were repeated at 24 h interval in the same embryos (tg(cmlc2:EGFP) line) from 48-120 hpf. A. Heart rate slightly increased over the time period but with no statistical significant changes. B. Cardinal vein blood velocity also increased over the time period, with statistical significant changes between 48 hpf and other time point. A repeated measures one-way ANOVA was employed to compare means, followed by Bonferroni's multiple comparison test. N=3 experiments.

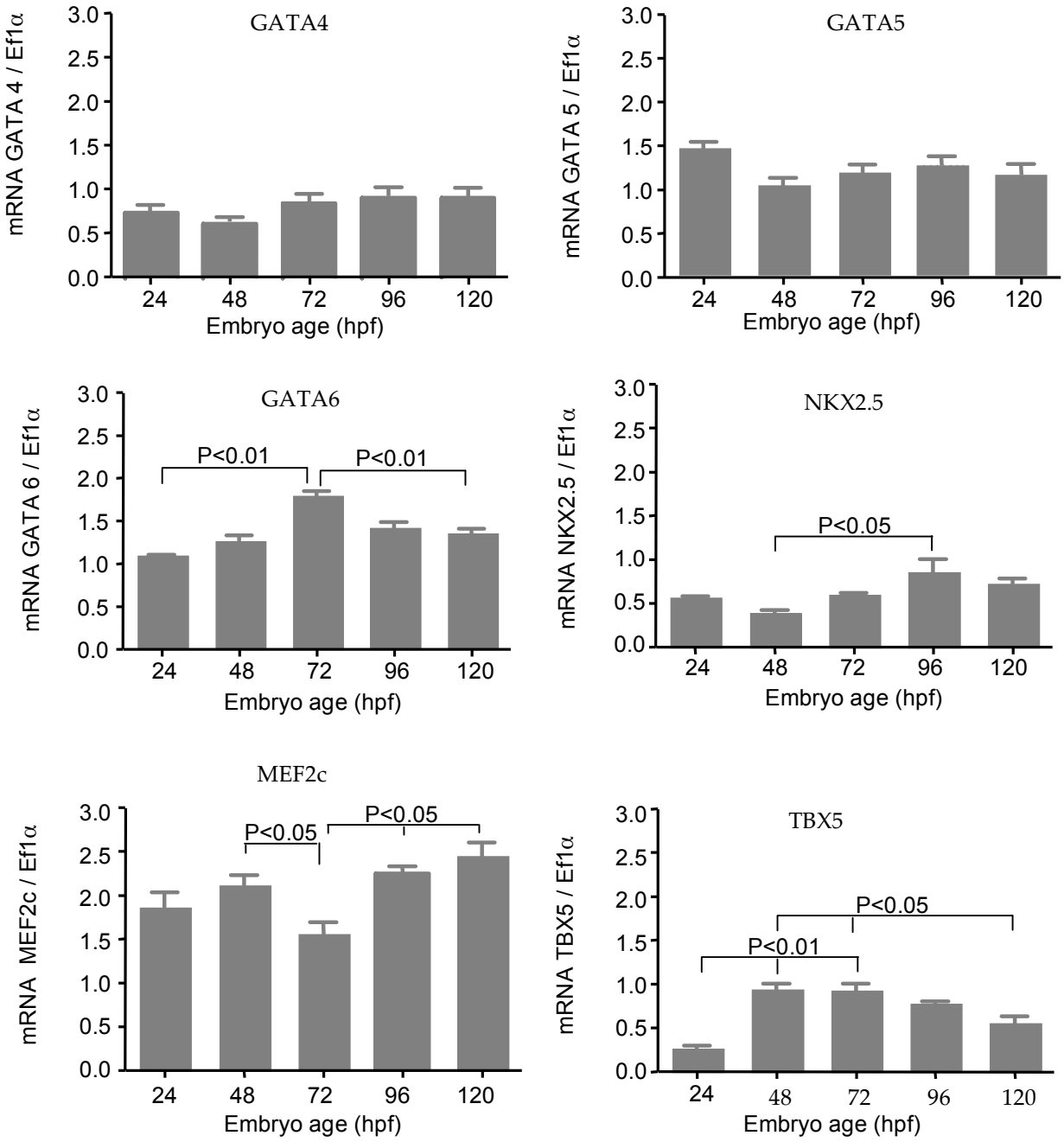

Figure 3.6 – Expression of cardiac relevant transcription factors genes in the zebrafish whole embryo. mRNA levels were assessed by Q-PCR during normal development from 24 to 120 hpf and were normalised against the housekeeping gene Ef1α. One-way ANOVA was employed followed by Bonferroni's multiple comparison test. N=3 experiments. Each time-course was studied in 1 clutch of eggs, at least 10 embryos from the clutch were used to generate each time point. The data represents an average from studies in 3 clutches of eggs.

TBX5 showed the lowest value of mRNA level at 24 hpf that increased significantly at 48 and 72 hpf ($P<0.01$) and then decreased again up to 120 hpf ($P<0.05$) (figure 3.6).

3.3.3.2 In Isolated Hearts

Q-PCR analysis in the embryonic and adult heart showed a general increased expression of most of the genes (figure 3.7). GATA4, 5 and 6 showed very similar level of mRNA at 48 hpf. Then at 96 hpf GATA 4 and 6 showed a high significant increase in mRNA levels ($P<0.01$) that were maintained at 120 hpf and in the 6 month (adult) heart. GATA 5 did not change between 48 and 96 hpf while it significantly increased between 96 and 120 hpf ($P<0.05$) and in the adult heart ($P<0.01$). MEF2c reported the lowest level of mRNA at 24 hpf compared to all other genes, while it showed a significant increase between 48 or 96 and 120 hpf ($P<0.05$). MEF2c continued to increase in adult heart ($P<0.01$, versus 48 hpf). NKX25 and TBX5 showed a very similar pattern of expression, with a slight increase between 48 and 96 hpf followed by a significant reduction at 120hpf and in the adult heart (figure 3.7).

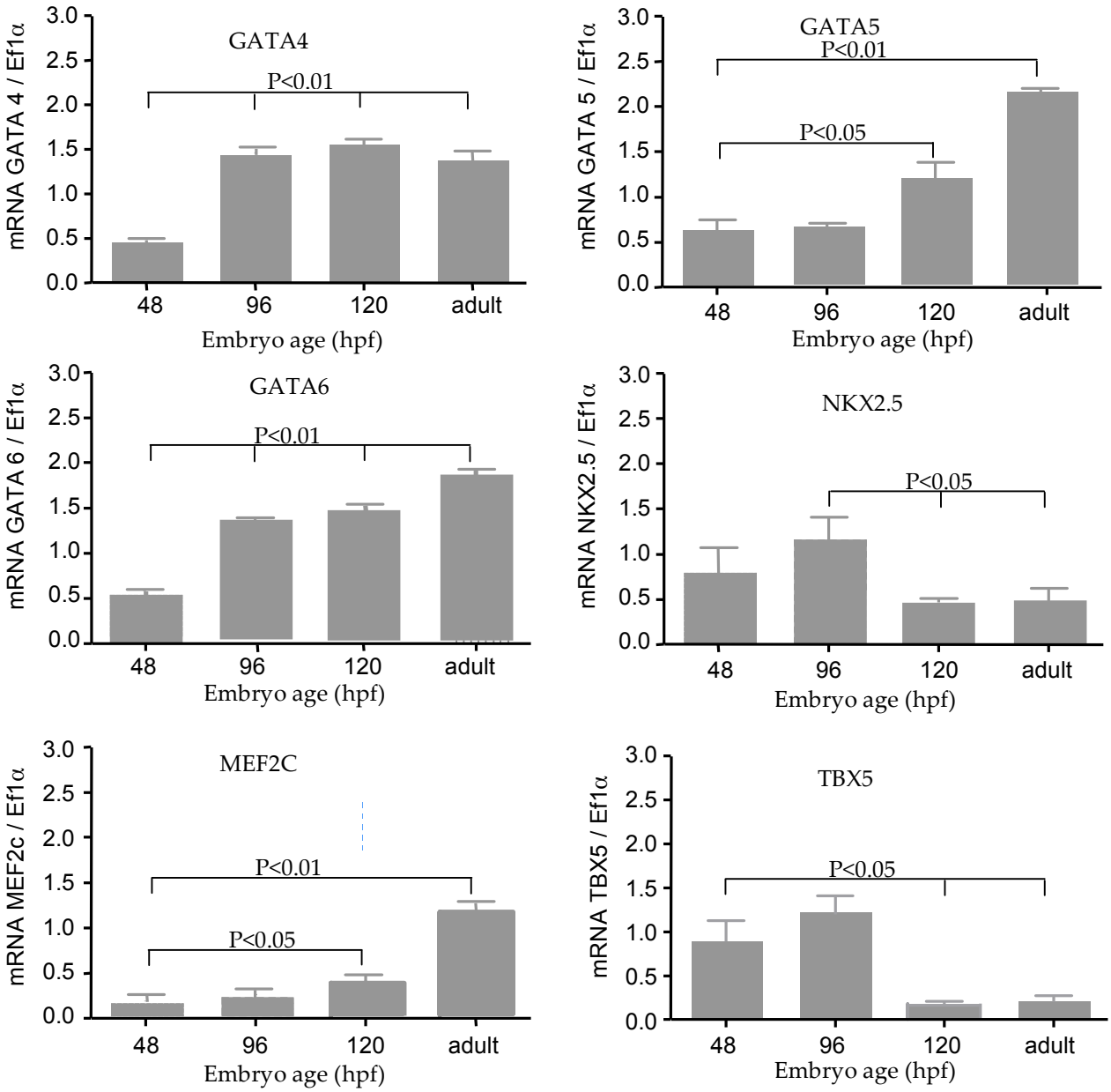

Figure 3.7 - Expression of cardiac relevant transcription factors genes in the zebrafish embryonic heart. mRNA levels were assessed by Q-PCR during normal development at 48, 96 and 120 hpf, and in the adult (6 month age) heart. mRNA was normalised against the housekeeping gene Ef1α. One-way ANOVA was employed followed by Bonferroni's multiple comparison test. N=3 experiments. Each time-course was studied in 1 clutch of eggs, at least 10 embryos from the clutch were used to generate each time point. The data represents an average from studies in 3 clutches of eggs.

3.4. Discussion

This chapter has addressed the changes in cardiomyocyte proliferation and cardiac function in the zebrafish embryo during early development defined here as 48-120 hpf. Integrated structural and functional studies examining the changes in cardiac and haemodynamic function during this time period have not been previously published.

3.4.1 Cardiac Growth

The current study incorporated repeat measurements of cardiovascular function and ventricle size in the same zebrafish embryo thus permitting repeat comparisons using ANOVA. The cardiac size, here expressed as ventricle diastolic area, showed a consistent increase over the time period studied.

The maximal ventricle size is reached at 96hpf and remains in this range at 120hpf, although slightly lower. Conversely, Sedletcaia and co-worker (Sedletcaia and Evans, 2011) reported lower values of diastolic area of the ventricle (VDA) at 48 and 72 hpf and with no increase between 48 and 72 hpf. This discrepancy could be ascribed to the different anesthesia approach used, that is known to affect the measure (Denvir *et al.*, 2008). The diastolic area, as a measure of heart size, has the advantage to be easy to calculate. Also, it is assessed in the in-vivo beating heart, therefore the measure is not affected by the artifacts than can follow the organ fixation. However, as the diastolic area is very sensitive to the level of anaesthesia, the solution of tricaine must be carefully prepared.

In our experiments, trabecular formation was not observed before 48 hpf, as already shown by Hu et al. in the zebrafish heart ventricle (Hu *et al.*, 2000), while in embryonic heart ventricle 72 hpf trabeculae were observed for the first time. This also means that the trabeculation process must be appeared between 48 and 72 hpf, and this is supported by a recent report showing that in the zebrafish heart the first discernible protrusion of cardiomyocytes from the outer curvature into the ventricular lumen appear by 60 hpf (Peshkovsky *et al.*, 2011).

An acceleration in trabecular network formation was observed in our lab in the period 96-120 hpf. A similar finding was described by Hu et al. (Hu *et al.*, 2000). However, the authors did not identify the developmental time period this formed. Interestingly, in this same developmental stage the VDA showed a slight decrease. Therefore, in the cardiac maturation process it seems that the heart reduces its external growth in the period 96-120 hpf and starts to increase internal myocardial mass that eventually create elaborated lacunae through which blood flows.

As expected, the increase in cardiac size was mirrored by the augmentation in ventricle cardiomyocyte number in the period 48-120 hpf. The highest increase in cardiomyocyte number was observed between 96 and 120 hpf, about 50%.

In respect with the published literature we reported higher number of total ventricle cardiomyocyte (TVCn) at 48 hpf compared to Targoff et al. (Targoff *et al.*, 2008), that reported a value of about 120 cardiomyocytes, counted as Mef2-positive nuclei, in zebrafish heart ventricle at 52 hpf. The discrepancy between the MEF2 and DAPI positive nuclei may be explained by the inter-observer variation that could over or underestimate the number of cardiomyocyte, for example by including in the count some parts of bulbus arteriosus and atrio ventricular cushion. Our experiments have examined inter- and intra-observer variation. Fibroblasts that account for the majority of non-muscle cells in mammals and could be referred to explain this difference are rare in zebrafish and occur randomly interspersed within the subepicardial layer (Ausoni and Sartore, 2009).

Furthermore, the number of cardiomyocytes assessed by DAPI could be affected by blood cells, which are nucleated in fish. As this could have represented a possible source of a systematic error, I examined this in detail. In two separate experiments, I counted cardiomyocyte in tg(cmlc2:EGFP;GATA1:dsRed) double transgenic zebrafish line. This zebrafish line expresses dsRed in red blood cells (Long *et al.*, 1997) and GFP in cardiomyocytes. Both cell type were positive to DAPI. Red blood cells which nuclei are both dsRed and DAPI positive were clearly visible in the ventricle under confocal microscopy and, on average, they represented a 5% of the

total DAPI positive nuclei in the ventricle. Bostrom et al (Bostrom *et al.*, 2010) also counted cardiomyocyte as DAPI positive nuclei and reported at 36 hpf about 240 cardiomyocytes in the two chambers.

In another report, Antkiewitz et al (Antkiewicz *et al.*, 2005) used a line of zebrafish that expresses Discosoma red fluorescent protein (RFP) from the promoter of the cmlc2. The RFP expressed in these fish contains a nuclear localization sequence fused in frame that restricts the RFP to the nuclei of cardiomyocytes (Tg(cmlc2:dsRed-nuc)) (Baird *et al.*, 2000), therefore cardiomyocyte nucleus will appear in red. With this method, cardiomyocyte number reported in the whole embryo heart were between 240 and 330 in the period 48-96 hpf (Antkiewicz *et al.*, 2005) that however is similar to the numbers we observed in the ventricle alone. One limitation of this technique lies in the fact that the dsRed2-nuc protein takes a significant amount of time to fold and localize (Bevis and Glick, 2002), such that its nuclear fluorescence is not evident until approximately 24 h after activation of the cmlc2 promoter (Lepilina *et al.*, 2006). Therefore, some of the differences in cardiomyocyte number observed between my study and others could be ascribed to the method used and also due to simple inter-observer variation. Moreover, I counted as cardiomyocytes all DAPI stained nuclei matching GFP signal and this does not exclude that some epicardial and/or endocardial cells could have caused an overestimation of these values. While I feel this would not have contributed significantly to errors in estimating cardiomyocyte number in my series of studies I certainly would plan to adopt a more cardiomyocyte-specific staining for any future experiments of this type or use the recently developed zebrafish with cardiomyocyte-specific nuclear tagging (tg(cmlc2:DsRed-nuc)).

3.4.2 Cardiac function

To assess cardiac performance sequentially during development I used Fractional Area Change and for consistency I have referred to this as Ejection Fraction throughout my thesis. This approach to measuring ventricle systolic assessment has been used in man for quantifying changes in the left ventricular systolic function

(see paragraphs 1.5 and 2.6.2 for a more detailed explanation) (Domanski *et al.*, 1992). While there is little in the literature regarding using this method in the zebrafish embryo the method is simple and transparent, and does not make assumptions of any complex geometrical shape of the ventricle as used in other techniques. The mean Ejection Fraction (EF) of 22% that I reported at 2 dpf was similar to that reported from Shu *et al*. (Shu *et al.*, 2003) in embryos of the same age. However, he used a different formula that measured the diameter instead of the area. Other authors reported values of Ejection Fraction (EF) of 40-45% in the period 72-120 hpf (Kim *et al.*, 2007) and in the period 76-84 hpf (Carney *et al.*, 2006). In these cases, they used different approaches (Coucelo and Joaquim, 2000) derived from volumetric analysis of end-diastole and end-systole, instead of the area as we did. In some studies, for example Kim *et al.*, embryos were anaesthetised using a higher dose of Tricaine than we used and this is well recognised to affect cardiac function (Denvir *et al.*, 2008). Interestingly, the EF remained fairly stable throughout the first 120 hpf in our experiments. Speculating on why this might be the case, it is worthwhile considering the method of estimating EF in more detail.

Cardiac function has been measured optically through video analysis of area changes of the beating hearts in systole and diastole. Though powerful, this has the problem to be performed in a planar field with two dimensions, while the vertebrate heart develops asymmetrically in three dimensions.

Performing some further modeling of the potential output from the heart during the first 120hpf reveals that the cardiac output may in fact rise dramatically as heart rate and circulating blood volume increase, as normally reported in mammals (Hamill *et al.*, 2011). Taking the mean values for diastolic and systolic area for each developmental time point and assuming the ventricle was shaped as a prolate spheroid (Bagatto and Burggren, 2006) gives a mean volume change of a 6% per day from 48 to 120 hpf. With this assumption the stroke volume in the zebrafish embryonic heart raises, on average, from 0.4 nL at 48 hpf to 0.7 nL at 120 hpf. With the heart rate at 120-160 bpm during this time period this yields a cardiac output of

50 nL/min at 48 hpf rising at 110 nL/min at 120hpf, similarly to data showed by other authors (Antkiewicz *et al.*, 2006; Jacob *et al.*, 2002; Kopp *et al.*, 2010). These data are in agreement with the increasing metabolic demands in embryos during this developmental time period to sustain newly forming organs. Although the data of ejection fraction here presented do not give an immediate information on the cardiac output, this method is still very helpful when the aim of the study is the comparison of cardiac function in different groups.

3.4.3 Gene Expression

The set of genes here analysed are evolutionarily highly conserved in all the vertebrates including zebrafish at the level of sequence, expression pattern and function and are critical for normal cardiac development (Brand, 2003; Molkentin, 2000; Xavier-Neto *et al.*, 2007). All genes reported here were analysed in the whole embryo and then in the isolated embryonic (48-120hpf) and adult heart (6 month age).

GATA4 regulatory mechanisms have been intensively studied and its levels and activity are crucial for normal heart specification and development (Zhou *et al.*, 2012). GATA4 null mice display defects in heart morphogenesis and ventral foregut closure, resulting in embryonic lethality by embryonic day E8.5 (Molkentin *et al.*, 1997). Early cardiac-specific deletion of GATA4 also results in myocardial thinning, abnormal endocardial cushion development, and right ventricular hypoplasia (Zeisberg *et al.*, 2005). Cardiac-specific deletion at later time points results in reduced cardiac function and an inability to undergo hypertrophy after pressure overload or exercise (Xin *et al.*, 2006) (Oka *et al.*, 2006), a process also mediated by CDK9 (Sunagawa *et al.*, 2010). GATA4 in the zebrafish heart showed a similar gene expression pattern as found in the whole embryo at 48 hpf, while it was significantly increased at later time-points and resulted more than double at 96, 120 hpf and in the adult heart compared to the whole embryo. Conversely, a report by Huang et al. (Huang *et al.*, 2004) in normal fetal mouse heart at E16.5, E17.5 and E18.5, showed no change in the expression in GATA4.However, the data here

presented are not directly comparable with the above report either for the different specie or the different cardiac developmental stage analysed. Nevertheless, I also found very similar level in the GATA4 expression at 96 and 120 hpf. Huang and colleagues also found no changes in NKX2.5 in the same time period, while our data showed a significant decrease in the expression of the gene at 120 hpf compared to earlier time points.

Indeed, GATA4 forms protein complexes with several other transcription factors expressed in the heart (Xin *et al.*, 2006). Their synergistic interactions have been proposed to regulate cardiac gene transcription, and disruption of these interactions has been reported to underlie some cases of congenital heart disease (Zhou *et al.*, 2012). GATA4 and 6 were found to have a similar pattern of expression and this agrees with a previous report showing that GATA4 and 6 co-express during early murine development, with both expressed in the pericardial mesoderm, the embryonic heart tube, and the developing endoderm (Morrisey *et al.*, 1996) and continue to be expressed in the adult heart (Morrisey *et al.*, 1997). Indeed, GATA4 and GATA6 proteins physically interact and synergistically activate target gene transcription, in particular the CEF-1 nuclear protein-binding site in the cardiac-specific cTnC transcriptional enhancer (Charron *et al.*, 2001). In contrast, GATA5 is expressed in a temporally and spatially restricted pattern during early embryonic mammalian cardiac development but it is seems not present in the mature heart (Morrisey *et al.*, 1997).

GATA4 also form complexes with MEF2 (Lin *et al.*, 1997), NKX2.5 (Sepulveda *et al.*, 1998; Durocher *et al.*, 1997) and TBX5 (Garg *et al.*, 2003). GATA4, MEF2c and NKX2 showed similar expression pattern as for GATA6 in the zebrafish whole embryo. While TBX5 expression is very low at 48 hpf as previously shown (Garrity *et al.*, 2002) it then registers a fast increase at 72 hpf and then slowly decreases up to 120 hpf.

A gene that has not been included in the above list but which would be important to consider for future experiments is the basic helix-loop-helix transcription factor Hand. This factor shows specific expression patterns during cardiac development in

several organisms including mouse, chick, frog and zebrafish embryos (McFadden *et al.*, 2005). Mammalians retain two genes, Hand 1 and Hand 2, while zebrafish genome appears to encode only Hand 2 (Yelon *et al.*, 2000). Zebrafish mutants with Hand knock-out (Hands off) show a more severe phenotype compared to Hand2 knockout mice and it has been speculated that this is due to the lack of compensatory activity of a second Hand gene in the zebrafish (McFadden *et al.*, 2005).

In conclusion, in this chapter I have characterized several aspects of the developmental dynamics of the zebrafish heart ventricle in the period 48-120 hpf, including changes in cardiac function, ventricle diastolic area and the pattern of change cardiomyocytes number and gene expression. The functional characteristics of the heart appear to be established early in development, at around 48 hours, with no significant increase in ejection fraction after this time. However, given that the heart rate increases progressively over this time period the overall cardiac output is likely to rise in order to supply the growing needs of the embryo. I also demonstrated that the period of greatest increase in size of the heart does not correspond to the period of greatest increase in cardiomyocyte number. This apparent paradox may be explained by changes in blood volume and transmural forces within the ventricle cavity causing dilatation preceding a period of wall thickening and accelerated cardiomyocyte proliferation at around day 5. This highlights the fact that the heart's early structure and function involves an interplay between cardiac growth and organization combined with physical forces which change at different rates during this rapid early developmental phase. I also showed a complex and changing pattern of expression of several growth factors during development in whole embryos and in isolated embryonic hearts. These changes are critical for the final morphology of the heart and ultimately for cardiac functional capacity (Chicurel *et al.*, 1998; Conlon and Raff, 1999; Day and Lawrence, 2000).

Chapter 4

Modulation of CDK9 in the zebrafish embryo

INTRODUCTION

Cyclin-dependent Kinase (CDK)9 acts by phosphorylating the carboxy-terminal domain of RNA polymerase II and promote cellular RNA synthesis. It is therefore of fundamental importance to cellular function and for this reason it is also closely regulated. In general, it is active when combined with Cyclins (P-TEFb complex) and it is repressed when other molecules, *i.e.* 7SK-RNA, HEXIM and LARP7, join the P-TEFb complex, forming an inhibitory complex. This pathway is likely to be important in driving the increased RNA and protein synthesis typically observed in cardiac hypertrophy and has been proposed as a key regulator of the cardiac hypertrophic response (Sano *et al.*, 2002). However, the therapeutic potential of this pathway arises not only from the possible inhibition of an abnormal hypertrophic response but a further overlooked possibility includes the activation of CDK9 to induce a favorable hypertrophic response such as that seen in pregnancy or with exercise training. Therefore, in this chapter I set out to compare and contrast both inhibition and activation of CDK9 in order to assess the potential therapeutic benefits on the heart and simultaneously examine the wider impact on the whole zebrafish embryo.

This Chapter has therefore been split in two complementary parts.

Part 1 describes the role of CDK9 and the effects of its inhibition during zebrafish development, with emphasis on cardiac development and function.

Part 2 focuses on the effects of CDK9 upregulation by LARP7 knockdown in the same model.

CHAPTER 4

PART 1

Effects of CDK9 inhibition on global and cardiac development in the zebrafish embryo

4.1.1 Introduction

Cyclin-dependent kinase (CDK)9 is a regulatory molecule activated following binding to Cyclin T (Peng *et al.*, 1998), forming a heterodimer that is the core element of the positive-acting transcription elongation factor (P-TEFb) (Zhou and Yik, 2006). It is ubiquitously expressed in many organs (Shore *et al.*, 2005), which relative abundance depends on the developmental stage and cell commitment (Kohoutek, 2009). It has been involved in several mechanisms during the development. In growth control of primordial germ cells (PGCs) (Okamura *et al.*, 2012). In mouse oocytes and preimplantation embryos CDK9 inhibition causes developmental arrest at the two-cell stage (Oqani *et al.*, 2011). CDK9 also modulates the endoderm-inducing activity of Mix.3 during embryonic development (Zhu *et al.*, 2009).

A tissue-specific role for CDK9 in development has been indicated in zebrafish embryos, where loss of CDK9 selectively blocks definitive hematopoiesis (Meier *et al.*, 2006).

In adulthood, CDK9 and P-TEFb activity appears to be highly expressed in terminally differentiated cells and tissues (Bagella *et al.*, 1998), this suggests a role for this kinase in specialized cellular functions.

Because of its central role in the transcription regulation (Garriga and Grana, 2004), CDK9 has been implicated in pathologic cellular processes (Krystof *et al.*, 2010). In cardiac remodeling, this hypothesis is supported by previous research indicating that CDK9 expression is up-regulated and activity enhanced in cardiac hypertrophy (Sano *et al.*, 2002) and chronic activation of CDK9 predisposes to heart failure in adult mouse myocardium. A major finding in different models was the fact that both hypertrophy and normal cardiac development correspond to an enlargement of the cardiomyocytes with increased RNA and protein synthesis.

Surprisingly, very few data are available on the role of CDK9 during cardiac development (Wagner *et al.*, 2008).

Persistent endogenous CDKs inhibition in cardiomyocytes has been proposed as one reason why adult cardiomyocytes fail to re-enter the cell cycle following injury

or in response to stress (Di Stefano *et al.*, 2011). In fact, Di Stefano et al. induced knockdown of endogenous CDK inhibitors by small interfering RNA in cultured mouse cardiomyocytes, thereby activating or dis-inhibiting CDK9. This triggered both neonatal and adult cardiomyocytes to re-enter the cell cycle resulting in proliferation of previously quiescent cells (Di Stefano *et al.*, 2011). However, these workers did not identify which specific CDK or CDKs were activated. CDK9 has also been shown to regulate cell-cycle and is involved in differentiation of cardiomyocytes from mice embryonic stem cell (Kaichi *et al.*, 2011).

There are a few studies suggesting a potential link between CDK9 and cardiomyocyte proliferation (Kaichi *et al.*, 2011; Sunagawa *et al.*, 2010). We planned to explore this in the zebrafish embryonic heart.

General aim

Describe and define the role of CDK9 on global development and cardiac development in the zebrafish embryo.

Key questions

- What is the normal pattern of expression of CDK9 in the whole embryo and the heart during normal zebrafish development?
- What are the effects of pharmacological manipulation of CDK9 on whole embryo and heart development?
- What are the effects of genetic down regulation of CDK9 on whole embryo and heart development?

4.1.2 Materials and Methods

4.1.2.1 Zebrafish lines

Zebrafish transgenic cmlc2:EGFP embryos were used in all experiments, unless stated.

4.1.2.2 Whole embryo and cardiac phenotype

Assessment of whole embryo and cardiac phenotype was described in Chapter 2, section 2.13.5.

4.1.2.3 Total body length and Heart-to-body length ratio

Body length was used as a simple way of assessing whether there was reduced growth of the embryos. Zebrafish embryo total body embryo was measured as the distance from the snout to the posterior tip of the notochord. Heart-to-body length ratio was also used as a simple method to show how the organ grows in relation to the whole embryo. Heart-to-body length ratio was assessed only in embryos where the whole embryo length could be accurately measured, *i.e.* in embryos exposed to flavopiridol and was expressed as μm/mm.

4.1.2.4 Cardiovascular function

Cardiovascular function was assessed using techniques and methods outlined in Chapter 2, Section 2.6; these included ejection fraction (EF), heart rate (HR), ventricular diastolic area (VDA), total (TVCn) and proliferating (PVCn) ventricular cardiomyocyte number analysis.

4.1.2.5 CDK9 Gene knockdown

Morpholino technology by injection of antisense oligonucleotides (oligos) was used to block mRNA transcription (splice blocking) or mRNA translation (translation blocking) (see table 4.1.1). A detailed description of the technique is reported in Chapter 2, Section 2.13. A volume of 0.5nL of oligos (100 μM for CDK9 splice

Table 4.1.1 – CDK9 morpholino oligonucleotides sequences.	
Danio rerio cyclin-dependent kinase 9 (CDC2-related kinase) mRNA Pubmed Accession number NM_212591.1	
Morpholino sequences	
Splice blocking	5’-CTTTCTTCCCCATTCTTTTACGTGG-3’ (exon 3 / intron 3)
Mismatch	5’-CTTTgTTgCCgATTgTTTTACcTGG-3’
Translation blocking	5’-CCTACGTCGCGCTGTTTTGGCCTTC-3’

blocking, 20 μM for CDK9 translation blocking) was injected in eggs at 1-4 cell stage, therefore delivering about 0,5 ng and 0,1 ng oligonucleotides with each injection respectively for the splice blocking and the translation blocking morpholino.

4.1.2.6 Pharmacological treatment of embryos

Flavopiridol is a well-recognized specific CDK9 inhibitor (Chao *et al.*, 2000). Zebrafish embryos 24hpf were placed in embryo medium containing Flavopiridol 3μM (Sigma) previously diluted in DMSO. No DMSO was added in the embryo medium. Solutions were replaced at 48, 72 and 96hpf. The concentration of Flavopiridol used was chosen after a dose ranging study at concentrations of 1μM - 5μM. Embryo survival, gross body phenotype and gross cardiac morphology were assessed following exposure to various concentrations of flavopiridol (see section 2.14.2). The final concentration selected for all subsequent experiments was 3μM as this resulted in the lowest degree of non-specific toxicity to the whole embryo while also resulting in a significant decrease in CDK9 activity confirmed by reduced phosphorylation of the serine 2 residue of RNA polymerase II.

4.1.2.7 Gene expression analysis

Q-PCR technique, described in details in section 2.12, was used to assess the mRNA levels. The time-course in the period 24 to 120 hpf for CDK9 was assessed in the whole embryo (section 2.12.1) and in isolated embryonic hearts (section 2.12.2) and adult (6 month age) hearts. mRNA levels of CDK9, LARP7, GATA4, 5 and 6, MEF2C, TBX5 and NKX2.5 following flavopiridol exposure and morpholino injection were also assessed in the whole embryo at 48 and 96 hpf.

I performed an assessment of various housekeeping genes in these experiments.

Ef1α was found to be constant during normal development and was chosen to enable quantitation of CDK9 gene expression between 24-120 hpf. Whereas I identified that the gene β-actin remained the most stable during exposure to

flavopiridol and in the embryos treated with MO-CDK9 (figure 2.11 in Chapter 2). I, therefore, used the house keeping gene ß-actin to enable quantitation of gene expression according to the amount of cDNA loaded for both flavopiridol and MO-CDK9 treated embryos.

4.1.2.8 Protein analysis

Polyacrylamide Gel Electrophoresis and Western blotting were used for semi-quantitative analysis of CDK9 protein, assessed by densitometric quantitation of the membrane bands (see Section 2.11.8 for a full explanation). To correct for variations in the total amount of total protein loaded on the membrane, the amounts of target protein (CDK9 or P-Ser2) were normalised to a loading control protein that is highly unlikely to change in the various embryo groups. In all experiments with Flavopiridol, the loading control protein used was vitellogenin. Vitellogenin is the most abundant egg yolk protein, present as fragment of different size (the band showed in figure 4.1.8 correspond to the 110kDa fragment) used as source of nutrients in the early development (Bugel *et al.*, 2013). Before being blotted, the membrane was stained in Red Ponceau (Romero-Calvo *et al.*, 2010) for 5 min, then washed in tap water until the red bands clearly appear. A digital image of the membrane was then captured by CCD cameras and bands were quantified as above. In later experiments, all those involving the injection of morpholinos, the structural protein tubulin was used as loading control.

Anti-CDK9 antibody was produced in rabbit (C12F7, Cell Signalling Technology). Anti-P-Ser2 was produced in mice (ab24758, Abcam). Both were diluted 1:1000 in PBS.

4.1.2.9 Statistics

Data were presented as means ± standard error of the mean (SEM). ANOVA test followed by Bonferroni post-hoc test, were used to compare means within and between groups (see also Section 2.15).

4.1.3 Results

4.1.3.1 CDK9 gene expression during normal zebrafish development

CDK9 mRNA was detected in the whole embryo from 24 to 120 hpf (figure 4.1.1A). Significant variations were observed. The CDK9 mRNA level increased significantly between 24 and 72 hpf ($p<0.01$) and then decreased significantly at 120 hours of development ($p<0.01$). CDK9 mRNA was clearly detected also in isolated hearts at 48, 96, 120 hpf and in the adult (6 months) heart. The highest concentration was detected at 48 and 96 hpf, then the CDK9 mRNA level decreased significantly in the embryonic, at 120 hpf, and in the adult heart ($p<0.01$) (figure 4.1.1B).

4.1.3.2 Pharmacological inhibition of CDK9

4.1.3.2.1 Embryo survival following exposure to flavopiridol

Embryo survival was assessed at 6, 24, 48, 72, 96 after exposure to flavopiridol (figure 4.1.2), that started at 24 hpf. Overall, the survival of embryos at 120 hpf, *i.e.* at 96 hours post-exposure to Flavopiridol 3μM was 77% in the group exposed to the drug compared to the 91% survival in the control group.

4.1.3.2.2 Effect of flavopiridol on whole-embryo and cardiac phenotype

Gross morphological screening showed a significant reduction in total body length of zebrafish embryos exposed to flavopiridol 3μM at 96 hpf compared to the control (figure 4.1.3). H&E analysis and in-vivo images of the zebrafish embryonic heart 96 hpf (figure 4.1.4 A-D) showed pericardial oedema, ranging from mild to severe, evident in up to 50% of embryos exposed to flavopiridol 3μM compared with 5% in controls. A smaller heart was also evident in most embryos exposed to Flavopiridol 3μM compared to controls (figure 4.1.4 C-D). This was clearly shown by the significant reduction in heart-to-total body length ratio (figure 4.1.4 E) in the embryos exposed to the drug.

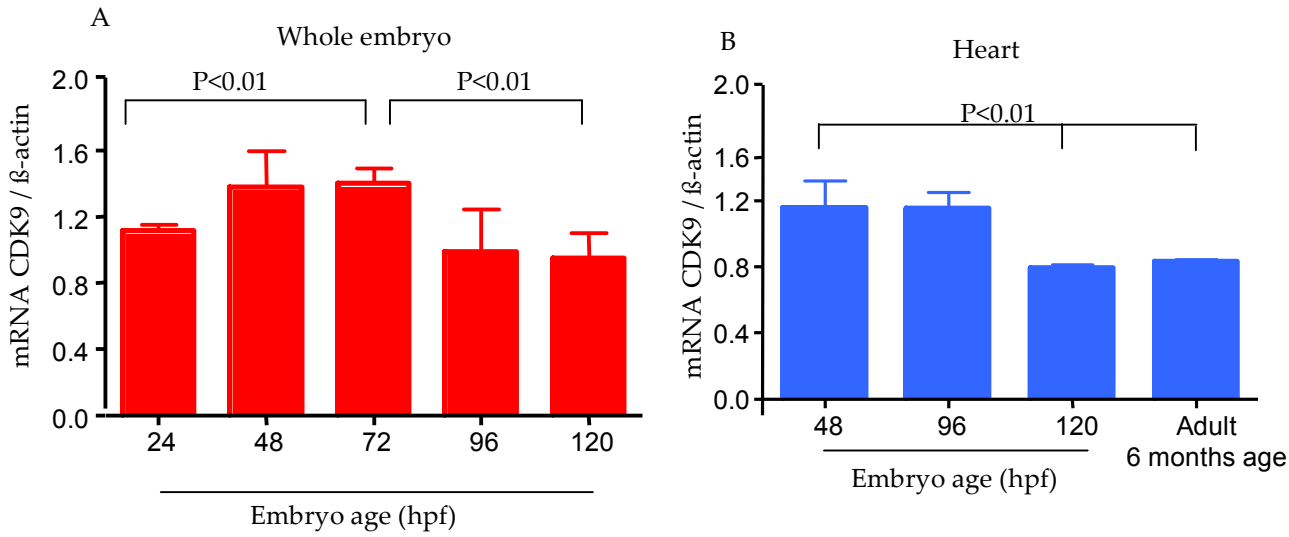

Figure 4.1.1 – Assessment of CDK9 gene expression during normal zebrafish development. This was assessed in whole embryos collected from 24 to 120 hpf (A) and in isolated embryonic hearts at 48, 96, 120 hpf and adult heart (6 months age) (B). Data were compared by one-way ANOVA followed by Bonferroni's multiple comparison test. Each time-course was studied in 1 clutch of eggs, at least 10 embryos from the clutch were used to generate each time point. The data represents an average from studies in 3 clutches of eggs.

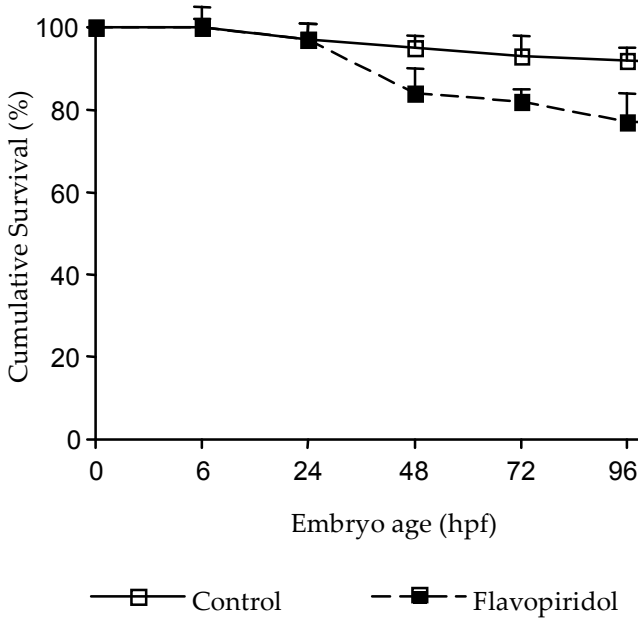

Figure 4.1.2 - Cumulative survival curve following exposed to flavopiridol 3μM. Embryos from the same clutch of eggs were continuously exposed to flavopiridol 3μM from 24 to 120 hpf. Surviving embryos were counted at 6, 24, 48, 72, 96 hpf. Mean ± SEM, N= 4 experiments with at least 70 embryos per group.

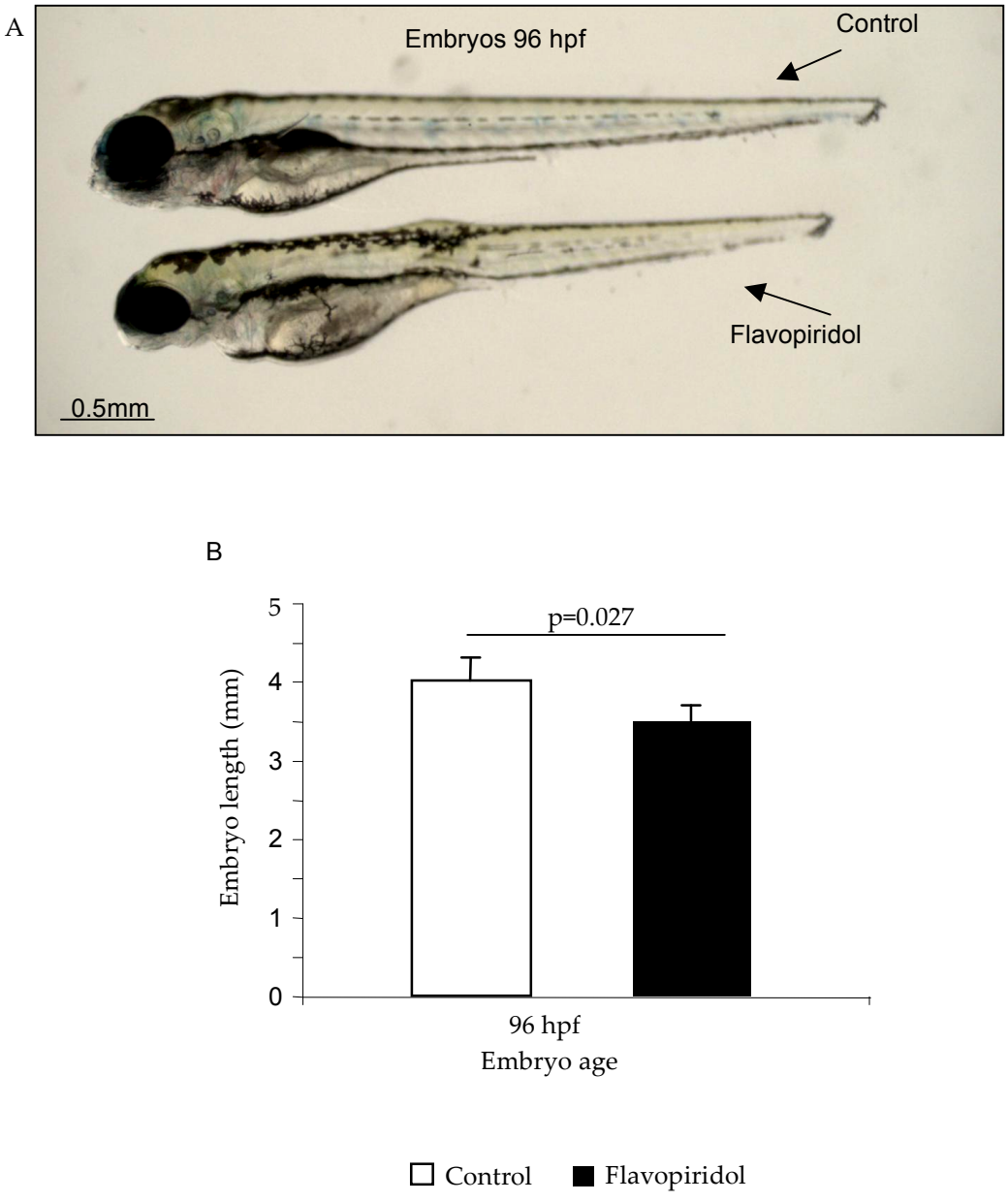

Figure 4.1.3 - Effects of Flavopiridol on zebrafish embryo total body length. Panel A – Images showing the difference between embryos 96hpf control or exposed to the drug. This is graphically reported in Panel B, where embryo length was measured as the distance from the snout to the posterior tip of the notochord. The experiment was performed in at least 5 embryos per group. N=3 experiments, for each experiment embryos derived from the same clutch of eggs. Student's t-test was used to assess difference between the two groups of embryos.

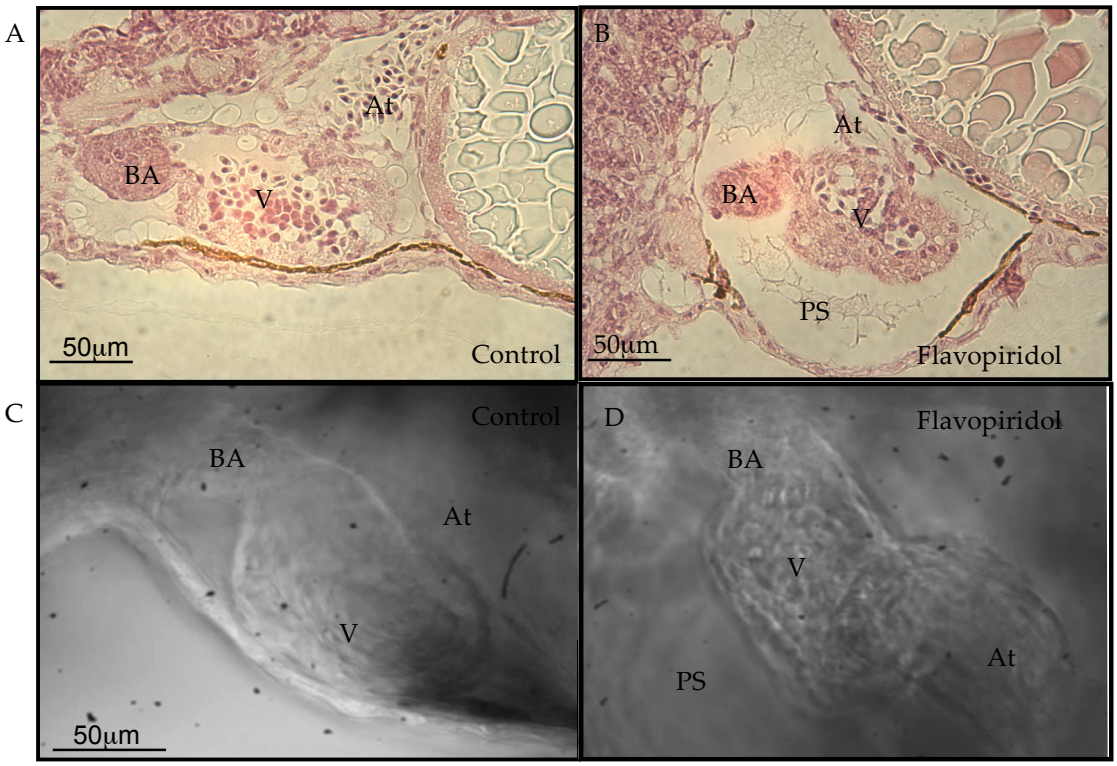

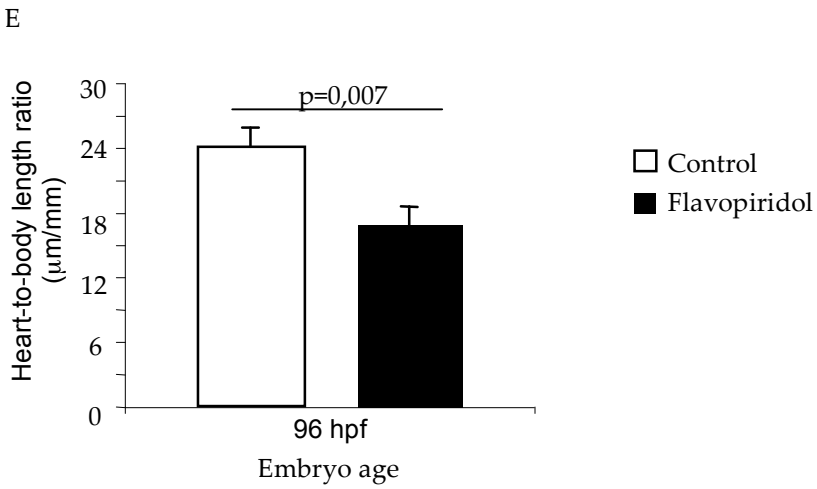

Figure 4.1.4 - Effect of Flavopiridol 3µM on the zebrafish embryonic cardiac phenotype. H&E sections showing the reduced size and the extensive pericardial edema in the heart exposed to the drug (B) compared to control (A). Heart images of in-vivo ventricle in diastole show pericardial edema again and a reduced ventricle area in the ventricle exposed to the drug (D) compared to control (C). Images were captured in embryo 96hpf. E- Graph showing the heart-to-total body length ratio, significantly reduced in embryos exposed to the drug compared to control. The experiment was performed in at least 5 embryos per group. N=3 experiments, for each experiment embryos derived from the same clutch of eggs. PS=pericardial sac, V=ventricle, At=atrium, BA=bulbus arteriosus.

4.1.3.2.3 Effects of flavopiridol on cardiac function

During normal development, zebrafish embryos showed a progressive increase in heart size, measured as diastolic area in-vivo, in the period 72-120 hpf (figure 4.1.5 A), with a maximum diastolic area of 12.5 $x10^3$ μm^2 by 120hpf. Conversely, embryos exposed to flavopiridol 3μM showed a significantly reduced heart size by 20% at 72 hpf and by 55% at 120 hpf compared to controls. Ejection fraction was also significantly reduced in embryos exposed to flavopiridol 3μM (mean of 7% at 72 hpf and 50% at 120 hpf) compared to controls (figure 4.1.5 B).

4.1.3.2.4. Effects of flavopiridol on cardiomyocyte proliferation

While total ventricle cardiomyocyte number (TVCn) increased progressively during development in controls, embryos exposed to flavopiridol 3μM showed no difference in the number of cardiomyocyte between 72hpf and 120hpf. Values for TVCn, were significantly lower in hearts exposed to flavopiridol 3μM compared to controls at 72 hpf (20% lower) and at 120 hpf (45% lower), (figure 4.1.6 A and B).

Exposure of embryos to flavopiridol 3μM also significantly reduced the number of mitotic cardiomyocytes in isolated hearts (figure 4.1.6 A and C) as illustrated by a 55% and 65% reduction, respectively at 72 and 120 hpf, in the number of Phospho-histone H3 positive nuclei in embryos exposed to the drug.

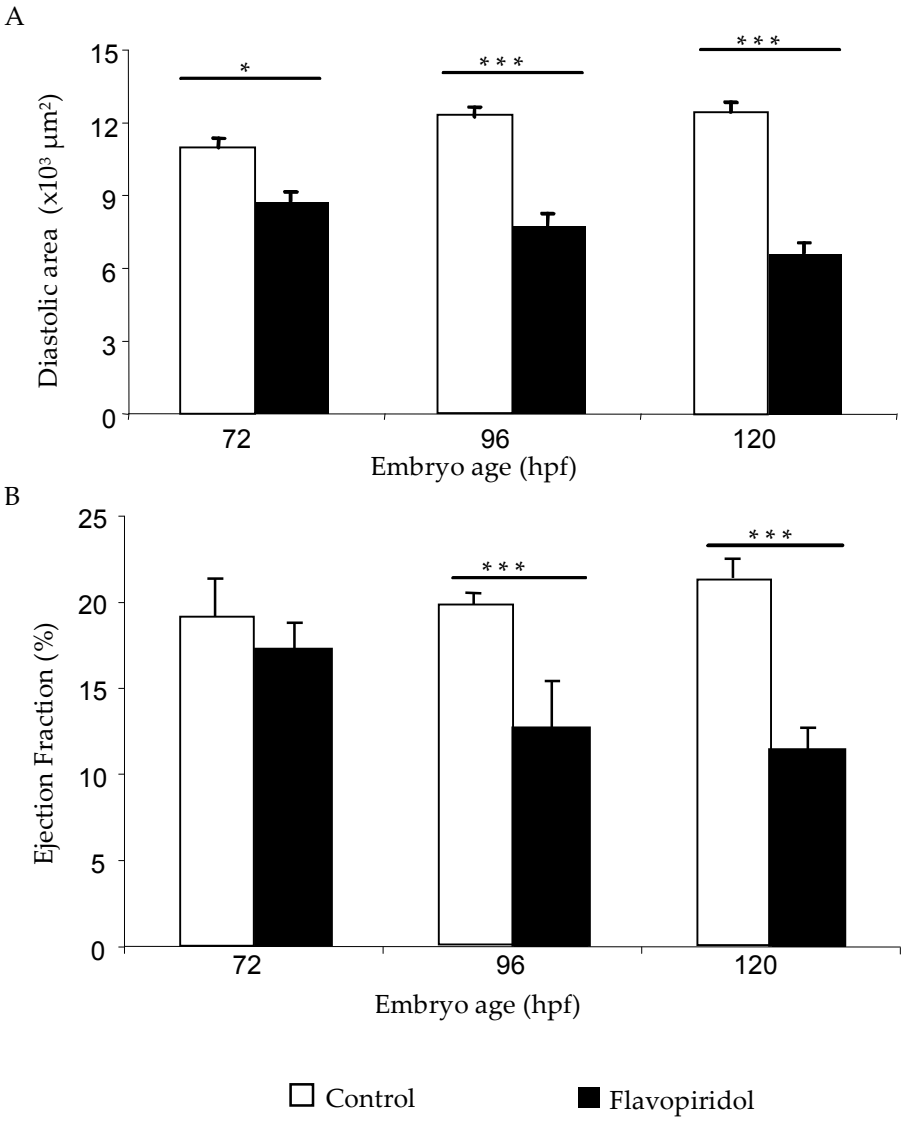

Figure 4.1.5 - Effect of flavopiridol on the zebrafish embryonic heart ventricle. Embryos from the same clutch of eggs were continuously exposed to flavopiridol 3μM from 24 to 120 hpf. Ventricle diastolic area (A) and ejection fraction (B) were assessed in the same embryos, control and exposed to the drug, at 72, 96 and 120 hpf. N=3 experiments, *=p<0.05, **=p<0.01, ***=p<0.001. Two-way ANOVA test for repeated measures was used to compare means.

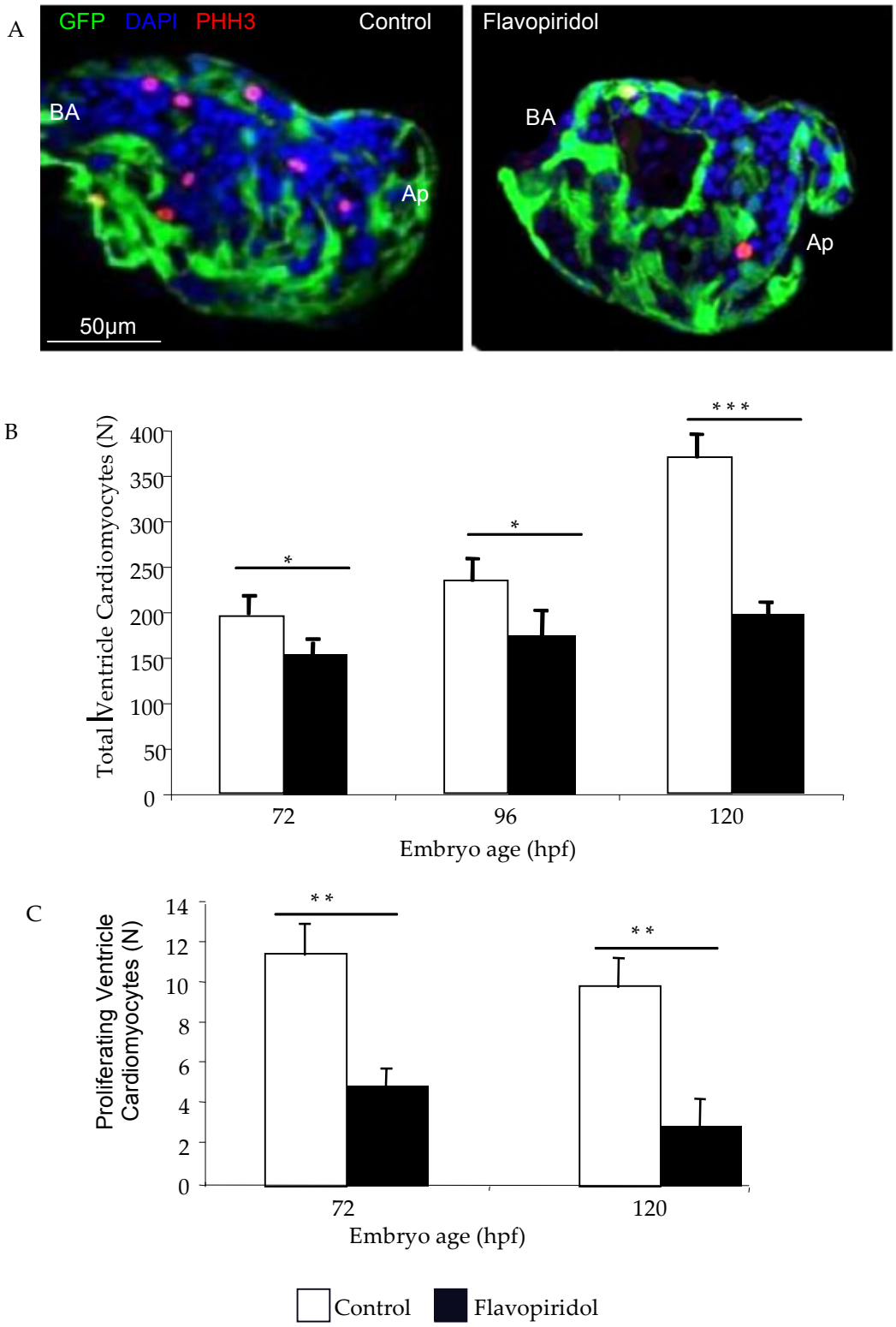

Figure 4.1.6 - Effects of flavopiridol on ventricle cardiomyocyte proliferation. Embryos from the same clutch of eggs were continuously exposed to flavopiridol 3µM from 24 to 120 hpf. Hearts from at least 5 embryos per group, control or exposed to the drug, were dissected and stained with DAPI for total cardiomyocyte number at 72, 96 and 120 hpf (A) or anti PHH3 for mitotic cardiomyocytes number analysis at 72 and 120 hpf. Representative confocal images of stained cmlc2;GFP hearts are shown in the panel A, the blue DAPI staining marks the nuclei while the red PHH3 positive nuclei mark proliferating cardiomyocytes. Mean±SEM, N=3 experiments, *=p<0.05, **=p<0.01 ***=p<0.001, two-way ANOVA test was used to assess differenc between means. Key- BA= bulbus arteriosus, Ap=Apex

4.1.3.2.5 Effects of flavopiridol on gene expression

CDK9, LARP7, GATA4 and TBX5 showed a significant decrease in mRNA level at 48 hpf in embryo exposed to flavopiridol 3μM compared to controls ($p<0.05$), figure 4.1.7. MEF2c was also slightly reduced in embryo exposed to the drug, while other genes did not change. At 72 hpf, the mRNA level of TBX5 was still significantly reduced in embryos exposed to the flavopiridol compared to controls. All other genes, excluding NKX2.5, were also slightly reduced following exposure to flavopiridol. Whereas at 96 hpf we assisted to a significant increase in the mRNA level of GATA4, 5 and 6, and NKX2.5 and to a slight increase of CDK9 and MEF2c in embryos exposed to the drugs compared to controls (figure 4.1.7).

4.1.3.2.6 Effects of flavopiridol on protein expression

The activity of CDK9, detected by the level of the phosphorylated form of the serine-2 residue of RNAPII (P-Ser2), in whole embryos control increased between 48 and 72 hpf and then decrease at 96 hpf at the level detected at 48 hpf. In embryos exposed to flavopiridol 3μM, the P-Ser2 was significantly reduced of approximately 50% at 48hpf and 70% lower at 72hpf compared to controls (figure 4.1.8 A and B). However, at 96 hpf the level of P- Ser2 increased in embryos exposed to the drug to the same level detected in controls.

CDK9 protein was detected at all developmental time points studied. The level of the CDK9 protein did not change in control group over the time period. In embryos exposed to flavopiridol 3μM the level of CDK9 at 48 hpf was the same as the controls. However, CDK9 was found to be progressively and significantly increased at 72 and 96 hpf in embryos treated with flavopiridol 3μM compared to controls (figure 4.1.8 C).

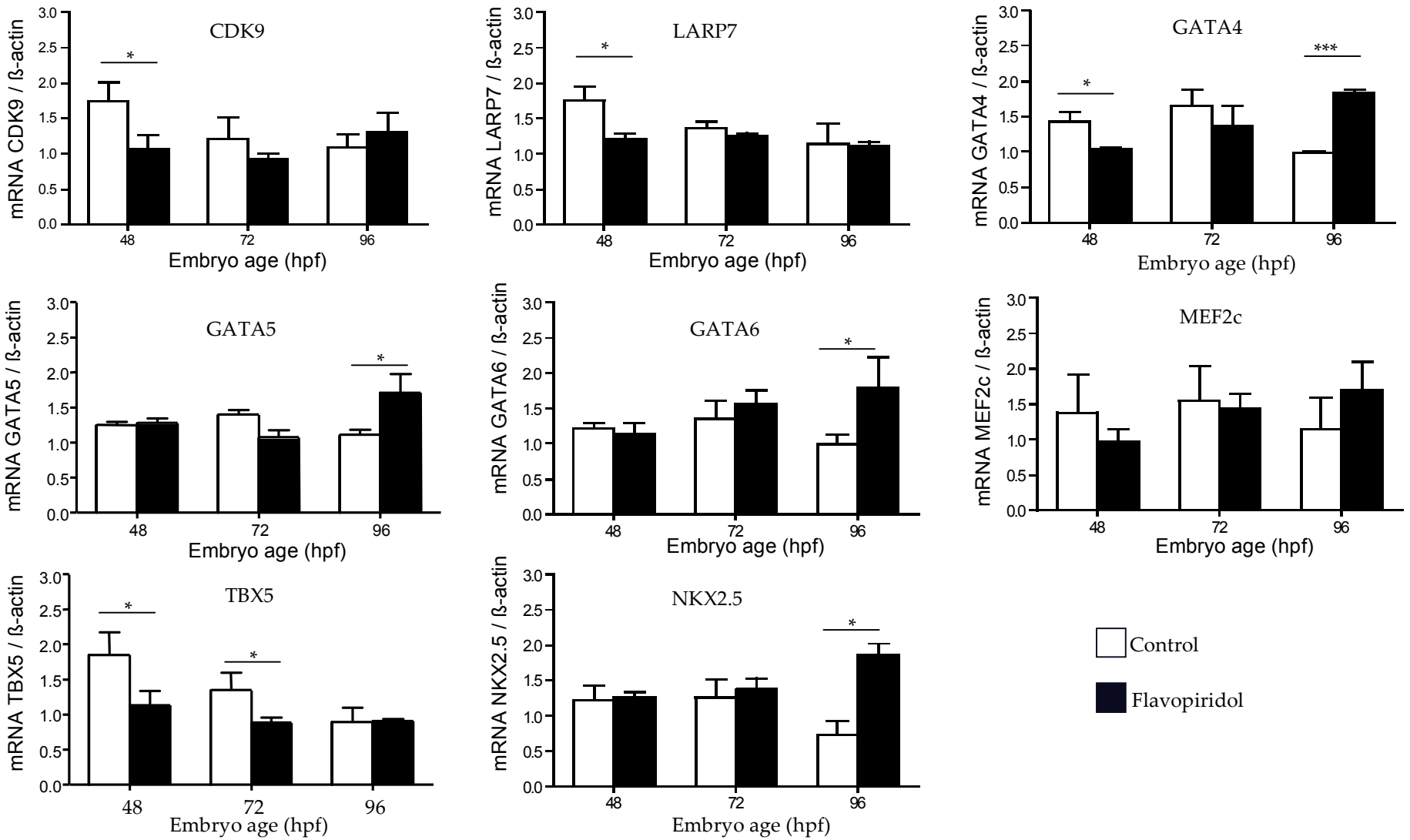

Figure 4.1.7 - Effects of Flavopiridol on the gene expression. Embryos from the same clutch of eggs were continuously exposed to flavopiridol 3μM from 24 to 120 hpf. At 48, 72 and 96 hpf mRNA was extracted from whole embryos (at least 10 embryo per group). Level of CDK9, LARP7 and relevant gene for cardiac development GATA4, 5 and 6, MEF2c and TBX5 were detected by Q-PCR analysis. mRNA were normalised to the housekeeping gene ß-actin. N=3 experiments, *=p<0.05, ***=p<0.001, two-way ANOVA test followed by Bonferroni's post-hoc test.

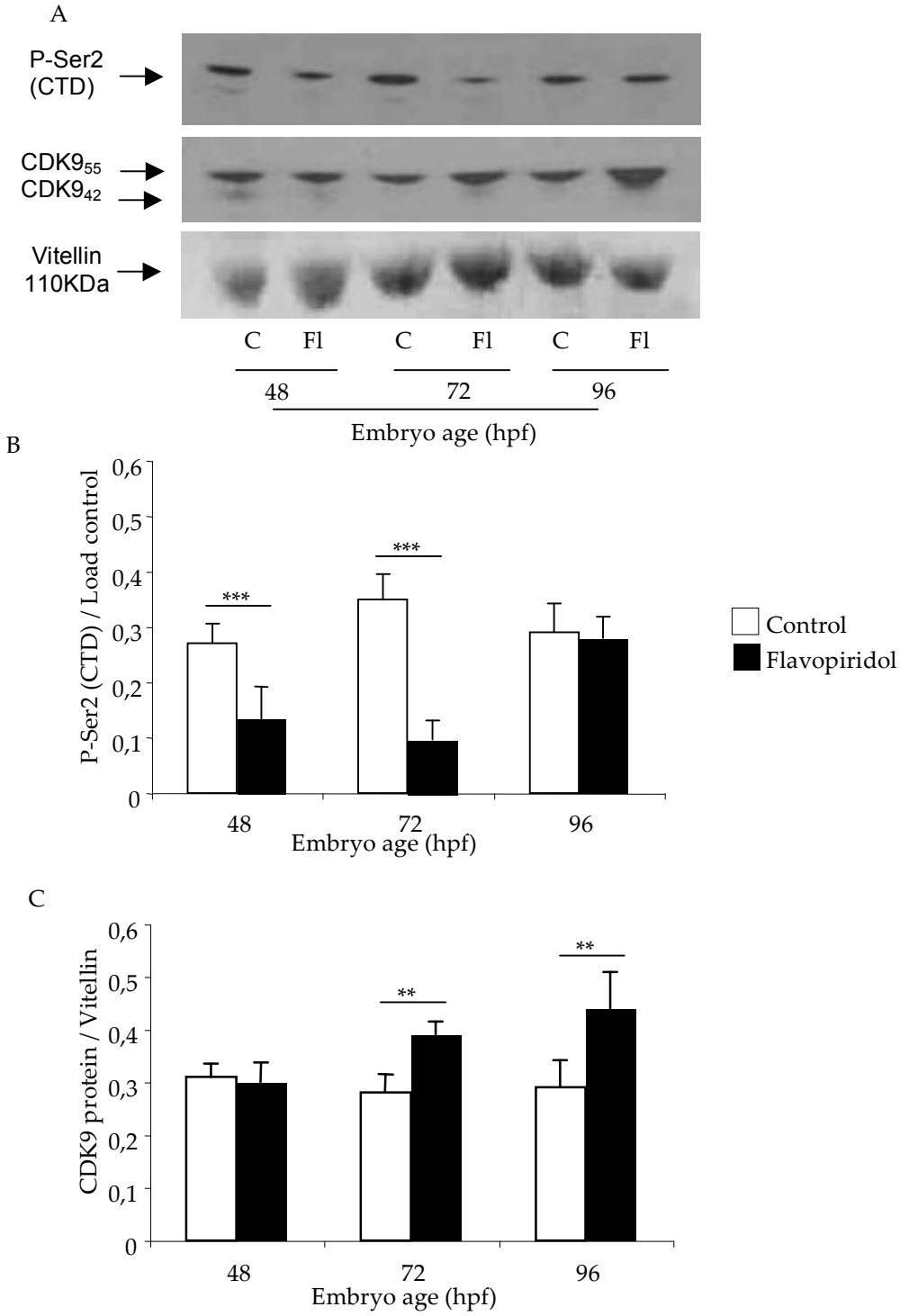

Figure 4.1.8 - Effects of Flavopiridol on the protein expression. Embryos from the same clutch of eggs were continuously exposed to flavopiridol 3μM from 24 to 120 hpf. At 48, 72 and 96 hpf protein were extracted from whole embryos and separated by gel electrophoresis followed by western blot (A). Membrane were blotted against Phospho-Ser2 (CTD) (B) or CDK9 (C). Protein level are normalised to vitellin (fragment 110KDa) to compare control and treated group at the same time point. N= 3 experiments, at least 5 embryo per group were used in each experiment, **=p<0.01, ***=p<0.001, two-way ANOVA test was used to compare means, followed by Bonferroni's post-hoc test.

4.1.3.3 Genetic reduction/inhibition of CDK9 by Morpholino treatment

4.1.3.3.1 Embryo survival following MO-CDK9 injection

Embryo survival (figure 4.1.9) was assessed at 24, 48, 72, 96 and 120 hpf and showed reduced survival in all MO injected embryos (translation blocking, splice-site and mismatches) compared to non-injected controls. Overall by 120 hpf survival was 47% in MO-CDK9transl group, 87% in MO-CDK9mism and 77% in MO-CDK9splice. These striking differences in mortality occurred despite a 5 times lower concentration of translation-blocking MO than MO-CDK9splice.

4.1.3.3.2 Effects of MO-CDK9 on CDK9 transcription and protein expression

The MO-CDK9mismatch did not produce significant difference in CDK9 expression compared to control non-injected embryos.

The MO-CDK9splice, that blocks the formation of the mRNA, produced a 70% and a 45% reduction of CDK9 mRNA in the whole embryo, respectively at 48 hpf and 96 hpf, compared to controls (figure 4.1.10 A). The MO-CDK9transl caused about a 20% reduction of CDK9 protein in whole embryos compared to control, as assessed at 48 and 96 hpf (figure 4.1.10 B). Although the low reduction in CDK9 protein in embryos injected with CDK9trans, the mortality observed was very high in these embryos at 120 hpf. Therefore, it was decided to use only MO-CDK9splice for further experiments of CDK9 knockdown.

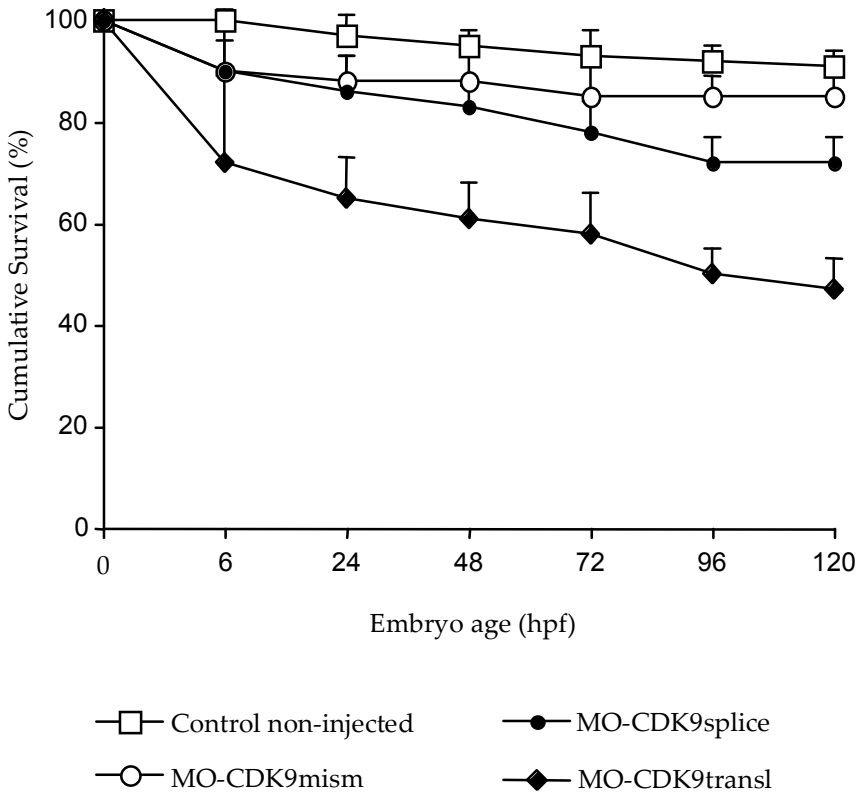

Figure 4.1.9- Cumulative survival curve following CDK9 genetic knockdown. Zebrafish eggs from the same clutch were injected at 1-2 cell stage with CDK9 morpholino mismatch, splice or translation blocking. Surviving embryos were counted at 6, 24, 48, 72, 96 and 120 hpf. Non-injected group represent a basic control to for the egg quality. N=4 experiments, at least 60 embryos were included in each group.

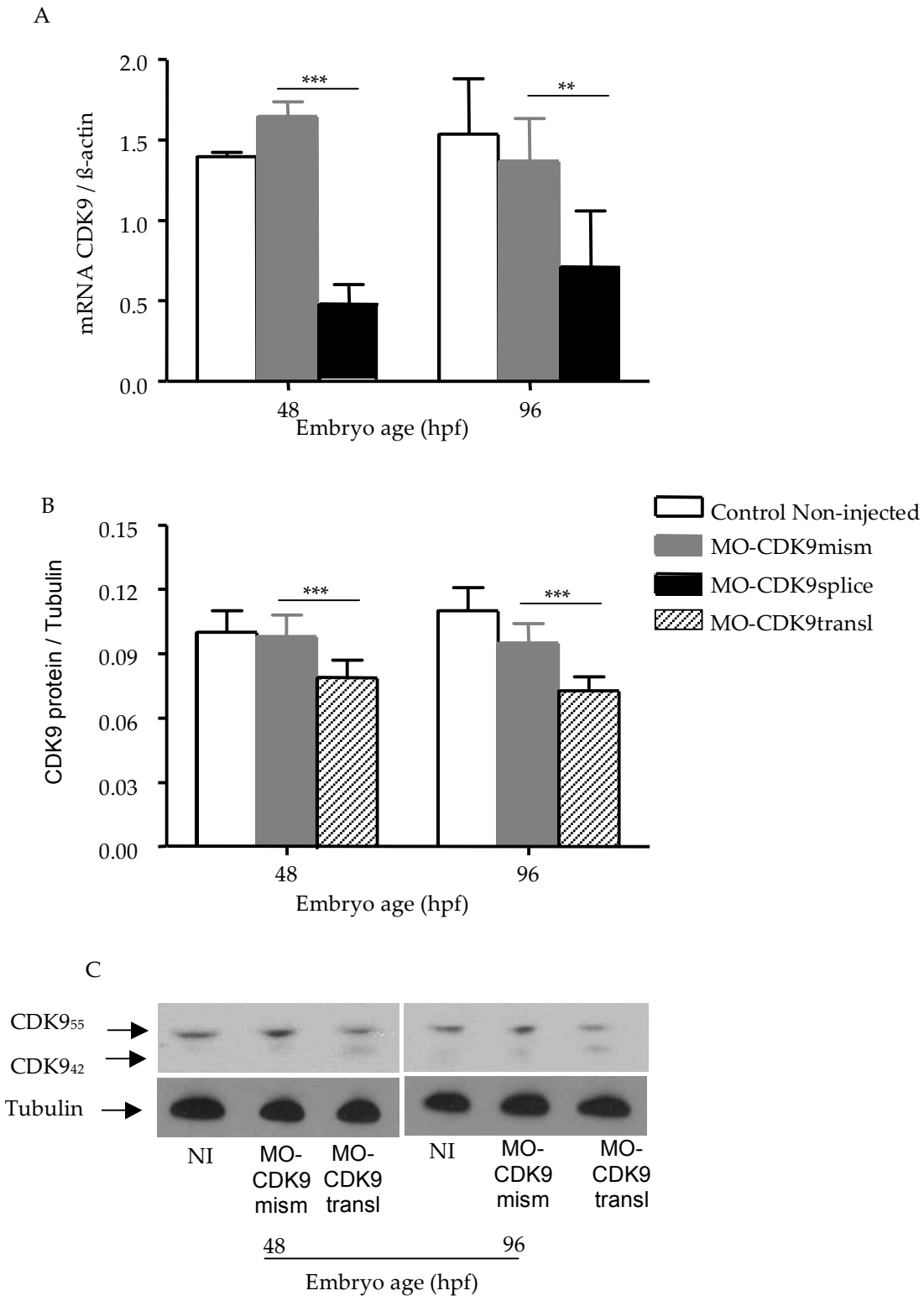

Figure 4.1.10 – Effect of MO-CDK9 injection on the CDK9 expression. CDK9 mRNA (A) and protein (B) level were assessed at 48 and 96 hpf and were significantly reduced following injection of MO-CDK9splice blocking and MO-CDK9 translation blocking, respectively. Panel C shows western blot membranes with the CDK9 isoform of 55KDa more abundant than the smaller one (42KDa). ß-actin was used to normalize mRNA level, while tubulin was used to normalize protein level. N=3 experiments, at least 10 embryos per group, **=p<0.01, ***=p<0.001, one-way ANOVA test was used to compare means, followed by Bonferroni's post-hoc test. Key: NI – Control non-injected

4.1.3.3.3 Characterisation of the phenotype following MO-CDK9 injection

The phenotypes of the whole embryo and heart were assessed at 72hpf following injection of the CDK9 morpholino. The different phenotypes are reported graphically in figure 4.1.11 and as images in figure 4.1.12. Phenotypes of MO-CDK9 mismatch were not affected compared to controls (figure 4.1.11 and 4.1.12 a & b). In contrast, the MO-CDK9splice (figure 4.1.11 and 4.1.12 c) caused a number of abnormalities in whole embryos: deformity of body, trunk and tail curvature that produced evident difficulties in swimming, microcephaly, pericardial oedema, low circulation and a clear developmental delay compared to MO-CDK9mism group. The heart was abnormal: cardiac chambers had a reduced size and often formed a continuous tubular structure, with absence of chamber switching and ballooning. These embryo contained blood islands mainly in the pericardial sac and also around the yolk sac. Compared to the MO-CDK9splice, the MO-CDK9transl caused more frequent and more profound abnormalities (figure 4.1.11 and 4.1.12 d). Most of these embryos did not hatch and development ceased at an early stage as shown by persistence of an intact yolk sac. The heart was reduced in size and had a stringy appearance, when present, without any clear well-defined chamber or valve structure and function. Due to the profound effects of MO-CDK9transl, even at lowest dose, I elected to use only embryos injected with MO-CDK9splice for further experiments reported subsequently in this and other chapters in my thesis.

4.1.3.3.4 Effects of MO-CDK9 on the cardiac function, growth and cardiomyocyte proliferation

Ejection fraction (EF) in embryos treated with MO-CDK9mism was similar to control non-injected (figure 4.1.13 A). Embryonic heart ventricles of embryos injected with MO-CDK9splice had significantly reduced EF throughout development: 10%, 22% and 32% lower than in MO-CDK9mism embryos, respectively at 72, 96 and 120 hpf (figure 4.1.13 A).

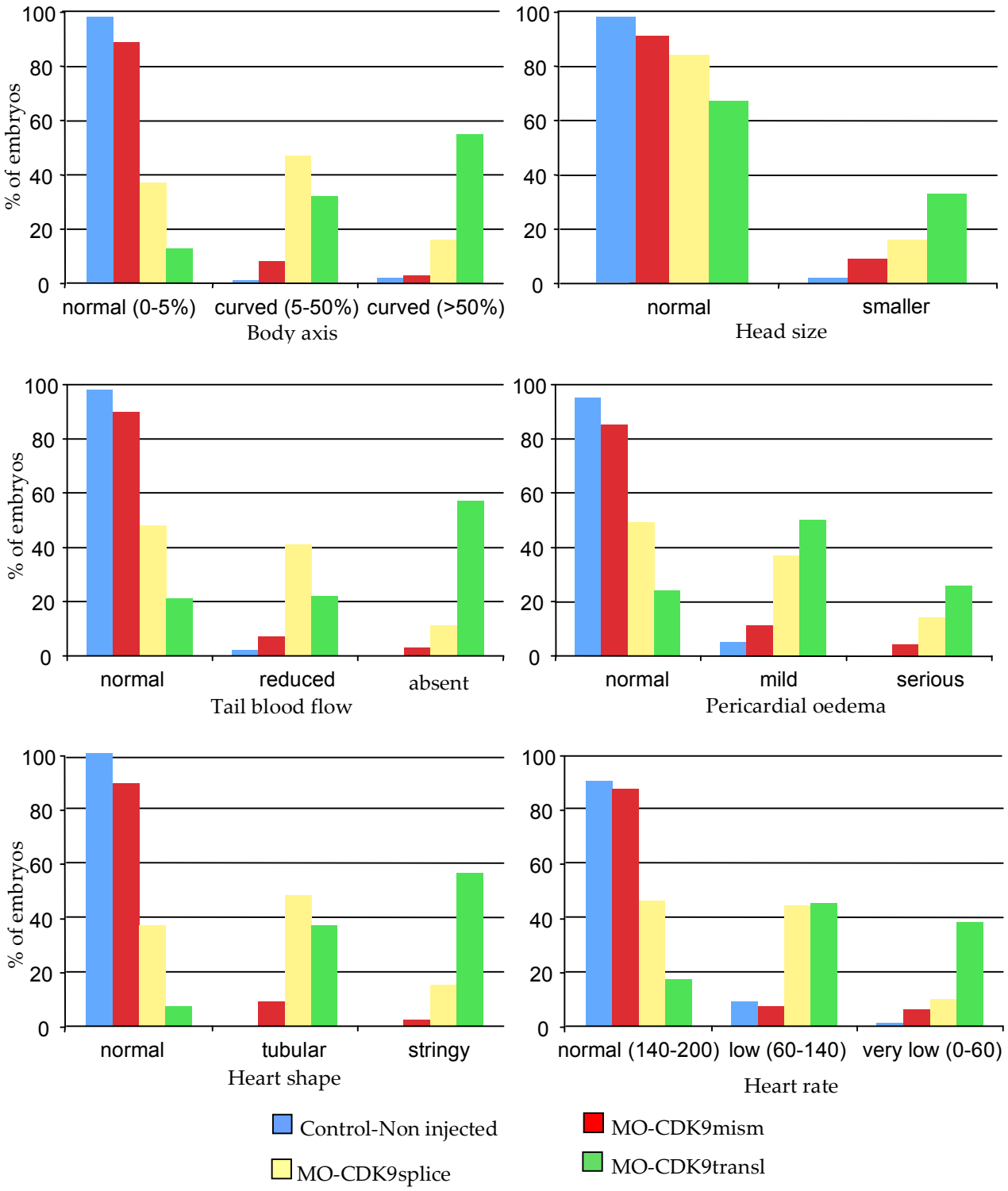

Figure 4.1.11- Characterisation of the 72hpf zebrafish embryo and cardiac phenotype following CDK9 morpholino treatment. Each diagram report on the X axis a specific trait, which phenotypic severity increase from left to right. On the Y axis is reported the percentage of embryos retaining that phenotype. The first two diagrams with body axis and head shape explain the embryo body phenotype while lower diagrams with tail blood flow, pericardial edema, heart shape and heart rate are related to the cardiac phenotype. N=4 experiments, at least 60 embryos were included in each group.

Zebrafish embryos 72 hpf Control non-injected

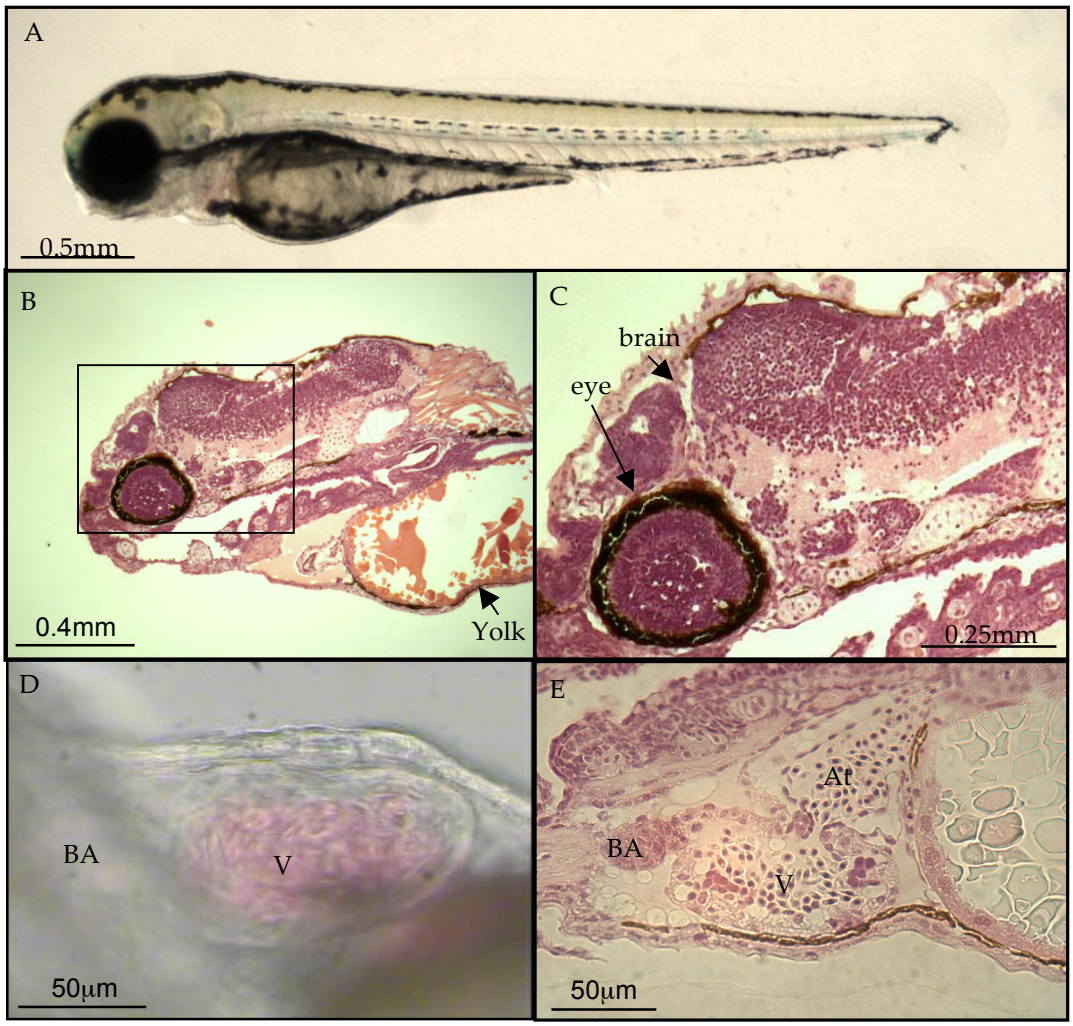

Figure 4.1.12a – Zebrafish embryo control non-injected. In all morpholino experiment, a control group of non-injected embryo is included to take into account of the variability in the quality of the eggs'clutch. Indeed, each clutch is different and can present a different mortality and this must be taken into account in the assessment of the mortality in embryos injected with morpholino. Image A shows an in-vivo zebrafish embryo 72 hpf. Image B shows a H&E stained embryo section at 72 hpf, with the boxed area reported at higher magnification in C. Image D and E show respectively an in-vivo image of the zebrafish beating heart and an H&E stained heart section. Key: BA - bulbus arteriosus, V - ventricle, At - atrium

Zebrafish embryos 72 hpf injected with MO-CDK9mismatch

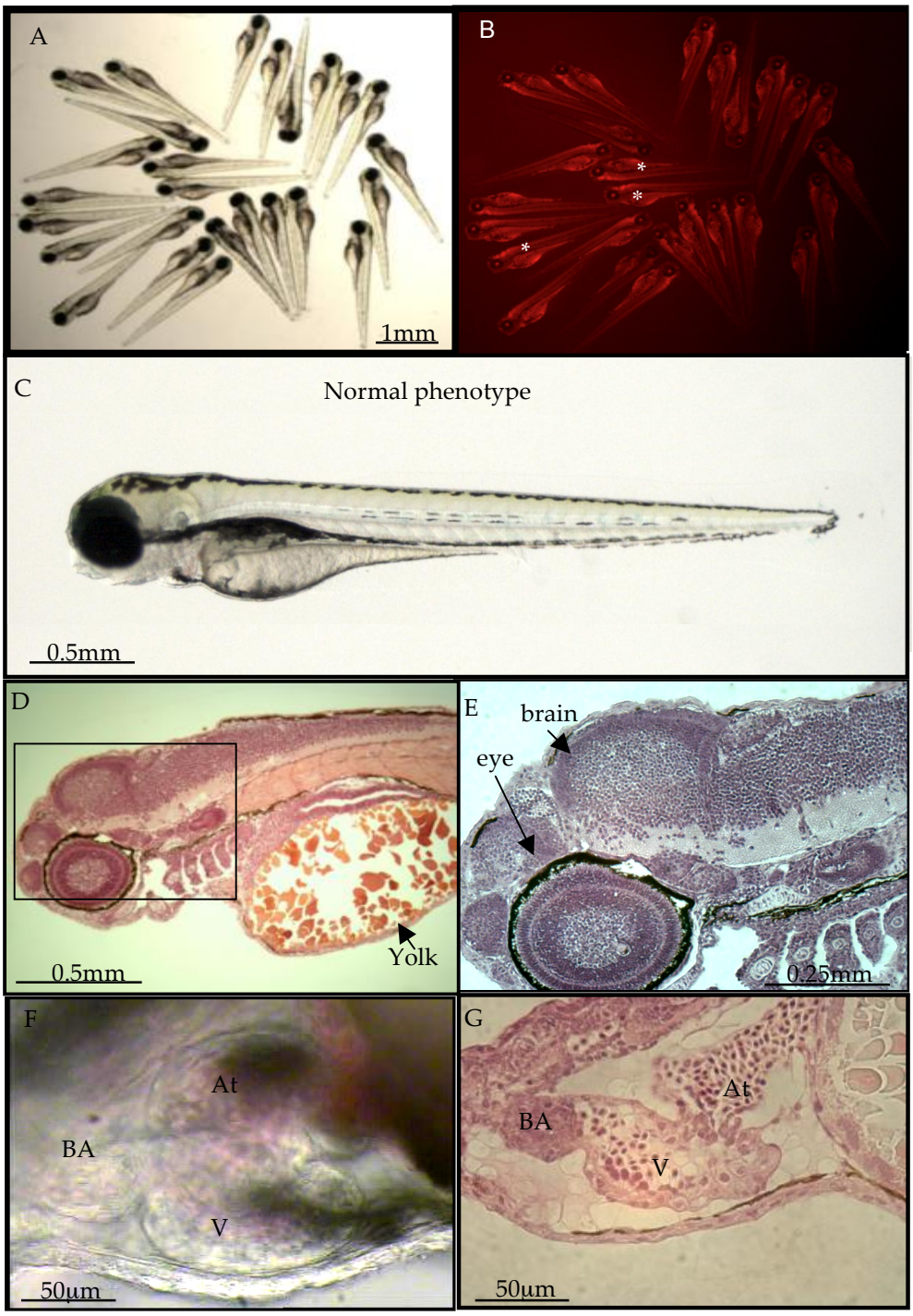

Figure 4.1.12b – Effect of MO-CDK9mismatch injection in the zebrafish embryo. Zebrafish eggs were injected at 1-4 cell stage with this control morpholino. Image A and B show an overall view of embryos at 72 hpf under white and fluorescence light to show the successful injection by the morpholino-linked red lissamine (white star). One of the embryos is shown at higher magnification in image C. Image D shows a H&E stained embryo section, with the boxed area reported at higher magnification in E. Image F shows an in-vivo image of beating heart while image G shows a H&E stained heart section. Key: BA - bulbus arteriosus, V - ventricle, At - atrium

Zebrafish embryos 72 hpf injected with MO-CDK9splice

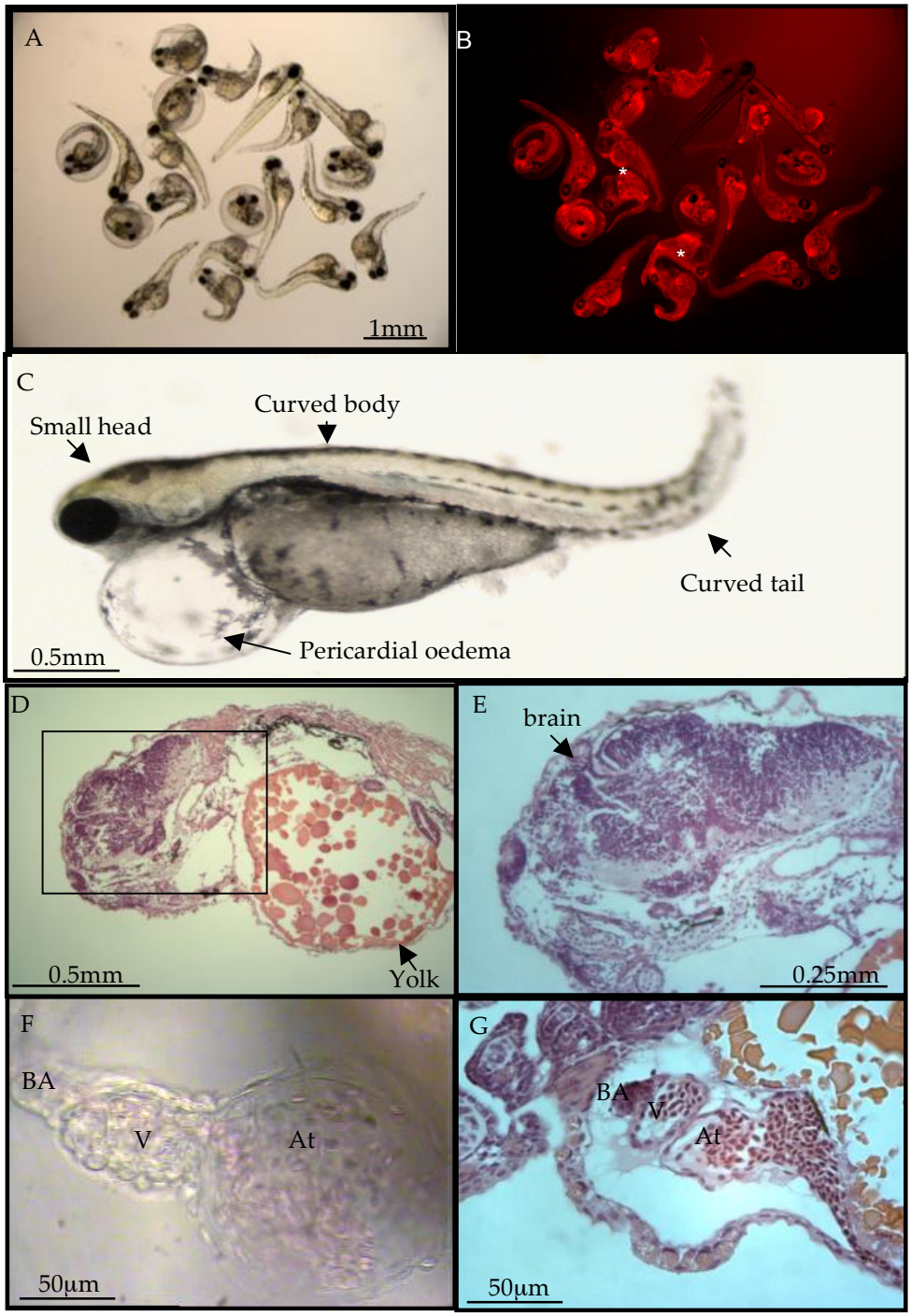

Figure 4.1.12c – Effect of MO-CDK9splice blocking injection in the zebrafish embryo. Zebrafish eggs were injected at 1-4 cell stage. Image A and B show an overall view of embryos at 72 hpf under white and fluorescence light to show the successful injection by the morpholino-linked red lissamine (white star). One of the embryos is shown at higher magnification in image C. Image D shows a H&E stained embryo section, with the boxed area reported at higher magnification in E. Image F shows an in-vivo image of beating heart while image G shows a H&E stained heart section. Key: BA - bulbus arteriosus, V - ventricle, At - atrium

Zebrafish embryos 72 hpf injected with MO-CDK9translation

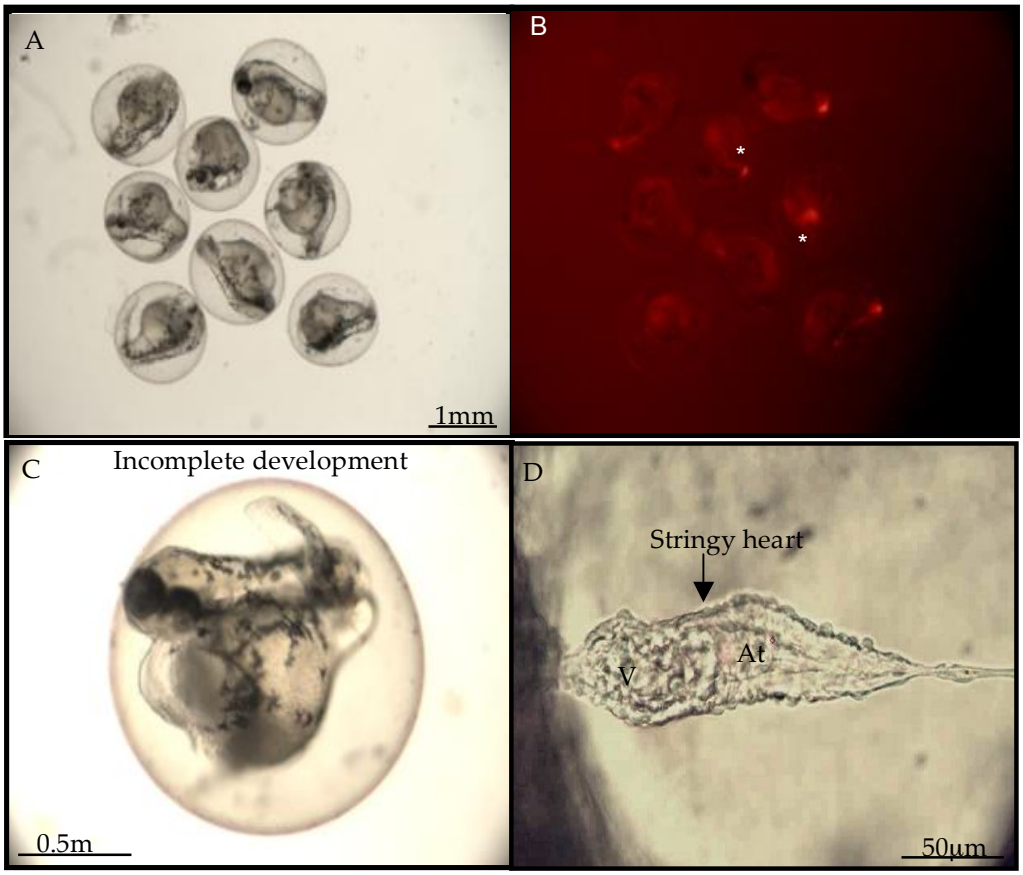

Figure 4.1.12d – Effect of MO-CDK9translation blocking in the zebrafish embryo. Images A and B show an overall view of embryos at 72 hpf under white and fluorescence light to show the successful injection by the morpholino-linked red lissamine (white star). One of the embryos is shown at higher magnification in image C. Image D shows an in-vivo image of beating heart. Key: V - ventricle, At - atrium

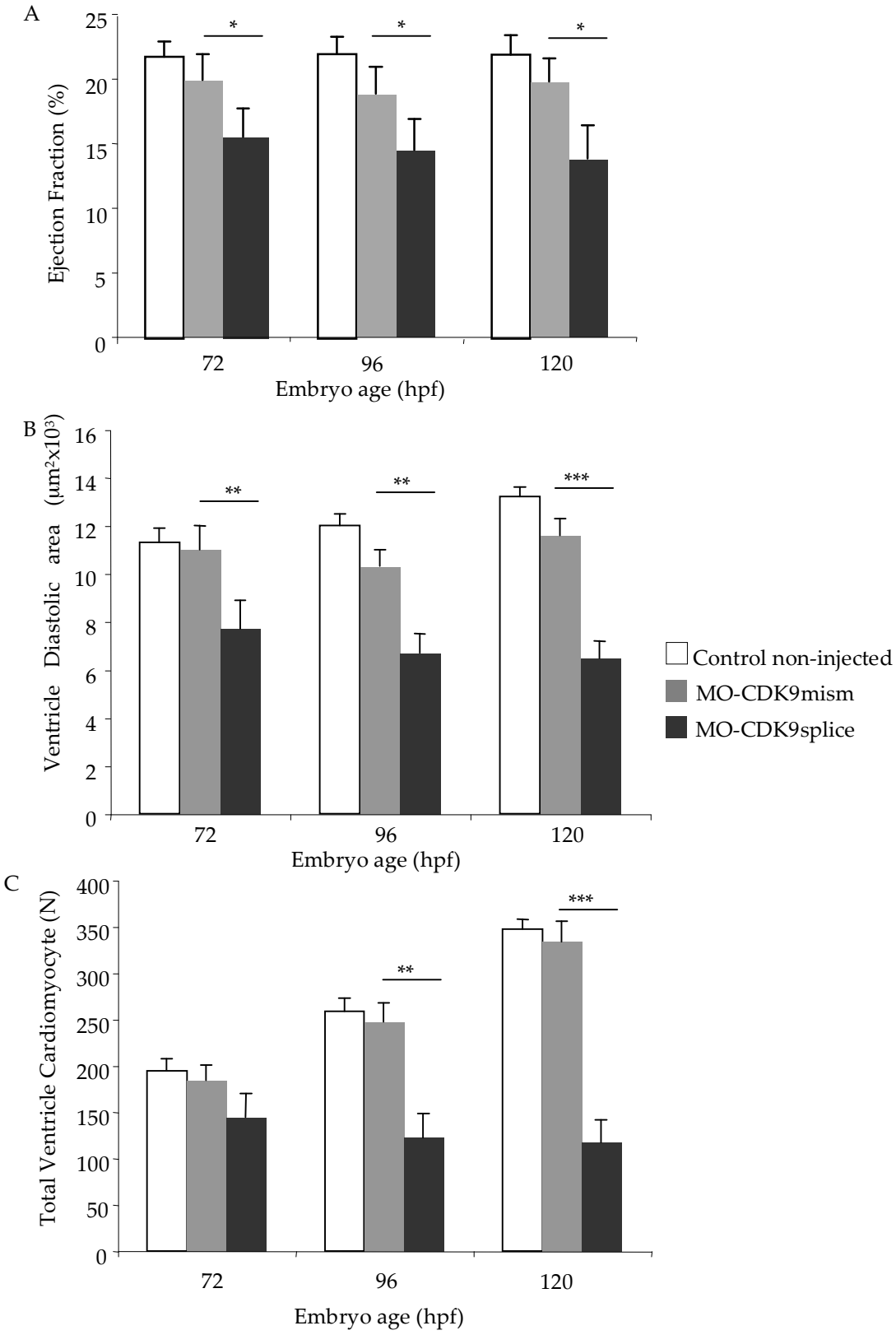

Figure 4.1.13 - Effects of CDK9 genetic knockdown on cardiac structure and function. Embryo eggs 1-4 cell stage from the same clutch were injected with MO-CDK9 splice blocking or MO-CDK9 mismatch. (A) Ejection fraction, (B) Ventricle diastolic area and (C) Total ventricle cardiomyocyte number in the zebrafish embryonic heart were assessed at 72, 96 and 120 hpf. N=3 experiments, *=p<0.05, **=p<0.01, ***=p<0.001,two-way ANOVA test was used to compare means, followed by Bonferroni's post-hoc test.

Cardiac growth, measured simply as ventricular diastolic area (VDA), in the group MO-CDK9mism showed an overall increase between 72 and 120 hpf. This pattern was very similar to non-injected controls (figure 4.1.13 B). Whereas, VDA was significantly reduced in the MO-CDK9splice group of embryos at all time points studied compared to the MO-CDK9mism, with a reduction of about 30% at 72hpf and 96 hpf and 45% at 120 hpf (figure 4.1.13 B). Total ventricle cardiomyocyte number (TVCn) in embryos injected with MO-CDK9mism showed similar values as non injected controls with a similar increase during development from 72 to 120 hpf (figure 4.1.13 C). In contrast embryonic ventricles treated with MO-CDK9splice had significantly lower TVCn compared with MO-CDK9mism with a reduction of 25%, 48% and 70% respectively at 72, 96 and 120 hpf (figure 4.1.13 C).

4.1.3.3.5 Effects of CDK9 MO treatment on whole embryo gene expression

Quantitative PCR analysis for transcription factors genes, markers of cardiac development, and LARP7 were assessed at 48 and 96hpf in embryos treated with MO-CDK9splice and mismatch controls (figure 4.1.14). This analysis revealed reduced level of mRNA of the members of the GATA family and MEF2c at both time points in MO-CDK9splice injected embryos compared to mismatch controls. For GATA 6 and MEF2c this reduction was statistically significant at 96 hpf. LARP7 was also found slightly reduced. The marker of cardiac development TBX5 was elevated, particularly at 96 hpf in embryos injected with MO-CDK9splice compared to mismatch controls. (figure 4.1.14).

4.1.3.3.6 Immunohistochemistry with CDK9 antibody

Immunostaining to detect CDK9 in whole-mount embryos identified fairly ubiquitous presence particularly in the tail region (figure 4.1.15 A). Confocal imaging showed that CDK9 staining forms a linear pattern created by multiple spots along the tail that could coincide with growing vessels. High power images (figure 4.1.15 C) suggest that staining is located in the cytoplasm although some co-location around the nucleus is also evident. CDK9 staining was also present in the

heart although confined in the area of the bulbus arteriosus (figure 4.1.15 B). In embryos injected with MO-CDK9splice blocking, the staining was significantly reduced confirming successful knockdown of protein production throughout the embryo (figure 4.1.15 D).

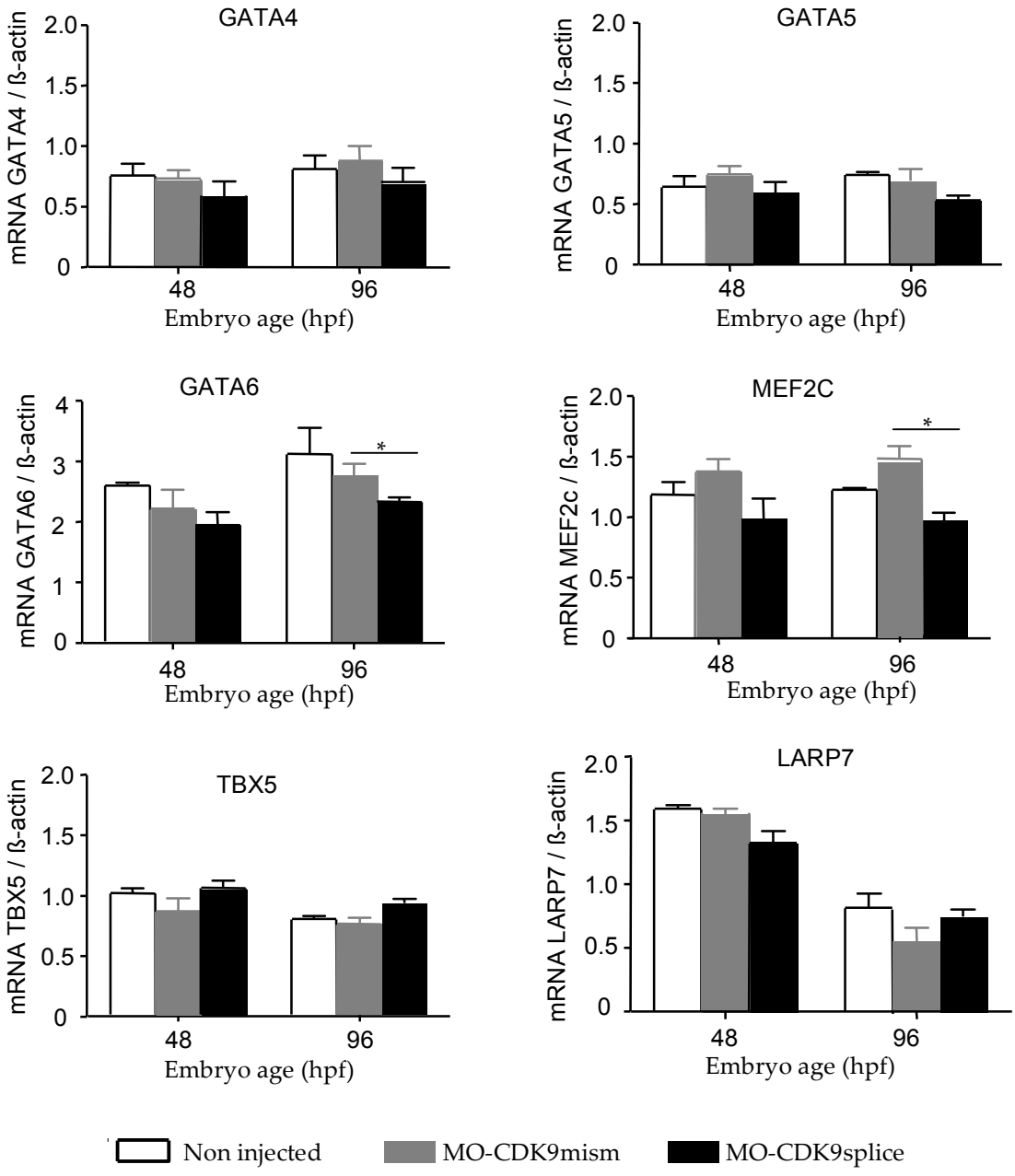

Figure 4.1.14 – Effects of CDK9 genetic knockdown on the gene expression. Embryo eggs 1-4 cell stage from the same clutch were injected with MO-CDK9 splice blocking or MO-CDK9 mismatch. At 48 and 96 hpf, mRNA was extracted from whole embryos (at least 10 embryo per group). Level of relevant gene for cardiac development GATA4, 5 and 6, MEF2c, TBX5 and LARP7 were detected by Q-PCR analysis. mRNA level were normalised to the housekeeping gene ß-actin. N=3 experiments, *=$p<0.05$, two-way ANOVA test followed by Bonferroni's post-hoc test.

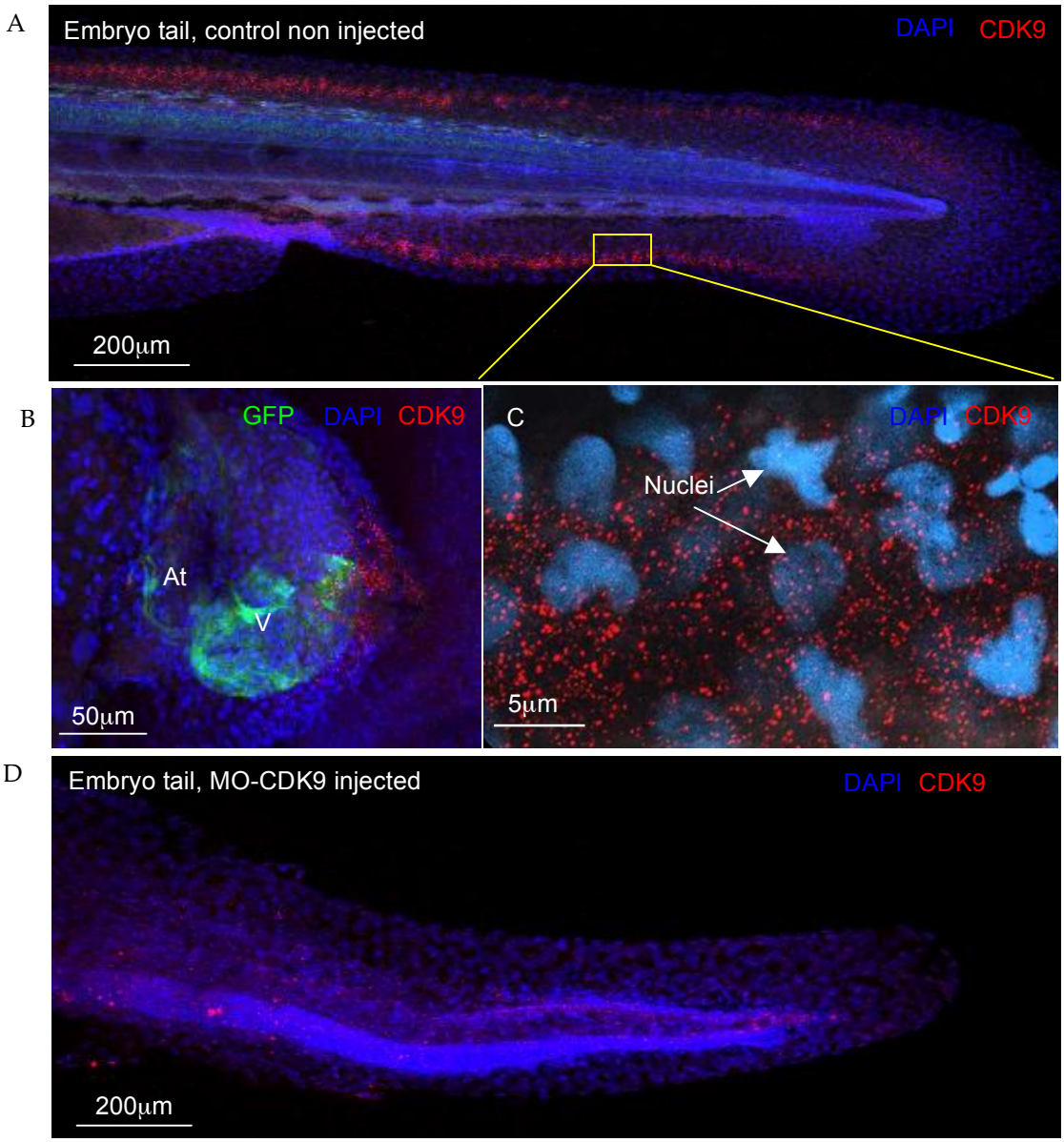

Figure 4.1.15 – CDK9 immunohistochemistry in a whole mount zebrafish embryo. Confocal images of cmlc2:GFP zebrafish embryo 72 hpf immunostained with anti-CDK9 antibody, in red, and counterstained with DAPI. In control embryos (A), the staining showed a diffused presence of CDK9 in both nucleus and cytoplasm through the whole embryo body, here presented only in the tail. The boxed area is shown at higher magnification in C. While image B shows the GFP heart with anti-CDK9 staining in the area of the bulbus arteriosus. In the image D, embryos injected with MO-CDK9splice did not show the red pattern observed in A.

4.1.4 Discussion

4.1.4.1 Role and expression of CDK9 in zebrafish during normal development

In the whole zebrafish embryo, CDK9 mRNA levels were found to be similar at 24, 96 and 120 hpf. However, higher concentrations were detected at 48 and 72 hpf. While this suggests a key constitutive role for this molecule throughout development, the increase observed in some stages suggest also a specific role of CDK9 in some developmental processes. Constitutive genes may be defined as genes that are equally expressed in all cells of an organism, and under most if not all environmental conditions, characterized by an unregulated promoter (Geisel, 2011). Indeed, Liu and Rice (Liu and Rice, 2000) found that CDK9 gene promoter possesses high constitutive activity and contains features characteristic of a housekeeping gene, including GC-rich sequences and absence of a functional TATA element (Garriga *et al*., 2003). Indeed, human fibroblasts and glioblastoma cells demonstrate the same levels of CDK9 throughout their cell cycle and also when cells exit the cell cycle and differentiate along various lineages. Therefore, CDK9 does not appear to be regulated by the cell cycle phase. However, Sano et al., (Sano *et al*., 2002) found that CDK9 protein and activity decline with increasing age in mouse and this finding are similar to our data observed particularly in the heart where CDK9 level decreased at later developmental stage.

In our study, while abundant levels of CDK9 transcripts were found at all three embryonic time points, P-Ser2 was not detected at the earliest time point, 48 hpf.

4.1.4.2 Pharmacological modulation of CDK9: Impacts on global and cardiac development and on gene expression

CDK9 has been manipulated in the zebrafish embryo in different ways. Firstly, CDK9 inhibition was achieved by exposure to flavopiridol which acts by competing with ATP at the ATP-binding site of CDK9. Flavopiridol has been previously tested in zebrafish embryos. A dose of 35μM was used for acute exposure of zebrafish

embryos by Bai *et al*., (Bai *et al*., 2010), but I considered this dose not suitable for long-term exposure, according to the purpose of this study. Whereas Seng *et al*. (Seng *et al*., 2004) found a dose of flavopiridol 3μM suitable to inhibit angiogenesis. Because of different lipophilicity properties of compounds, including Flavopiridol, the calculation of dose to use in zebrafish embryo is challenging. After a series of experiments to optimize the drug, looking at the survival of embryos following exposure at different dose of drug (see section 2.14.2), I also adopted the dose of 3μM. In this study, the effects of Flavopiridol 3μM on the CDK9 inactivation were confirmed by Western blot analysis assessing the Phosphorylation levels of RNAPII. When I did the experiments assessing the optimal dose of Flavopiridol I did not have the Westerns set-up. If I had more time I would have used this technique to construct a dose-response curve and characterize the effect on the Phosphorylation levels of RNAPII.

Flavopiridol has been shown to decrease global levels of transcription in Drosophila (Chao *et al*., 2000), in HeLa or 293 cells (Chao and Price, 2001; Salerno *et al*., 2007) and in chronic lymphocytic leukemia cells (Chen *et al*., 2005). This global inhibition of transcription is similar to that seen with other molecules such as Actinomycin D and DRB (Garriga *et al*., 2010; Lam *et al*., 2001).

In our study, CDK9 inactivation was confirmed by reduced phosphorylation of the Phospho-Serine 2 (P-Ser2), *i.e*. the direct target of CDK9 activity. Chao and Price (Chao and Price, 2001) found a similar result into the Drosophila where they detected a reduced amount of ^{32}P incorporated RNA polymerase II following exposure to flavopiridol.

Decreased P-Ser2 and consequent reduced transcription could explain the embryonic developmental delay, measured as a 10% reduction in total body length and may also explain the effective reduction in heart size as shown by the heart-to-total body length ratio in embryos exposed to the drug compared to controls.

In this thesis the body lenght was used as a simple morphometric analysis to evaluate developmental progress. Infact, considering the length of the period of

study, 48-120 hpf, different methods should have been used to outline a particular developmental stage (Morin-Kensicki and Eisen, 1997) and therefore to assess the possible developmental delay arisen following exposure to flavopiridol. For example, the somite counting can be converted to standard hours of development (Hanneman and Westerfield, 1989) but can be used to stage embryos in the first 24 hours post-fertilization (Kimmel *et al.*, 1995), while myotome counting, in which the somite develop, can be used by 24 up to 72-96 hpf to stage embryos. Shortly after hatching, a prominent change is the inflation and float up of the swim bladder (Robertson *et al.*, 2007). In fish, including zebrafish, the measure of the standard body length has been used to outline developmental stage (Fuiman et al., 1998;Bird and Mabee, 2003;Campinho et al., 2004) and it seems to be highly correlated with other size measurements, such as eye diameter, head at nape or flexion angle of notochord (Parichy *et al.*, 2009) that I could also have used. I think that a limitation in my measurements is not the technique used, that is quite versatile as it can be used for several developmental stages, but is that this has been the sole method used. Therefore in future experiment I would use also a second methods, such as the flexion of notochord or the head size, to corroborate my data.

In our study, embryos exposed to flavopiridol showed a significant decrease between 48-72 hpf in mRNA levels of CDK9 and most of other transcription factors transcripts. Interestingly, at 96 hpf some of them showed an increase, such as CDK9 and MEF2c, that for GATA 4,5, and 6 and NKX2.5 was statistical significant.
CDK9 activity, but not the gene and protein expression, can be increased in mouse myocardium by Gq, calcineurin and chronic mechanical signals for hypertrophic growth (Sano *et al.*, 2002) or decreased as neutrophils age in culture and enter apoptosis (Liu *et al.*, 2012). Our finding that embryos 96 hpf, continuously exposed to flavopiridol 3 μM from 24 hpf, increases the expression of some of the genes we studied is new and raises the prospect that a hitherto undefined feedback mechanism, activated by flavopiridol exposure, could be responsible. This intriguing finding clearly requires further investigation.

Garriga et al. (Garriga *et al.*, 2010) reported that despite the impact of flavopiridol on general transcription, a significant number of transcripts are rapidly down- or upregulated following treatment with this molecule, the percentage of which can differ depending on the concentration and time-exposure. Moreover, specific inhibition of CDK9 activity by treating cells with a dominant negative form of CDK9 leads to a distinctive pattern of changes in gene expression compared to that obtained with flavopiridol (Garriga *et al.*, 2010).

This suggests that flavopiridol probably impedes transcription by other mechanisms in addition to CDK9 inhibition. Indeed, flavopiridol is known to inhibit other CDKs, although with lower efficacy. For example, the phosphorylation of the Ser5 on the CTD of the RNAPII is also reduced by flavopiridol because of its inhibitory effect on CDK7 in human glioblastoma T98G cell line (Caracciolo *et al.*, 2012). In addition, in a recent screen for binding of 20 kinase inhibitors to a panel of 119 kinases Fabian *et al*. has indicated that flavopiridol also binds the transcription regulator Calcium/Calmodulin kinase 1 and with higher affinity than to the CDKs and CDK-related kinases tested, although unfortunately they did not test CDK9 (Fabian *et al.*, 2005). The effects of the flavopiridol were also evident on cardiac performance. Ejection fraction and ventricular diastolic area were progressively and significantly affected during incubation with the drug. These findings were accompanied by reduced cardiomyocyte numbers compared with controls and reduced numbers of proliferating cardiomyocytes, indicated by PHH3 immunostaining. This suggest a role of the flavopiridol as a cell cycle-inhibitor. In fact, the total number of ventricle cardiomyocyte number did not change at the different time-points, in contrast with the constant increase observed in untreated embryos. The effects of flavopiridol on cardiac growth and function shown here closely mirror the effects we observed following exposure to aphidicolin, a well known cell cycle inhibitor (see chapter 5). Flavopiridol was reported to possess potent antiproliferative action on 60 human cancer cell lines in the US National Cancer Institute screen panel (Sedlacek *et al.*, 1996) and currently is being evaluated in numerous studies for treating hematologic and solid cancers. In the

cardiovascular system, flavopiridol is also known to inhibit smooth muscle cell proliferation and migration in vitro (Ruef *et al.*, 1999) (Jaschke *et al.*, 2004). Considering the plethora of downstream effects that the flavopiridol can have (Schmerwitz *et al.*, 2011) it is not unexpected that a cardiac phenotype results from prolonged exposure during embryonic development.

For example, reduced numbers of cardiomyocytes could affect the development of the hearts structure. Secondly, there appears to be a direct cardiotoxic effect of CDK inhibitors, as clinical use of these molecules have shown (Liu *et al.*, 2012). However, the mechanism by which they exert their cardiotoxicity is not well understood. Hasinoff and Patel showed in neonatal rat ventricular myocytes that flavopiridol, and other kinases inhibitors, cause the release of the cytosolic enzyme lactate dehydrogenase into the media, a widely used measure of drug-induced damage to myocytes (Hasinoff and Patel, 2010). An additional mechanism involves apoptosis which flavopiridol also induces programmed cell death in certain settings (Arguello *et al.*, 1998).

4.1.4.3 Genetic modulation of CDK9: impact on global and cardiac development and gene expression

Genetic knock-down was performed either by injecting a molecule blocking CDK9 pre-mRNA splicing or CDK9 mRNA translation.

The concentration of morpholino (MO) to inject was chosen on the basis of a series of dose-response experiments in which the survival and phenotype were carefully documented over 120hpf.

A 0.5nL constant volume of MO was injected in each egg as this was found to be ideal in causing homogenous distribution into the developing embryo from the early cell-division stage, *i.e.* < 4-cell. The determination of knockdown efficiency is clearly an essential step in this process (Eisen and Smith, 2008). At a concentration of 100μM, MO-CDK9splice blocking produced about 70% reduction of CDK9 mRNA, that reduced at 45% at 96 hpf cause the time-dependent decrease in morpholino efficacy as development proceeds (Matson *et al.*, 2008) (Nutt *et al.*, 2001;

Summerton, 2007). However, it is important to note that a percentage reduction in mRNA levels does not necessarily lead to the same reduction in protein levels.

Despite performing careful dose response studies I found that injection of the MO-CDK9 translation blocking produced a very high embryo mortality associated with profound developmental defects. This was in spite of the much lower concentration used compared to the MO-CDK9splice, which produced a 20% of knockdown of CDK9 protein. Therefore, it was decided to use only the MO-CDK9splice blocking for further experiments.

The different mortality observed following injection of the translation or splice blocking is an observation reported also by other authors (Granero-Molto *et al.*, 2008). Indeed, different morpholino sequences have different properties, in terms of strand affinity and rate of binding. This is one reason why translation and splice blocking, at the same concentration, can produce a different mortality and morphant phenotype. While the more severe phenotype with the translation blocking morpholino compared to the splice blocking could be ascribed to the presence of maternal CDK9 transcripts into the eggs. These transcripts, ready to be translated in CDK9 protein, cannot be affected by the splice blocking but can still be blocked by the translation blocking morpholino.

While embryos injected with MO-CDK9mismatch did not show appreciable change in their morphology and global phenotype, multiple developmental defects were observed in MO-CDK9splice treated embryos, such as increased body curvature and curled tail, pericardial edema and reduced tail blood flow. In addition, morphant embryos showed tube-shaped deformities of cardiac chambers, somatic blood islands and intra-cardiac blood congestion.

Histological sections revealed that the pericardial sac was either severely congested with blood or a proteinaceous exudate. MO-CDK9splice produced an increased percentage of defects in all the traits chosen to describe the whole embryo phenotype compared to the mismatch, including body axis, head shape, blood flow, pericardial edema, cardiac shape and heart rate although as stated above these were

less frequent and less severe than those seen with the translation blocking MO.

Typical cardiac defects included abnormalities of shape and rhythm. In addition, diastolic area and ejection fraction were also significantly reduced and there was a significantly lower number of total ventricular cardiomyocytes in each heart. Therefore, MO-CDK9splice appeared to inhibit cardiomyocyte proliferation, in a way similar to flavopiridol. These are novel observations with no previously published reports with which to compare our data.

An underlying and increasingly recognised problem with the use of MOs is that they may have 'off-target' effects (Eisen and Smith, 2008). This means that they can affect the production of other genes, and the observed phenotype may be only partially the result of the gene under observation. Therefore, some of the defects we observed in embryo injected could be non-specific. To partially overcome this problem, it is common to inject in separate experiments the mismatch as a control (MO-CDK9mismatch in our case), that is the same gene targeting morpholino (MO-CDK9splice blocking in our study) with 5 out of 25 nucleotide changes along the sequence. In the case of CDK9, this control caused few developmental defects, suggesting that the phenotype observed in embryos injected with MO-CDK9splice blocking was specific. On the contrary, the phenotype traits associated with injection of MO-CDK9 translation blocking were probably in part caused by off-target effects.

In order to reveal the spatial organization of the CDK9 and the P-TEFb complex, the CDK9 antibody used to assess the presence of the protein by western blotting was also used for immunohistochemistry in the whole embryo. The resulting immunostaining pattern suggests widespread distribution of CDK9 throughout the embryo with a strong presence along the length of the tail-fin. This pattern was not found in embryos exposed only to the secondary antibody and has not been seen in other whole mount immunostaining in our Institute. I feel it is highly unlikely to be due to artefact. However, at this stage I am unable to fully explain the particular pattern of staining observed. An hypothesis is that the structures stained could be blood vessels but further experiments will be required to assess this. One way could

be performing a DAB (3,3'-Diaminobenzidine) staining on embryo section. The DAB is an immunostaining (Seligman *et al.*, 1968) producing an easily observable brown color under white light and therefore would allow to visualize exactly the tissue were the CDK9 seems to be more concentrated and also to corroborate data obtained with confocal microscopy.

This ubiquitous presence supports the hypothesis that CDK9 represents a master regulator essential in early zebrafish embryo development (Oqani et al., 2011). A more detailed observation of the staining at higher magnification revealed a diffuse distribution throughout the cell predominantly in cytoplasm but also in the nucleus. Conversely, Dow et al. (Dow *et al.*, 2010) immunostained HeLa cells with the phospho-Thr186-CDK9 antiserum, that is the activated form of CDK9, and reported a predominantly nucleplasmic localization of the immuno-fluorescent pattern. Other reports support the nuclear localization of CDK9 (Oqani *et al.*, 2011; Herrmann and Mancini, 2001). In our experiments, we used a CDK9 antiserum that labels either the phosphorylated and non- phosphorylated forms of CDK9. Unfortunately, a phospho-Thr-CDK9 antibody for zebrafish was not available, therefore we could not distinguish between the two forms and I am therefore unable to compare directly with published data. However, Napolitano et al. indicated that CDK9 was predominantly located in the nucleus but could also be visualized in the cytoplasm (Napolitano *et al.*, 2002). They interpreted their observations as suggesting that CDK9 is actively exported from the nucleus to the cytoplasm and that leptomycin B, a specific inhibitor of nuclear export, inhibits this process.

In the present immunostaining experiments, labelled puncta had different size. Indeed, CDK9 exists in complexes of different magnitude. One study found a 1:1:1 ratio for CDK9, cyclin T1 and HEXIM molecules in the large P-TEFb complex (Dulac *et al.*, 2005). However, since HEXIM homodimerizes through its coiled-coil regions, it was proposed that two HEXIM molecules and one 7SK snRNA associate with two cyclin T1/CDK9 heterodimers to form the inactive P-TEFb complex (Blazek *et al.*, 2005; Murphy *et al.*, 2005). When the CDK9 immunostaining was repeated in

embryos injected with MO-CDK9splice blocking, the presence of red speckles was much reduced and, very interestingly, looked smaller. Red puncta observed in the MO injected embryos might reflect either a residual CDK9 presence detected by the immunostaining or might represent the MO tag red lissamine. A non-red secondary antibody was tested but unfortunately it did not work.

There are several cell-type specific transcription factors essential during the developmental processes of cardiomyocytes (Sachinidis *et al*., 2003), also working in co-operation (Garg *et al.*, 2003). We have assessed the expression of some of these factors and found that, overall, the expression of these genes was slightly reduced, and significantly reduced at 96 hpf for GATA 6 and MEF2c, in embryos injected with MO-CDK9 splice compared to MO-CDK9 mismatch.

Among these, the zinc finger protein GATA4 could be very important. DNA-binding transcription factors involved in myocardial differentiation are expressed at the earliest stages of heart development (Grepin *et al.*, 1997; Kuo *et al.*, 1997; Molkentin *et al*., 1997). CDK9 forms a complex with GATA4 in mouse embryonic stem cells and is involved in their differentiation into cardiomyocytes (Kaichi *et al.*, 2011). In addition, CDK9 activity is required for P300 HAT activity and for the p300/GATA4 transcriptional pathway during hypertrophic responses in cardiomyocytes (Sunagawa *et al*., 2010).

GATA4 functionally and physically interacts with other transcription factors, including GATA6 and MEF2C (Charron *et al.*, 1999; Morin *et al*., 2000). Whereas these interactions regulate the transcriptional potential of GATA4 downstream of hypertrophy signaling pathways, disruption of this complex results in the inhibition of hypertrophic responses.

The reduced gene expression for these markers fit with the reduced cardiomyocyte proliferation and cardiac performances observed following CDK9 inhibition/knockdown. Indeed, the roles of CDK9 in the regulation of transcription and RNA processing are gene specific, such that expression of certain genes is highly sensitive to CDK9 inhibition, while the expression of the remaining RNAPII-dependent genes may be partially or totally independent of CDK9 activity (Garriga

et al., 2010). One example is represented by the constitutive gene glyceraldehyde 3-phosphate dehydrogenase, that is affected by the P-TEFb complex, of which CDK9 is part (He *et al.*, 2006). This gene specificity may result from more potent inhibition of elongation of certain gene transcripts by negative elongation factors requiring dedicated recruitment of P-TEFb by inducible transcription factors and BRD4.

How and why CDK9 pharmacological inhibition can trigger selectively the expression of some of these genes but not others, while CDK9 genetic knockdown reduce them remains unknown. The possibility of a positive feedback control mechanism either for CDK9 or other transcription factors certainly merits further investigation.

In conclusion, these experiments assessing the effects of pharmacological inhibition and genetic knockdown of CDK9 have revealed the key importance of CDK9 on global zebrafish growth and development. They have also highlighted the importance of CDK9 on cardiac development and function during early embryonic stages. Cardiomyocyte proliferation was severely impaired by CDK9 inhibition and this had a significant impact on cardiac function and subsequently tail blood flow. While there was a significant global developmental impact of CDK9 inhibition, the effect on the heart was more marked with dramatic effects on shape, size and function where many other organ systems appeared to be functioning normally. This does suggest that it plays a very important role in the growth and development of the heart.

Interestingly, CDK9 pharmacological inhibition appeared to result in enhanced expression, after an initial inhibition, of genes associated with cardiomyocyte proliferation and development, including CDK9 itself. There was also clear evidence for increased levels of CDK9 protein and reduced activity of CDK9 reflected in reduced phosphorylation of its target site on RNAPII.

This finding supports the suggestion that CDK9 is a key, but not exclusive, regulator of transcription during zebrafish development and raises the possibility of a feedback mechanism which permits transcription to proceed, possibly at a higher

rate, via other pathways when it is either inhibited or where CDK9 protein levels are reduced.

These important and completely novel aspects of CDK9 function now need to be confirmed to mammalian model systems including further investigation on the role of CDK9 on mammalian cardiomyocyte proliferation.

CHAPTER 4

PART 2

Effects of LARP7 on global and cardiac development in the zebrafish embryo

4.2.1 Introduction

The deleterious effect of genetic knockdown and pharmacological inhibition of CDK9 in zebrafish embryos, described in the part 1 of this chapter, suggest a role for this protein as an important regulator of cardiomyocyte proliferation. The mechanism for this is likely to be due to CDK9's role in gene transcription achieved by relieving the block on transcriptional elongation, when it binds with Cyclin T (Peterlin and Price, 2006). CDK9 is inactive when enveloped in the 7SK Ribonucleoprotein (7SK-RNP) complex (Zhou and Yik, 2006). Among other members of this complex is La-related protein (LARP)7 also called PIP7S (He *et al.*, 2008)). LARP7 is specialized in RNA binding, it provides a bridge between 7SK-RNA and HEXIM, so as to stabilize the CDK9-inactivating complex and acts as a crucial factor in the regulation of the P-TEFb complex (Markert *et al.*, 2008; Krueger *et al.*, 2008).

A previous study (Markert *et al.*, 2008) has shown that LARP7 ablation by RNA interfering-mediated silencing produced upregulation in RNA pol II transcription. Therefore, while CDK9 inhibition has been proposed as a therapeutic strategy for inhibiting cardiac hypertrophy, it is also possible that enhancing CDK9 activity may increase hypertrophy. While this could obviously be deleterious in certain circumstances, including the presence of pre-existing cardiac hypertrophy, we hypothesised that it could be beneficial in certain pathological settings since it could potentially stimulate and support cardiomyocyte growth and possibly proliferation. Previously, numerous approaches have been explored to increase the number of cardiomyocytes in mammals: by interfering with the machinery for apoptosis, necrosis, autophagy (Pattingre *et al.*, 2005; Chen *et al.*, 2010; Diwan *et al.*, 2008), with oxidative stress (Li *et al.*, 2009) or stress-activated cascades (Krishnan *et al.*, 2009) or by enhancing cell survival pathways (Harada *et al.*, 2005; Oh *et al.*, 2001; Oshima *et al.*, 2009; Takagi *et al.*, 2010). However, while these mechanisms have been shown to prevent or reduce cell death, they have had limited success in repopulating significant numbers of cardiac muscle cells. Stimulating endogenous regenerative pathways in the human heart is attractive as it could potentially provide a non-

invasive therapy and circumvent the need for exogenous stem cell approaches or the need for immunosuppression associated with the use of allografts (Bergmann and Steller, 2010).

In this chapter I explore the possibility of upregulating CDK9 activity in the zebrafish embryo by utilising a strategy of LARP7 genetic knockdown using morpholino.

General aim

Describe and assess the effect of LARP7 knockdown on global and cardiac development in the zebrafish embryo.

Key questions

- What is the normal pattern of expression of LARP7 in the whole embryo and the heart during normal zebrafish development?
- What are the effects of genetic knockdown of LARP7 on the whole embryo and the heart development?

4.2.2 Methods

4.2.2.1 Zebrafish lines

Zebrafish transgenic cmlc2:EGFP embryos were used for all experiments, unless stated.

4.2.2.2 Embryo survival and phenotype

Embryo survival was assessed at 6, 24, 48, 72, 96 and 120 hpf. Whole embryo and cardiac phenotype were described as stated in chapter 2, section 2.13.5.

4.2.2.3 Cardiovascular function and cardiomyocyte analysis

Ejection fraction (EF), heart rate (HR), ventricular diastolic and atrial area (VDA, ADA) and total ventricular cardiomyocyte number (TVCn) were assessed. Methods are described in detail in chapter 2, section 2.6 and 2.9.2.

4.2.2.4 LARP7 gene knockdown

Morpholino antisense oligonucleotides were used to inhibit LARP7 mRNA splicing (MO-LARP7splice) or mRNA translation blocking (MO-LARP7trans) (see table 4.2.1). A mismatch oligonucleotide (MO-LARP7mism) was used as a control. A volume of 0.5 nL of MO-LARP7 (containing 200 μM for either MO-LARP7splice or MO-LARP7trans) was injected in the zebrafish eggs yolk sac at 1-4 cell stage. A detailed description of this technique is described in Chapter 2, section 2.13.

4.2.2.5 Gene expression analysis

Quantitative PCR has been used to examine LARP7 expression in the whole embryo and in isolated embryonic and adult hearts during normal development and to detect the expression of CDK9, GATA 4, 5 and 6, MEF2C and TBX5 following LARP7 knockdown in whole embryos. I performed an assessment of various housekeeping genes in these experiments. Ef1α was chosen to normalise LARP7 gene expression between 24-120 hpf as it did not vary during this developmental

time-period. Whereas β-actin was chosen to enable quantitation of gene expression according to the amount of cDNA loaded for MO-LARP7 treated embryos because it remained the most stable in these experimental conditions (figure 2.10 and 2.11 in Chapter 2).

4.2.2.6 Protein analysis

Polyacrylamide Gel Electrophoresis and Western blotting (see section 2.11) were used for semiquantitative analysis of LARP7 (antibody produced in rabbit; AV40848, Sigma-Aldrich) in whole embryos injected with morpholino and respective controls.

4.2.2.7 Statistics

See chapter 2, section 2.15 for a detailed statistical analysis.

Table 4.2.1 – LARP7 morpholino oligonucleotides sequences.

Danio rerio La-ribonucleoprotein domain family, member 7 (LARP7), mRNA. Pubmed Accession number NM_199930.1	
Morpholino sequences	
Splice blocking	5'-TCATCTCCATACTAAACCAAACTGT-3' (exon 3 / intron 3)
Mismatch	5'-TgATgTCCATAgTAAACgAAACTcT-3'
Translation blocking	5'-TACTTTCACACAGTTGCGTTCTGCT-3'

4.2.3 Results

4.2.3.1 LARP7 gene expression during normal zebrafish development

LARP7 mRNA was detected by Q-PCR in the whole embryo, as well as in the embryonic and adult hearts (6 month old) (figure 4.2.1). In the whole embryo, LARP7 expression reached the peak at 48 hpf and then significantly decreased towards 72, 96 and 120 hpf. In isolated embryonic hearts, LARP7 mRNA increased slightly between 48 and 96 hpf and then significantly reduced at 120 hpf where it showed the lowest value. In the adult heart, LARP7 mRNA level was significantly higher compared to the embryonic heart at 120 hpf and similar to those observed at earlier developmental stages (figure 4.2.1).

4.2.3.2 LARP7 Morpholino knockdown

4.2.3.2.1 Embryo survival following morpholino injection

Embryo survival, at 120 hpf, was 91%, 80% and 78%, respectively in the group injected with MO-LARP7mism, MO-LARP7splice and MO-LARP7transl (see embryo survival curve in figure 4.2.2).

4.2.3.2.2 Effects of MO-LARP7 on LARP7 gene and protein levels

Injection of either LARP7 splice (MO-LARP7splice) or translation (MO-LARP7transl) blocking and control mismatch (MO-LARP7mism) morpholino oligos were performed. Following injection of MO-LARP7splice, Q-PCR confirmed a reduction of about 40% at 48 hpf and 45% at 96 hpf of LARP7 mRNA compared to the mismatch control embryos (figure 4.2.3 A). Embryos injected with MO-LARP7transl had a 70% reduction in LARP7 protein at 48 hpf (figure 4.2.3 B) compared to the MO-mismatch embryos.

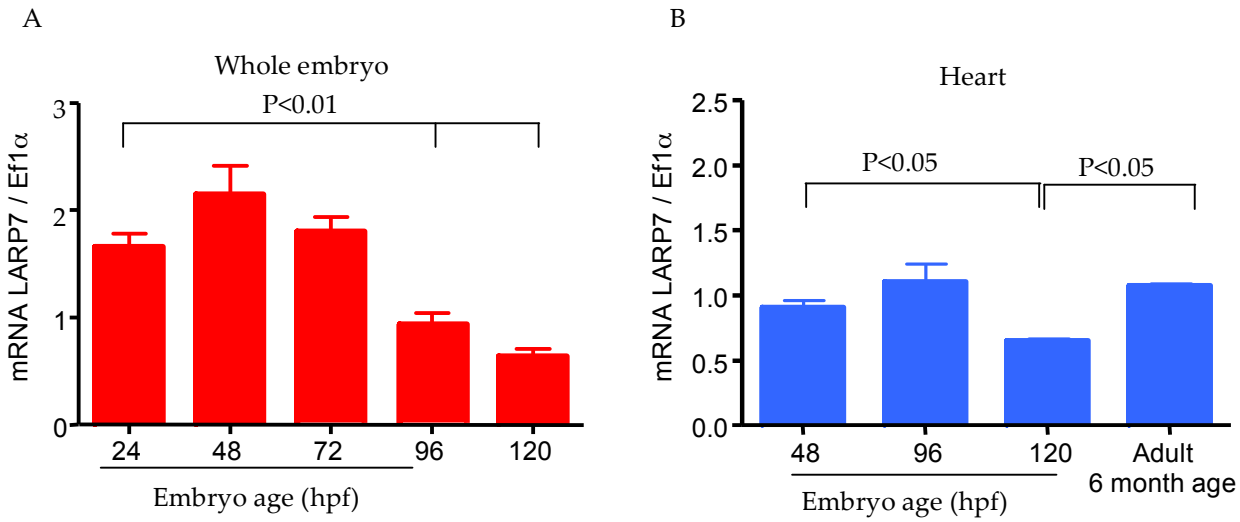

Figure 4.2.1 – Assessment of LARP7 gene expression during normal zebrafish development. This was assessed in whole embryos collected from 24 to 120 hpf (A) and in isolated hearts at 48, 96, 120 hpf and adult heart (B). Data were compared by one-way ANOVA followed by Bonferroni multiple comparison test. Each time-course was studied in 1 clutch of eggs, at least 10 embryos from the clutch were used to generate each time point. The data represents an average from studies in 3 clutches of eggs.

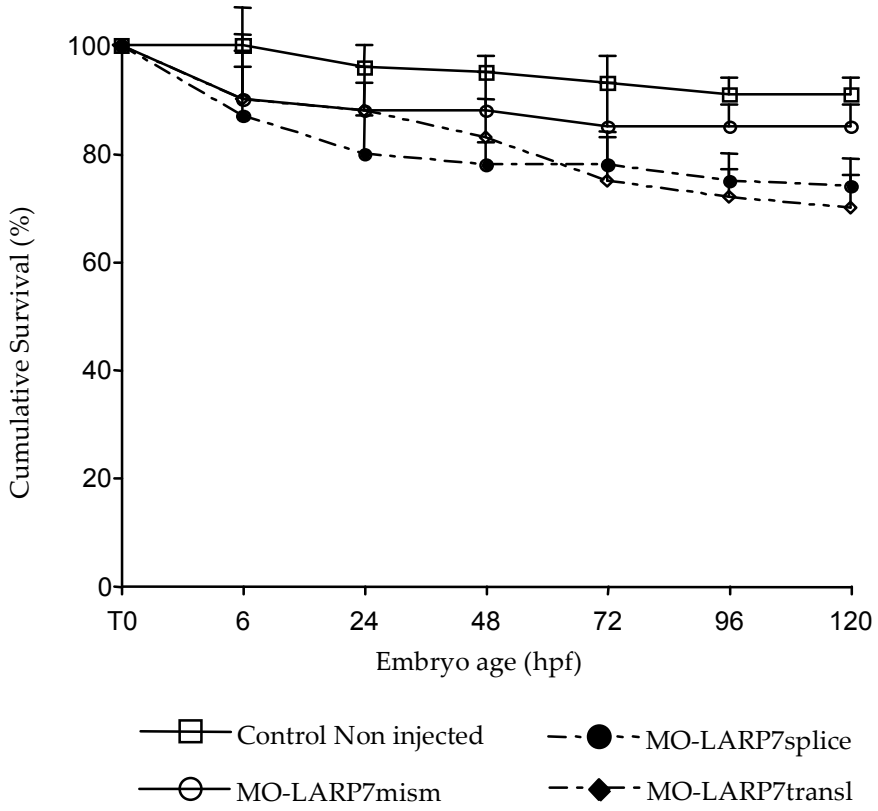

Figure 4.2.2- Cumulative survival curve following LARP7 genetic knockdown. Zebrafish eggs from the same clutch were injected at 1-4 cell stage with LARP7 morpholino mismatch, splice or translation blocking. Surviving embryos were counted at 6, 24, 48, 72, 96 and 120 hpf. Non-injected group represent a basic control to for the egg quality. N=3 experiments, at least 50 embryos were included in each group.

4.2.3.2.3 Effect of MO-LARP7 injection on gross and cardiac phenotype

The phenotypes of the whole embryo and heart were assessed at 72hpf following injection of the LARP7 morpholino. The different phenotypes are reported graphical in figure 4.2.4 and as images in figure 4.2.5 (for images of control non–injected embryos see figure 4.1.11a). Embryos injected with MO-LARP7splice and MO-LARP7transl showed a mild increase in developmental abnormalities compared to the MO-LARP7mism group (figure 4.2.4 & 4.2.5 a-c).

MO-LARP7splice morphants showed more pericardial odema compared with controls (38% vs 10% respectively), curved-up body axis (30% vs 8%) and reduced tail blood flow (23% vs 9%) at 120 hpf (figure 4.2.4 and 4.2.5 a-c). Marked atrial dilation was a very clear and dominant feature (35% vs 0%) and a reduced heart rate (<100bpm) in the 32% vs 2% in controls. MO-LARP7transl morphants showed pericardial edema in a 27% of cases, curved body-axis in the 33% and reduced blood flow in the 42%. Atrial dilation was also evident in about 32% of MO-LARP7transl morphants while the heart rate was reduced in 46% (figure 4.2.4 and 4.2.5 a-c).

4.2.3.2.4 Effects of MO-LARP7 on cardiac growth, function and cardiomyocyte proliferation

Ventricle ejection fraction (EF) (figure 4.2.6 A) was slightly reduced in embryonic ventricles injected with MO-LARP7splice and MO-LARP7transl by 3-5%, 7-10% and 15% respectively at 72, 96 and 120 hpf, compared to MO-LARP7mism.

Embryos injected with MO-mism and non injected controls showed a positive time-trend in total ventricle cardiomyocyte number (TVCn) 72, 96 and 120 hpf with values similar to those I reported in chapter 3 (figure 4.2.6 B). Embryos injected with translation blocking and splice site MO also showed a positive upward trend in TVCn during development with a small non significant increase in TVCn of 9% and 15% at 96 and 120 hpf respectively compared to controls (figure 4.2.5 B).

Ventricular diastolic area showed a positive trend for all groups in the period of

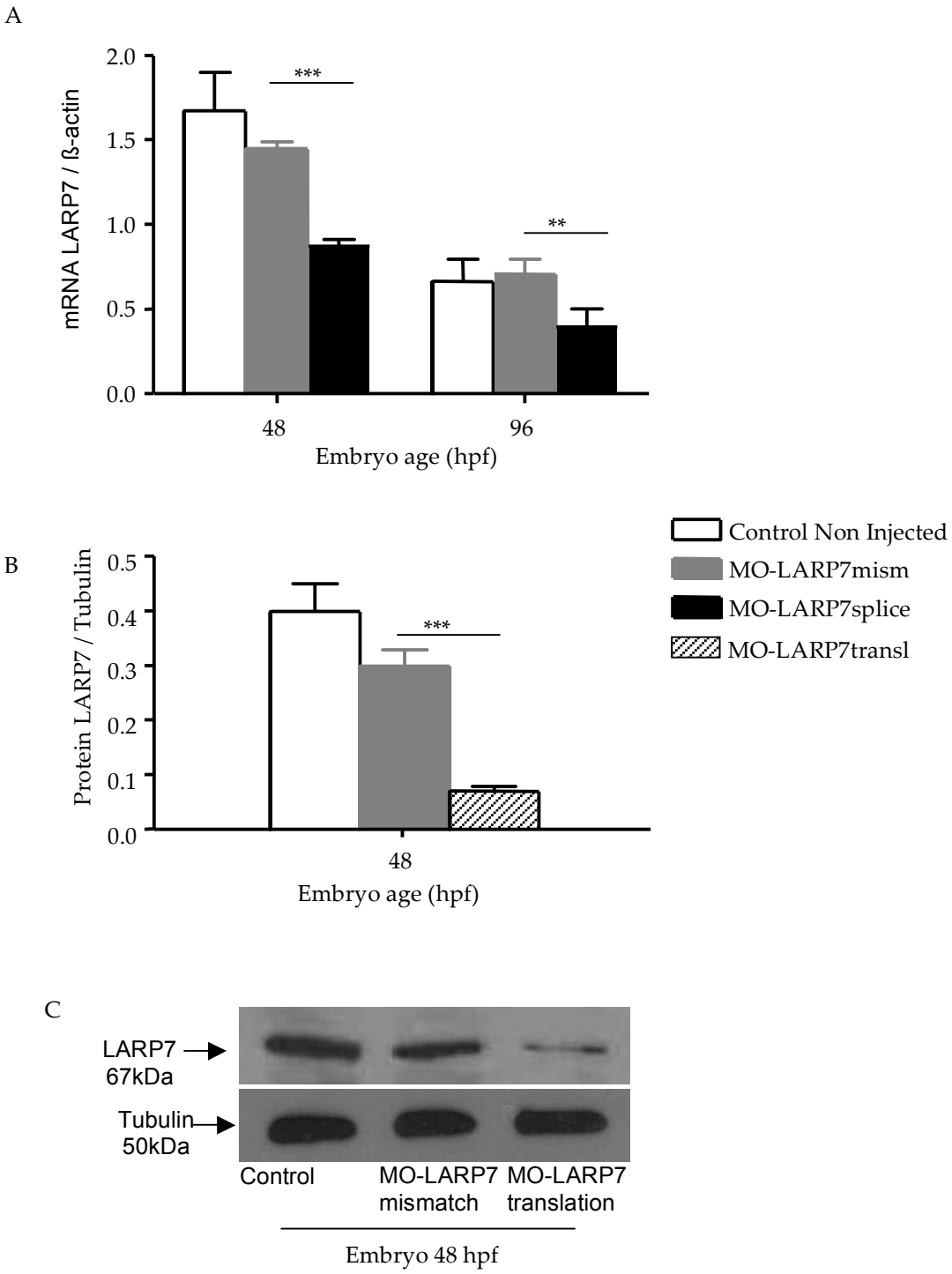

Figure 4.2.3 – Effect of MO-LARP7 injection on the LARP7 expression. LARP7 mRNA (A) level was assessed at 48 and 96 hpf, protein (B) level was assessed at 48 hpf. mRNA and protein were significantly reduced following injection of MO-CDK9splice blocking and MO-CDK9 translation blocking, respectively. Panel C shows western blot membranes following ECL detection. ß-actin was used to normalize mRNA level, while tubulin was used to normalize protein level. N=3 experiments, **=p<0.01, ***=p<0.001, one-way ANOVA test was used to compare means, followed by Bonferroni's post-hoc test.

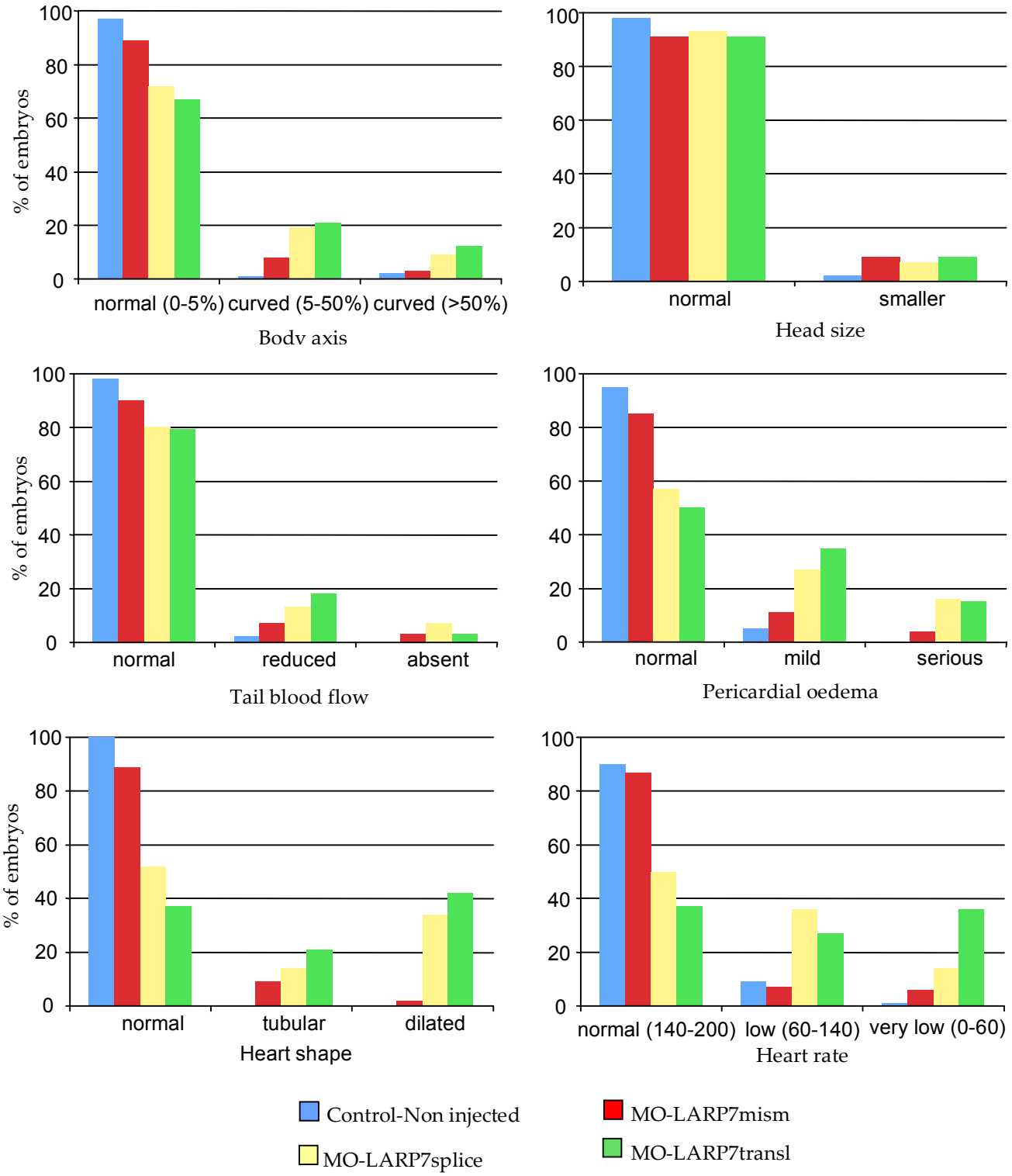

Figure 4.2.4- Characterisation of the 72 hpf zebrafish embryo and cardiac phenotype following LARP7 morpholino treatment. Each diagram report on the X axis a specific trait, which phenotypic severity increase from left to right. On the Y axis is reported the percentage of embryos retaining that phenotype. The first two diagrams, with body axis and head shape, explain the embryo body phenotype while lower diagrams, with tail blood flow, pericardial edema, heart shape and heart rate, are related to the cardiac phenotype. N=3 experiments, at least 50 embryos were included in each group.

Zebrafish embryos 72 hpf injected with MO-LARP7mismatch

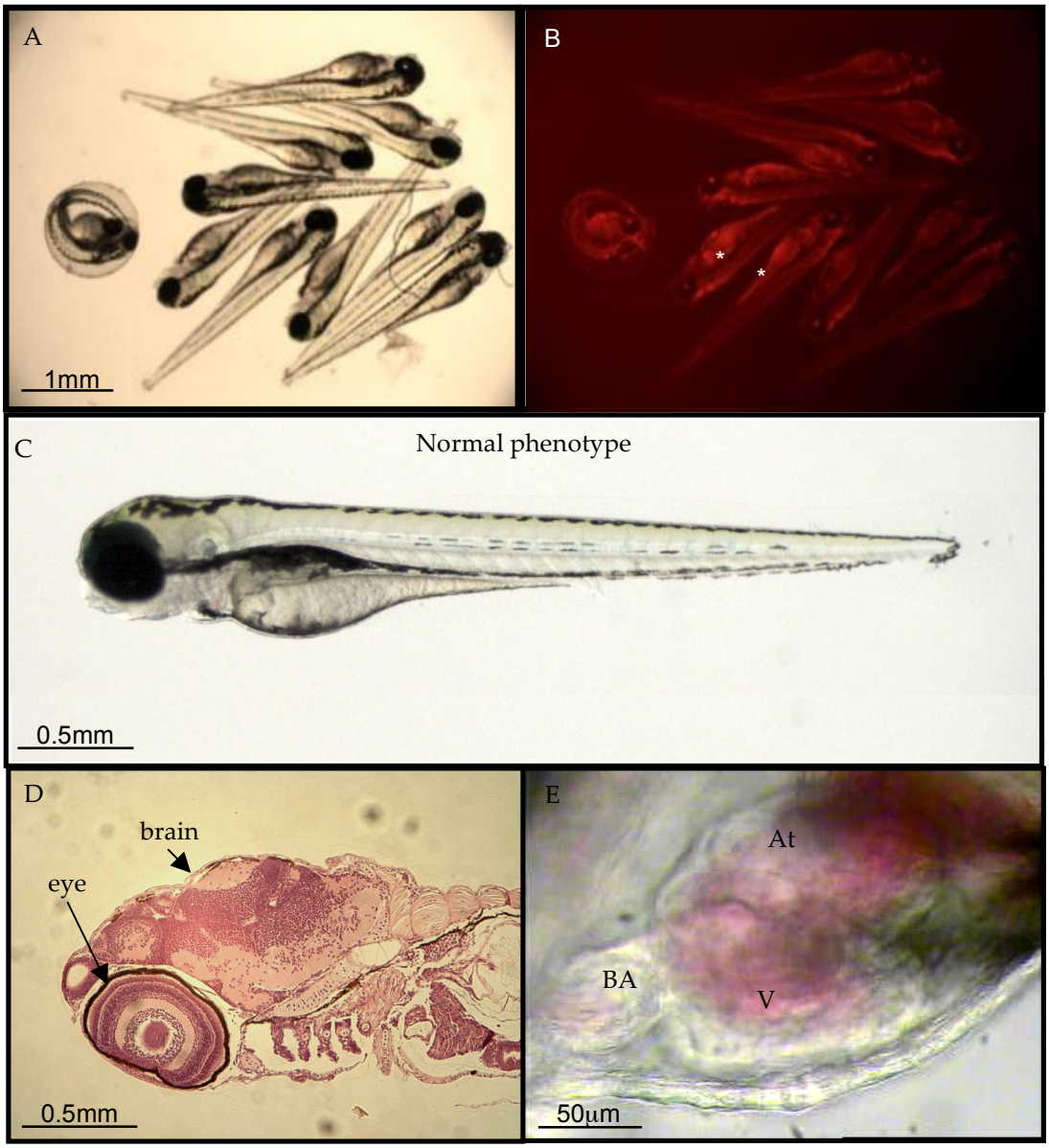

Figure 4.2.5a – Effect of MO-LARP7mismatch injection on the zebrafish embryo. Zebrafish eggs were injected at 1-4 cell stage with this control morpholino. A shows an overall view of embryos at 72 hpf under white light. B is the same image captured under fluorescence light to show the successful injection by the morpholino-linked red lissamine (white star). One of the embryos is shown at higher magnification in C. Image D shows an H&E stained embryo, while E shows a still image from a video of an in-vivo beating heart. Key: BA - bulbus arteriosus, V - ventricle, At - atrium

Zebrafish embryos 72 hpf injected with MO-LARP7splice

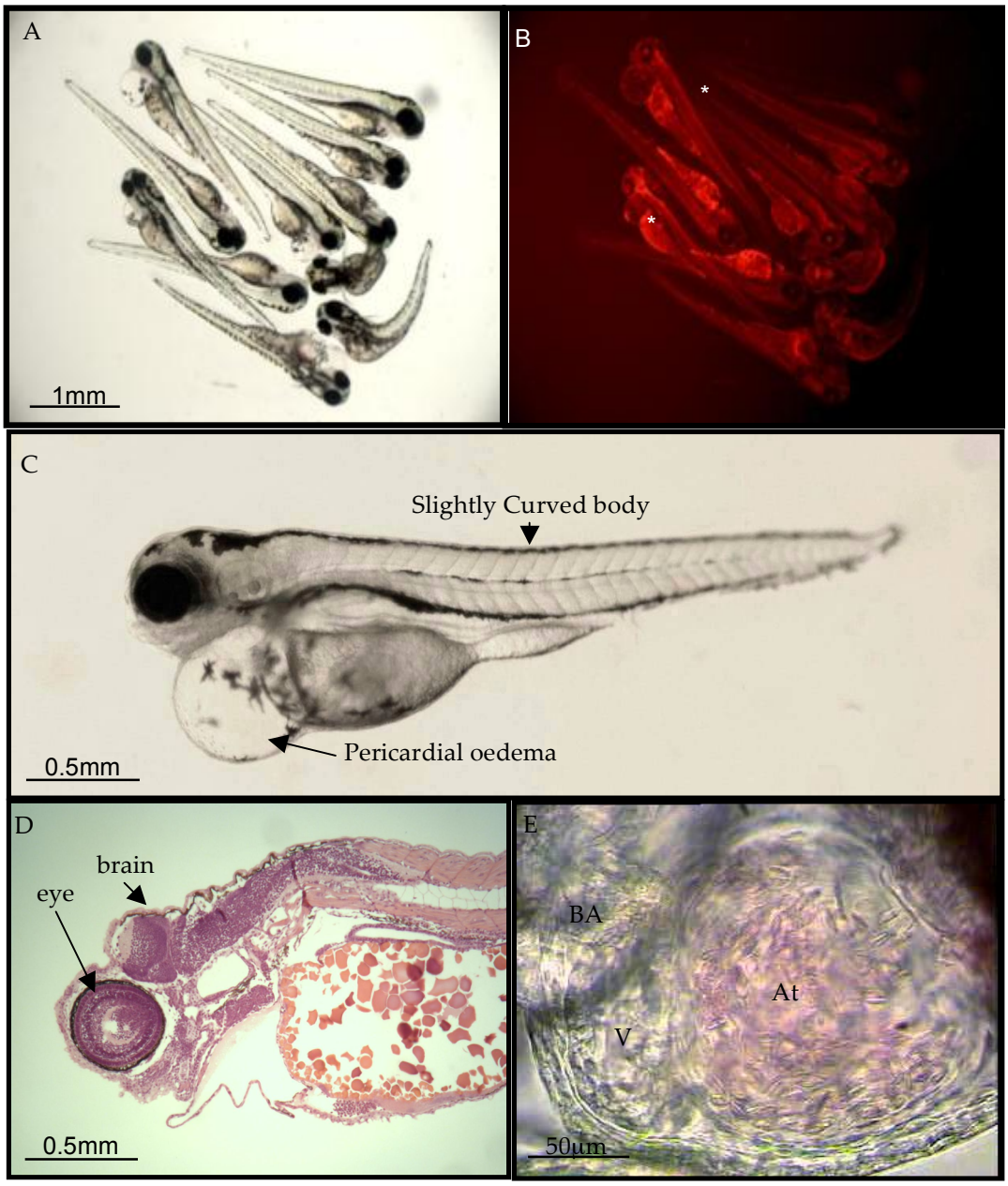

Figure 4.2.5B – Effect of MO-LARP7splice blocking injection on the zebrafish embryo. Zebrafish eggs were injected at 1-4 cell stage with this control morpholino. A shows an overall view of embryos at 72 hpf under white light. B is the same iamge captured under fluorescence light to show the successful injection by the morpholino-linked red lissamine (white star). One of the embryos is shown at higher magnification in C. D shows an H&E stained embryo section, E shows a still image of the heart captured from a video of an in-vivo beating heart. Key: BA - bulbus arteriosus, V - ventricle, At - atrium

Zebrafish embryos 72 hpf injected with MO-LARP7translation

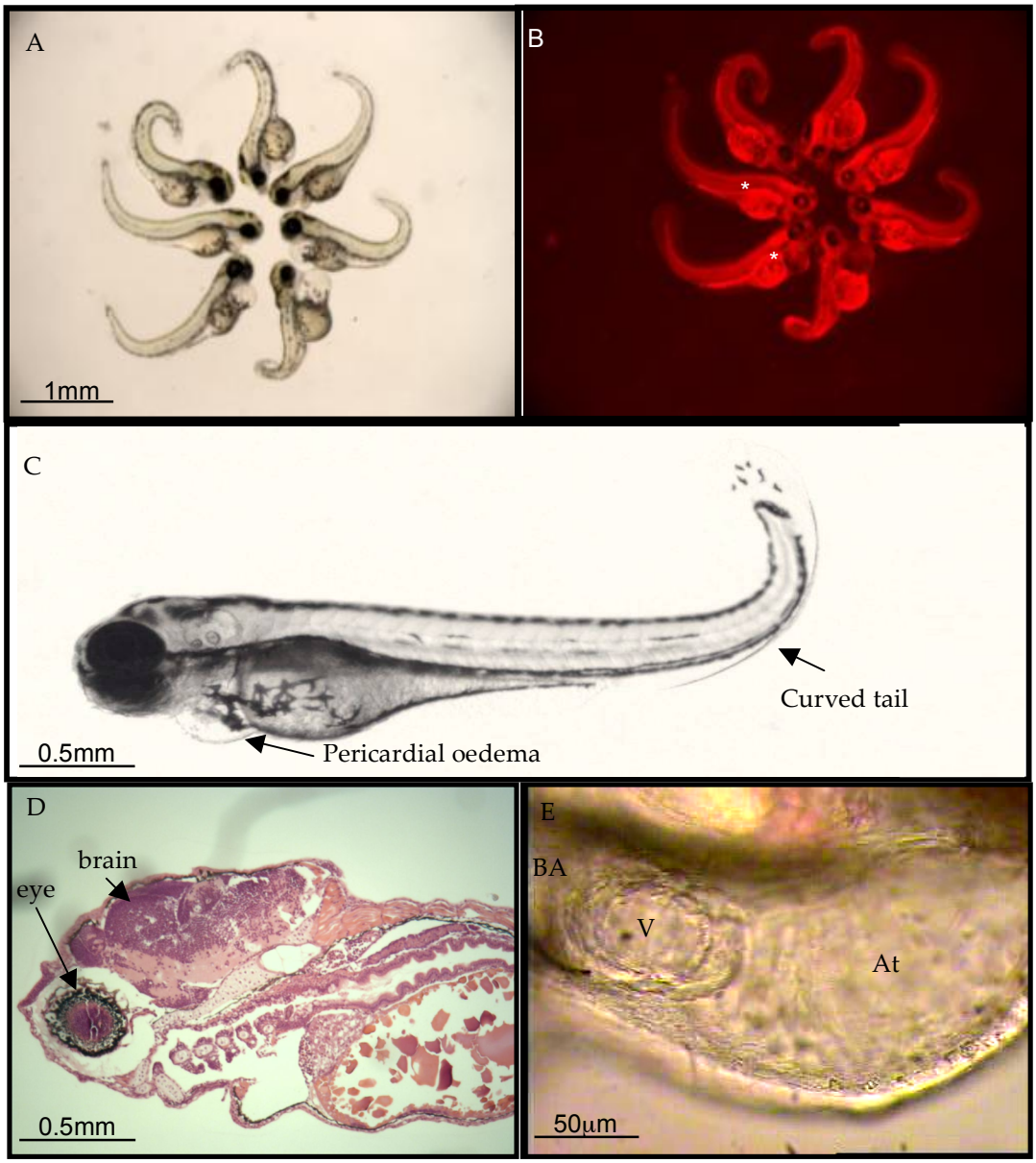

Figure 4.2.5C – Effect of MO-LARP7 translation blocking injection on the zebrafish embryo. Zebrafish eggs were injected at 1-4 cell stage with this control morpholino. A shows an overall view of embryos at 72 hpf under white light. B is the same iamge captured under fluorescence light to show the successful injection by the morpholino-linked red lissamine (star). One of the embryos is shown at higher magnification in C. D shows an H&E stained embryo section, E shows a still image of the heart captured from a video of an in-vivo beating heart. Key: BA - bulbus arteriosus, V - ventricle, At - atrium

study (figure 4.2.6 C). However, this increase was less evident in MO-LARP7splice and MO-LARP7transl compared to MO-LARP7mism (figure 4.2.6 C). Conversely, MO-LARP7transl and MO-LARP7mism injected embryos showed a greater increase in atrial diastolic area by 20%, 15% and 14%, at 72, 96 and 120 hpf respectively compared to controls (figure 4.2.6 D).

4.2.3.2.5 Effects of MO-LARP7 on gene expression

Analysis of gene expression in whole embryos showed generally non significant changes in embryos injected with MO-LARP7splice blocking compared to mismatch controls, although several variations were observed figure 4.2.7). CDK9 was slightly reduced at 48 and 96 hpf. GATA4 and 6 were increased at 48 and 96 hpf in embryos injected with MO-LARP7splice blocking compared to mismatch controls, while GATA 5 mRNA level was increased at 48 hpf and reduced at 96 hpf. MEF2c showed no change at 48 hpf but it increased at 96 hpf. Whereas TBX5 mRNA level was reduced at 48 hpf but was significantly increased at 96 hpf in embryos injected with MO-LARP7splice blocking compared to mismatch controls (figure 4.2.7).

4.2.3.2.6 Effects on phosphorylation of serine 2 residue of RNAPII

Western blotting revealed that the phosphorylated form of Ser2 in the carboxyterminal domain of the RNAPII was significantly increased following MO-LARP7transl injections compared to the control MO-LARP7mism (figure 4.2.8). Unexpectedly, this was found to be slightly reduced in MO-LARP7splice injected embryos.

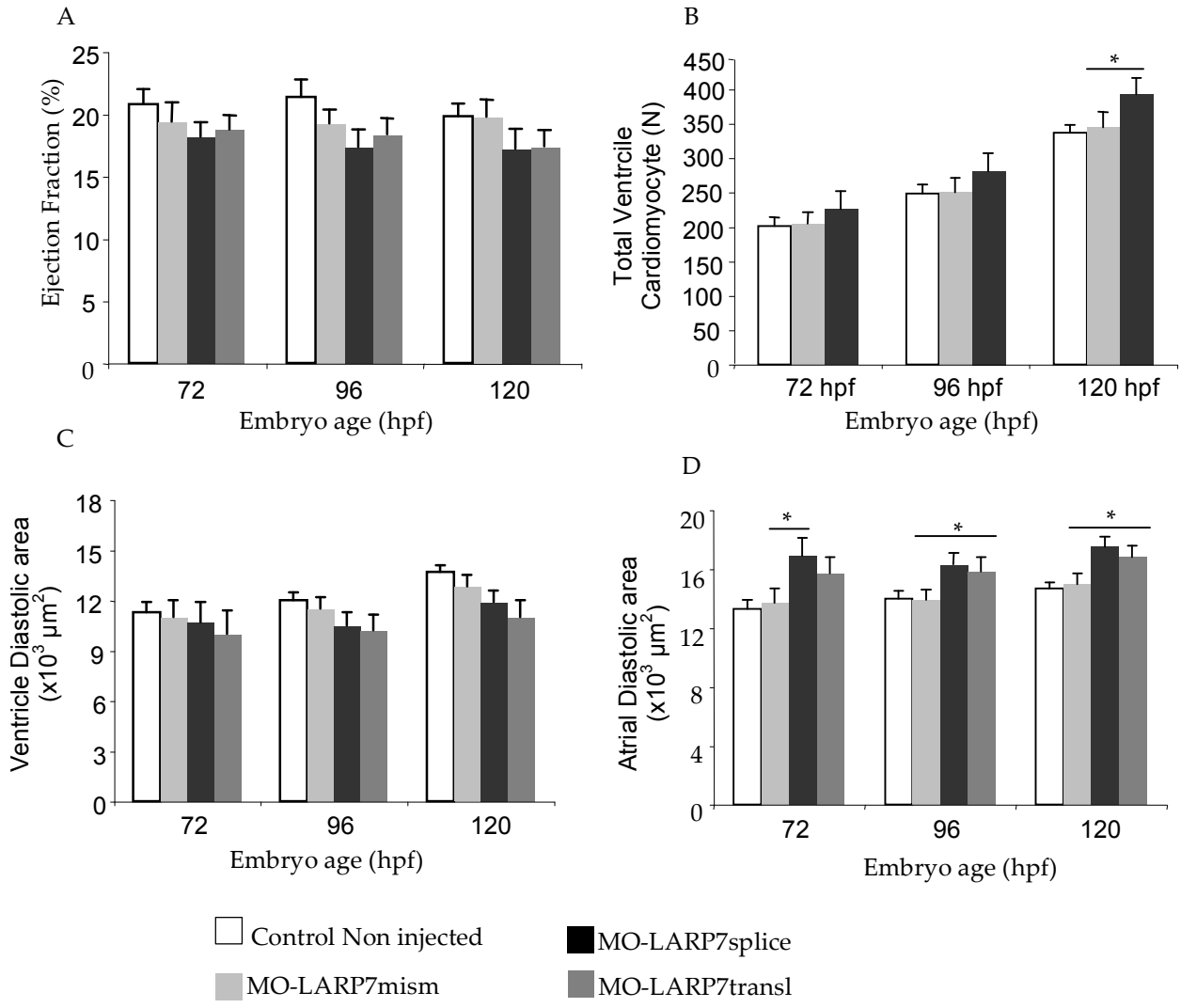

Figure 4.2.6 - Effects of LARP7 genetic knockdown on cardiac structure and function. Embryo eggs 1-4 cell stage from the same clutch were injected with MO-LARP7 splice or MO-LARP7 translation blocking or MO-CDK9 mismatch. Ejection fraction (A), Total ventricle cardiomyocyte number (B) and Ventricle (C) and Atrial (D) diastolic area were assessed in zebrafish embryonic heart at 72, 96 and 120 hpf. Cardiomyocyte analysis is reported only for MO-LARP7splice embryonic heart. N=3 experiments, *=$p<0.05$, two-way ANOVA test for repeated measures was used to assess difference between means, excluding cardiomyocyte analysis where a normal two-way ANOVA test was used.

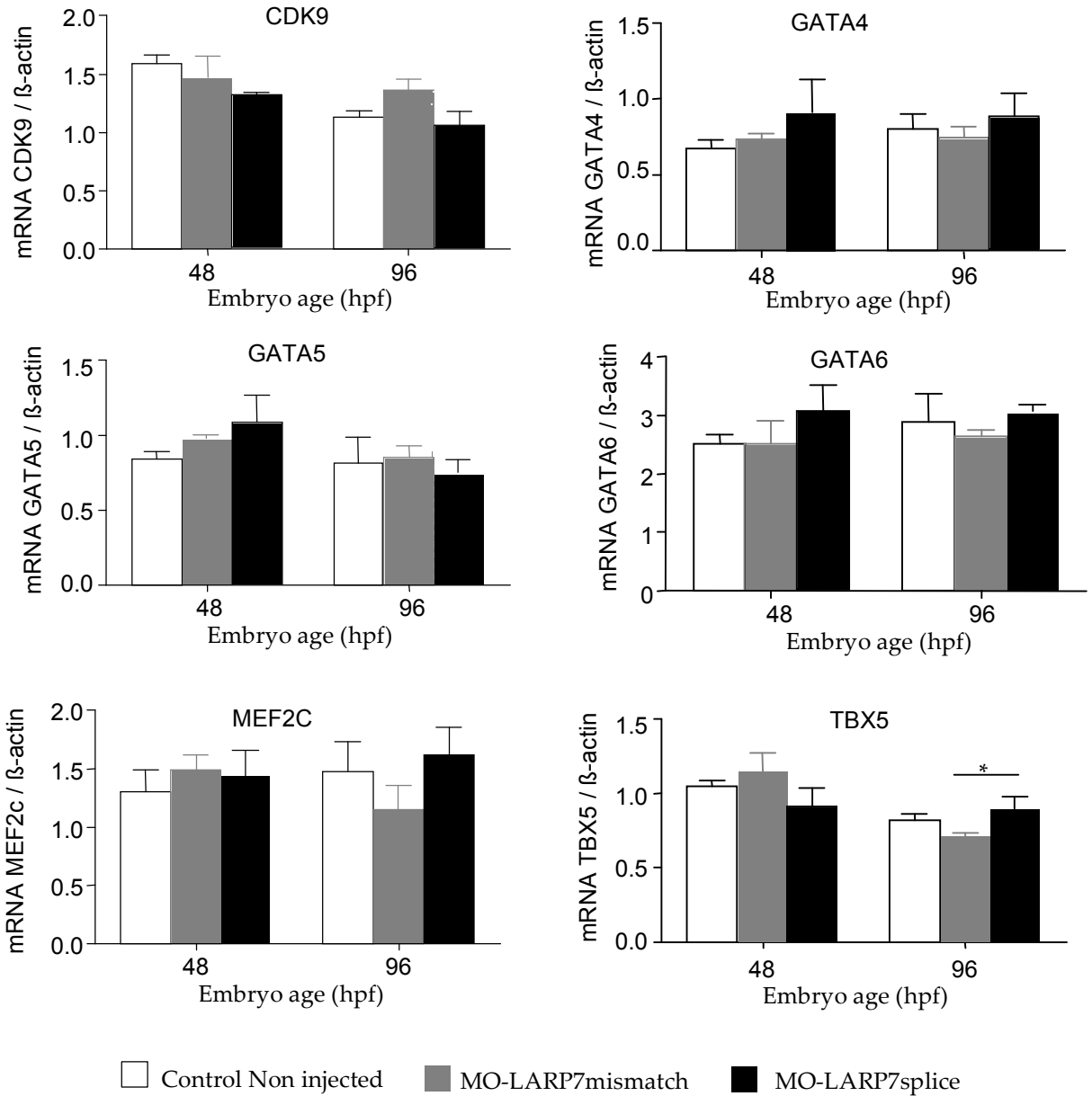

Figure 4.2.7 – Effects of LARP genetic knockdown on the gene expression. Embryo eggs 1-4 cell stage from the same clutch were injected with MO-LARP7 splice blocking or MO-LARP7 mismatch. At 48 and 96 hpf mRNA was extracted from whole embryos (at least 10 embryo per group). Level of CDK9 mRNA and relevant gene for cardiac development GATA4, 5 and 6, MEF2c, TBX5 mRNA was detected by Q-PCR analysis. mRNA level were normalised to the housekeeping gene ß-actin. N= 3 experiments, *=$p<0.05$, two-way ANOVA test followed by Bonferroni's post-hoc test.

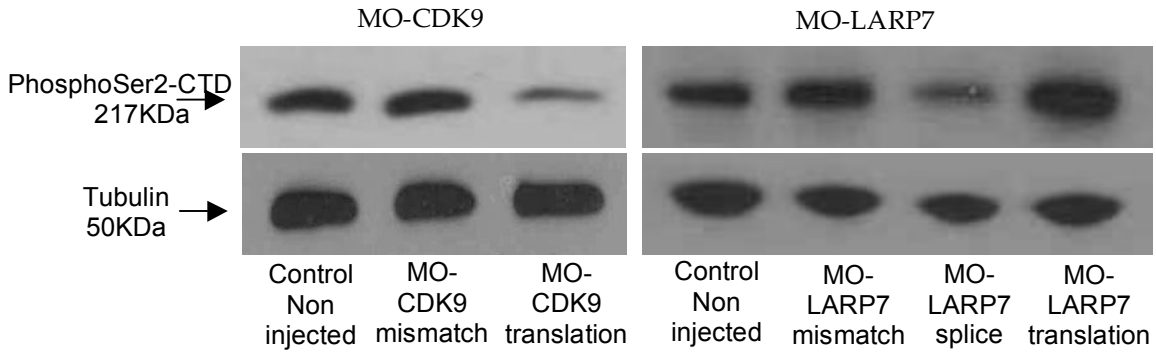

Figure 4.2.8 Effects of CDK9 and LARP7 knockdown on the Phosphorylation of Ser2-CTD. Western blotting membranes showing the level of PosphoSer2-CTD in the zebrafish whole embryos 72 hpf, tubulin was used as loading control. Embryo eggs 1-4 cell stage were injected with MO-CDK9 mismatch or splice blocking or were injected with the MO-LARP7 mismatch, splice or translation blocking. N=1 experiment.

4.2.4 Discussion

CDK9 is known to be involved in many cellular mechanisms, mainly involving gene regulation. Activation of CDK9 acts to increase cell division and growth although this appears to dependent on the particular organ or tissue . In adult mice heart, for example, CDK9 is hyperactivated during cardiac hypertrophic growth, either by means of increased activity of Cyclin T in cardiac-specific gain-of-function transgenic mice (Sano et al., 2002) or by repression of CDK9 inhibitors (Sano *et al.*, 2002; Yang *et al.*, 2001), such as 7SK small nuclear RNA and HEXIM (Egloff *et al.*, 2006; Michels *et al.*, 2004). A putative role of CDK9 in increasing cell number has been described but may be related to reduced cell apoptosis via upregulation of antiapoptotic molecules, e.g. MCL-1 (Wang *et al.*, 2012a). Whether CDK9 has a direct role in cell proliferation remains unclear.

La-related protein (LARP)7 is an RNA binding molecule and a key player in the snRNP complex, possibly of underestimated importance. In fact, LARP7 directly interacts with 7SK snRNA (Bayfield *et al.*, 2010), which by turn acts as a molecular scaffold bringing together various components into what is called the 7SK snRNP complex (Michels *et al.*, 2003) (Yik *et al.*, 2003) and leading eventually to CDK9 repression. Therefore, I hypothesized that LARP7 knockdown could decrease the activity and or abundance of this inactive complex and lead to an activation of CDK9 action.

In situ hybridization on whole mount mouse embryos have shown a large and ubiquitous presence of LARP7 (Alazami *et al.*, 2012), while previous reports showed the presence of LARP7 also in human embryonic kidney cells (Krueger *et al.*, 2008) and HeLa cell extracts (Markert *et al.*, 2008; He *et al.*, 2008). Barboric and colleagues (Barboric *et al.*, 2009) also described ubiquitous presence of LARP7 in the early-stage zebrafish embryo (up to 48 hpf), with its abundance more apparent in the anterior part of the body, particularly the brain. In my experiments, LARP7 was investigated in the zebrafish whole embryo from 24 to 120 hpf and also specifically in the developing heart from 48 to 120 hpf and in the adult heart. LARP7 mRNA was detected at all time points, in the whole embryo and in the heart, with the highest

concentration found in the whole embryo in the period 24-72 hpf. Both MOs, splice and translation blocking, diffused widely throughout the embryo as shown by morpholino oligos-associated red lissamine and effectively inhibited LARP7 expression.

Barboric described an altered body axis formation at 24 hpf, although the major axial polarity including the anteroposterior and dorsoventral axes appeared largely normal in LARP7 morphants. He also observed high mortality among LARP7 morphants at 48 hpf, associated with selective darkening of the brain region indicative of neurodegeneration. These features, however, could be non specific for the down-regulated gene. In fact, off-target effects can be a confounding variable when using MOs for the assignment of function in zebrafish. Some well-described and relatively consistent phenotype are p53-dependent neural toxicity (Nasevicius *et al.*, 2000; Robu *et al.*, 2007), shortened and gnarled tails, massive body curvatures and small heads and eyes (Woods and Schier, 2008). Mild body and tail curvature upward were common phenotypic features observed in my LARP7 morphants. However, the mortality I observed remained very low even at 120 hpf while signs of neurodegeneration were not clearly described, either in vivo or in hematoxylin and eosin stained sections. Moreover, in my experiments LARP7 morphants showed swimming ability and behavioural profile similar to controls.

The heart of LARP7 morphants showed an interesting phenotype. In 30-35% of embryos, the atrium was markedly dilated, severely in some cases, first observed at 48 hpf. This LARP7 knockdown specific phenotype could have several origins: atrial hyperplasia or hypertrophy or increased atrial pressure caused by a reduced ventricular function or compliance. The dilation was only observed in the atrium and as its wall is formed by only one cardiomyocyte cell layer it could be more susceptible to enlargment due to increases in intravascular pressure. Assessment of atrium cardiomyocyte number or size was not feasible because the thin atrial wall, formed by only one or two cell layers at 48-96 hpf, collapses following embryonic fixation and make very challenging a correct count of cardiomyocytes.

In the ventricle, characterized by a thicker wall, total cardiomyocyte number was

assessed and was found to be significantly higher in MO-LARP7 morphants embryos compared to controls. These data do suggest a role for LARP7 in cardiomyocyte proliferation. Several authors report contrasting data on the role of LARP7 on cell proliferation. For example, (Cheng *et al.*, 2012) reported that LARP7 knockdown increased proliferation and migration of gastric epithelial cells and promote gastric tumorigenesis via p-TEFb dysregulation. He and co-workers (2008) showed that LARP7 (reported as PIP7S) knockdown produced a significant increase in transcription of both PTHLH and TGM-2 genes, normally associated with human mammary epithelial cell transformation, through activating P-TEFb. However, a genetic study in human (Alazami *et al.*, 2012) has shown that LARP7 depletion caused primordial dwarfism (PD), a clinical phenotype characterized by severe growth restriction that has its onset in utero.

My experimental findings suggests that upregulation of CDK9 due to LARP7 knockdown could be responsible for the observed increase in ventricle cardiomyocyte number, the dilated atrial hyperplasia and/or hypertrophy and the slightly reduced cardiac function. The detailed mechanism for these changes requires further study and further confirmation in mammalian model systems.

Chapter 5

Development and validation of a heart laser injury model in the zebrafish embryo

5.1 Introduction

The adult mammalian heart has little or no proliferative capacity (Pasumarthi and Field, 2002; Faucherre and Jopling, 2012) while the neonatal mouse heart retains the capacity to regenerate for up to 7 days following birth (Porrello *et al.*, 2011). In contrast, the adult zebrafish heart undergoes a regenerative process following resection or cryoinjury, which results in complete functional recovery (Gonzalez-Rosa *et al.*, 2011; Poss *et al.*, 2002). The regenerative process in the adult zebrafish heart has been ascribed to dedifferentiation and proliferation of existing cardiomyocytes which demonstrate reactivation of a number of cardiac markers typically observed during early embryonic development (Gardiner *et al.*, 2002), including NKX2.5, TBX20, and hand2 (Lepilina *et al.*, 2006), notch1b and delta-C, (Raya *et al.*, 2003) or the cell-cycle regulator Mps1 (Poss, 2010; Poss *et al.*, 2002).

The zebrafish embryo also activates a genomic response following brain injury (Kizil *et al.*, 2012) or fin resection (Gonzalez-Rosa *et al.*, 2011) by upregulating injury-induced regenerative genes similar as in the adult (Mathew *et al.*, 2009). In Chapter 4 CDK9 has shown to be involved in cardiomyocyte proliferation during normal development. This poses the question whether CDK9 is involved in the cardiomyocyte proliferative process also following injury.

Therefore, a cardiac injury and repair model needs to be developed in the zebrafish embryo. In particular, a model that could be produced easily using a high throughput approach with a shorter time for response and repair that would also complement present models in the adult (Poss *et al.*, 2002).

Laser ablation techniques have been used in the zebrafish to induce kidney injury (Johnson *et al.*, 2011), thrombosis (Jagadeeswaran *et al.*, 2011; Gray *et al.*, 2007) and brain injury (Sieger *et al.*, 2012). Laser injury of the atrioventricular cushion of the embryonic chick heart has been demonstrated but requires induction of bradycardia by thermal cooling to allow targeted injury (Yalcin *et al.*, 2010). The zebrafish embryonic heart is considerably smaller than the chick heart at equivalent developmental stages and is a more challenging structure in which to create

precision injury (Happel *et al.*, 2010).

Here, it is presented a technique, which permits targeted and highly localized injury of the zebrafish embryonic heart at physiological heart rates. The precision is achieved by virtue of novel image-gating software which permits temporal synchronization between the cardiac cycle and delivery of the laser pulse. It was demonstrated the functional and histological consequences of laser injury in different heart regions and it was also provided evidence that the mechanism of recovery from laser injury to the ventricle is dependent on proliferation of cardiomyocytes**.**

Aims of this chapter are:

- Development of a cardiac laser injury model in the zebrafish embryo
- Assessment of the functional, molecular and histological effects of laser injury to the embryonic ventricle
- Assessment of the potential for testing pharmacological agents affecting cardiac ventricle injury and repair
- Assessment of the effects of multiple laser pulses into the embryonic ventricle
- Assessment of the effects of laser injury on other specific cardiac structures including the atrioventricular cushions and bulbous arteriosus.

5.2 Methods

5.2.1 Heart laser injury protocol

For a detailed description of the heart laser injury model see Section 2.7 in Chapter 2. Anaesthetized embryos 72 hours post fertilization (hpf) were placed on a plain glass microscope slide lying on their side (figure 5.1). Images were captured by a digital video camera mounted on a microscope and displayed on a monitor as a live video image of the sample. The average energy delivered per pulse, from each of the lasers, was consistently 0.9mJ over a duration of 3ms (300mW) directed at a ventricle area of approximately 10μm. After injury, each embryo was immediately placed in embryo medium to recover for a further 48 h.

5.2.1.1 Single pulse injury

In single pulse cardiac injury (figure 5.1), two different laser systems were compared and their effects on the embryonic heart were analysed: the PALM Microbeam (section 2.7.1) and the XYClone laser ablator (section 2.7.2).

5.2.1.2 Intra-cardiac structures injury

To assess the response to injury in different ventricle regions, this was divided arbitrarily into 3 regions (basal (B), mid (M) and apical (A), figure 5.6). The effects of a single laser pulse to each of these regions on heart rate and function was assessed. Also, the effect of the laser on specific intra-cardiac structures such as the atrioventricular (AV) cushions and bulbus arteriosus were also assessed (figure 5.6); for these studies, the XYClone laser ablator with the Optical Gating system (section 5.2.2) was employed.

5.2.1.3 Multi-pulses injury

The multi-pulses cardiac injury protocol involved the delivery of 1 to 5 laser pulses to the mid-region of the ventricle at 1 minute intervals during ventricular diastole. This approach could be achieved without creating significant injury to nearby cardiac structures using by virtue of the Optical Gating system (Section 5.2.2).

5.2.2 Optical Gating System

The Optical Gating system was described in detail in Section 2.7.2.2. It was set up in combination with the XYClone laser ablator (section 2.7.2.1) to overcome the difficulty in delivering the laser beam to a specific area of the rapidly beating zebrafish embryo heart.

This novel approach also permitted the assessment of multiple-pulses injury (section 2.5.1.2) on the heart ventricle and precise targeting of specific intra-cardiac structures (section 2.5.1.3).

5.2.3 Evaluation of Cardiovascular function

Methods for cardiovascular functional measurements have been detailed in section 2.6; these included ejection fraction (EF) and ventricular diastolic area (VDA), heart rate (HR) and cardinal vein blood flow (CVBF).

5.2.4 Exposure of embryos to drugs

5.2.4.1 Exposure to Aphidicolin

To assess the effect of cell cycle inhibition following laser injury, embryos were bathed from 24 hpf in embryo medium containing 30 μM aphidicolin (Lyons *et al.*, 2005) solubilized in Dimethyl Sulfoxide (DMSO) 1%. Laser injury was induced at 72 hpf and embryos maintained in aphidicolin until 120 hpf. Control embryos incubated in vehicle (DMSO 1%) from 24 hpf were treated in an identical manner with laser injury at 72 hpf. A control group of embryos exposed to aphidicolin with no laser injury was also included.

5.2.4.2 Exposure to Colchicine

A similar protocol described in paragraph 5.2.4.1 was used for colchicine treatment, another cell cycle inhibitor, at 100μM. As for the Aphidicolin, this was solubilized in DMSO 1% and DMSO 1% was used in all control solutions.

5.2.5 Immunohistochemistry

Immunohistochemistry was performed on microdissected zebrafish hearts as

described in Section 2.8.1.

5.2.5.1 Cardiomyocyte number analysis

Total and Proliferating Ventricle Cardiomyocyte number analysis was performed as described in section 2.9.2 .

5.2.5.2 Apoptosis assays

TUNEL and Acridine Orange staining were performed as described respectively in section 2.10.1 and 2.10.2.

5.2.6 Histopathology

Haematoxylin & Eosin staining was performed as described in section 2.9.4.

5.2.7 Statistical analysis

Experiments were performed in triplicate with on average 20-30 embryos per experiment, unless otherwise stated. Data are presented as mean ± standard error of the mean (SEM). Statistical analyses were performed using GraphPad Prism 5. One-way or two-way repeated measures ANOVA followed by Bonferroni post-hoc test, were used to compare means within and between groups. P values <0.05 were considered significant. Student's t-test was used to compare outcomes from the two laser systems.

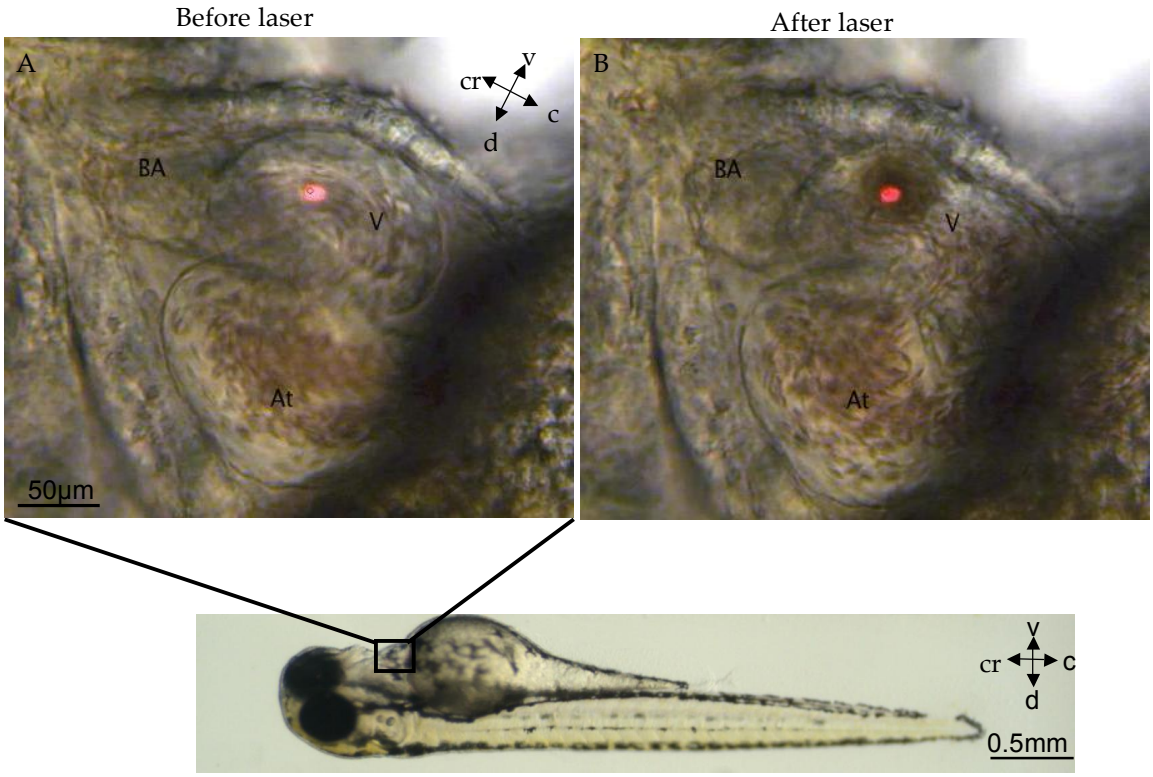

Figure 5.1- Cardiac laser injury. Zebrafish embryos 72 hpf (lower panel) were used for all experiments of laser injury. The laser pulse was delivered to the area of the ventricle indicated by the red dot (Panel A) and resulted in a clear burn-mark at the point of injury (Panel B), see also supplementary movie 1 (V – ventricle, BA – bulbus arteriosus, At – atrium). Position of the embryo is marked by compass lines (c-caudal, cr-cranial, d-dorsal, v-ventral).

5.3 Results

5.3.1 Effects of a single laser pulse to the ventricle

5.3.1.1 Heart function and cardinal vein blood flow

A single laser pulse to the mid-cavity of the ventricle resulted in instantaneous cardiac injury (figure 5.1), confirmed optically by a 2 to 4 s pause followed by marked bradycardia and a small amount of bleeding into the pericardial space. There then followed a gradual and progressive increase in heart rate (HR) over the following 2 to 3 min with persistent bradycardia and a reduced HR by 2h (117±11 vs 167±9 bpm, $p \leq 0.001$; figure 5.2 B). Laser injury also resulted in a temporary cessation of blood flow to the tail, followed by reduced blood flow in the posterior cardinal vein at 2h post-laser (103±15 vs 316±13 $\mu m.s^{-1}$, $p \leq 0.001$; figure 5.2 C). At the same time-point, laser injury produced a reduced ejection fraction (EF) (14.1±1.8 vs 20.1±1.3%, $p \leq 0.001$; figure 5.2 D) and ventricle diastolic area (VDA) (5.3±0.8 vs 10.1±0.6·10^3 μm^2; $p \leq 0.001$; figure 5.2 E). These parameters recovered to control levels by 24h and remained comparable to controls at 48h post-laser (figure 5.2 A-E).

For the purposes of direct injury to the mid-ventricle, a detailed comparison of the effects of each laser systems, PALM Microbeam and XYClone Ablator, indicated that there was no significant differences in EF, HR, VDA and total ventricular cardiomyocyte number (TVCn) following single pulse injury at 2h and 24h post-laser (table 5.1). However, XYClone in combination with the Optical Gating System was found to significantly increase the accuracy and precision of injury to specific regions of the ventricle while also reducing the need to repeatedly manipulate the embryo into a favorable position for the laser.

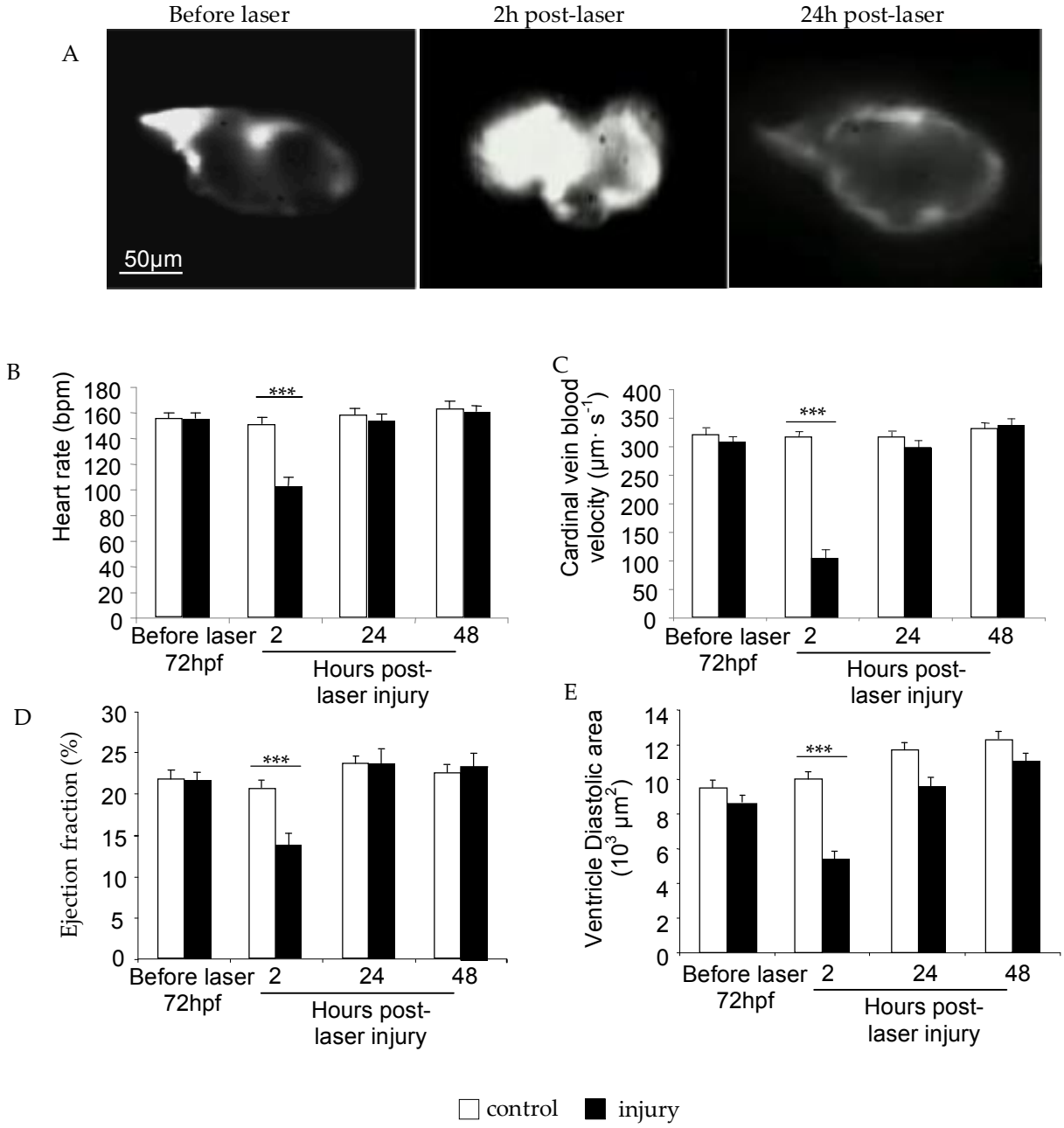

Figure 5.2- Effects of a single laser pulse on cardiovascular function. Data presented here were obtained from embryos injured with the PALM laser system at 72 hpf. A. Images captured under fluorescence microscope with a B&W video camera showing the same zebrafish embryonic heart ventricle before laser injury, at 2h and 24h post-laser injury. Embryos were maintained at 28.5°C between the measures. B-E Heart rate, cardinal vein blood velocity, ejection fraction and ventricle diastolic area were assessed before laser and 2, 24, 48h post-laser injury (Mean±sem, N=5 experiments). **=p<0.05, ***=p<0.001, two-way ANOVA test for repeated measures was used to assess difference between means, followed by Bonferroni post-hoc test).

Table 5.1- Comparison of the PALM Microbeam and XYClone Ablator systems. Single laser pulse injury to the mid-ventricle from each laser system resulted in similar changes in ejection fraction, heart rate, ventricle diastolic area and cardiomyocyte number at 2h and 24h post-laser (mean±sem, N=20 per group, 3 experiments, Student's t-test).

Laser System	Ejection Fraction (%)		Heart Rate (beats per minute)		Ventricle Diastolic Area (x 10^3 $\mu m^{2)}$		Total ventricle cardiomyocyte (n)	
	Hours post-laser							
	2	24	2	24	2	24	2	24
PALM Microbeam	14.5±1.5	22.5±1.9	109±10	158±10	5.4±0.5	9.7±0.9	199 ±13	285±13
XYClone Ablator	14.1±1.8	24±2.1	117±11	152±7	5.3±0.8	9.3±0.6	195 ±15	290±21
T-test	p=0.56	p=0.62	p=0.37	p=0.33	p=0.66	p=0.7	p=0.51	p=0.19

5.3.1.2 Cardiomyocyte number analysis

The zebrafish embryo heart ventricle demonstrated a progressive increase in total ventricle cardiomyocyte (TVCn) between 72h and 120h post-fertilization (figure 5.3 D) consistent with normal development of control hearts. At 2h post-laser, we observed a statistically significant mean 18% reduction in the number of cardiomyocytes in injured ventricles (195±15 vs 238±15, $p \leq 0.05$; figure 5.3) that recovered to control levels by 24h post-laser. However, between 2h and 24h post-laser we observed a mean 20% increase in TVCn in controls and a mean 49% increase in injured ventricles (figure 5.3A, B & D; table 5.1). The proportional increase in the time-period 2h to 48h post-laser injury was 53% in controls and 82% in injured ventricles. Proliferating ventricle cardiomyocytes (PVCn) were identified by anti-PhosphoHistone H3 (PHH3). At 2h and 24h post-laser injury, numbers of PHH3 positive nuclei identified were, respectively, 5.5±0.6 and 6.8±1.0 ($p=0.24$) in controls and 4.7±0.9 and 7.9±1 ($p=0.04$) (figure 5.3 C & E).

5.3.1.3 Histology

In laser-injured ventricles 2h post-laser there was histological evidence of focal fibrinoid necrosis of the pericardium and myocardium as evidenced by the presence of amorphous hyper-acidophilic debris containing pyknotic and karyorrhectic nuclear remnants (figure 5.4 A).

Mild haemorrhage and accumulation of eosinophilic proteinaceous oedema fluid was present within the pericardial space. Apoptotic nuclei were recognized as shown by Acridine Orange staining (figure 5.4 B). At 24h post-laser injury although active necrosis was absent there was moderate segmental reduction in thickness of the mural myocardium compared to controls with multifocal adhesions of the pericardium to the thoracic wall.

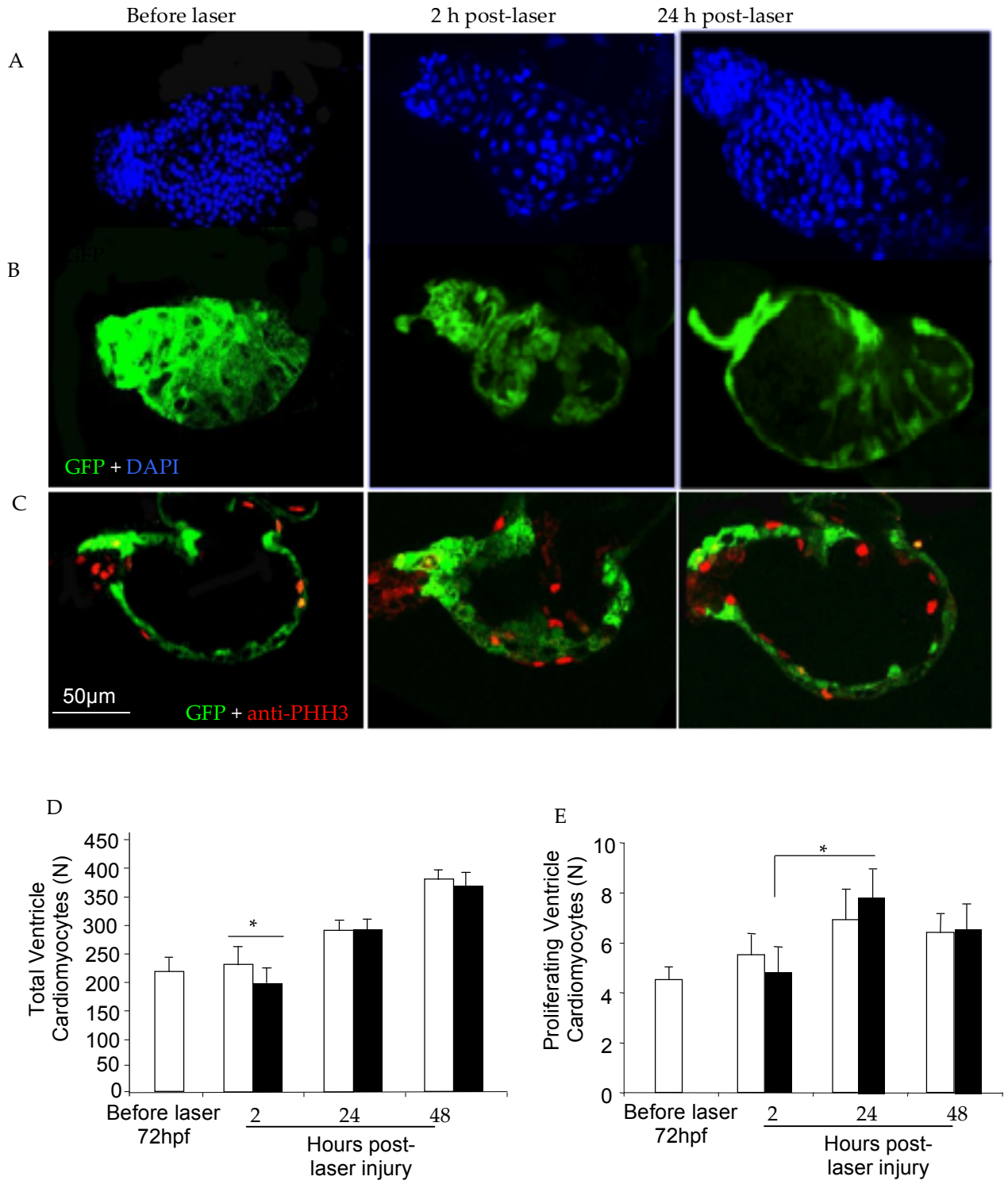

Figure 5.3- Effect of a single laser pulse on total and proliferating ventricle cardiomyocyte number. Panel **A**. DAPI stained nuclei counted as total number of ventricle cardiomyocytes (TVCn) in cmlc2:EGFP hearts, shown in the lower panel (**B**). **C.** PhosphoHistone H3 stained nuclei, in red, represent proliferating cardiomyocytes (PVCm). Total (**D**) and proliferating (**E**) ventricle cardiomyocyte number variations during normal development, from 72 to 120 hpf (48 h post-laser), and following laser injury (Mean±sem, N=5 experiments, *= $p<0.05$, two-way ANOVA test followed by Bonferroni post-hoc test was used to compare means).

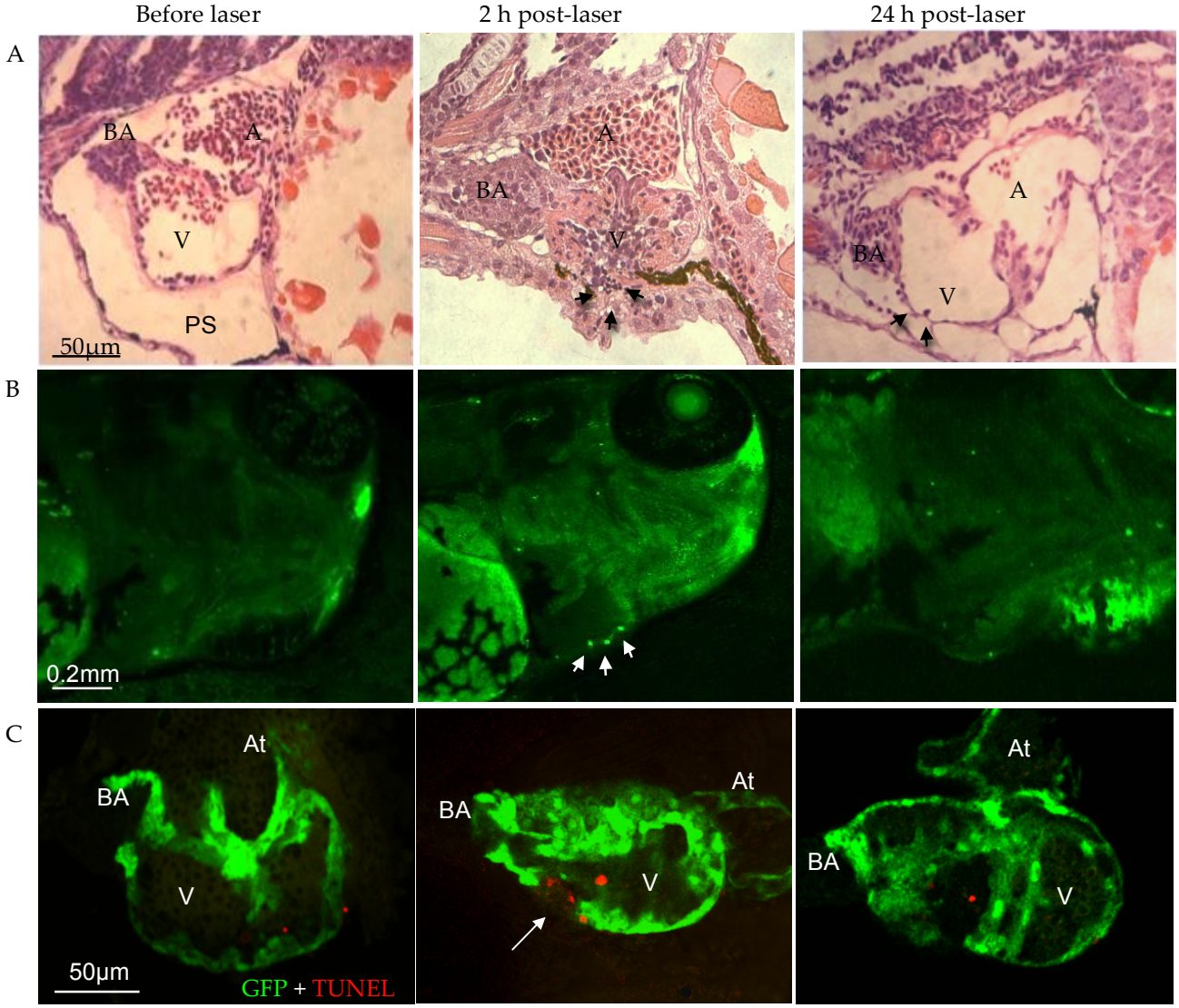

Figure 5.4 - Histological and apoptotic cell assessment of zebrafish heart ventricle laser injury. Panel row **A**. Haematoxylin and Eosin staining showing apoptotic/necrotic bodies in the area of laser damage (black arrowhead) at 2h post-laser injury and their absence at 24h post-laser injury. Laser-injury also resulted in a reduction in thickness of the mural myocardium at 24h post-laser (black arrowhead). Panel row **B**. Whole mounted zebrafish embryos (Wik wild type strain), stained with acridine orange, show positive nuclei at 2h post-laser (white arrows) in the area of laser injury. No apoptotic/necrotic bodies were detectable before laser or at 24h post-laser in the site of injury. Panel row **C**. Whole mounted zebrafish embryonic hearts following TUNEL assay, showing apoptotic bodies at 2 h post-laser (white arrows) in the area of laser injury. Few apoptotic bodies were detectable before laser or at 24 h post-laser in the site of injury (N=6 per group). V – ventricle, BA – bulbus arteriosus, At – atrium).

In fish receiving 3 or more laser shots there were residual foci of necrosis and more extensive cardiac / thoracic wall adhesions. These features were not observed at 48h post-laser injury. A greater number of apoptotic bodies was more evident in injured ventricle hearts as shown by TUNEL assay (figure 5.4 C) particularly around the region of the laser burn at 2 h post-laser injury (laser 5.2±1.0 vs controls 1.3±0.4). The number of apoptotic bodies had returned to control levels by 24 h post-laser.

5.3.2 Effects of multiple laser pulse injury

To assess the potential recovery ability of the zebrafish embryonic heart, I assessed the effect of multiple laser injury to the ventricle, using 1 to 5 pulses to the mid-ventricle during diastole (table 5.2). This experiments wanted to answer the question: how much injury the heart is able to tolerate before loosing the recovery ability? The XYClone laser in combination with Optical Gating System system was used for these experiments. Increasing the number of laser pulses was associated with a steady fall in ejection fraction at 2h post-laser. Ventricles treated with a single or double laser pulse recovered fully by 24h and 48h post-laser. Ventricles injured with 3 laser pulses showed some functional recovery at 48h post-laser, 4 or 5 laser pulses resulted in a significantly lower ejection fraction at 2h and these ventricles failed to recover function by 48h post-laser injury. In addition, increasing the number of laser pulses resulted in a progressive decrease in TVCn at 2 h post-laser (table 5.2) followed by a mean increase of 20 %, 49 % and 68 % in TVCn by 24h in ventricles treated with 3, 4 and 5 laser pulses respectively.

5.3.3 Effects of laser injury to different heart regions

5.3.3.1 Effects of regionally targeted single laser pulse injury to the zebrafish embryo heart ventricle.

To understand if the recovery ability of the heart was the same in the entire ventricle, a single laser pulse was directed at different regions of the ventricle (basal, mid and apical) using the XYClone laser in combination with Optical Gating System

Table 5.2- Effects of multiple laser pulses on the zebrafish embryo heart ventricle. Effects of increasing number of laser pulses (1 to 5) on ejection fraction and ventricle cardiomyocyte number at 2, 24 and 48h post-laser injury. Laser-Optical Gating System system allowed multiple laser pulses injury in the same ventricle area, with each pulse delivered in the diastolic phase (mean±sem, N=16, 3 experiments, *= p<0.05 compared to control at 2h post-laser, one-way ANOVA test).

		Number of pulses					
		Control	1	2	3	4	5
Ejection fraction (%)	Before laser	20.1±1.5	21.1±1.5	19.9±1.5	20.4±1.5	20.8±1.5	20±1.5
	2h post-laser	19.5±2.2	14.5±2.3***	10.2±2.5***	5.6±2.3***	1.7±2.2***	0.8±1.2***
	24h post-laser	22.3±2.4	23.1±3.2	17.4±1.2	12±3	7.5±3.3	1.6±2.8
	48h post-laser	22.2±0.9	22.5±2	21.8±4.3	14.8±2.3	9.4±2.7	1.7±5.7
Total ventricle cardiomyocytes (n)	2h post-laser	238±15	195±15*	168±16*	156±12*	145.6±19*	130±10*
	24h post-laser	285±11	290±7	257±21	237±36	203±21	219±3
	48h post-laser	365±10	355±9	301±17	317±21	293±16	252±17

system (figure 5.5). Heart rate (HR) reduction was more marked at 2h post-laser following injury to the mid and basal regions compared to the apical region (97±10 vs 113±10 figure 5.5 A), while at 24h post-laser the HR was comparable to controls for all regions analysed. Changes in ejection fraction were similar following injury to the three specified regions (data not shown).

5.3.3.2 Effects of single laser pulse injury to the atrioventricular cushions and bulbus arteriosus

Injury to the AV cushion resulted in heart block observed as a marked reduction in ventricular rate with preserved atrial rate (Ventricle : Atrium Rate ratio 1±0.06 vs 0.6±0.1, $p \leq 0.01$; figure 5.5 B), consistent with a degree of AV conduction block. Injury to the AV cushion also resulted in marked regurgitation of blood cells from the ventricle into the atrium with evidence of reversed pulsatile flow extending into the caudal vein suggestive of valvular regurgitation. Laser injury to the bulbus arteriosus (BA) consistently resulted in a marked temporary or permanent thrombotic occlusion of the outflow tract, typified by a build-up of erythrocytes within the ventricle cavity and cessation of circulation to the gills and tail. In some cases, flow in the BA resumed after a period of time with reduced flow into the gills.

5.3.4 Effects of pharmacological agents on response to cardiac laser injury

5.3.4.1 Aphidicolin

Embryos incubated with the cell cycle inhibitor aphidicolin 30 μM showed a similar reduction in ejection fraction and cardiomyocyte number at 2h post-laser injury compared to controls (figure 5.6 A). At 24h post-laser, ejection fraction did not recover in embryos exposed to aphidicolin, but did recover in laser-injured embryos incubated in vehicle (9.1±2.1 vs 18.8±2.3, $p \leq 0.001$; figure 5.6 A). Aphidicolin 30 μM exposure was associated with a significant reduction in cardiomyocyte number at 24h and 48h post-laser injury compared to vehicle (169±19 vs 342±18 at 48h, $p \leq 0.001$; figure 5.6 B).

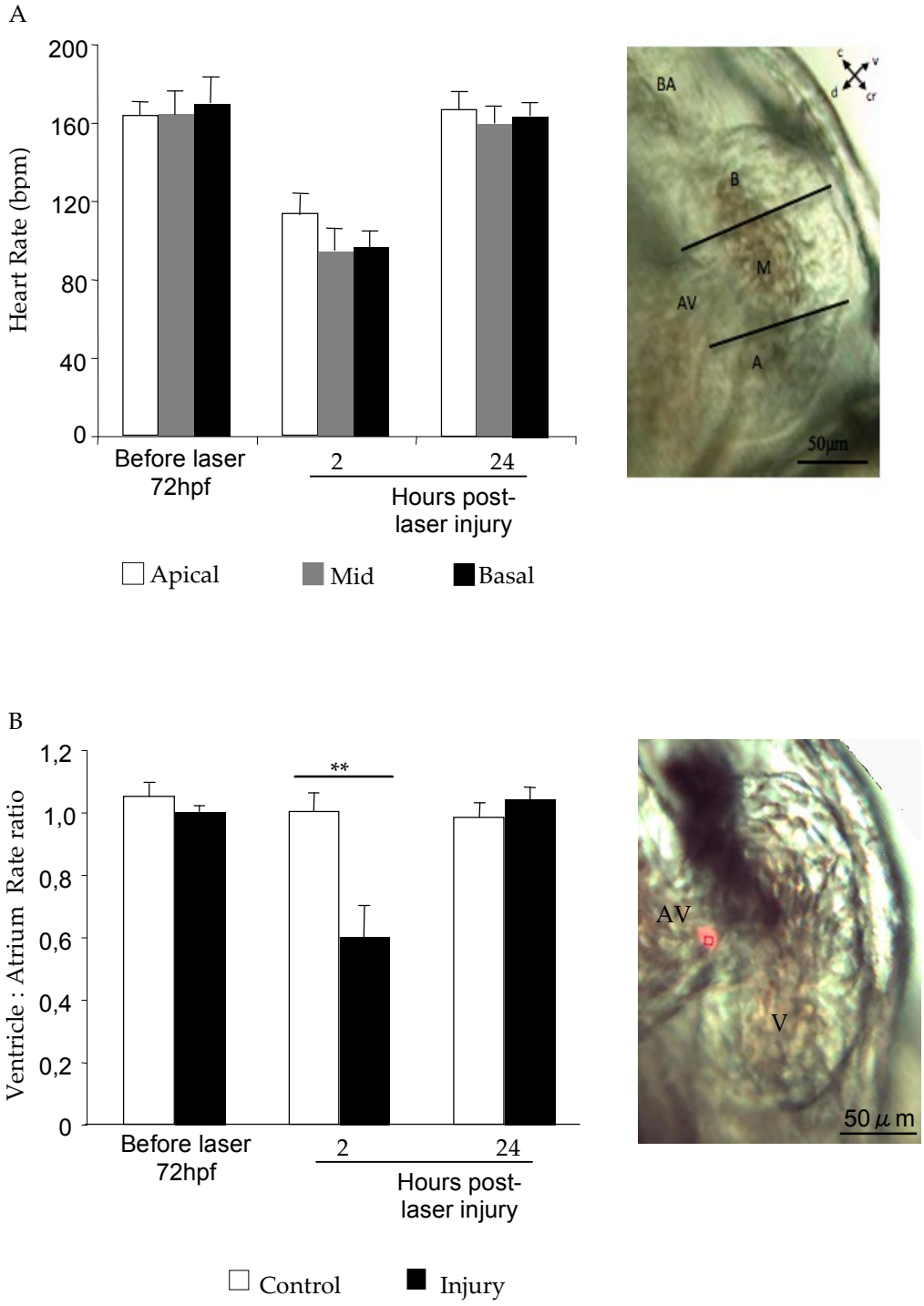

Figure 5.5 – Effects of laser injury to different heart regions. A. Effects of regionally-targeted single laser pulse injury in the zebrafish embryo heart ventricle. Heart ventricle was injured into three different ventricle regions: basal (B), middle (M) and apical. The diagram shows the heart rate before laser, 2h and 24h following laser injury to the 3 specified zones of the ventricle. B. Effects of single laser pulse injury in the atrioventricular cushion. Ventricle : atrium heart rate ratio was used as a marker of AV block, following laser injury to the AV cushions. Data were presented as mean±sem, N=2 experiments, $p<0.05$, ANOVA followed by Bonferroni's post-hoc test. Key – Ventricle=V, AV= atrioventricular, BA=bulbus arteriosus

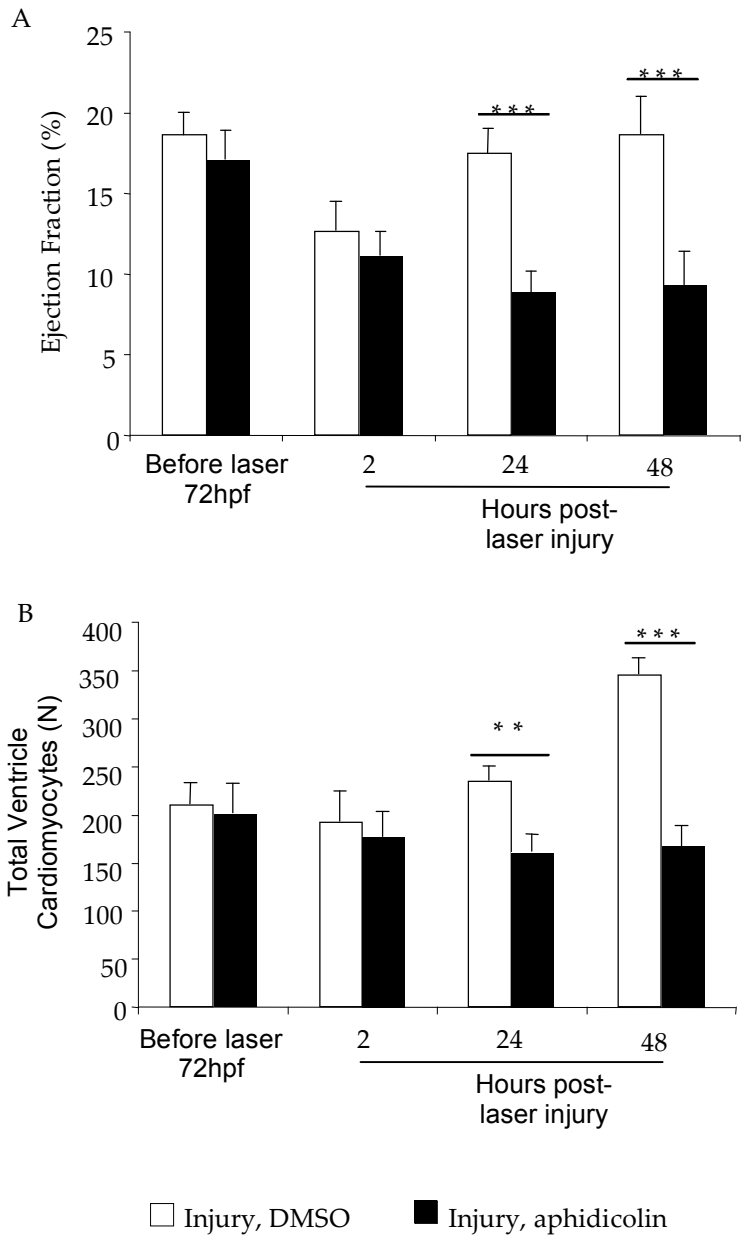

Figure 5.6 - Effects of cell cycle inhibition on cardiac recovery following laser injury in zebrafish embryonic hearts. Embryos from the same clutch of eggs were continuously exposed to Aphidicolin 30μM from 24 to 120 hpf. Some embryos were laser-injured at the mid-ventricle at 72 hpf and ejection fraction (diagram A) and ventricle cardiomyocyte number (diagram B) were assessed before laser and then at 2, 24 and 48 h post-laser injury. (mean±sem, N=3 experiments, *= $p<0.05$, **= $p<0.01$, ANOVA followed by Bonferroni's post-hoc test)

5.3.4.1 Colchicine

Embryos incubated with the cell cycle inhibitor colchicine 100µM, showed a reduction in ventricular diastolic area before laser and at 2 h post-laser injury (figure 5.7). Conversely, at 24 and 48 h post-laser, embryos treated with this drug didn't show any recovery and VDA was significantly lower compared to controls.

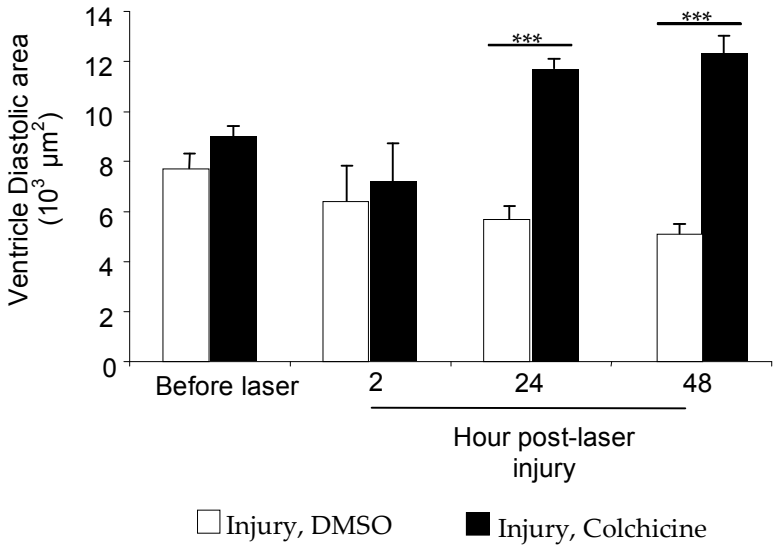

Figure 5.7- Effects of Colchicine 100µM on the ventricle diastolic area in zebrafish embryonic heart following cardiac laser injury. Embryos from the same clutch of eggs were continuously exposed to Colchicine 100µM from 24 to 120 hpf. Some embryos were laser-injured at the mid-ventricle at 72 hpf and ventricle diastolic area was assessed before laser and then at 2, 24 and 48 h post-laser injury. (mean±sem, N=3 experiments, *=p<0.05, **=p<0.01, ANOVA by Bonferroni's post-hoc test)

5.4 Discussion

5.4.1 Development of a novel cardiac laser injury model

5.4.1.1 Comparison of three different approaches

The initial approach described here utilised a single laser pulse from two different laser systems, PALM Microbeam and XYClone Ablator, targeted at the mid-point of the ventricle. While this resulted in reproducible damage to the ventricle, it was clear that the rapid cardiac cycle in the zebrafish heart affects the accuracy of delivering the laser beam to a specific cardiac regions and/or anatomical structures. Moreover, atrium and ventricle are typically overlapping in the embryonic zebrafish heart providing further difficulties in targeting specific heart structures without injuring nearby structures. Our initial approach was to optimally position the embryo on the slide to ensure there was minimal overlap of cardiac structures and thus provide a clear target for the laser. However, repositioning the embryo multiple times was time consuming and could result in stress and injury to the embryo. We identified the need to develop a system that addressed this problem allowing more precise targeting of specific cardiac structures. We also wanted to assess the impact of injury to different regions of the embryonic ventricle. Therefore, a further approach that allowed the user to trigger the laser pulse during a specific phase of the cardiac cycle was developed. This was achieved using a previously validated Optical Gating technique (Taylor *et al.*, 2011). This system was readily linked to the XYClone Ablator (Laser-Optical Gating System), which was also in routine use for other purposes within our institute. This new tool permitted highly accurate targeting of the laser to different regions of the heart at specific time points of the cardiac cycle.

While our data suggest there was no difference between the two laser systems in the resulting injury to the heart from a single laser pulse, the Laser-Optical Gating System was significantly easier to use and did not require constant manual repositioning of the embryo on the slide in order to obtain a clearer view of the

ventricle without overlap of the atrium. This allowed a faster throughput of embryos with the possibility of injuring 50 to 100 embryos per hour. This technique has the potential to be used to assess pharmacological and molecular pathways associated with and contributing to injury and recovery in the heart. The only comparable high-throughput model reported in the literature in the zebrafish embryo is a transgenic chemical cell ablation approach in the zebrafish embryonic heart (Curado *et al.*, 2007). However, this chemical-ablation approach produced a diffuse cardiomyocyte cell death that occurs 2 to 3 hour after metronidazole exposure of the whole embryo. The laser injury model presented here does not need pharmacological intervention to induce damage and results in regional damage of a nature similar to the regional damage occurring with ligation of a coronary artery in mammals.

5.4.1.2 Zebrafish embryonic ventricle recovers following laser injury

Significant injury was immediate as demonstrated by cardiac arrest and cessation of tail blood flow. This was followed by a significant fall in EF, VDA and HR at 2h post-laser injury, which recovered by 24h post-laser injury. In addition, at 2h post-laser injury we observed a loss of ventricle cardiomyocytes. Histology indicated pyknotic nuclear remnants in the damaged region suggestive of cell death by necrosis. Apoptosis, assessed by AO staining, also partially contributed to cardiomyocyte loss following injury as demonstrated by chromatin clumping at 2h post-laser. These histological appearances could have resulted from vaporization and pyrolysis of cells at the site of laser injury accompanied by a more delayed attrition of cardiomyocytes in regions more distant from the direct site of injury. Interestingly, at 24h post-laser necrosis nor apoptosis were not observed whilst there was a moderate reduction in thickness of the mural myocardium compared to controls at this time point, at a time when cardiac function returned to normal.

5.4.1.3 Cardiomyocyte proliferation drives the functional recovery of injured ventricles

Cardiomyocyte number increased by 20% in control non-lasered ventricles between 72 hpf and 96 hpf as part of normal development. During this same time-period, we observed a far greater proportional increase in the number of cardiomyocytes in lasered ventricles by almost 50% suggesting that the proliferative process had been accelerated by laser injury. These changes are significantly greater than the intra-observer variation and are therefore likely to reflect a true change in cardiomyocyte number.

Enhanced proliferation of cardiomyocytes was further supported by significantly more PHH3 nuclei in lasered ventricles. The underlying mechanism for this apparent acceleration of cardiomyocyte proliferation is possibly related to laser-induced release of local factors enhancing proliferative change in surviving cardiomyocytes or could be due to circulating factors responding to the compromise in the circulatory system. A further intriguing observation is that ventricles treated with multiple laser pulses showed significant reductions in cardiomyocytes in keeping with more widespread cell death at 2h followed by a significantly greater increase in cardiomyocytes in the lasered ventricles compared to controls at 24 and 48h post-laser. This was observed despite the ventricles not showing signs of functional recovery. Indeed, our observations are consistent findings in the adult zebrafish (Poss *et al.*, 2002) and the mouse where cardiac injury has been shown to trigger epicardial cell proliferation (Zhou *et al.*, 2011).

5.4.1.4 Effects of multiple laser pulses into the embryonic ventricle

Once we had established the ability of the zebrafish embryo to undergo complete functional recovery following a single laser pulse, we then assessed the effects of more severe laser damage in a dose dependent manner using 1 to 5 laser pulses.

This experiment aimed to assess how much damage load the zebrafish embryonic heart at 72 hpf is capable to sustain before loosing its ability to recover functionally.

Using 3 or 4 laser pulses resulted in a marked reduction in ejection fraction by 2h

post-laser and very limited recovery of function by 24 and 48h post-laser. Ventricles treated with 5 pulses showed no recovery of function at 48h post-laser despite an increase in cardiomyocyte number identified by DAPI staining. This could be due to the inability of newly formed cardiomyocytes to function and assemble in a manner that can generate a coordinated contraction in the ventricle. Some embryos receiving three or more laser pulses, demonstrated histological foci of residual necrosis at 24h post-laser.

5.4.1.5 Effect of pharmacological agents on the recovery ability

Further evidence to indicate that proliferation of new cardiomyocytes contributed to functional recovery of the lasered ventricles was provided by the experiments showing that the cell cycle inhibitor aphidicolin (30 μM) effectively inhibited recovery of ejection fraction and that this was associated with reduced cardiomyocyte proliferation. These findings suggest that the repair and recovery mechanism following laser injury is largely mediated by newly formed cardiomyocytes (Poss *et al.*, 2002; Jopling *et al.*, 2010) although we cannot completely exclude cardiomyocyte hypertrophy as part of the recovery process. Our observations suggest that laser injury could increase cardiomyocyte proliferation in the zebrafish embryonic heart. Although there are now numerous published studies indicating that the adult zebrafish has an astonishing ability to repair following resection or injury, we do not fully understand its total regenerative reserve. We do know that, in-vivo, removal of more than 20% usually results in death in adults. We also do not know how this capacity changes between embryonic and adult stages.

Another aspect to mention is the effect of colchicine (100 μM) on the cardiac recovery following injury. As an actin-polymerization inhibitor, Colchicine impedes the formation of the mitotic fuse and therefore inhibits cell division. Incubation of embryos with colchicine 100μM, had no impact on the initial injury response but significantly impaired recovery of HF and VDA at 24 hours post-laser injury. The colchicine could have blocked the cardiac recovery in two different way: by inhibiting either the cell cycle or the F-actin polymerization needed to organize the

ventricle architecture (Taber, 2006; Voronov *et al.*, 2004) perturbed following injury.

5.4.2 Additional applications of the Laser-Optical Gating System in the zebrafish embryo heart

5.4.2.1 Laser-induced occlusion of cardiac outflow as a model of volume and pressure overload

Laser technology has been previously used to induce proximal aortic occlusion to investigate arteriogenesis and collateral blood vessel development in the zebrafish embryo (Gray *et al.*, 2007). Here, we have used our laser model to induce complete or partial ventricle outflow obstruction in the beating zebrafish embryo heart. One or two laser pulses to the BA caused temporary or permanent obstruction to cardiac outflow. Following outflow occlusion, the atrium continued to contract vigorously while erythrocytes accumulated rapidly in the ventricle. The ventricle appeared to show signs of volume and possibly pressure overload. This also resulted in AV regurgitation from the ventricle to the atrium during ventricle systole and in clear thickening of the ventricle wall. This technique should be explored further as a potential model of acute or chronic volume and possibly pressure overload hypertrophy.

5.4.2.2 Laser-induced injury into the atrioventricular cushion as a model of heart block and mitral valve insufficiency

In non-mammalian vertebrates, a cardiac conducting system with properties similar to those of the mammalian hearts has been inferred (Sedmera *et al.*, 2003; Chi *et al.*, 2008) although detailed anatomical structures have not been described. In zebrafish, the pacemaker region becomes defined at approximately 72 hpf (Arrenberg *et al.*, 2010), with the atrioventricular canal contributing to the conduction of the electrical activity from atrium to ventricle.

We have used our laser model to influence atrioventricular conduction by injuring the AV cushions. Single laser pulse resulted in immediate bradycardia, lasting for a few seconds, followed by a significant reduction in ventricular rate compared to the atrial rate, that gradually normalized over the following few hours, finally returning

to normal by 24h h post-laser. Injury to the AV cushion also resulted in marked regurgitation of blood cells from the ventricle into the atrium with evidence of pulsatile flow reversal extending backwards into the caudal vein. This AV regurgitation mimics mitral or tricuspid valve regurgitation and could result in a model of chronic volume overload of the ventricle.

This study has demonstrated the feasibility and reproducibility of a novel method of injury to the zebrafish embryonic heart. With this approach, for the first time was shown the ability of the zebrafish embryo heart to recover from laser injury by 24h after laser by a mechanism largely dependent on the proliferation of new cardiomyocytes. Furthermore, laser injury appeared to stimulate this proliferative process. The ability to synchronize the laser pulse with the cardiac cycle permits more precise and targeted injury of specific structures within the embryonic heart. In addition, the Laser-Optical Gating System has shown to increase the utility of the laser, providing new models of outflow tract obstruction, heart block and AV valve regurgitation. Taken together, these models could permit the study of novel mechanisms related to molecular and cellular repair and recovery of the heart using a high throughput approach.

Chapter 6

Effects of inhibition and derepression of CDK9 on the embryonic heart response to laser injury

6.1 Introduction

The limited ability of adult mammals to repair the heart following an injury starkly contrasts with the highly effective cardiac regenerative process in lower vertebrates. In contrast, embryonic and fetal hearts of most Vertebrates typically show some degree of regenerative capacity which is lost in early post-natal life. In Chapter 5 we demonstrated the ability of the embryonic zebrafish heart to regenerate and repair functionally following laser injury. Recently, underlying mechanisms of heart regeneration in the adult zebrafish have become clearer with evidence that mature cardiomyocytes dedifferentiate, re-enter the cell cycle and then proliferate to support repair and replacement of injured myocardium (Mercola *et al.*, 2011);(Jopling *et al.*, 2010). Moreover, injury-induced regenerative genetic programs appear to be activated after injury in zebrafish heart, as already shown in the zebrafish brain (Kizil *et al.*, 2012), where CDK9 and the P-TEFb complex could play a significant role. For example, it has been reported that CDK9$_{55}$ was specifically induced in injured skeletal muscle and its activity was strictly required for the achievement of the muscle regeneration process (Giacinti *et al.*, 2008). In addition, transplanted HEXIM1-haplodeficient satellite cells improved muscle regeneration after injury, while HEXIM1 overexpression restrained satellite cell proliferation and impeded muscle regeneration (Hong *et al.*, 2012). Conversely, in adult stem cells CDK9 protein and mRNA are downregulated (Freter *et al.*, 2010) and this inhibition resulted in enhanced survival of cells.

The possible role of CDK9 activation in the response to injury in the zebrafish heart is not supported by published microarray data but that does not completely exclude the possibility that activation of CDK9 could support and possibly enhance the reparative process. In this chapter I intend to explore this possibility by assessing the possible role of CDK9 in the response to heart injury following down- and up-regulation of CDK9 activity using genetic and pharmacological tools in the zebrafish embryo.

Overall aim

Assess the role of CDK9 on the response of the heart to laser-injury in the zebrafish embryo.

Key questions:

- How does decreased CDK9 activity, by pharmacological and genetic manipulation, impact on recovery from heart laser injury in the zebrafish embryo?
- How does increased CDK9 activity, induced by LARP7 knockdown, impact on the recovery from heart laser injury in the zebrafish embryo?

6.2 Methods

Zebrafish transgenic cmlc2:EGFP embryos were used for all experiments, unless stated.

6.2.1 Cardiovascular function and cardiomyocyte analysis

Ejection fraction (EF) and total ventricular cardiomyocyte number (TVCn) were assessed. Methods are described in detail in chapter 2, section 2.6 and 2.9.2.

6.2.2 CDK9 and LARP7 Gene knockdown

Morpholino splice blocking oligonucleotides were used to inhibit CDK9 (MO-CDK9splice) (for CDK9 morpholino sequence see table 4.1.1) and LARP7 (MO-LARP7splice) (see table 4.2.1) mRNA splicing. A mismatch oligo (MO-CDK9mism and MO-LARP7mism) was used as a control. The amount of morpholino injected were the same as described in Chapter 4. A detailed description of the morpholino knockdown is reported in Chapter 2, section 2.13.

6.2.3 Pharmacological treatment of embryos

Flavopiridol was used to inhibit CDK9 activity as reported in Section 4.1.2.6.

6.2.4 Gene expression analysis

Quantitative PCR (Section 2.12) has been used to examine CDK9 expression in the whole embryo before and after cardiac laser injury.

6.2.5 Laser technique

The laser technique and related protocol of cardiac injury has been discussed in chapter 2 (section 2.7) and chapter 5 (section 5.2.1).

6.2.6 Statistics

See chapter 2, section 2.15 for a detailed description of statistical analysis used.

6.3 Results

6.3.3 Effect of CDK9 modulation following cardiac laser injury

6.3.3.1 Expression of CDK9 in the whole embryo following cardiac laser injury

This experiment has been done only once, therefore data have not been statistically analysed. Q-PCR was performed before laser, 10 min and 1, 3 and 24 hours post laser injury. CDK9 gene expression, measured in the whole embryo, was increased in cardiac laser-injured embryos compared to non-injured embryos at all time points (figure 6.1).

6.3.3.2 Cardiac function and cardiomyocyte number in CDK9 knockdown embryos following laser injury

In control embryos of all three treatments reported in figure 6.2, ejection fraction (EF) and total ventricular cardiomyocyte number (TVCn) were reduced at 2 h post-laser and both parameters recovered fully at 24 h post-laser, confirming data shown in Chapter 5.

Embryos injected with MO-CDK9 mismatch showed similar pattern in EF and TVCn compared to control non-injected although the recovery at 24 h post-laser was not complete. In embryos injected with MO-CDK9 splice blocking, instead, the EF was significantly reduced and TVCn slightly reduced compared to MO-CDK9 mismatch and control non-injected hearts that had been lasered (fig. 6.2 A & B). At 24 h post-laser injury MO-CDK9splice injected embryos did not show any recovery in cardiac function that, together with TVCn continued to decrease (fig. 6.2 A&B). Embryos exposed to flavopiridol 3μM, showed reduced EF and TVCn compared to controls lasered hearts. At 24h post-laser embryos exposed to the drug were not able to recovery cardiac function that had a similar value as the MO-CDK9splice injected

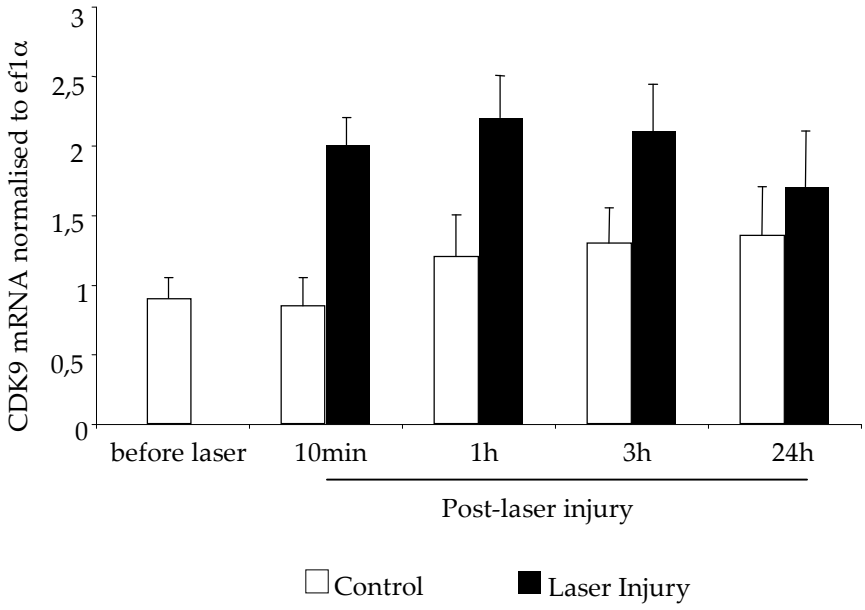

Figure 6.1- CDK9 gene expression in the zebrafish whole embryo following cardiac laser injury. Q-PCR was performed before laser and then at 10 min, 1 h, 3 h and 24 h post laser injury. This experiment was performed once, therefore no statistic analysis was done. Although more experiments are needed to corroborate these data, in the future this experiment should be possibly done in the embryonic heart, where the laser injury is directed.

embryos. However, the cardiomyocyte number showed a slight increase in flavopiridol-exposed embryos. (fig. 6.2 C & D).

6.3.3.3 Cardiac function and cardiomyocyte numbers in LARP7 knockdown embryos following laser injury

In embryos injected with MO-LARP7mismatch and MO-LARP7splice blocking, EF and TVCn showed a very similar pattern at all the time points compared to lasered non-injected controls (fig. 6.2 E & F), including a full recovery in cardiac function and TVCn to similar levels as controls A small change in MO-LARP7splice injected embryos is that the EF at 24 h post-laser injury was slightly higher than other groups.

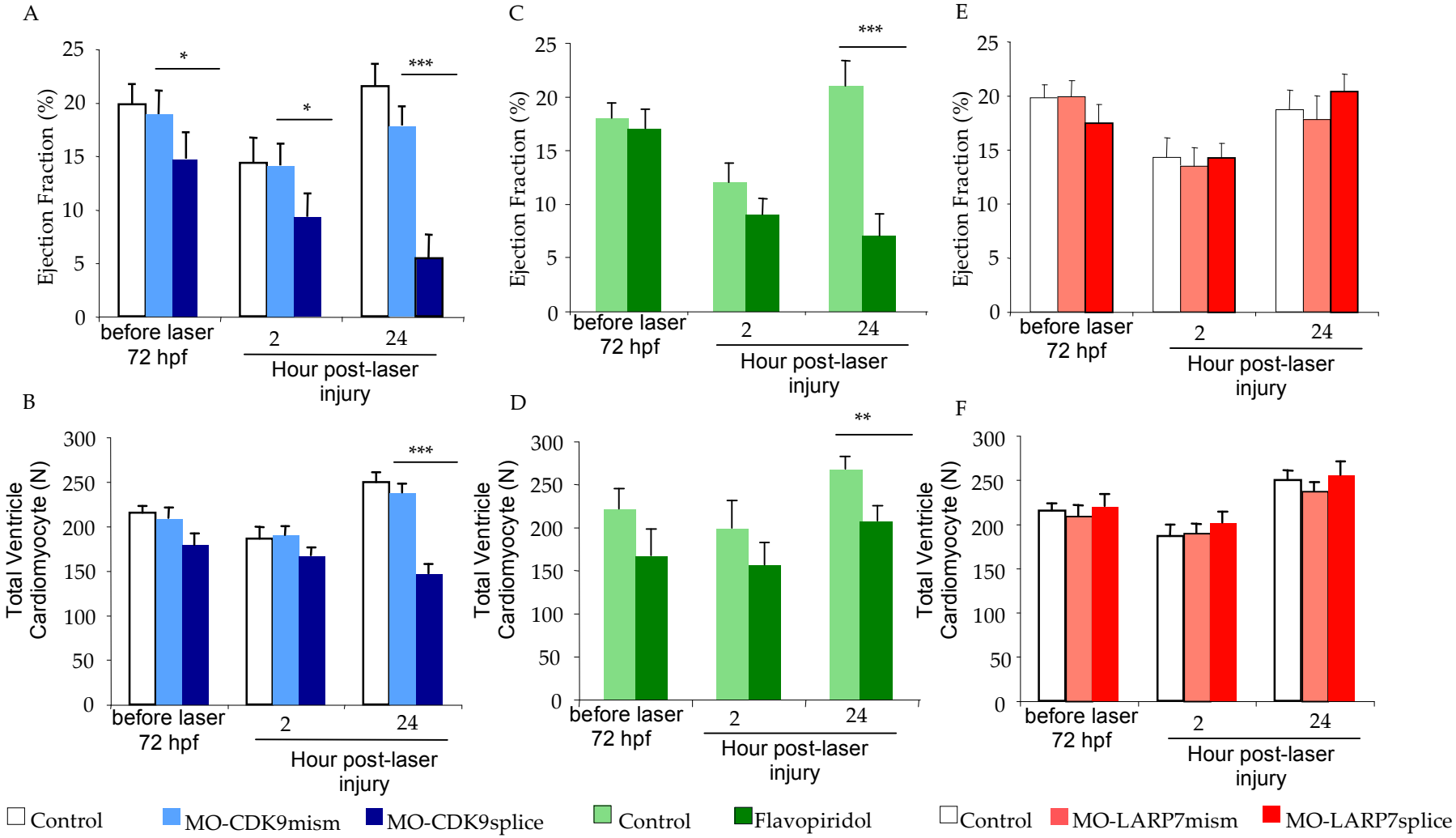

Figure 6.2- Effects of CDK9 modulation combined to cardiac laser injury in the zebrafish embryonic heart. CDK9 was inhibited genetically (**A-B**) by injection of MO-CDK9 splice blocking 100 µM (0,5nL per embryo) in eggs at 1-2 cell stage, or pharmacologically (**C-D**) by continuous exposure to flavopiridol 3µM from 24 up to 120 hpf. CDK9 was genetically upregulated (**E-F**) by injection of MO-LARP7 splice blocking 200 µM (0,5nL per embryo). Ejection fraction and cardiomyocyte number analysis were performed before laser and then at 2 and 24 h post-laser injury. N=3 experiments, two-way ANOVA test was used to compare groups followed by Bonferroni's post-hoc test; *=p<0.05, **=p<0.01, ***=p<0.001).

6.4 Discussion

In this Chapter I investigated the effects of CDK9 and LARP7 knockdown on the response of the heart to laser-induced injury. The activation of specific genetic and epigenetic programs following an external insult such as stress or injury has been described in several organisms (Bergmann and Steller, 2010; Dilworth and Blais, 2011; King and Newmark, 2012; Monaghan *et al.*, 2012; Wang *et al.*, 2012b).

I hypothesized that the zebrafish embryonic heart following laser injury could switch-on specific molecular pathways that modulate P-TEFb activity in way that is different from normal development.

CDK9 inhibition, by morpholino or flavopiridol, combined with ventricle laser injury resulted in loss of the ability of the zebrafish embryo to recover cardiac function by 24h post-laser injury. For both morpholino and flavopiridol treatments, this was associated with reduced proliferation of cardiomyocytes compared to controls.

When laser-injury was applied during normal development the recovery of cardiac function occurred in parallel with an increase in cardiomyocyte proliferation. Therefore, I concluded that recovery from laser-injury is, at least in part, associated with cardiomyocyte proliferation leading to restoration of cardiac function. During normal development, exposure to the flavopiridol, sustained from 24 up to 120 hpf (3μM), significantly inhibited cardiomyocyte proliferation. The inhibitory effect was slight lower than the aphidicolin (see Section 5.3.4). Therefore, the lack of recovery in ventricle function following laser-injury in the presence of flavopiridol must be at least partly explained by a failure of cardiomyocyte proliferation. However, flavopiridol could influence other cellular mechanisms that could contribute to the inability of the heart to recover. For example, flavopiridol is known to inhibit inflammation by attenuating leukocyte-endothelial interaction via inhibition of cyclin-dependent kinase 9 (Schmerwitz *et al.*, 2011). Inflammation is known to activate cell proliferation, also in the adult zebrafish (Kyritsis *et al.*, 2012). The immune system of zebrafish closely resembles that of mammals with definitive hematopoiesis thought to originate in cells within or near the dorsal aorta from 24 hpf and it is fully competent by 72 hpf. However, a major driving force for

inflammation, such as with blood vessel growth, is by hypoxia within surrounding tissue. At 72 hpf oxygen can still freely diffuse into the zebrafish embryo, therefore it seems unlikely the oxygen can be limiting for normal cell functions. Nevertheless, I have not measured the level of oxygen nor the infiltration of inflammatory cells into the injured ventricle. Therefore hypoxic microenvironments created by blood clot around the area of injury cannot be entirely excluded.

A lack of inflammation could also be argued to explain the non-recovery in CDK9-MO treated embryos. However, in this case the fall in ejection fraction observed at 24 h post-laser was associated with no increase in cardiomyocyte number, as observed with flavopiridol. This difference in cell proliferation between the two treatments definitely suggests a strong role of the CDK9 in cardiomyocyte proliferation and could be a consequence of the observed greater reduction in the phosphorylated form of Ser2 in RNAPII produced by morpholino knockdown.

In mammals, enhanced CDK9 activity is associated with cardiac hypertrophy (Sano *et al.*, 2002) following myocardial infarction. Flavopiridol has been proposed as treatment in heart failure because of its selectivity for CDK9 over other CDKs. There are, however, at least two problems to resolve. Firstly, from my data, this molecule could induce cardio-toxicity by inhibiting the normal responses to haemodynamic stress associated with exercise and mild hypertension. Similar problems have been encountered with the introduction of tyrosine kinase inhibitors for treatment of breast cancer. Secondly, there is certainly no evidence that flavopiridol is selective for the heart in any way. This leaves the possibility that it could have toxic effects on other organs including the liver and bone marrow. Therefore, there is scope for the development of more cardiac-specific anti-CDK9 drugs. The finding of two different CDK9 isoforms, $CDK9_{55}$ and $CDK9_{42}$, which are expressed differentially in some cell types and tissues, raises this possibility. Therefore, a first step could be finding if one of the CDK9 isoforms is more or exclusively expressed in the heart and then try to build a CDK9 inhibitor targeted at the heart.

On the other hand, we showed that LARP7 knockdown increased cardiomyocyte number and was associated with normal recovery following laser injury. Indeed the increased cardiomyocyte proliferation that I demonstrated following LARP7

knockdown during normal development (see chapter 4) suggests that targeting this molecule could provide benefits for cardiac repair. A pro-CDK9 therapy to treat heart failure could potentially increase cardiomyocyte proliferation and increase the expression of prosurvival factors leading to inhibition of apoptosis following injury. Therefore, I hypothesize that LARP7 knockdown and, potentially, anti-LARP7 drugs could have beneficial effects in cardiac injury if they could be targeted to the heart or even to the damaged area early after injury. However, LARP7 knockdown has been shown to cause malignant transformation by activation of key tumor-related genes and this possible side effect could limit their use. Clearly, further studioes are required to assess this potentially useful cardiac cellular repair mechanism.

Chapter 7
Conclusion and future perspectives

7.1 Role Of CDK9 In Cell Division And Growth

CDK9 is involved in a plethora of molecular pathways in many tissues and organs, including the heart. Molecular pathways linked to CDK9 appear to be more strongly associated with cell growth and less linked to cell cycle, which appears to be more influenced by other CDKs. The key original observation that inspired the work contained in this thesis was the increase in the CDK9 observed during cardiac hypertrophy in mammals (Sano *et al.*, 2002) and that a dominant-negative CDK9 was able to block ET-1-induced hypertrophy in mouse cultured cardiomyocytes. While it was clear that this process was not associated with cardiomyocyte proliferation, for me, it raised the possibility that it could be since the fetal gene program is well known to be reactivated during cardiac hypertrophy and these gene include a plethora of transcription factors, *i.e.* GATA4, TBX5 and MEF2c just to mention a few, that drive cardiomyocyte proliferation during the development.

The zebrafish provided a unique opportunity to test this hypothesis given the heart's capacity in the adult to regenerate following resection by a process driven by cardiomyocyte dedifferentiation and proliferation. One key question, which I have raised in this work, is whether CDK9 plays a role in such processes in mammalian myocardium where regenerative capacity is lost early after birth as shown recently in mice (Porrello *et al.*, 2011).

7.2 Role Of CDK9 During Embryonic Development

Cardiac CDK9 activity is normally highest in embryonic life and decreases after birth (Sano and Schneider, 2004) in mammals. Interestingly, we showed in the zebrafish that CDK9 is more strongly expressed in the first 96hpf of embryonic heart development when cardiomyocyte proliferation rate was higher. This posed the question as to whether CDK9 manipulation impacted on cardiomyocyte proliferation during embryonic development and subsequently on cardiovascular function.

To assess this, I quantified, for the first time, detailed characteristics of cardiomyocyte number and mitotic rate in the zebrafish embryonic heart ventricle in the period 48-120 hpf. I clearly showed that total ventricle cardiomyocytes number

increased rapidly, particularly in the period 96-120 hpf, particularly in association with trebeculation of the heart. To give me confidence in my in my data, I took into account possible sources of systematic error. For example, intra ventricular presence of nucleated blood cells was assessed by counting ventricle DAPI positive nuclei in a double transgenic line expressing either a red fluorochrome (DsRed) linked to the GATA1 promoter, specifically expressed in red blood cells, or a green fluorochrome (GFP) linked to the promoter of the cardiac specific myosin light chain 2 (cmlc2).

I also analysed the intra- and inter-observer variations in cardiomyocyte analysis by Bland-Altman plot before comparing our data with published literature. Indeed, very few reports were available to permit comparison during developmental stages that I chose to study as others had focused on earlier stages of cardiac development. In addition to developmental changes in cardiomyocyte proliferation, I highlighted several other developmental aspects of the heart including ventricular function and size, heart rate and cardinal vein blood flow changes during the first 120hpf and explored potential relationship among these factors. I demonstrated that between 96 and 120 hpf, in spite of the highest cardiomyocyte proliferation rate, this was not associated with a concomitant increase in ventricle diastolic area, a measure of heart growth, as observed in the first 96 hours of development. These findings suggest that increases in cardiomyocyte cell number and increases in heart size do not occur contemporaneously and that periods of hyperplastic growth are inter-spersed with hypertrophic growth. Furthermore, these developmental stages were characterized by a gradual and progressive increase in cardiac output, as a result of increasing heart rate, important to cover the increasing metabolic demands of newly forming organs.

A further reason to adopt the zebrafish embryo as a model for the present studies was its suitability for both pharmacological and genetic studies. The addition of Flavopiridol, a CDK9-specific inhibitor, in the fish water produced a significant decrease in the CDK9 activity, while injection of CDK9-targeting morpholino oligonucleotides in the eggs also resulted in a reduced CDK9 expression and activity. CDK9 Morpholino treatment produced a number of phenotypic traits which were more severe than those observed with flavopiridol treatment. Cardiovascular

function was affected in both cases, with a dramatic reduction in cardiomyocyte proliferation, cardiac function and tail blood flow. Table 7.1 and 7.2 show a summary of the effects of CDK9 modulation on molecular regulation, cardiovascular function and cardiomyocyte proliferation described in this thesis. We found that the two treatments produced a different effect on gene expression. Concomitant to the reduced phosphorylated form of the CTD, following exposure to the Flavopiridol or injection of CDK9-targeting morpholino there was the upregulation of all the genes we investigated in the first case and of GATA 4-6 and TBX5 in the second case. This confirm that while CDK9, or the P-TEFb complex is essential for the expression of most protein-coding genes (Chao and Price, 2001), apparently not all class II genes depend on P-TEFb for transcription (Zhou and Yik, 2006). For example, a recent report suggests that certain genes within the p53 pathway are able to bypass the requirement for P-TEFb. Furthermore, P-TEFb is not an essential elongation factor for the intronless histone H2b and the U2 snRNA genes (Medlin *et al.*, 2005). Similarly, Garriga and Grana (Garriga and Grana, 2004) performed microarray analysis of thousands gene of glioblastoma T98G cells following treatment with flavopiridol or a kinase-dead CDK9 dominant-negative mutant. They found that in both cases certain genes were upregulated while others were downregulated, with a distinctive pattern of changes by the two treatment modalities. Other reports have shown that flavopiridol upregulate a number of primary response genes (Keskin *et al.*, 2012) and also activates caspases by which apoptosis is induced (Rapoport *et al.*, 2001).

7.3 CDK9 As A Pharmacological Therapeutic Target For Heart Disease

7.3.1. Switching It Off!

CDK9 activity is actually being evaluated in pre-clinical and clinical studies for the treatment of cardiac hypertrophy, and several other pathologies, whose principal goal in the heart is to reduce cardiomyocyte hypertrophy by inhibiting RNA and protein synthesis.

Table 7.1 - Summary of the effects of the CDK9 modulation on the zebrafish embryo gene and protein expression.											
Treatment	Gene expression								Protein expression		
	GATA4	GATA5	GATA6	MEF2c	TBX5	NKX2.5	CDK9	LARP7	CDK9	LARP7	CTD
Flavopiridol	↓ ↑	↑↑	↑↑	↓ ↑	↓↓	↑↑	↓	↓	↑↑		↓↓
MO-CDK9	↔	↔	↓	↓	↔		↓↓↓	↔	↓↓↓		↓↓
MO-LARP7	↔	↔	↔	↔	↑	↔	↔	↓↓↓		↓↓↓	↔

Effect on gene or protein expression: (↑,↓) mild, (↑↑,↓↓) medium or (↑↑↑,↓↓↓) strong increase/decrease or (↔) unchanged.

Table 7.2 – Summary of the effects of the CDK9 modulation on the global zebrafish embryo and on the cardiovascular function, cardiac growth and cardiomyocyte proliferation.									
Treatment	Gene expression								
	Mortality	Global phenotype	Cardiac phenotype	EF	HR	CVBF	VDA	ADA	TVCn
Flavopiridol	+	+	++	↓↓	↔	↓↓↓	↓↓↓	↓↓↓	↓↓
MO-CDK9	+++	+++	+++	↓↓↓	↔	↓↓↓	↓↓↓	↓↓↓	↓↓↓
MO-LARP7	+	+	+	↔	↔	↔	↔	↑↑↑	↑

Degree of mortality or phenotype: (+) mild, (++), medium or (+++) severe. Effect on Cardiovascular function: (↑,↓) mild, (↑↑,↓↓) medium or (↑↑↑,↓↓↓) strong increase/decrease or (↔) unchanged

As Flavopiridol upregulates gene expression, it is important that we fully understand the molecular pathways by which Flavopiridol produces these effects (figure 7.1 A). Indeed, upregulation of genes including transcription factors GATA 4, 5 and 6, are among the drivers of the cardiac development and cardiomyocyte proliferation. Among these, GATA4 is also part of the complex network of signaling pathways within cardiac myocytes and it is known to be activated following certain stressors (pressure or volume load, reactive oxygen species, etc.) (Cappola, 2008). Of particular interest is the fact that GATA4 forms a complex with CDK9, promoted by the intrinsic histone acetyltransferase p300 that is also required for the kinase activity of CDK9, which is in turn required for transcriptional pathway activation during cardiomyocyte hypertrophy (Sunagawa *et al.*, 2010). While CDK9 inhibition could be responsible for reduced cardiomyocyte proliferation, on the other hand the observed upregulation of target genes could conversely herald an increase in cardiomyocytes proliferation via GATA-related pathways. It is possible that CDK9 knockdown activates a feedback loop that upregulates these transcription factors which in turn attempt to reestablish normal cardiomyocyte number and cardiovascular function.

7.3.2 Switching It On!

On the other hand, LARP7 knockdown (figure 7.1 B) provoked an increase in ventricle cardiomyocyte number, although not accompanied by an increase in the ventricle chamber size suggesting a more predominant hyperplastic response. LARP7 specifically binds to and enhances the stability of the complex 7SK snRNA-HEXIM-CDK9. The hypothesis was that this inhibitory complex would collapse following LARP7 knockdown and subsequently increase CDK9 activity. I observed in fact that LARP7 knockdown produced a profound increase in the atrial chamber size. For technical reasons I could not accurately assess atrial cardiomyocyte number, but it seems likely that both hyperplasia, and hypertrophy occur in the atrium to produce this phenotype. Some contribution of altered ventricular chamber stiffness could also contribute to the observed atrial dilatation.

7.4 Role Of CDK9 In Response To Injury

Switch of specific genetic and epigenetic programs, such as the activation of the above genes following CDK9 modulation, have also been reported following injury, in several organisms (Bergmann and Steller, 2010; Dilworth and Blais, 2011; King and Newmark, 2012; Monaghan *et al.*, 2012; Wang *et al.*, 2012b), including zebrafish (Kizil *et al.*, 2012). I developed a cardiac laser injury model to create an acute cardiac stress in the zebrafish embryonic heart ventricle. This high throughput embryonic model has similarities to myocardial infarction models in mammals in that it generates a sudden loss of myocardial tissue in a regional distribution. It is highly versatile and reproducible, and has allowed me to show the remarkable capability of the zebrafish embryonic heart to recover from profound injury. In fact, at 2 hours after ventricular laser injury there was markedly reduced cardiac function accompanied by a reduced number of cardiomyocyte and increased apoptosis in the area of injury which recovered fully within 24 hours. I suggest, from my findings, that recovery was promoted by the acceleration of cardiomyocyte proliferation reported in the period 2-24 hours post-laser. The process by which some adult vertebrates repair their lost components, e.g. the surgical resected zebrafish cardiac apex or the salamander limb, by invoking the proliferation of newly formed cells from differentiated cells is called "regeneration". The regeneration is characterized by a series of events that unfolds resulting in reactivation of a fetal gene program. The repair phenomenon observed in the zebrafish embryonic heart occurs when the fetal gene program is already in operation and as such these cardiomyocyte are not yet fully differentiated.

It would be inappropriate therefore to use the term regeneration in this case. This study confirms the importance of studying molecular processes that orchestrate organ development and to observe the (re)generative processes of adulthood from a different perspective (Alexander and Bruneau, 2010; Mercola *et al.*, 2011).

I hypothesized that the zebrafish embryonic hearts following laser injury could switch molecular pathways that modulate the P-TEFb activity in a way that was different from normal development.

CDK9 inhibition activate gene expression

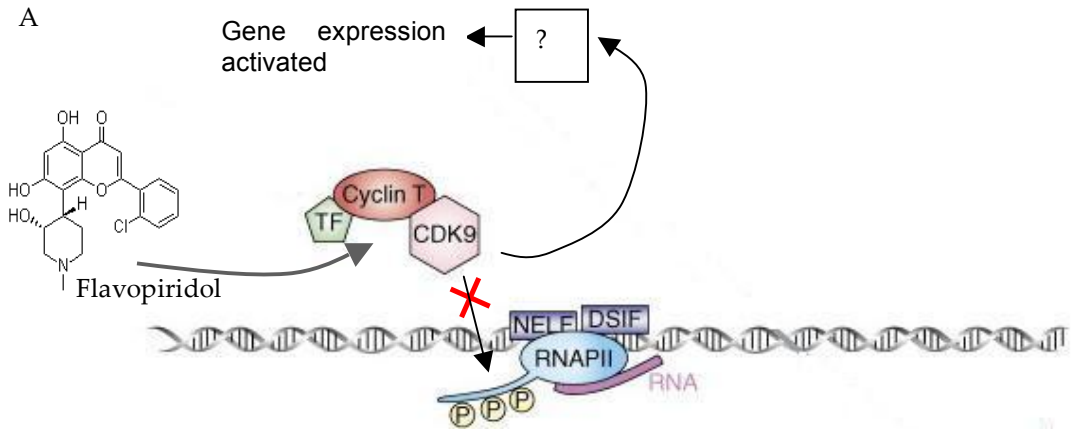

LARP7 knockdown upregulates CDK9 and increase scardiomyocyte proliferation

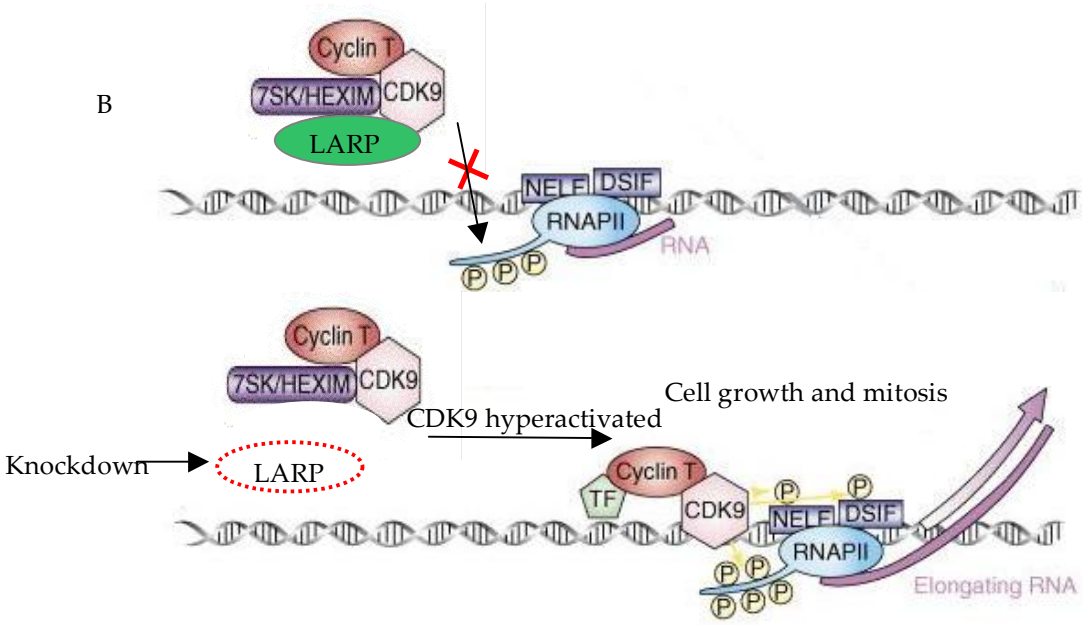

Figure 7.1- Two possible models to explain the opposite role of the CDK9. A. Following CDK9 inhibition by pharmacological (or genetic) agents, a feedback loop activate gene expression by a hitherto undefined mechanisms. B. Following knockdown of the CDK9 repressor LARP7, the inactivation of the CDK9-inhibitory complex increase CDK9 activity and promote RNA synthesis and cell growth. In the zebrafish this has also shown to increase cardiomyocyte proliferation.

When the laser injury was associated with CDK9 modulation, recovery in ventricle function was only observed when LARP7 was reduced by morpholino knockdown. This suggests that reduced CDK9 activity or lack of CDK9 inhibits recovery after laser injury as a result of altered cardiomyocyte proliferation. LARP7 knockdown on the other hand did not significantly affect cardiac recovery, which was similar to non-injected controls following laser injury. I could however have missed a difference in the rate of recovery between the 2 and 24 hr time points. Nevertheless, the increased basal cardiomyocyte number in LARP7 knockdown embryonic hearts suggests that this pathway could stimulate cell proliferation in the heart and should be further explored. For example, considering that the inactive P-TEFb complex includes HEXIM and 7SK, co-inhibiting two or more of these CDK9 repressors could be a promising therapeutic strategy. Following injury, mammalian hearts display some of the tissue/cellular reactions typical of cardiac regeneration but in a way that is unable to repair extensive cardiac damage. Understanding of CDK9 modulation may allow alternative therapeutic approaches to help address heart failure in humans (Martin-Puig *et al.*, 2012).

7.6 Limitations of the work in this thesis

At the end of my thesis, I have realized that I would change or improve some aspects of my studies if this was to be repeated. For future morpholino experiments, for example, I would add more controls either by performing 'rescue' experiments with mRNA (see section 1.5.3.2 for a detailed explanation) or by injecting the p53 morpholino to assess the p53-dependent apoptosis. This should give more confidence that the phenotype observed in the zebrafish embryo is genuinely related to my targeted gene.

I would improve flavopiridol optimization by doing a curve dose-effect where for each increment in the concentration of drug I would assess the level of phospho-Ser2, for which the antibody is already available. I would also measure phospho-CDK9, *i.e.* the activated form that should be reduced following exposure to flavopiridol, if a good antibody would be available.

For protein analysis in the experiments with flavopiridol it would be better to use

tubulin to normalize protein level, instead of vitellin that is rapidly metabolised from the embryo and that did not allow me to compare groups at different time point.
To assess cardiomyocyte proliferation I would adopt a BrdU pulse labelling protocol. This method gives detailed information on the total number of cells that passed through S phase in a selected time window. In my experiment, for example, the exposure of cardiac injured or non-injured embryos to the BrdU immediately after laser delivery would give information on the number of cardiac cell cycle up to 2 h post-laser or other selected time.

7.5 Future work

My findings highlight the need for further studies of CDK9 in mammalian models. A first step could be studying the CDK9 expression pattern in mice neonatal heart and analysing its role in the regenerating ability following cardiac apex resection (Porrello *et al.*, 2011). Then move CDK9 studies in the adult mammals. It would be very important to understand whether the heart synthesizes a specific CDK9 isoform, so that new developed drugs could be targeted at cardiac specific CDK9 with less effect on other organs and tissues. Particularly interesting would be investigating the effect of CDK9 upregulation by LARP7 knockdown, or other CDK9 repressors, on the cardiac remodeling following ischemic injury in the heart, or on neoangiogenesis in the femoral artery following ischemia. Indeed, upregulation of CDK9 at levels similar to those observed in mammalians fetal life could allow the same heart plasticity that drives cardiac formation. This could be a powerful tool for proangiogenic and stem cell therapies, not only by directly promoting cell proliferation but also by promoting the expression of endogenous growth factors aimed to establish the ideal environment whereby newly formed cells can engraft.

Bibliography

Abarbanell, A. M., Herrmann, J. L., Weil, B. R., Wang, Y., Tan, J., Moberly, S. P., Fiege, J. W. & Meldrum, D. R. 2010. Animal models of myocardial and vascular injury. J Surg Res, 162, 239-49.

Ackermann, G. E. & Paw, B. H. 2003. Zebrafish: a genetic model for vertebrate organogenesis and human disorders. Front Biosci, 8, d1227-53.

Ahuja, P., Sdek, P. & Maclellan, W. R. 2007. Cardiac myocyte cell cycle control in development, disease, and regeneration. Physiol Rev, 87, 521-44.

Akhtar, M. S., Heidemann, M., Tietjen, J. R., Zhang, D. W., Chapman, R. D., Eick, D. & Ansari, A. Z. 2009. TFIIH kinase places bivalent marks on the carboxy-terminal domain of RNA polymerase II. Mol Cell, 34, 387-93.

Akoulitchev, S., Chuikov, S. & Reinberg, D. 2000. TFIIH is negatively regulated by cdk8-containing mediator complexes. Nature, 407, 102-6.

Alazami, A. M., Al-Owain, M., Alzahrani, F., Shuaib, T., Al-Shamrani, H., Al-Falki, Y. H., Al-Qahtani, S. M., Alsheddi, T., Colak, D. & Alkuraya, F. S. 2012. Loss of function mutation in LARP7, chaperone of 7SK ncRNA, causes a syndrome of facial dysmorphism, intellectual disability, and primordial dwarfism. Hum Mutat, 33, 1429-34.

Alcon, A., Cagavi Bozkulak, E. & Qyang, Y. 2012. Regenerating functional heart tissue for myocardial repair. Cell Mol Life Sci, 69, 2635-56.

Alexander, J. M. & Bruneau, B. G. 2010. Lessons for cardiac regeneration and repair through development. Trends Mol Med, 16, 426-34.

Antkiewicz, D. S., Burns, C. G., Carney, S. A., Peterson, R. E. & Heideman, W. 2005. Heart malformation is an early response to TCDD in embryonic zebrafish. Toxicol Sci, 84, 368-77.

Antkiewicz, D. S., Peterson, R. E. & Heideman, W. 2006. Blocking expression of AHR2 and ARNT1 in zebrafish larvae protects against cardiac toxicity of 2,3,7,8-tetrachlorodibenzo-p-dioxin. Toxicol Sci, 94, 175-82.

Anversa, P., Li, P., Zhang, X., Olivetti, G. & Capasso, J. M. 1993. Ischaemic myocardial injury and ventricular remodelling. Cardiovasc Res, 27, 145-57.

Aoki, H., Sadoshima, J. & Izumo, S. 2000. Myosin light chain kinase mediates sarcomere organization during cardiac hypertrophy in vitro. Nat Med, 6, 183-8.

Arguello, F., Alexander, M., Sterry, J. A., Tudor, G., Smith, E. M., Kalavar, N. T., Greene, J. F., Jr., Koss, W., Morgan, C. D., Stinson, S. F., Siford, T. J., Alvord, W. G.,

Klabansky, R. L. & Sausville, E. A. 1998. Flavopiridol induces apoptosis of normal lymphoid cells, causes immunosuppression, and has potent antitumor activity In vivo against human leukemia and lymphoma xenografts. Blood, 91, 2482-90.

Arrenberg, A. B., Stainier, D. Y., Baier, H. & Huisken, J. 2010. Optogenetic control of cardiac function. Science, 330, 971-4.

Auman, H. J., Coleman, H., Riley, H. E., Olale, F., Tsai, H. J. & Yelon, D. 2007. Functional modulation of cardiac form through regionally confined cell shape changes. PLoS Biol, 5, e53.

Ausoni, S. & Sartore, S. 2009. From fish to amphibians to mammals: in search of novel strategies to optimize cardiac regeneration. J Cell Biol, 184, 357-64.

Bagatto, B. & Burggren, W. 2006. A three-dimensional functional assessment of heart and vessel development in the larva of the zebrafish (Danio rerio). Physiol Biochem Zool, 79, 194-201.

Bagella, L., Maclachlan, T. K., Buono, R. J., Pisano, M. M., Giordano, A. & De Luca, A. 1998. Cloning of murine CDK9/PITALRE and its tissue-specific expression in development. J Cell Physiol, 177, 206-13.

Bai, X., Kim, J., Yang, Z., Jurynec, M. J., Akie, T. E., Lee, J., Leblanc, J., Sessa, A., Jiang, H., Dibiase, A., Zhou, Y., Grunwald, D. J., Lin, S., Cantor, A. B., Orkin, S. H. & Zon, L. I. 2010. TIF1gamma controls erythroid cell fate by regulating transcription elongation. Cell, 142, 133-43.

Baird, G. S., Zacharias, D. A. & Tsien, R. Y. 2000. Biochemistry, mutagenesis, and oligomerization of DsRed, a red fluorescent protein from coral. Proc Natl Acad Sci U S A, 97, 11984-9.

Bakkers, J. 2011. Zebrafish as a model to study cardiac development and human cardiac disease. Cardiovasc Res, 91, 279-88.

Barboric, M., Kohoutek, J., Price, J. P., Blazek, D., Price, D. H. & Peterlin, B. M. 2005. Interplay between 7SK snRNA and oppositely charged regions in HEXIM1 direct the inhibition of P-TEFb. EMBO J, 24, 4291-303.

Barboric, M., Lenasi, T., Chen, H., Johansen, E. B., Guo, S. & Peterlin, B. M. 2009. 7SK snRNP/P-TEFb couples transcription elongation with alternative splicing and is essential for vertebrate development. Proc Natl Acad Sci U S A, 106, 7798-803.

Barboric, M., Nissen, R. M., Kanazawa, S., Jabrane-Ferrat, N. & Peterlin, B. M. 2001. NF-kappaB binds P-TEFb to stimulate transcriptional elongation by RNA polymerase II. Mol Cell, 8, 327-37.

Barboric, M., Yik, J. H., Czudnochowski, N., Yang, Z., Chen, R., Contreras, X., Geyer, M., Matija Peterlin, B. & Zhou, Q. 2007. Tat competes with HEXIM1 to increase the active pool of P-TEFb for HIV-1 transcription. Nucleic Acids Res, 35, 2003-12.

Bark-Jones, S. J., Webb, H. M. & West, M. J. 2006. EBV EBNA 2 stimulates CDK9-dependent transcription and RNA polymerase II phosphorylation on serine 5. Oncogene, 25, 1775-85.

Baumli, S., Endicott, J. A. & Johnson, L. N. 2010. Halogen bonds form the basis for selective P-TEFb inhibition by DRB. Chem Biol, 17, 931-6.

Baumli, S., Lolli, G., Lowe, E. D., Troiani, S., Rusconi, L., Bullock, A. N., Debreczeni, J. E., Knapp, S. & Johnson, L. N. 2008. The structure of P-TEFb (CDK9/cyclin T1), its complex with flavopiridol and regulation by phosphorylation. EMBO J, 27, 1907-18.

Bayfield, M. A., Yang, R. & Maraia, R. J. 2010. Conserved and divergent features of the structure and function of La and La-related proteins (LARPs). Biochim Biophys Acta, 1799, 365-78.

Becker, J. R., Deo, R. C., Werdich, A. A., Panakova, D., Coy, S. & Macrae, C. A. 2011. Human cardiomyopathy mutations induce myocyte hyperplasia and activate hypertrophic pathways during cardiogenesis in zebrafish. Dis Model Mech, 4, 400-10.

Begemann, G. & Ingham, P. W. 2000. Developmental regulation of Tbx5 in zebrafish embryogenesis. Mech Dev, 90, 299-304.

Bellan, C., De Falco, G., Lazzi, S., Micheli, P., Vicidomini, S., Schurfeld, K., Amato, T., Palumbo, A., Bagella, L., Sabattini, E., Bartolommei, S., Hummel, M., Pileri, S., Tosi, P., Leoncini, L. & Giordano, A. 2004. CDK9/CYCLIN T1 expression during normal lymphoid differentiation and malignant transformation. J Pathol, 203, 946-52.

Beltrami, A. P., Barlucchi, L., Torella, D., Baker, M., Limana, F., Chimenti, S., Kasahara, H., Rota, M., Musso, E., Urbanek, K., Leri, A., Kajstura, J., Nadal-Ginard, B. & Anversa, P. 2003. Adult cardiac stem cells are multipotent and support myocardial regeneration. Cell, 114, 763-76.

Beltrami, A. P., Urbanek, K., Kajstura, J., Yan, S. M., Finato, N., Bussani, R., Nadal-Ginard, B., Silvestri, F., Leri, A., Beltrami, C. A. & Anversa, P. 2001. Evidence that human cardiac myocytes divide after myocardial infarction. N Engl J Med, 344, 1750-7.

Berberich, N., Uhl, B., Joore, J., Schmerwitz, U. K., Mayer, B. A., Reichel, C. A., Krombach, F., Zahler, S., Vollmar, A. M. & Furst, R. 2011. Roscovitine blocks leukocyte extravasation by inhibition of cyclin-dependent kinases 5 and 9. Br J Pharmacol, 163, 1086-98.

Berdougo, E., Coleman, H., Lee, D. H., Stainier, D. Y. & Yelon, D. 2003. Mutation of weak atrium/atrial myosin heavy chain disrupts atrial function and influences ventricular morphogenesis in zebrafish. Development, 130, 6121-9.

Berenji, K., Drazner, M. H., Rothermel, B. A. & Hill, J. A. 2005. Does load-induced

ventricular hypertrophy progress to systolic heart failure? Am J Physiol Heart Circ Physiol, 289, H8-H16.

Bergmann, A. & Steller, H. 2010. Apoptosis, stem cells, and tissue regeneration. Sci Signal, 3, re8.

Bergmann, O., Bhardwaj, R. D., Bernard, S., Zdunek, S., Barnabe-Heider, F., Walsh, S., Zupicich, J., Alkass, K., Buchholz, B. A., Druid, H., Jovinge, S. & Frisen, J. 2009. Evidence for cardiomyocyte renewal in humans. Science, 324, 98-102.

Bettayeb, K., Tirado, O. M., Marionneau-Lambot, S., Ferandin, Y., Lozach, O., Morris, J. C., Mateo-Lozano, S., Drueckes, P., Schachtele, C., Kubbutat, M. H., Liger, F., Marquet, B., Joseph, B., Echalier, A., Endicott, J. A., Notario, V. & Meijer, L. 2007. Meriolins, a new class of cell death inducing kinase inhibitors with enhanced selectivity for cyclin-dependent kinases. Cancer Res, 67, 8325-34.

Bevis, B. J. & Glick, B. S. 2002. Rapidly maturing variants of the Discosoma red fluorescent protein (DsRed). Nat Biotechnol, 20, 83-7.

Bicknell, K. A., Coxon, C. H. & Brooks, G. 2007. Can the cardiomyocyte cell cycle be reprogrammed? J Mol Cell Cardiol, 42, 706-21.

Bicknell, K. A., Surry, E. L. & Brooks, G. 2003. Targeting the cell cycle machinery for the treatment of cardiovascular disease. J Pharm Pharmacol, 55, 571-91.

Bill, B. R., Petzold, A. M., Clark, K. J., Schimmenti, L. A. & Ekker, S. C. 2009. A primer for morpholino use in zebrafish. Zebrafish, 6, 69-77.

Bisgrove, B. W., Essner, J. J. & Yost, H. J. 1999. Regulation of midline development by antagonism of lefty and nodal signaling. Development, 126, 3253-62.

Bishopric, N. H. 2005. Evolution of the heart from bacteria to man. Ann N Y Acad Sci, 1047, 13-29.

Black, B. L. O., E. N. Academic, San & Diego 1999. Academic, San Diego.

Bland, J. M. & Altman, D. G. 1986. Statistical methods for assessing agreement between two methods of clinical measurement. Lancet, 1, 307-10.

Blazek, D., Barboric, M., Kohoutek, J., Oven, I. & Peterlin, B. M. 2005. Oligomerization of HEXIM1 via 7SK snRNA and coiled-coil region directs the inhibition of P-TEFb. Nucleic Acids Res, 33, 7000-10.

Bostrom, P., Mann, N., Wu, J., Quintero, P. A., Plovie, E. R., Panakova, D., Gupta, R. K., Xiao, C., Macrae, C. A., Rosenzweig, A. & Spiegelman, B. M. 2010. C/EBPbeta controls exercise-induced cardiac growth and protects against pathological cardiac remodeling. Cell, 143, 1072-83.

Boyer, M. J. & Cheng, T. 2008. The CDK inhibitors: potential targets for therapeutic

stem cell manipulations? Gene Ther, 15, 117-25.

Brand, T. 2003. Heart development: molecular insights into cardiac specification and early morphogenesis. Dev Biol, 258, 1-19.

Bres, V., Yoh, S. M. & Jones, K. A. 2008. The multi-tasking P-TEFb complex. Curr Opin Cell Biol, 20, 334-40.

Bruneau, B. G., Logan, M., Davis, N., Levi, T., Tabin, C. J., Seidman, J. G. & Seidman, C. E. 1999. Chamber-specific cardiac expression of Tbx5 and heart defects in Holt-Oram syndrome. Dev Biol, 211, 100-8.

Buccini, S., Haider, K. H., Ahmed, R. P., Jiang, S. & Ashraf, M. 2012. Cardiac progenitors derived from reprogrammed mesenchymal stem cells contribute to angiomyogenic repair of the infarcted heart. Basic Res Cardiol, 107, 301.

Buckingham, M., Meilhac, S. & Zaffran, S. 2005. Building the mammalian heart from two sources of myocardial cells. Nat Rev Genet, 6, 826-35.

Bugel, S. M., White, L. A. & Cooper, K. R. 2013. Inhibition of vitellogenin gene induction by 2,3,7,8-tetrachlorodibenzo-p-dioxin is mediated by aryl hydrocarbon receptor 2 (AHR2) in zebrafish (Danio rerio). Aquat Toxicol, 126, 1-8.

Bullrich, F., Maclachlan, T. K., Sang, N., Druck, T., Veronese, M. L., Allen, S. L., Chiorazzi, N., Koff, A., Heubner, K., Croce, C. M. & Et Al. 1995. Chromosomal mapping of members of the cdc2 family of protein kinases, cdk3, cdk6, PISSLRE, and PITALRE, and a cdk inhibitor, p27Kip1, to regions involved in human cancer. Cancer Res, 55, 1199-205.

Buratowski, S. 2009. Progression through the RNA polymerase II CTD cycle. Mol Cell, 36, 541-6.

Burns, C. G. & Macrae, C. A. 2006. Purification of hearts from zebrafish embryos. Biotechniques, 40, 274, 276, 278 passim.

Burns, C. G., Milan, D. J., Grande, E. J., Rottbauer, W., Macrae, C. A. & Fishman, M. C. 2005. High-throughput assay for small molecules that modulate zebrafish embryonic heart rate. Nat Chem Biol, 1, 263-4.

Busk, P. K. & Hinrichsen, R. 2003. Cyclin D in left ventricle hypertrophy. Cell Cycle, 2, 91-5.

Cai, C. L., Liang, X., Shi, Y., Chu, P. H., Pfaff, S. L., Chen, J. & Evans, S. 2003. Isl1 identifies a cardiac progenitor population that proliferates prior to differentiation and contributes a majority of cells to the heart. Dev Cell, 5, 877-89.

Candela, H. & Hake, S. 2008. The art and design of genetic screens: maize. Nat Rev Genet, 9, 192-203.

Canduri, F., Perez, P. C., Caceres, R. A. & De Azevedo, W. F., Jr. 2008. CDK9 a potential target for drug development. Med Chem, 4, 210-8.

Capasso, J. M., Bruno, S., Cheng, W., Li, P., Rodgers, R., Darzynkiewicz, Z. & Anversa, P. 1992. Ventricular loading is coupled with DNA synthesis in adult cardiac myocytes after acute and chronic myocardial infarction in rats. Circ Res, 71, 1379-89.

Cappola, T. P. 2008. Molecular remodeling in human heart failure. J Am Coll Cardiol, 51, 137-8.

Caracciolo, V., Laurenti, G., Romano, G., Carnevale, V., Cimini, A. M., Crozier-Fitzgerald, C., Gentile, E., Russo, G. & Giordano, A. 2012. Flavopiridol induces phosphorylation of AKT in a human glioblastoma cell line, in contrast to siRNA-mediated silencing of Cdk9: Implications for drug design and development. Cell Cycle, 11, 1202-16.

Carney, S. A., Chen, J., Burns, C. G., Xiong, K. M., Peterson, R. E. & Heideman, W. 2006. Aryl hydrocarbon receptor activation produces heart-specific transcriptional and toxic responses in developing zebrafish. Mol Pharmacol, 70, 549-61.

Casadei, R., Pelleri, M. C., Vitale, L., Facchin, F., Lenzi, L., Canaider, S., Strippoli, P. & Frabetti, F. 2011. Identification of housekeeping genes suitable for gene expression analysis in the zebrafish. Gene Expr Patterns, 11, 271-6.

Chao, S. H., Fujinaga, K., Marion, J. E., Taube, R., Sausville, E. A., Senderowicz, A. M., Peterlin, B. M. & Price, D. H. 2000. Flavopiridol inhibits P-TEFb and blocks HIV-1 replication. J Biol Chem, 275, 28345-8.

Chao, S. H. & Price, D. H. 2001. Flavopiridol inactivates P-TEFb and blocks most RNA polymerase II transcription in vivo. J Biol Chem, 276, 31793-9.

Charron, F., Paradis, P., Bronchain, O., Nemer, G. & Nemer, M. 1999. Cooperative interaction between GATA-4 and GATA-6 regulates myocardial gene expression. Mol Cell Biol, 19, 4355-65.

Charron, F., Tsimiklis, G., Arcand, M., Robitaille, L., Liang, Q., Molkentin, J. D., Meloche, S. & Nemer, M. 2001. Tissue-specific GATA factors are transcriptional effectors of the small GTPase RhoA. Genes Dev, 15, 2702-19.

Chen, C. H., Wang, S. S., Wei, E. I., Chu, T. Y. & Hsieh, P. 2013. Hyaluronan enhances bone marrow cell therapy for myocardial repair after infarction. Mol Ther, 21, 670-9.

Chen, H., Zhang, W., Li, D., Cordes, T. M., Mark Payne, R. & Shou, W. 2009a. Analysis of ventricular hypertrabeculation and noncompaction using genetically engineered mouse models. Pediatr Cardiol, 30, 626-34.

Chen, H. H., Wang, Y. C. & Fann, M. J. 2006. Identification and characterization of the CDK12/cyclin L1 complex involved in alternative splicing regulation. Mol Cell Biol, 26, 2736-45.

Chen, H. H., Wong, Y. H., Geneviere, A. M. & Fann, M. J. 2007. CDK13/CDC2L5 interacts with L-type cyclins and regulates alternative splicing. Biochem Biophys Res Commun, 354, 735-40.

Chen, J. N., Van Eeden, F. J., Warren, K. S., Chin, A., Nusslein-Volhard, C., Haffter, P. & Fishman, M. C. 1997. Left-right pattern of cardiac BMP4 may drive asymmetry of the heart in zebrafish. Development, 124, 4373-82.

Chen, R., Keating, M. J., Gandhi, V. & Plunkett, W. 2005. Transcription inhibition by flavopiridol: mechanism of chronic lymphocytic leukemia cell death. Blood, 106, 2513-9.

Chen, R., Wierda, W. G., Chubb, S., Hawtin, R. E., Fox, J. A., Keating, M. J., Gandhi, V. & Plunkett, W. 2009b. Mechanism of action of SNS-032, a novel cyclin-dependent kinase inhibitor, in chronic lymphocytic leukemia. Blood, 113, 4637-45.

Chen, Y., Lewis, W., Diwan, A., Cheng, E. H., Matkovich, S. J. & Dorn, G. W., 2nd 2010. Dual autonomous mitochondrial cell death pathways are activated by Nix/BNip3L and induce cardiomyopathy. Proc Natl Acad Sci U S A, 107, 9035-42.

Cheng, Y., Jin, Z., Agarwal, R., Ma, K., Yang, J., Ibrahim, S., Olaru, A. V., David, S., Ashktorab, H., Smoot, D. T., Duncan, M. D., Hutcheon, D. F., Abraham, J. M., Meltzer, S. J. & Mori, Y. 2012. LARP7 is a potential tumor suppressor gene in gastric cancer. Lab Invest, 92, 1013-9.

Chi, N. C., Shaw, R. M., Jungblut, B., Huisken, J., Ferrer, T., Arnaout, R., Scott, I., Beis, D., Xiao, T., Baier, H., Jan, L. Y., Tristani-Firouzi, M. & Stainier, D. Y. 2008. Genetic and physiologic dissection of the vertebrate cardiac conduction system. PLoS Biol, 6, e109.

Chicurel, M. E., Chen, C. S. & Ingber, D. E. 1998. Cellular control lies in the balance of forces. Curr Opin Cell Biol, 10, 232-9.

Cho, H., Orphanides, G., Sun, X., Yang, X. J., Ogryzko, V., Lees, E., Nakatani, Y. & Reinberg, D. 1998. A human RNA polymerase II complex containing factors that modify chromatin structure. Mol Cell Biol, 18, 5355-63.

Cho, S., Schroeder, S. & Ott, M. 2010. CYCLINg through transcription: posttranslational modifications of P-TEFb regulate transcription elongation. Cell Cycle, 9, 1697-705.

Choi, W. Y., Gemberling, M., Wang, J., Holdway, J. E., Shen, M. C., Karlstrom, R. O. & Poss, K. D. 2013. In vivo monitoring of cardiomyocyte proliferation to identify chemical modifiers of heart regeneration. Development, 140, 660-6.

Christoffels, V. M., Burch, J. B. & Moorman, A. F. 2004. Architectural plan for the heart: early patterning and delineation of the chambers and the nodes. Trends Cardiovasc Med, 14, 301-7.

Christoffels, V. M., Habets, P. E., Franco, D., Campione, M., De Jong, F., Lamers, W. H., Bao, Z. Z., Palmer, S., Biben, C., Harvey, R. P. & Moorman, A. F. 2000. Chamber formation and morphogenesis in the developing mammalian heart. Dev Biol, 223, 266-78.

Clamp, M., Fry, B., Kamal, M., Xie, X., Cuff, J., Lin, M. F., Kellis, M., Lindblad-Toh, K. & Lander, E. S. 2007. Distinguishing protein-coding and noncoding genes in the human genome. Proc Natl Acad Sci U S A, 104, 19428-33.

Clubb, F. J., Jr. & Bishop, S. P. 1984. Formation of binucleated myocardial cells in the neonatal rat. An index for growth hypertrophy. Lab Invest, 50, 571-7.

Conlon, I. & Raff, M. 1999. Size control in animal development. Cell, 96, 235-44.

Corey, D. R. & Abrams, J. M. 2001. Morpholino antisense oligonucleotides: tools for investigating vertebrate development. Genome Biol, 2, REVIEWS1015.

Coucelo, J. & Joaquim, N. 2000. Calculation of volumes and systolic indices of heart ventricle from Halobatrachus didactylus: echocardiographic noninvasive method. J Exp Zool, 286, 585-95.

Curado, S., Anderson, R. M., Jungblut, B., Mumm, J., Schroeter, E. & Stainier, D. Y. 2007. Conditional targeted cell ablation in zebrafish: a new tool for regeneration studies. Dev Dyn, 236, 1025-35.

Day, S. J. & Lawrence, P. A. 2000. Measuring dimensions: the regulation of size and shape. Development, 127, 2977-87.

De Falco, G. & Giordano, A. 2002. CDK9: from basal transcription to cancer and AIDS. Cancer Biol Ther, 1, 342-7.

De Pater, E., Clijsters, L., Marques, S. R., Lin, Y. F., Garavito-Aguilar, Z. V., Yelon, D. & Bakkers, J. 2009. Distinct phases of cardiomyocyte differentiation regulate growth of the zebrafish heart. Development, 136, 1633-41.

Denvir, M. A., Tucker, C. S. & Mullins, J. J. 2008. Systolic and diastolic ventricular function in zebrafish embryos: influence of norepenephrine, MS-222 and temperature. BMC Biotechnol, 8, 21.

Detrich, H. W., 3rd 2008. Fluorescent proteins in zebrafish cell and developmental biology. Methods Cell Biol, 85, 219-41.

Di Stefano, V., Giacca, M., Capogrossi, M. C., Crescenzi, M. & Martelli, F. 2011. Knockdown of cyclin-dependent kinase inhibitors induces cardiomyocyte re-entry in the cell cycle. J Biol Chem, 286, 8644-54.

Dilworth, F. J. & Blais, A. 2011. Epigenetic regulation of satellite cell activation during muscle regeneration. Stem Cell Res Ther, 2, 18.

Diwan, A., Wansapura, J., Syed, F. M., Matkovich, S. J., Lorenz, J. N. & Dorn, G. W., 2nd 2008. Nix-mediated apoptosis links myocardial fibrosis, cardiac remodeling, and hypertrophy decompensation. Circulation, 117, 396-404.

Domanski, M. J., Cunnion, R. E. & Roberts, W. C. 1992. Analysis of fractional area change at various levels in the normal left ventricle. Am J Cardiol, 70, 1367-8.

Dorosz, J. L., Lezotte, D. C., Weitzenkamp, D. A., Allen, L. A. & Salcedo, E. E. 2012. Performance of 3-dimensional echocardiography in measuring left ventricular volumes and ejection fraction: a systematic review and meta-analysis. J Am Coll Cardiol, 59, 1799-808.

Dow, E. C., Liu, H. & Rice, A. P. 2010. T-loop phosphorylated Cdk9 localizes to nuclear speckle domains which may serve as sites of active P-TEFb function and exchange between the Brd4 and 7SK/HEXIM1 regulatory complexes. J Cell Physiol, 224, 84-93.

Dragneva, G., Korpisalo, P. & Yla-Herttuala, S. 2013. Promoting blood vessel growth in ischemic diseases: challenges in translating preclinical potential into clinical success. Dis Model Mech.

Draper, B. W., Morcos, P. A. & Kimmel, C. B. 2001. Inhibition of zebrafish fgf8 pre-mRNA splicing with morpholino oligos: a quantifiable method for gene knockdown. Genesis, 30, 154-6.

Dulac, C., Michels, A. A., Fraldi, A., Bonnet, F., Nguyen, V. T., Napolitano, G., Lania, L. & Bensaude, O. 2005. Transcription-dependent association of multiple positive transcription elongation factor units to a HEXIM multimer. J Biol Chem, 280, 30619-29.

Durocher, D., Charron, F., Warren, R., Schwartz, R. J. & Nemer, M. 1997. The cardiac transcription factors Nkx2-5 and GATA-4 are mutual cofactors. EMBO J, 16, 5687-96.

Egloff, S., Van Herreweghe, E. & Kiss, T. 2006. Regulation of polymerase II transcription by 7SK snRNA: two distinct RNA elements direct P-TEFb and HEXIM1 binding. Mol Cell Biol, 26, 630-42.

Eisen, J. S. & Smith, J. C. 2008. Controlling morpholino experiments: don't stop making antisense. Development, 135, 1735-43.

Engel, F. B. 2005. Cardiomyocyte proliferation: a platform for mammalian cardiac repair. Cell Cycle, 4, 1360-3.

Espinoza-Derout, J., Wagner, M., Shahmiri, K., Mascareno, E., Chaqour, B. & Siddiqui, M. A. 2007. Pivotal role of cardiac lineage protein-1 (CLP-1) in transcriptional elongation factor P-TEFb complex formation in cardiac hypertrophy. Cardiovasc Res, 75, 129-38.

Eswaran, J. & Knapp, S. 2010. Insights into protein kinase regulation and inhibition

by large scale structural comparison. Biochim Biophys Acta, 1804, 429-32.

Fabian, M. A., Biggs, W. H., Treiber, D. K., Atteridge, C. E., Azimioara, M. D., Benedetti, M. G., Carter, T. A., Ciceri, P., Edeen, P. T., Floyd, M., Ford, J. M., Galvin, M., Gerlach, J. L., Grotzfeld, R. M., Herrgard, S., Insko, D. E., Insko, M. A., Lai, A. G., Lelias, J. M., Mehta, S. A., Milanov, Z. V., Velasco, A. M., Wodicka, L. M., Patel, H. K., Zarrinkar, P. P. & Lockhart, D. J. 2005. A small molecule-kinase interaction map for clinical kinase inhibitors. Nat Biotechnol, 23, 329-36.

Falco, G. D., Neri, L. M., Falco, M. D., Bellan, C., Yu, Z., Luca, A. D., Leoncini, L. & Giordano, A. 2002. Cdk9, a member of the cdc2-like family of kinases, binds to gp130, the receptor of the IL-6 family of cytokines. Oncogene, 21, 7464-70.

Faucherre, A. & Jopling, C. 2012. The heart's content-renewable resources. Int J Cardiol.

Feldman, B., Gates, M. A., Egan, E. S., Dougan, S. T., Rennebeck, G., Sirotkin, H. I., Schier, A. F. & Talbot, W. S. 1998. Zebrafish organizer development and germ-layer formation require nodal-related signals. Nature, 395, 181-5.

Firestein, R., Bass, A. J., Kim, S. Y., Dunn, I. F., Silver, S. J., Guney, I., Freed, E., Ligon, A. H., Vena, N., Ogino, S., Chheda, M. G., Tamayo, P., Finn, S., Shrestha, Y., Boehm, J. S., Jain, S., Bojarski, E., Mermel, C., Barretina, J., Chan, J. A., Baselga, J., Tabernero, J., Root, D. E., Fuchs, C. S., Loda, M., Shivdasani, R. A., Meyerson, M. & Hahn, W. C. 2008. CDK8 is a colorectal cancer oncogene that regulates beta-catenin activity. Nature, 455, 547-51.

Fisher, R. P. 2005. Secrets of a double agent: CDK7 in cell-cycle control and transcription. J Cell Sci, 118, 5171-80.

Folland, E. D., Parisi, A. F., Moynihan, P. F., Jones, D. R., Feldman, C. L. & Tow, D. E. 1979. Assessment of left ventricular ejection fraction and volumes by real-time, two-dimensional echocardiography. A comparison of cineangiographic and radionuclide techniques. Circulation, 60, 760-6.

Foskett, S. M., Ghose, R., Tang, D. N., Lewis, D. E. & Rice, A. P. 2001. Antiapoptotic function of Cdk9 (TAK/P-TEFb) in U937 promonocytic cells. J Virol, 75, 1220-8.

Foubert, P., Matrone, G., Souttou, B., Lere-Dean, C., Barateau, V., Plouet, J., Le Ricousse-Roussanne, S., Levy, B. I., Silvestre, J. S. & Tobelem, G. 2008. Coadministration of endothelial and smooth muscle progenitor cells enhances the efficiency of proangiogenic cell-based therapy. Circ Res, 103, 751-60.

Freter, R., Osawa, M. & Nishikawa, S. 2010. Adult stem cells exhibit global suppression of RNA polymerase II serine-2 phosphorylation. Stem Cells, 28, 1571-80.

Frey, N., Mckinsey, T. A. & Olson, E. N. 2000. Decoding calcium signals involved in cardiac growth and function. Nat Med, 6, 1221-7.

Frey, N. & Olson, E. N. 2003. Cardiac hypertrophy: the good, the bad, and the ugly. Annu Rev Physiol, 65, 45-79.

Fu, T. J., Peng, J., Lee, G., Price, D. H. & Flores, O. 1999. Cyclin K functions as a CDK9 regulatory subunit and participates in RNA polymerase II transcription. J Biol Chem, 274, 34527-30.

Furutani-Seiki, M. & Wittbrodt, J. 2004. Medaka and zebrafish, an evolutionary twin study. Mech Dev, 121, 629-37.

Gallagher, J. J., Sealy, W. C., Anderson, R. W., Kasell, J., Millar, R., Campbell, R. W., Harrison, L., Pritchett, E. L. & Wallace, A. G. 1977. Cryosurgical ablation of accessory atrioventricular connections: a method for correction of the pre-excitation syndrome. Circulation, 55, 471-9.

Gan, D. D., Macaluso, M., Cinti, C., Khalili, K. & Giordano, A. 2003. How does a normal human cell become a cancer cell? J Exp Clin Cancer Res, 22, 509-16.

Gardiner, D. M., Endo, T. & Bryant, S. V. 2002. The molecular basis of amphibian limb regeneration: integrating the old with the new. Semin Cell Dev Biol, 13, 345-52.

Garg, V., Kathiriya, I. S., Barnes, R., Schluterman, M. K., King, I. N., Butler, C. A., Rothrock, C. R., Eapen, R. S., Hirayama-Yamada, K., Joo, K., Matsuoka, R., Cohen, J. C. & Srivastava, D. 2003. GATA4 mutations cause human congenital heart defects and reveal an interaction with TBX5. Nature, 424, 443-7.

Garriga, J., Bhattacharya, S., Calbo, J., Marshall, R. M., Truongcao, M., Haines, D. S. & Grana, X. 2003. CDK9 is constitutively expressed throughout the cell cycle, and its steady-state expression is independent of SKP2. Mol Cell Biol, 23, 5165-73.

Garriga, J. & Grana, X. 2004. Cellular control of gene expression by T-type cyclin/CDK9 complexes. Gene, 337, 15-23.

Garriga, J., Xie, H., Obradovic, Z. & Grana, X. 2010. Selective control of gene expression by CDK9 in human cells. J Cell Physiol, 222, 200-8.

Garrity, D. M., Childs, S. & Fishman, M. C. 2002. The heartstrings mutation in zebrafish causes heart/fin Tbx5 deficiency syndrome. Development, 129, 4635-45.

Geisel, N. 2011. Constitutive versus responsive gene expression strategies for growth in changing environments. PLoS One, 6, e27033.

Giacinti, C., Bagella, L., Puri, P. L., Giordano, A. & Simone, C. 2006. MyoD recruits the cdk9/cyclin T2 complex on myogenic-genes regulatory regions. J Cell Physiol, 206, 807-13.

Giacinti, C., Musaro, A., De Falco, G., Jourdan, I., Molinaro, M., Bagella, L., Simone, C. & Giordano, A. 2008. Cdk9-55: a new player in muscle regeneration. J Cell Physiol, 216, 576-82.

Glover-Cutter, K., Larochelle, S., Erickson, B., Zhang, C., Shokat, K., Fisher, R. P. & Bentley, D. L. 2009. TFIIH-associated Cdk7 kinase functions in phosphorylation of C-terminal domain Ser7 residues, promoter-proximal pausing, and termination by RNA polymerase II. Mol Cell Biol, 29, 5455-64.

Gonzalez-Rosa, J. M., Martin, V., Peralta, M., Torres, M. & Mercader, N. 2011. Extensive scar formation and regression during heart regeneration after cryoinjury in zebrafish. Development, 138, 1663-74.

Gonzalez-Rosa, J. M. & Mercader, N. 2012. Cryoinjury as a myocardial infarction model for the study of cardiac regeneration in the zebrafish. Nat Protoc, 7, 782-8.

Gopinathan, L., Ratnacaram, C. K. & Kaldis, P. 2011. Established and novel Cdk/cyclin complexes regulating the cell cycle and development. Results Probl Cell Differ, 53, 365-89.

Grana, X., De Luca, A., Sang, N., Fu, Y., Claudio, P. P., Rosenblatt, J., Morgan, D. O. & Giordano, A. 1994. PITALRE, a nuclear CDC2-related protein kinase that phosphorylates the retinoblastoma protein in vitro. Proc Natl Acad Sci U S A, 91, 3834-8.

Granero-Molto, F., Sarmah, S., O'rear, L., Spagnoli, A., Abrahamson, D., Saus, J., Hudson, B. G. & Knapik, E. W. 2008. Goodpasture antigen-binding protein and its spliced variant, ceramide transfer protein, have different functions in the modulation of apoptosis during zebrafish development. J Biol Chem, 283, 20495-504.

Gray, C., Packham, I. M., Wurmser, F., Eastley, N. C., Hellewell, P. G., Ingham, P. W., Crossman, D. C. & Chico, T. J. 2007. Ischemia is not required for arteriogenesis in zebrafish embryos. Arterioscler Thromb Vasc Biol, 27, 2135-41.

Greer, S., Honeywell, R., Geletu, M., Arulanandam, R. & Raptis, L. 2010. Housekeeping genes; expression levels may change with density of cultured cells. J Immunol Methods, 355, 76-9.

Grepin, C., Nemer, G. & Nemer, M. 1997. Enhanced cardiogenesis in embryonic stem cells overexpressing the GATA-4 transcription factor. Development, 124, 2387-95.

Grunwald, D. J. & Eisen, J. S. 2002. Headwaters of the zebrafish -- emergence of a new model vertebrate. Nat Rev Genet, 3, 717-24.

Guadix, J. A., Ruiz-Villalba, A., Lettice, L., Velecela, V., Munoz-Chapuli, R., Hastie, N. D., Perez-Pomares, J. M. & Martinez-Estrada, O. M. 2011. Wt1 controls retinoic acid signalling in embryonic epicardium through transcriptional activation of Raldh2. Development, 138, 1093-7.

Haider, A. W., Larson, M. G., Benjamin, E. J. & Levy, D. 1998. Increased left ventricular mass and hypertrophy are associated with increased risk for sudden death. J Am Coll Cardiol, 32, 1454-9.

Hami, D., Grimes, A. C., Tsai, H. J. & Kirby, M. L. 2011. Zebrafish cardiac development requires a conserved secondary heart field. Development, 138, 2389-98.

Hamill, N., Yeo, L., Romero, R., Hassan, S. S., Myers, S. A., Mittal, P., Kusanovic, J. P., Balasubramaniam, M., Chaiworapongsa, T., Vaisbuch, E., Espinoza, J., Gotsch, F., Goncalves, L. F. & Lee, W. 2011. Fetal cardiac ventricular volume, cardiac output, and ejection fraction determined with 4-dimensional ultrasound using spatiotemporal image correlation and virtual organ computer-aided analysis. Am J Obstet Gynecol, 205, 76 e1-10.

Hanneman, E. & Westerfield, M. 1989. Early expression of acetylcholinesterase activity in functionally distinct neurons of the zebrafish. J Comp Neurol, 284, 350-61.

Happel, C. M., Klose, C., Witton, G., Angrisani, G. L., Wienecke, S., Groos, S., Bach, F. W., Bormann, D., Manner, J. & Yelbuz, T. M. 2010. Non-destructive, high-resolution 3-dimensional visualization of a cardiac defect in the chick embryo resembling complex heart defect in humans using micro-computed tomography: double outlet right ventricle with left juxtaposition of atrial appendages. Circulation, 122, e561-4.

Harada, M., Qin, Y., Takano, H., Minamino, T., Zou, Y., Toko, H., Ohtsuka, M., Matsuura, K., Sano, M., Nishi, J., Iwanaga, K., Akazawa, H., Kunieda, T., Zhu, W., Hasegawa, H., Kunisada, K., Nagai, T., Nakaya, H., Yamauchi-Takihara, K. & Komuro, I. 2005. G-CSF prevents cardiac remodeling after myocardial infarction by activating the Jak-Stat pathway in cardiomyocytes. Nat Med, 11, 305-11.

Hartwell, L. H. 1974. Saccharomyces cerevisiae cell cycle. Bacteriol Rev, 38, 164-98.

Harvey, R. P. 2002. Patterning the vertebrate heart. Nat Rev Genet, 3, 544-56.

Hasinoff, B. B. & Patel, D. 2010. The lack of target specificity of small molecule anticancer kinase inhibitors is correlated with their ability to damage myocytes in vitro. Toxicol Appl Pharmacol, 249, 132-9.

He, N., Jahchan, N. S., Hong, E., Li, Q., Bayfield, M. A., Maraia, R. J., Luo, K. & Zhou, Q. 2008. A La-related protein modulates 7SK snRNP integrity to suppress P-TEFb-dependent transcriptional elongation and tumorigenesis. Mol Cell, 29, 588-99.

He, N., Pezda, A. C. & Zhou, Q. 2006. Modulation of a P-TEFb functional equilibrium for the global control of cell growth and differentiation. Mol Cell Biol, 26, 7068-76.

Heasman, J. 2002. Morpholino oligos: making sense of antisense? Dev Biol, 243, 209-14.

Heineke, J. & Molkentin, J. D. 2006. Regulation of cardiac hypertrophy by intracellular signalling pathways. Nat Rev Mol Cell Biol, 7, 589-600.

Herrmann, C. H. & Mancini, M. A. 2001. The Cdk9 and cyclin T subunits of TAK/P-TEFb localize to splicing factor-rich nuclear speckle regions. J Cell Sci, 114, 1491-503.

Ho, Y. L., Shau, Y. W., Tsai, H. J., Lin, L. C., Huang, P. J. & Hsieh, F. J. 2002. Assessment of zebrafish cardiac performance using Doppler echocardiography and power angiography. Ultrasound Med Biol, 28, 1137-43.

Hong, P., Chen, K., Huang, B., Liu, M., Cui, M., Rozenberg, I., Chaqour, B., Pan, X., Barton, E. R., Jiang, X. C. & Siddiqui, M. A. 2012. HEXIM1 controls satellite cell expansion after injury to regulate skeletal muscle regeneration. J Clin Invest, 122, 3873-87.

Hou, P. C. & Burggren, W. W. 1995. Cardiac output and peripheral resistance during larval development in the anuran amphibian Xenopus laevis. Am J Physiol, 269, R1126-32.

Hove, J. R., Koster, R. W., Forouhar, A. S., Acevedo-Bolton, G., Fraser, S. E. & Gharib, M. 2003. Intracardiac fluid forces are an essential epigenetic factor for embryonic cardiogenesis. Nature, 421, 172-7.

Howe, K., Clark, M. D., Torroja, C. F., Torrance, J., Berthelot, C., Muffato, M., Collins, J. E., Humphray, S., Mclaren, K., Matthews, L., Mclaren, S., Sealy, I., Caccamo, M., Churcher, C., Scott, C., Barrett, J. C., Koch, R., Rauch, G. J., *et al*. 2013. The zebrafish reference genome sequence and its relationship to the human genome. Nature, 496, 498-503.

Hu, N., Sedmera, D., Yost, H. J. & Clark, E. B. 2000. Structure and function of the developing zebrafish heart. Anat Rec, 260, 148-57.

Huang, F., Wagner, M. & Siddiqui, M. A. 2002. Structure, expression, and functional characterization of the mouse CLP-1 gene. Gene, 292, 245-59.

Huang, F., Wagner, M. & Siddiqui, M. A. 2004. Ablation of the CLP-1 gene leads to down-regulation of the HAND1 gene and abnormality of the left ventricle of the heart and fetal death. Mech Dev, 121, 559-72.

Iankova, I., Petersen, R. K., Annicotte, J. S., Chavey, C., Hansen, J. B., Kratchmarova, I., Sarruf, D., Benkirane, M., Kristiansen, K. & Fajas, L. 2006. Peroxisome proliferator-activated receptor gamma recruits the positive transcription elongation factor b complex to activate transcription and promote adipogenesis. Mol Endocrinol, 20, 1494-505.

Isogai, S., Horiguchi, M. & Weinstein, B. M. 2001. The vascular anatomy of the developing zebrafish: an atlas of embryonic and early larval development. Dev Biol, 230, 278-301.

Iwasaki, H., Kawamoto, A., Tjwa, M., Horii, M., Hayashi, S., Oyamada, A., Matsumoto, T., Suehiro, S., Carmeliet, P. & Asahara, T. 2011. PlGF repairs myocardial ischemia through mechanisms of angiogenesis, cardioprotection and recruitment of myo-angiogenic competent marrow progenitors. PLoS One, 6, e24872.

Jacob, E., Drexel, M., Schwerte, T. & Pelster, B. 2002. Influence of hypoxia and of hypoxemia on the development of cardiac activity in zebrafish larvae. Am J Physiol Regul Integr Comp Physiol, 283, R911-7.

Jagadeeswaran, P., Carrillo, M., Radhakrishnan, U. P., Rajpurohit, S. K. & Kim, S. 2011. Laser-induced thrombosis in zebrafish. Methods Cell Biol, 101, 197-203.

Jang, M. K., Mochizuki, K., Zhou, M., Jeong, H. S., Brady, J. N. & Ozato, K. 2005. The bromodomain protein Brd4 is a positive regulatory component of P-TEFb and stimulates RNA polymerase II-dependent transcription. Mol Cell, 19, 523-34.

Jaschke, B., Milz, S., Vogeser, M., Michaelis, C., Vorpahl, M., Schomig, A., Kastrati, A. & Wessely, R. 2004. Local cyclin-dependent kinase inhibition by flavopiridol inhibits coronary artery smooth muscle cell proliferation and migration: Implications for the applicability on drug-eluting stents to prevent neointima formation following vascular injury. FASEB J, 18, 1285-7.

Jenuwein, T. & Allis, C. D. 2001. Translating the histone code. Science, 293, 1074-80.

Jin, S. W., Beis, D., Mitchell, T., Chen, J. N. & Stainier, D. Y. 2005. Cellular and molecular analyses of vascular tube and lumen formation in zebrafish. Development, 132, 5199-209.

Johnson, C. S., Holzemer, N. F. & Wingert, R. A. 2011. Laser ablation of the zebrafish pronephros to study renal epithelial regeneration. J Vis Exp.

Jopling, C., Sleep, E., Raya, M., Marti, M., Raya, A. & Izpisua Belmonte, J. C. 2010. Zebrafish heart regeneration occurs by cardiomyocyte dedifferentiation and proliferation. Nature, 464, 606-9.

Kaichi, S., Takaya, T., Morimoto, T., Sunagawa, Y., Kawamura, T., Ono, K., Shimatsu, A., Baba, S., Heike, T., Nakahata, T. & Hasegawa, K. 2011. Cyclin-dependent kinase 9 forms a complex with GATA4 and is involved in the differentiation of mouse ES cells into cardiomyocytes. J Cell Physiol, 226, 248-54.

Kajstura, J., Zhang, X., Reiss, K., Szoke, E., Li, P., Lagrasta, C., Cheng, W., Darzynkiewicz, Z., Olivetti, G. & Anversa, P. 1994. Myocyte cellular hyperplasia and myocyte cellular hypertrophy contribute to chronic ventricular remodeling in coronary artery narrowing-induced cardiomyopathy in rats. Circ Res, 74, 383-400.

Kang, P. M. & Izumo, S. 2003. Apoptosis in heart: basic mechanisms and implications in cardiovascular diseases. Trends Mol Med, 9, 177-82.

Kao, S. Y., Calman, A. F., Luciw, P. A. & Peterlin, B. M. 1987. Anti-termination of transcription within the long terminal repeat of HIV-1 by tat gene product. Nature, 330, 489-93.

Karsner, H. T., Saphir, O. & Todd, T. W. 1925. The State of the Cardiac Muscle in Hypertrophy and Atrophy. Am J Pathol, 1, 351-372 1.

Kearns-Jonker, M., Dai, W., Gunthart, M., Fuentes, T., Yeh, H. Y., Gerczuk, P., Pera, M., Mummery, C. & Kloner, R. A. 2012. Genetically Engineered Mesenchymal Stem Cells Influence Gene Expression in Donor Cardiomyocytes and the Recipient Heart. J Stem Cell Res Ther, S1.

Keegan, B. R., Meyer, D. & Yelon, D. 2004. Organization of cardiac chamber progenitors in the zebrafish blastula. Development, 131, 3081-91.

Kelly, R. G. & Buckingham, M. E. 2002. The anterior heart-forming field: voyage to the arterial pole of the heart. Trends Genet, 18, 210-6.

Keskin, H., Garriga, J., Georlette, D. & Grana, X. 2012. Complex effects of flavopiridol on the expression of primary response genes. Cell Div, 7, 11.

Kikuchi, K., Holdway, J. E., Werdich, A. A., Anderson, R. M., Fang, Y., Egnaczyk, G. F., Evans, T., Macrae, C. A., Stainier, D. Y. & Poss, K. D. 2010. Primary contribution to zebrafish heart regeneration by gata4(+) cardiomyocytes. Nature, 464, 601-5.

Kim, K. H., Antkiewicz, D. S., Yan, L., Eliceiri, K. W., Heideman, W., Peterson, R. E. & Lee, Y. 2007. Lrrc10 is required for early heart development and function in zebrafish. Dev Biol, 308, 494-506.

Kimmel, C. B., Ballard, W. W., Kimmel, S. R., Ullmann, B. & Schilling, T. F. 1995. Stages of embryonic development of the zebrafish. Dev Dyn, 203, 253-310.

King, R. S. & Newmark, P. A. 2012. The cell biology of regeneration. J Cell Biol, 196, 553-62.

Kizil, C., Kyritsis, N., Dudczig, S., Kroehne, V., Freudenreich, D., Kaslin, J. & Brand, M. 2012. Regenerative neurogenesis from neural progenitor cells requires injury-induced expression of gata3. Dev Cell, 23, 1230-7.

Kohoutek, J. 2009. P-TEFb- the final frontier. Cell Div, 4, 19.

Kopp, R., Schwerte, T., Egg, M., Sandbichler, A. M., Egger, B. & Pelster, B. 2010. Chronic reduction in cardiac output induces hypoxic signaling in larval zebrafish even at a time when convective oxygen transport is not required. Physiol Genomics, 42A, 8-23.

Krishnan, J., Suter, M., Windak, R., Krebs, T., Felley, A., Montessuit, C., Tokarska-Schlattner, M., Aasum, E., Bogdanova, A., Perriard, E., Perriard, J. C., Larsen, T., Pedrazzini, T. & Krek, W. 2009. Activation of a HIF1alpha-PPARgamma axis underlies the integration of glycolytic and lipid anabolic pathways in pathologic cardiac hypertrophy. Cell Metab, 9, 512-24.

Krueger, B. J., Jeronimo, C., Roy, B. B., Bouchard, A., Barrandon, C., Byers, S. A., Searcey, C. E., Cooper, J. J., Bensaude, O., Cohen, E. A., Coulombe, B. & Price, D. H. 2008. LARP7 is a stable component of the 7SK snRNP while P-TEFb, HEXIM1 and hnRNP A1 are reversibly associated. Nucleic Acids Res, 36, 2219-29.

Krystof, V., Baumli, S. & Furst, R. 2012. Perspective of cyclin-dependent kinase 9 (CDK9) as a drug target. Curr Pharm Des, 18, 2883-90.

Krystof, V., Chamrad, I., Jorda, R. & Kohoutek, J. 2010. Pharmacological targeting of CDK9 in cardiac hypertrophy. Med Res Rev, 30, 646-66.

Krystof, V. & Uldrijan, S. 2010. Cyclin-dependent kinase inhibitors as anticancer drugs. Curr Drug Targets, 11, 291-302.

Kuo, C. T., Morrisey, E. E., Anandappa, R., Sigrist, K., Lu, M. M., Parmacek, M. S., Soudais, C. & Leiden, J. M. 1997. GATA4 transcription factor is required for ventral morphogenesis and heart tube formation. Genes Dev, 11, 1048-60.

Kyritsis, N., Kizil, C., Zocher, S., Kroehne, V., Kaslin, J., Freudenreich, D., Iltzsche, A. & Brand, M. 2012. Acute inflammation initiates the regenerative response in the adult zebrafish brain. Science, 338, 1353-6.

Laflamme, M. A. & Murry, C. E. 2011. Heart regeneration. Nature, 473, 326-35.

Laguerre, L., Soubiran, F., Ghysen, A., Konig, N. & Dambly-Chaudiere, C. 2005. Cell proliferation in the developing lateral line system of zebrafish embryos. Dev Dyn, 233, 466-72.

Lam, L. T., Pickeral, O. K., Peng, A. C., Rosenwald, A., Hurt, E. M., Giltnane, J. M., Averett, L. M., Zhao, H., Davis, R. E., Sathyamoorthy, M., Wahl, L. M., Harris, E. D., Mikovits, J. A., Monks, A. P., Hollingshead, M. G., Sausville, E. A. & Staudt, L. M. 2001. Genomic-scale measurement of mRNA turnover and the mechanisms of action of the anti-cancer drug flavopiridol. Genome Biol, 2, RESEARCH0041.

Lamason, R. L., Mohideen, M. A., Mest, J. R., Wong, A. C., Norton, H. L., Aros, M. C., Jurynec, M. J., Mao, X., Humphreville, V. R., Humbert, J. E., Sinha, S., Moore, J. L., Jagadeeswaran, P., Zhao, W., Ning, G., Makalowska, I., Mckeigue, P. M., O'donnell, D., Kittles, R., Parra, E. J., Mangini, N. J., Grunwald, D. J., Shriver, M. D., Canfield, V. A. & Cheng, K. C. 2005. SLC24A5, a putative cation exchanger, affects pigmentation in zebrafish and humans. Science, 310, 1782-6.

Langenau, D. M. & Zon, L. I. 2005. The zebrafish: a new model of T-cell and thymic development. Nat Rev Immunol, 5, 307-17.

Latronico, M. V., Elia, L., Condorelli, G. & Catalucci, D. 2008. Heart failure: targeting transcriptional and post-transcriptional control mechanisms of hypertrophy for treatment. Int J Biochem Cell Biol, 40, 1643-8.

Laugwitz, K. L., Moretti, A., Lam, J., Gruber, P., Chen, Y., Woodard, S., Lin, L. Z., Cai, C. L., Lu, M. M., Reth, M., Platoshyn, O., Yuan, J. X., Evans, S. & Chien, K. R. 2005. Postnatal isl1+ cardioblasts enter fully differentiated cardiomyocyte lineages. Nature, 433, 647-53.

Lee, K. C., Chang, H. T., Chou, K. J., Tang, K. Y., Wang, J. L., Lo, Y. K., Huang, J. K.,

Chen, W. C., Su, W., Law, Y. P. & Jan, C. R. 2001. Mechanism underlying histamine-induced intracellular Ca2+ movement in PC3 human prostate cancer cells. Pharmacol Res, 44, 547-52.

Lepilina, A., Coon, A. N., Kikuchi, K., Holdway, J. E., Roberts, R. W., Burns, C. G. & Poss, K. D. 2006. A dynamic epicardial injury response supports progenitor cell activity during zebrafish heart regeneration. Cell, 127, 607-19.

Levy, D., Kenchaiah, S., Larson, M. G., Benjamin, E. J., Kupka, M. J., Ho, K. K., Murabito, J. M. & Vasan, R. S. 2002. Long-term trends in the incidence of and survival with heart failure. N Engl J Med, 347, 1397-402.

Li, F., Wang, X., Capasso, J. M. & Gerdes, A. M. 1996. Rapid transition of cardiac myocytes from hyperplasia to hypertrophy during postnatal development. J Mol Cell Cardiol, 28, 1737-46.

Li, J. M., Poolman, R. A. & Brooks, G. 1998. Role of G1 phase cyclins and cyclin-dependent kinases during cardiomyocyte hypertrophic growth in rats. Am J Physiol, 275, H814-22.

Li, Q., Guo, Y., Ou, Q., Cui, C., Wu, W. J., Tan, W., Zhu, X., Lanceta, L. B., Sanganalmath, S. K., Dawn, B., Shinmura, K., Rokosh, G. D., Wang, S. & Bolli, R. 2009. Gene transfer of inducible nitric oxide synthase affords cardioprotection by upregulating heme oxygenase-1 via a nuclear factor-{kappa}B-dependent pathway. Circulation, 120, 1222-30.

Li, Q., Price, J. P., Byers, S. A., Cheng, D., Peng, J. & Price, D. H. 2005. Analysis of the large inactive P-TEFb complex indicates that it contains one 7SK molecule, a dimer of HEXIM1 or HEXIM2, and two P-TEFb molecules containing Cdk9 phosphorylated at threonine 186. J Biol Chem, 280, 28819-26.

Lien, C. L., Harrison, M. R., Tuan, T. L. & Starnes, V. A. 2012. Heart repair and regeneration: Recent insights from zebrafish studies. Wound Repair Regen.

Lieschke, G. J. & Currie, P. D. 2007. Animal models of human disease: zebrafish swim into view. Nat Rev Genet, 8, 353-67.

Lin, Q., Schwarz, J., Bucana, C. & Olson, E. N. 1997. Control of mouse cardiac morphogenesis and myogenesis by transcription factor MEF2C. Science, 276, 1404-7.

Lints, T. J., Parsons, L. M., Hartley, L., Lyons, I. & Harvey, R. P. 1993. Nkx-2.5: a novel murine homeobox gene expressed in early heart progenitor cells and their myogenic descendants. Development, 119, 969.

Linzbach, A. J. 1960. Heart failure from the point of view of quantitative anatomy. Am J Cardiol, 5, 370-82.

Lips, D. J., Dewindt, L. J., Van Kraaij, D. J. & Doevendans, P. A. 2003. Molecular determinants of myocardial hypertrophy and failure: alternative pathways for

beneficial and maladaptive hypertrophy. Eur Heart J, 24, 883-96.

Liu, H. & Herrmann, C. H. 2005. Differential localization and expression of the Cdk9 42k and 55k isoforms. J Cell Physiol, 203, 251-60.

Liu, H. & Rice, A. P. 2000. Genomic organization and characterization of promoter function of the human CDK9 gene. Gene, 252, 51-9.

Liu, J. & Stainier, D. Y. 2012. Zebrafish in the study of early cardiac development. Circ Res, 110, 870-4.

Liu, N. & Olson, E. N. 2010. MicroRNA regulatory networks in cardiovascular development. Dev Cell, 18, 510-25.

Liu, X., Shi, S., Lam, F., Pepper, C., Fischer, P. M. & Wang, S. 2012. CDKI-71, a novel CDK9 inhibitor, is preferentially cytotoxic to cancer cells compared to flavopiridol. Int J Cancer, 130, 1216-26.

Long, Q., Meng, A., Wang, H., Jessen, J. R., Farrell, M. J. & Lin, S. 1997. GATA-1 expression pattern can be recapitulated in living transgenic zebrafish using GFP reporter gene. Development, 124, 4105-11.

Loyer, P., Trembley, J. H., Katona, R., Kidd, V. J. & Lahti, J. M. 2005. Role of CDK/cyclin complexes in transcription and RNA splicing. Cell Signal, 17, 1033-51.

Lyons, D. A., Pogoda, H. M., Voas, M. G., Woods, I. G., Diamond, B., Nix, R., Arana, N., Jacobs, J. & Talbot, W. S. 2005. erbb3 and erbb2 are essential for schwann cell migration and myelination in zebrafish. Curr Biol, 15, 513-24.

Maclachlan, T. K., Sang, N., De Luca, A., Puri, P. L., Levrero, M. & Giordano, A. 1998. Binding of CDK9 to TRAF2. J Cell Biochem, 71, 467-78.

Macmahon, H. E. 1937. Hyperplasia and Regeneration of the Myocardium in Infants and in Children. Am J Pathol, 13, 845-854 5.

Malaga-Trillo, E., Solis, G. P., Schrock, Y., Geiss, C., Luncz, L., Thomanetz, V. & Stuermer, C. A. 2009. Regulation of embryonic cell adhesion by the prion protein. PLoS Biol, 7, e55.

Malumbres, M. 2011. Physiological relevance of cell cycle kinases. Physiol Rev, 91, 973-1007.

Malumbres, M. & Barbacid, M. 2005. Mammalian cyclin-dependent kinases. Trends Biochem Sci, 30, 630-41.

Malumbres, M. & Barbacid, M. 2007. Cell cycle kinases in cancer. Curr Opin Genet Dev, 17, 60-5.

Malumbres, M. & Barbacid, M. 2009. Cell cycle, CDKs and cancer: a changing

paradigm. Nat Rev Cancer, 9, 153-66.

Malumbres, M., Pevarello, P., Barbacid, M. & Bischoff, J. R. 2008. CDK inhibitors in cancer therapy: what is next? Trends Pharmacol Sci, 29, 16-21.

Markert, A., Grimm, M., Martinez, J., Wiesner, J., Meyerhans, A., Meyuhas, O., Sickmann, A. & Fischer, U. 2008. The La-related protein LARP7 is a component of the 7SK ribonucleoprotein and affects transcription of cellular and viral polymerase II genes. EMBO Rep, 9, 569-75.

Marques, S. R., Lee, Y., Poss, K. D. & Yelon, D. 2008. Reiterative roles for FGF signaling in the establishment of size and proportion of the zebrafish heart. Dev Biol, 321, 397-406.

Marshall, N. F., Peng, J., Xie, Z. & Price, D. H. 1996. Control of RNA polymerase II elongation potential by a novel carboxyl-terminal domain kinase. J Biol Chem, 271, 27176-83.

Marshall, R. M. & Grana, X. 2006. Mechanisms controlling CDK9 activity. Front Biosci, 11, 2598-613.

Martin-Puig, S., Fuster, V. & Torres, M. 2012. Heart repair: from natural mechanisms of cardiomyocyte production to the design of new cardiac therapies. Ann N Y Acad Sci, 1254, 71-81.

Mathew, L. K., Sengupta, S., Franzosa, J. A., Perry, J., La Du, J., Andreasen, E. A. & Tanguay, R. L. 2009. Comparative expression profiling reveals an essential role for raldh2 in epimorphic regeneration. J Biol Chem, 284, 33642-53.

Matson, C. W., Clark, B. W., Jenny, M. J., Fleming, C. R., Hahn, M. E. & Di Giulio, R. T. 2008. Development of the morpholino gene knockdown technique in Fundulus heteroclitus: a tool for studying molecular mechanisms in an established environmental model. Aquat Toxicol, 87, 289-95.

Mattick, J. S. 2011. The central role of RNA in human development and cognition. FEBS Lett, 585, 1600-16.

Matz, D. G., Oberpriller, J. O. & Oberpriller, J. C. 1998. Comparison of mitosis in binucleated and mononucleated newt cardiac myocytes. Anat Rec, 251, 245-55.

Mccurley, A. T. & Callard, G. V. 2008. Characterization of housekeeping genes in zebrafish: male-female differences and effects of tissue type, developmental stage and chemical treatment. BMC Mol Biol, 9, 102.

Mcfadden, D. G., Barbosa, A. C., Richardson, J. A., Schneider, M. D., Srivastava, D. & Olson, E. N. 2005. The Hand1 and Hand2 transcription factors regulate expansion of the embryonic cardiac ventricles in a gene dosage-dependent manner. Development, 132, 189-201.

Mcmurray, J. J. & Pfeffer, M. A. 2005. Heart failure. Lancet, 365, 1877-89.

Medlin, J., Scurry, A., Taylor, A., Zhang, F., Peterlin, B. M. & Murphy, S. 2005. P-TEFb is not an essential elongation factor for the intronless human U2 snRNA and histone H2b genes. EMBO J, 24, 4154-65.

Meier, N., Krpic, S., Rodriguez, P., Strouboulis, J., Monti, M., Krijgsveld, J., Gering, M., Patient, R., Hostert, A. & Grosveld, F. 2006. Novel binding partners of Ldb1 are required for haematopoietic development. Development, 133, 4913-23.

Meijer, L. & Raymond, E. 2003. Roscovitine and other purines as kinase inhibitors. From starfish oocytes to clinical trials. Acc Chem Res, 36, 417-25.

Menasche, P. 2011. Stem cell therapy for chronic heart failure: lessons from a 15-year experience. C R Biol, 334, 489-96.

Mercola, M., Ruiz-Lozano, P. & Schneider, M. D. 2011. Cardiac muscle regeneration: lessons from development. Genes Dev, 25, 299-309.

Michels, A. A., Fraldi, A., Li, Q., Adamson, T. E., Bonnet, F., Nguyen, V. T., Sedore, S. C., Price, J. P., Price, D. H., Lania, L. & Bensaude, O. 2004. Binding of the 7SK snRNA turns the HEXIM1 protein into a P-TEFb (CDK9/cyclin T) inhibitor. EMBO J, 23, 2608-19.

Michels, A. A., Nguyen, V. T., Fraldi, A., Labas, V., Edwards, M., Bonnet, F., Lania, L. & Bensaude, O. 2003. MAQ1 and 7SK RNA interact with CDK9/cyclin T complexes in a transcription-dependent manner. Mol Cell Biol, 23, 4859-69.

Molkentin, J. D. 2000. The zinc finger-containing transcription factors GATA-4, -5, and -6. Ubiquitously expressed regulators of tissue-specific gene expression. J Biol Chem, 275, 38949-52.

Molkentin, J. D., Lin, Q., Duncan, S. A. & Olson, E. N. 1997. Requirement of the transcription factor GATA4 for heart tube formation and ventral morphogenesis. Genes Dev, 11, 1061-72.

Monaghan, J. R., Athippozhy, A., Seifert, A. W., Putta, S., Stromberg, A. J., Maden, M., Gardiner, D. M. & Voss, S. R. 2012. Gene expression patterns specific to the regenerating limb of the Mexican axolotl. Biol Open, 1, 937-48.

Moorman, A. F. & Christoffels, V. M. 2003. Cardiac chamber formation: development, genes, and evolution. Physiol Rev, 83, 1223-67.

Moretti, A., Caron, L., Nakano, A., Lam, J. T., Bernshausen, A., Chen, Y., Qyang, Y., Bu, L., Sasaki, M., Martin-Puig, S., Sun, Y., Evans, S. M., Laugwitz, K. L. & Chien, K. R. 2006. Multipotent embryonic isl1+ progenitor cells lead to cardiac, smooth muscle, and endothelial cell diversification. Cell, 127, 1151-65.

Morgan, D. O. 1995. Principles of CDK regulation. Nature, 374, 131-4.

Morin, S., Charron, F., Robitaille, L. & Nemer, M. 2000. GATA-dependent recruitment of MEF2 proteins to target promoters. EMBO J, 19, 2046-55.

Morin-Kensicki, E. M. & Eisen, J. S. 1997. Sclerotome development and peripheral nervous system segmentation in embryonic zebrafish. Development, 124, 159-67.

Morrisey, E. E., Ip, H. S., Lu, M. M. & Parmacek, M. S. 1996. GATA-6: a zinc finger transcription factor that is expressed in multiple cell lineages derived from lateral mesoderm. Dev Biol, 177, 309-22.

Morrisey, E. E., Ip, H. S., Tang, Z., Lu, M. M. & Parmacek, M. S. 1997. GATA-5: a transcriptional activator expressed in a novel temporally and spatially-restricted pattern during embryonic development. Dev Biol, 183, 21-36.

Murphy, R. T., Mogensen, J., Mcgarry, K., Bahl, A., Evans, A., Osman, E., Syrris, P., Gorman, G., Farrell, M., Holton, J. L., Hanna, M. G., Hughes, S., Elliott, P. M., Macrae, C. A. & Mckenna, W. J. 2005. Adenosine monophosphate-activated protein kinase disease mimicks hypertrophic cardiomyopathy and Wolff-Parkinson-White syndrome: natural history. J Am Coll Cardiol, 45, 922-30.

Nag, A. C., Healy, C. J. & Cheng, M. 1979. DNA synthesis and mitosis in adult amphibian cardiac muscle cells in vitro. Science, 205, 1281-2.

Napolitano, G., Licciardo, P., Carbone, R., Majello, B. & Lania, L. 2002. CDK9 has the intrinsic property to shuttle between nucleus and cytoplasm, and enhanced expression of cyclin T1 promotes its nuclear localization. J Cell Physiol, 192, 209-15.

Nasevicius, A. & Ekker, S. C. 2000. Effective targeted gene 'knockdown' in zebrafish. Nat Genet, 26, 216-20.

Nasevicius, A., Larson, J. & Ekker, S. C. 2000. Distinct requirements for zebrafish angiogenesis revealed by a VEGF-A morphant. Yeast, 17, 294-301.

Nemeth, G., Varga, Z., Greff, Z., Bencze, G., Sipos, A., Szantai-Kis, C., Baska, F., Gyuris, A., Kelemenics, K., Szathmary, Z., Minarovits, J., Keri, G. & Orfi, L. 2011. Novel, selective CDK9 inhibitors for the treatment of HIV infection. Curr Med Chem, 18, 342-58.

Neufeld, T. P. & Edgar, B. A. 1998. Connections between growth and the cell cycle. Curr Opin Cell Biol, 10, 784-90.

Nguyen, V. H., Schmid, B., Trout, J., Connors, S. A., Ekker, M. & Mullins, M. C. 1998. Ventral and lateral regions of the zebrafish gastrula, including the neural crest progenitors, are established by a bmp2b/swirl pathway of genes. Dev Biol, 199, 93-110.

Nguyen, V. T., Kiss, T., Michels, A. A. & Bensaude, O. 2001. 7SK small nuclear RNA binds to and inhibits the activity of CDK9/cyclin T complexes. Nature, 414, 322-5.

Nurse, P. 1975. Genetic control of cell size at cell division in yeast. Nature, 256, 547-51.

Nurse, P. 2000. A long twentieth century of the cell cycle and beyond. Cell, 100, 71-8.

Nusslein-Volhard, C. 2012. The zebrafish issue of Development. Development, 139, 4099-103.

Nüsslein-Volhard, C., Dahm, R. 2002. Zebrafish, A Practical Approach, Oxford, Oxford University Press.

Nutt, S. L., Bronchain, O. J., Hartley, K. O. & Amaya, E. 2001. Comparison of morpholino based translational inhibition during the development of Xenopus laevis and Xenopus tropicalis. Genesis, 30, 110-3.

O'keeffe, B., Fong, Y., Chen, D., Zhou, S. & Zhou, Q. 2000. Requirement for a kinase-specific chaperone pathway in the production of a Cdk9/cyclin T1 heterodimer responsible for P-TEFb-mediated tat stimulation of HIV-1 transcription. J Biol Chem, 275, 279-87.

Oh, H., Taffet, G. E., Youker, K. A., Entman, M. L., Overbeek, P. A., Michael, L. H. & Schneider, M. D. 2001. Telomerase reverse transcriptase promotes cardiac muscle cell proliferation, hypertrophy, and survival. Proc Natl Acad Sci U S A, 98, 10308-13.

Oka, T., Maillet, M., Watt, A. J., Schwartz, R. J., Aronow, B. J., Duncan, S. A. & Molkentin, J. D. 2006. Cardiac-specific deletion of Gata4 reveals its requirement for hypertrophy, compensation, and myocyte viability. Circ Res, 98, 837-45.

Okamura, D., Maeda, I., Taniguchi, H., Tokitake, Y., Ikeda, M., Ozato, K., Mise, N., Abe, K., Noce, T., Izpisua Belmonte, J. C. & Matsui, Y. 2012. Cell cycle gene-specific control of transcription has a critical role in proliferation of primordial germ cells. Genes Dev, 26, 2477-82.

Olson, E. N. 2004. A decade of discoveries in cardiac biology. Nat Med, 10, 467-74.

Olson, E. N. & Schneider, M. D. 2003. Sizing up the heart: development redux in disease. Genes Dev, 17, 1937-56.

Oqani, R. K., Kim, H. R., Diao, Y. F., Park, C. S. & Jin, D. I. 2011. The CDK9/cyclin T1 subunits of P-TEFb in mouse oocytes and preimplantation embryos: a possible role in embryonic genome activation. BMC Dev Biol, 11, 33.

Orphanides, G., Lagrange, T. & Reinberg, D. 1996. The general transcription factors of RNA polymerase II. Genes Dev, 10, 2657-83.

Orphanides, G. & Reinberg, D. 2002. A unified theory of gene expression. Cell, 108, 439-51.

Oshima, Y., Ouchi, N., Shimano, M., Pimentel, D. R., Papanicolaou, K. N., Panse, K.

D., Tsuchida, K., Lara-Pezzi, E., Lee, S. J. & Walsh, K. 2009. Activin A and follistatin-like 3 determine the susceptibility of heart to ischemic injury. Circulation, 120, 1606-15.

Parichy, D. M., Elizondo, M. R., Mills, M. G., Gordon, T. N. & Engeszer, R. E. 2009. Normal table of postembryonic zebrafish development: staging by externally visible anatomy of the living fish. Dev Dyn, 238, 2975-3015.

Pasumarthi, K. B. & Field, L. J. 2002. Cardiomyocyte cell cycle regulation. Circ Res, 90, 1044-54.

Pattingre, S., Tassa, A., Qu, X., Garuti, R., Liang, X. H., Mizushima, N., Packer, M., Schneider, M. D. & Levine, B. 2005. Bcl-2 antiapoptotic proteins inhibit Beclin 1-dependent autophagy. Cell, 122, 927-39.

Pavletich, N. P. 1999. Mechanisms of cyclin-dependent kinase regulation: structures of Cdks, their cyclin activators, and Cip and INK4 inhibitors. J Mol Biol, 287, 821-8.

Peng, J., Zhu, Y., Milton, J. T. & Price, D. H. 1998. Identification of multiple cyclin subunits of human P-TEFb. Genes Dev, 12, 755-62.

Pennisi, D. J., Ballard, V. L. & Mikawa, T. 2003. Epicardium is required for the full rate of myocyte proliferation and levels of expression of myocyte mitogenic factors FGF2 and its receptor, FGFR-1, but not for transmural myocardial patterning in the embryonic chick heart. Dev Dyn, 228, 161-72.

Pennisi, E. 2012. Genomics. ENCODE project writes eulogy for junk DNA. Science, 337, 1159, 1161.

Perez-Pomares, J. M., Gonzalez-Rosa, J. M. & Munoz-Chapuli, R. 2009. Building the vertebrate heart - an evolutionary approach to cardiac development. Int J Dev Biol, 53, 1427-43.

Peshkovsky, C., Totong, R. & Yelon, D. 2011. Dependence of cardiac trabeculation on neuregulin signaling and blood flow in zebrafish. Dev Dyn, 240, 446-56.

Peterkin, T., Gibson, A. & Patient, R. 2009. Common genetic control of haemangioblast and cardiac development in zebrafish. Development, 136, 1465-74.

Peterlin, B. M. & Price, D. H. 2006. Controlling the elongation phase of transcription with P-TEFb. Mol Cell, 23, 297-305.

Pirngruber, J., Shchebet, A. & Johnsen, S. A. 2009a. Insights into the function of the human P-TEFb component CDK9 in the regulation of chromatin modifications and co-transcriptional mRNA processing. Cell Cycle, 8, 3636-42.

Pirngruber, J., Shchebet, A., Schreiber, L., Shema, E., Minsky, N., Chapman, R. D., Eick, D., Aylon, Y., Oren, M. & Johnsen, S. A. 2009b. CDK9 directs H2B monoubiquitination and controls replication-dependent histone mRNA 3'-end

processing. EMBO Rep, 10, 894-900.

Poolman, R. A. & Brooks, G. 1998. Expressions and activities of cell cycle regulatory molecules during the transition from myocyte hyperplasia to hypertrophy. J Mol Cell Cardiol, 30, 2121-35.

Porrello, E. R., Mahmoud, A. I., Simpson, E., Hill, J. A., Richardson, J. A., Olson, E. N. & Sadek, H. A. 2011. Transient regenerative potential of the neonatal mouse heart. Science, 331, 1078-80.

Poss, K. D. 2010. Advances in understanding tissue regenerative capacity and mechanisms in animals. Nat Rev Genet, 11, 710-22.

Poss, K. D., Wilson, L. G. & Keating, M. T. 2002. Heart regeneration in zebrafish. Science, 298, 2188-90.

Prelich, G. 2002. RNA polymerase II carboxy-terminal domain kinases: emerging clues to their function. Eukaryot Cell, 1, 153-62.

Price, D. H. 2000. P-TEFb, a cyclin-dependent kinase controlling elongation by RNA polymerase II. Mol Cell Biol, 20, 2629-34.

Quaini, F., Cigola, E., Lagrasta, C., Saccani, G., Quaini, E., Rossi, C., Olivetti, G. & Anversa, P. 1994. End-stage cardiac failure in humans is coupled with the induction of proliferating cell nuclear antigen and nuclear mitotic division in ventricular myocytes. Circ Res, 75, 1050-63.

Quaini, F., Urbanek, K., Beltrami, A. P., Finato, N., Beltrami, C. A., Nadal-Ginard, B., Kajstura, J., Leri, A. & Anversa, P. 2002. Chimerism of the transplanted heart. N Engl J Med, 346, 5-15.

Raju, T. N. 2000. The Nobel chronicles. 1995: Edward B Lewis (b 1918), Christiane Nusslein-Volhard (b 1942), and Eric Francis Wieschaus (b 1947). Lancet, 356, 81.

Rana, A. A., Collart, C., Gilchrist, M. J. & Smith, J. C. 2006. Defining synphenotype groups in Xenopus tropicalis by use of antisense morpholino oligonucleotides. PLoS Genet, 2, e193.

Rapoport, A. P., Simons-Evelyn, M., Chen, T., Sidell, R., Luhowskyj, S., Rosell, K., Obrig, T., Hicks, D., Hinkle, P. M., Nahm, M., Insel, R. A. & Abboud, C. N. 2001. Flavopiridol induces apoptosis and caspase-3 activation of a newly characterized Burkitt's lymphoma cell line containing mutant p53 genes. Blood Cells Mol Dis, 27, 610-24.

Raya, A., Koth, C. M., Buscher, D., Kawakami, Y., Itoh, T., Raya, R. M., Sternik, G., Tsai, H. J., Rodriguez-Esteban, C. & Izpisua-Belmonte, J. C. 2003. Activation of Notch signaling pathway precedes heart regeneration in zebrafish. Proc Natl Acad Sci U S A, 100 Suppl 1, 11889-95.

Reifers, F., Walsh, E. C., Leger, S., Stainier, D. Y. & Brand, M. 2000. Induction and differentiation of the zebrafish heart requires fibroblast growth factor 8 (fgf8/acerebellar). Development, 127, 225-35.

Reiter, J. F., Alexander, J., Rodaway, A., Yelon, D., Patient, R., Holder, N. & Stainier, D. Y. 1999. Gata5 is required for the development of the heart and endoderm in zebrafish. Genes Dev, 13, 2983-95.

Reiter, J. F., Verkade, H. & Stainier, D. Y. 2001. Bmp2b and Oep promote early myocardial differentiation through their regulation of gata5. Dev Biol, 234, 330-8.

Ren, S. & Rollins, B. J. 2004. Cyclin C/cdk3 promotes Rb-dependent G0 exit. Cell, 117, 239-51.

Rice, A. P. & Herrmann, C. H. 2003. Regulation of TAK/P-TEFb in CD4+ T lymphocytes and macrophages. Curr HIV Res, 1, 395-404.

Rider, S. A., Tucker, C. S., Del-Pozo, J., Rose, K. N., Macrae, C. A., Bailey, M. A. & Mullins, J. J. 2012. Techniques for the in vivo assessment of cardio-renal function in zebrafish (Danio rerio) larvae. J Physiol, 590, 1803-9.

Robertson, G. N., Mcgee, C. A., Dumbarton, T. C., Croll, R. P. & Smith, F. M. 2007. Development of the swimbladder and its innervation in the zebrafish, Danio rerio. J Morphol, 268, 967-85.

Robu, M. E., Larson, J. D., Nasevicius, A., Beiraghi, S., Brenner, C., Farber, S. A. & Ekker, S. C. 2007. p53 activation by knockdown technologies. PLoS Genet, 3, e78.

Rodriguez, C. R., Cho, E. J., Keogh, M. C., Moore, C. L., Greenleaf, A. L. & Buratowski, S. 2000. Kin28, the TFIIH-associated carboxy-terminal domain kinase, facilitates the recruitment of mRNA processing machinery to RNA polymerase II. Mol Cell Biol, 20, 104-12.

Rokas, A. 2008. The origins of multicellularity and the early history of the genetic toolkit for animal development. Annu Rev Genet, 42, 235-51.

Romano, G. & Giordano, A. 2008. Role of the cyclin-dependent kinase 9-related pathway in mammalian gene expression and human diseases. Cell Cycle, 7, 3664-8.

Romero-Calvo, I., Ocon, B., Martinez-Moya, P., Suarez, M. D., Zarzuelo, A., Martinez-Augustin, O. & De Medina, F. S. 2010. Reversible Ponceau staining as a loading control alternative to actin in Western blots. Anal Biochem, 401, 318-20.

Royse, C. F. & Royse, A. G. 2000. Afterload corrected fractional area change (FACac): a simple, relatively load-independent measurement of left ventricular contractility in humans. Ann Thorac Cardiovasc Surg, 6, 345-50.

Rubart, M. & Field, L. J. 2006. Cardiac regeneration: repopulating the heart. Annu Rev Physiol, 68, 29-49.

Ruef, J., Meshel, A. S., Hu, Z., Horaist, C., Ballinger, C. A., Thompson, L. J., Subbarao, V. D., Dumont, J. A. & Patterson, C. 1999. Flavopiridol inhibits smooth muscle cell proliferation in vitro and neointimal formation In vivo after carotid injury in the rat. Circulation, 100, 659-65.

Ruvinsky, I., Oates, A. C., Silver, L. M. & Ho, R. K. 2000. The evolution of paired appendages in vertebrates: T-box genes in the zebrafish. Dev Genes Evol, 210, 82-91.

Sabaliauskas, N. A., Foutz, C. A., Mest, J. R., Budgeon, L. R., Sidor, A. T., Gershenson, J. A., Joshi, S. B. & Cheng, K. C. 2006. High-throughput zebrafish histology. Methods, 39, 246-54.

Sachinidis, A., Fleischmann, B. K., Kolossov, E., Wartenberg, M., Sauer, H. & Hescheler, J. 2003. Cardiac specific differentiation of mouse embryonic stem cells. Cardiovasc Res, 58, 278-91.

Salerno, D., Hasham, M. G., Marshall, R., Garriga, J., Tsygankov, A. Y. & Grana, X. 2007. Direct inhibition of CDK9 blocks HIV-1 replication without preventing T-cell activation in primary human peripheral blood lymphocytes. Gene, 405, 65-78.

Sano, M., Abdellatif, M., Oh, H., Xie, M., Bagella, L., Giordano, A., Michael, L. H., Demayo, F. J. & Schneider, M. D. 2002. Activation and function of cyclin T-Cdk9 (positive transcription elongation factor-b) in cardiac muscle-cell hypertrophy. Nat Med, 8, 1310-7.

Sano, M. & Schneider, M. D. 2003. Cyclins that don't cycle--cyclin T/cyclin-dependent kinase-9 determines cardiac muscle cell size. Cell Cycle, 2, 99-104.

Sano, M. & Schneider, M. D. 2004. Cyclin-dependent kinase-9: an RNAPII kinase at the nexus of cardiac growth and death cascades. Circ Res, 95, 867-76.

Sano, M., Wang, S. C., Shirai, M., Scaglia, F., Xie, M., Sakai, S., Tanaka, T., Kulkarni, P. A., Barger, P. M., Youker, K. A., Taffet, G. E., Hamamori, Y., Michael, L. H., Craigen, W. J. & Schneider, M. D. 2004. Activation of cardiac Cdk9 represses PGC-1 and confers a predisposition to heart failure. EMBO J, 23, 3559-69.

Santo, L., Vallet, S., Hideshima, T., Cirstea, D., Ikeda, H., Pozzi, S., Patel, K., Okawa, Y., Gorgun, G., Perrone, G., Calabrese, E., Yule, M., Squires, M., Ladetto, M., Boccadoro, M., Richardson, P. G., Munshi, N. C., Anderson, K. C. & Raje, N. 2010. AT7519, A novel small molecule multi-cyclin-dependent kinase inhibitor, induces apoptosis in multiple myeloma via GSK-3beta activation and RNA polymerase II inhibition. Oncogene, 29, 2325-36.

Santoriello, C. & Zon, L. I. 2012. Hooked! Modeling human disease in zebrafish. J Clin Invest, 122, 2337-43.

Sayed, D., Hong, C., Chen, I. Y., Lypowy, J. & Abdellatif, M. 2007. MicroRNAs play an essential role in the development of cardiac hypertrophy. Circ Res, 100, 416-24.

Schlange, T., Andree, B., Arnold, H. H. & Brand, T. 2000. BMP2 is required for early heart development during a distinct time period. Mech Dev, 91, 259-70.

Schmerwitz, U. K., Sass, G., Khandoga, A. G., Joore, J., Mayer, B. A., Berberich, N., Totzke, F., Krombach, F., Tiegs, G., Zahler, S., Vollmar, A. M. & Furst, R. 2011. Flavopiridol protects against inflammation by attenuating leukocyte-endothelial interaction via inhibition of cyclin-dependent kinase 9. Arterioscler Thromb Vasc Biol, 31, 280-8.

Schnabel, K., Wu, C. C., Kurth, T. & Weidinger, G. 2011. Regeneration of cryoinjury induced necrotic heart lesions in zebrafish is associated with epicardial activation and cardiomyocyte proliferation. PLoS One, 6, e18503.

Schultheiss, T. M., Burch, J. B. & Lassar, A. B. 1997. A role for bone morphogenetic proteins in the induction of cardiac myogenesis. Genes Dev, 11, 451-62.

Sedlacek, H., Czech, J., Naik, R., Kaur, G., Worland, P., Losiewicz, M., Parker, B., Carlson, B., Smith, A., Senderowicz, A. & Sausville, E. 1996. Flavopiridol (L86 8275; NSC 649890), a new kinase inhibitor for tumor therapy. Int J Oncol, 9, 1143-68.

Sedletcaia, A. & Evans, T. 2011. Heart chamber size in zebrafish is regulated redundantly by duplicated tbx2 genes. Dev Dyn, 240, 1548-57.

Sedmera, D., Reckova, M., Dealmeida, A., Sedmerova, M., Biermann, M., Volejnik, J., Sarre, A., Raddatz, E., Mccarthy, R. A., Gourdie, R. G. & Thompson, R. P. 2003. Functional and morphological evidence for a ventricular conduction system in zebrafish and Xenopus hearts. Am J Physiol Heart Circ Physiol, 284, H1152-60.

Seligman, A. M., Karnovsky, M. J., Wasserkrug, H. L. & Hanker, J. S. 1968. Nondroplet ultrastructural demonstration of cytochrome oxidase activity with a polymerizing osmiophilic reagent, diaminobenzidine (DAB). J Cell Biol, 38, 1-14.

Seng, W. L., Eng, K., Lee, J. & Mcgrath, P. 2004. Use of a monoclonal antibody specific for activated endothelial cells to quantitate angiogenesis in vivo in zebrafish after drug treatment. Angiogenesis, 7, 243-53.

Sepulveda, J. L., Belaguli, N., Nigam, V., Chen, C. Y., Nemer, M. & Schwartz, R. J. 1998. GATA-4 and Nkx-2.5 coactivate Nkx-2 DNA binding targets: role for regulating early cardiac gene expression. Mol Cell Biol, 18, 3405-15.

Serluca, F. C. 2008. Development of the proepicardial organ in the zebrafish. Dev Biol, 315, 18-27.

Sheaff, R., Ilsley, D. & Kuchta, R. 1991. Mechanism of DNA polymerase alpha inhibition by aphidicolin. Biochemistry, 30, 8590-7.

Sherr, C. J. & Roberts, J. M. 1995. Inhibitors of mammalian G1 cyclin-dependent kinases. Genes Dev, 9, 1149-63.

Shin, J. T. & Fishman, M. C. 2002. From Zebrafish to human: modular medical models. Annu Rev Genomics Hum Genet, 3, 311-40.

Shin, J. T., Pomerantsev, E. V., Mably, J. D. & Macrae, C. A. 2010. High-resolution cardiovascular function confirms functional orthology of myocardial contractility pathways in zebrafish. Physiol Genomics, 42, 300-9.

Shore, S. M., Byers, S. A., Dent, P. & Price, D. H. 2005. Characterization of Cdk9(55) and differential regulation of two Cdk9 isoforms. Gene, 350, 51-8.

Shore, S. M., Byers, S. A., Maury, W. & Price, D. H. 2003. Identification of a novel isoform of Cdk9. Gene, 307, 175-82.

Shu, X., Cheng, K., Patel, N., Chen, F., Joseph, E., Tsai, H. J. & Chen, J. N. 2003. Na,K-ATPase is essential for embryonic heart development in the zebrafish. Development, 130, 6165-73.

Sieger, D., Moritz, C., Ziegenhals, T., Prykhozhij, S. & Peri, F. 2012. Long-range Ca2+ waves transmit brain-damage signals to microglia. Dev Cell, 22, 1138-48.

Simone, C. & Giordano, A. 2007. Abrogation of signal-dependent activation of the cdk9/cyclin T2a complex in human RD rhabdomyosarcoma cells. Cell Death Differ, 14, 192-5.

Sleep, E., Boue, S., Jopling, C., Raya, M., Raya, A. & Izpisua Belmonte, J. C. 2010. Transcriptomics approach to investigate zebrafish heart regeneration. J Cardiovasc Med (Hagerstown), 11, 369-80.

Smith, K. A., Chocron, S., Von Der Hardt, S., De Pater, E., Soufan, A., Bussmann, J., Schulte-Merker, S., Hammerschmidt, M. & Bakkers, J. 2008. Rotation and asymmetric development of the zebrafish heart requires directed migration of cardiac progenitor cells. Dev Cell, 14, 287-97.

Soonpaa, M. H., Kim, K. K., Pajak, L., Franklin, M. & Field, L. J. 1996. Cardiomyocyte DNA synthesis and binucleation during murine development. Am J Physiol, 271, H2183-9.

Stainier, D. Y. 2001. Zebrafish genetics and vertebrate heart formation. Nat Rev Genet, 2, 39-48.

Stainier, D. Y. & Fishman, M. C. 1992. Patterning the zebrafish heart tube: acquisition of anteroposterior polarity. Dev Biol, 153, 91-101.

Stainier, D. Y., Lee, R. K. & Fishman, M. C. 1993. Cardiovascular development in the zebrafish. I. Myocardial fate map and heart tube formation. Development, 119, 31-40.

Staudt, D. & Stainier, D. 2012. Uncovering the molecular and cellular mechanisms of heart development using the zebrafish. Annu Rev Genet, 46, 397-418.

Stein, L. D., Bao, Z., Blasiar, D., Blumenthal, T., Brent, M. R., Chen, N., Chinwalla, A., Clarke, L., Clee, C., Coghlan, A., Coulson, A., D'eustachio, P., Fitch, D. H., Fulton, L. A., Fulton, R. E., Griffiths-Jones, S., Harris, T. W., Hillier, L. W., Kamath, R., Kuwabara, P. E., Mardis, E. R., Marra, M. A., Miner, T. L., Minx, P., Mullikin, J. C., Plumb, R. W., Rogers, J., Schein, J. E., Sohrmann, M., Spieth, J., Stajich, J. E., Wei, C., Willey, D., Wilson, R. K., Durbin, R. & Waterston, R. H. 2003. The genome sequence of Caenorhabditis briggsae: a platform for comparative genomics. PLoS Biol, 1, E45.

Stevens, M., De Clercq, E. & Balzarini, J. 2006. The regulation of HIV-1 transcription: molecular targets for chemotherapeutic intervention. Med Res Rev, 26, 595-625.

Strahl, B. D. & Allis, C. D. 2000. The language of covalent histone modifications. Nature, 403, 41-5.

Streisinger, G., Walker, C., Dower, N., Knauber, D. & Singer, F. 1981. Production of clones of homozygous diploid zebra fish (Brachydanio rerio). Nature, 291, 293-6.

Summerton, J. & Weller, D. 1997. Morpholino antisense oligomers: design, preparation, and properties. Antisense Nucleic Acid Drug Dev, 7, 187-95.

Summerton, J. E. 2007. Morpholino, siRNA, and S-DNA compared: impact of structure and mechanism of action on off-target effects and sequence specificity. Curr Top Med Chem, 7, 651-60.

Sun, Y. & Weber, K. T. 2000. Infarct scar: a dynamic tissue. Cardiovasc Res, 46, 250-6.

Sunagawa, Y., Morimoto, T., Takaya, T., Kaichi, S., Wada, H., Kawamura, T., Fujita, M., Shimatsu, A., Kita, T. & Hasegawa, K. 2010. Cyclin-dependent kinase-9 is a component of the p300/GATA4 complex required for phenylephrine-induced hypertrophy in cardiomyocytes. J Biol Chem, 285, 9556-68.

Taber, L. A. 2006. Biophysical mechanisms of cardiac looping. Int J Dev Biol, 50, 323-32.

Takagi, H., Hsu, C. P., Kajimoto, K., Shao, D., Yang, Y., Maejima, Y., Zhai, P., Yehia, G., Yamada, C., Zablocki, D. & Sadoshima, J. 2010. Activation of PKN mediates survival of cardiac myocytes in the heart during ischemia/reperfusion. Circ Res, 107, 642-9.

Tang, R., Dodd, A., Lai, D., Mcnabb, W. C. & Love, D. R. 2007. Validation of zebrafish (Danio rerio) reference genes for quantitative real-time RT-PCR normalization. Acta Biochim Biophys Sin (Shanghai), 39, 384-90.

Targoff, K. L., Schell, T. & Yelon, D. 2008. Nkx genes regulate heart tube extension and exert differential effects on ventricular and atrial cell number. Dev Biol, 322, 314-21.

Taylor, J. M., Saunter, C. D., Love, G. D., Girkin, J. M., Henderson, D. J. & Chaudhry, B. 2011. Real-time optical gating for three-dimensional beating heart imaging. J

Biomed Opt, 16, 116021.

Tu, S. & Chi, N. C. 2012. Zebrafish models in cardiac development and congenital heart birth defects. Differentiation, 84, 4-16.

Urbanowicz, J. H., Shaaban, M. J., Cohen, N. H., Cahalan, M. K., Botvinick, E. H., Chatterjee, K., Schiller, N. B., Dae, M. W. & Matthay, M. A. 1990. Comparison of transesophageal echocardiographic and scintigraphic estimates of left ventricular end-diastolic volume index and ejection fraction in patients following coronary artery bypass grafting. Anesthesiology, 72, 607-12.

Van Den Bos, E. J., Mees, B. M., De Waard, M. C., De Crom, R. & Duncker, D. J. 2005. A novel model of cryoinjury-induced myocardial infarction in the mouse: a comparison with coronary artery ligation. Am J Physiol Heart Circ Physiol, 289, H1291-300.

Velez Rueda, J. O., Palomeque, J. & Mattiazzi, A. 2012. Early apoptosis in different models of cardiac hypertrophy induced by high renin-angiotensin system activity involves CaMKII. J Appl Physiol, 112, 2110-20.

Vermeulen, K., Van Bockstaele, D. R. & Berneman, Z. N. 2003. The cell cycle: a review of regulation, deregulation and therapeutic targets in cancer. Cell Prolif, 36, 131-49.

Vonbaer, K. 1828. Entwicklungsgeschichte der Tiere: Beobachting

und Reflexion. . Korningsberg: Borntrager.

Voronov, D. A., Alford, P. W., Xu, G. & Taber, L. A. 2004. The role of mechanical forces in dextral rotation during cardiac looping in the chick embryo. Dev Biol, 272, 339-50.

Wada, T., Takagi, T., Yamaguchi, Y., Ferdous, A., Imai, T., Hirose, S., Sugimoto, S., Yano, K., Hartzog, G. A., Winston, F., Buratowski, S. & Handa, H. 1998. DSIF, a novel transcription elongation factor that regulates RNA polymerase II processivity, is composed of human Spt4 and Spt5 homologs. Genes Dev, 12, 343-56.

Wagner, K. D., Wagner, N., Ghanbarian, H., Grandjean, V., Gounon, P., Cuzin, F. & Rassoulzadegan, M. 2008. RNA induction and inheritance of epigenetic cardiac hypertrophy in the mouse. Dev Cell, 14, 962-9.

Wang, H., Feng, L., Hu, J., Xie, C. & Wang, F. 2013. Differentiating vitreous proteomes in proliferative diabetic retinopathy using high-performance liquid chromatography coupled to tandem mass spectrometry. Exp Eye Res, 108, 110-9.

Wang, H., Zhang, X., Li, Y., Ma, Y., Zhang, Y., Liu, Z., Zhou, J., Lin, Q., Wang, Y., Duan, C. & Wang, C. 2010. Improved myocardial performance in infarcted rat heart by co-injection of basic fibroblast growth factor with temperature-responsive chitosan hydrogel. J Heart Lung Transplant, 29, 881-7.

Wang, H. U., Chen, Z. F. & Anderson, D. J. 1998. Molecular distinction and angiogenic interaction between embryonic arteries and veins revealed by ephrin-B2 and its receptor Eph-B4. Cell, 93, 741-53.

Wang, K., Hampson, P., Hazeldine, J., Krystof, V., Strnad, M., Pechan, P. & M, J. 2012a. Cyclin-dependent kinase 9 activity regulates neutrophil spontaneous apoptosis. PLoS One, 7, e30128.

Wang, S. & Fischer, P. M. 2008. Cyclin-dependent kinase 9: a key transcriptional regulator and potential drug target in oncology, virology and cardiology. Trends Pharmacol Sci, 29, 302-13.

Wang, X., Tredget, E. E. & Wu, Y. 2012b. Dynamic signals for hair follicle development and regeneration. Stem Cells Dev, 21, 7-18.

Weaver, J. 2011. Genetic origins of birth defects revealed by new animal model. PLoS Biol, 9, e1001180.

Weber, K. T., Pick, R., Jalil, J. E., Janicki, J. S. & Carroll, E. P. 1989. Patterns of myocardial fibrosis. J Mol Cell Cardiol, 21 Suppl 5, 121-31.

Wei, P., Garber, M. E., Fang, S. M., Fischer, W. H. & Jones, K. A. 1998. A novel CDK9-associated C-type cyclin interacts directly with HIV-1 Tat and mediates its high-affinity, loop-specific binding to TAR RNA. Cell, 92, 451-62.

Weinmann, H. & Metternich, R. 2005. Drug discovery process for kinase inhibitors. Chembiochem, 6, 455-9.

Westerfield, M. 2000. The Zebrafish Book: A Guide for the Laboratory Use of Zebrafish (Danio rerio). Univ. of Oregon Press, Eugene.

Wills, A. A., Holdway, J. E., Major, R. J. & Poss, K. D. 2008. Regulated addition of new myocardial and epicardial cells fosters homeostatic cardiac growth and maintenance in adult zebrafish. Development, 135, 183-92.

Woods, I. G. & Schier, A. F. 2008. Targeted mutagenesis in zebrafish. Nat Biotechnol, 26, 650-1.

Xavier-Neto, J., Castro, R. A., Sampaio, A. C., Azambuja, A. P., Castillo, H. A., Cravo, R. M. & Simoes-Costa, M. S. 2007. Parallel avenues in the evolution of hearts and pumping organs. Cell Mol Life Sci, 64, 719-34.

Xin, M., Davis, C. A., Molkentin, J. D., Lien, C. L., Duncan, S. A., Richardson, J. A. & Olson, E. N. 2006. A threshold of GATA4 and GATA6 expression is required for cardiovascular development. Proc Natl Acad Sci U S A, 103, 11189-94.

Xu, H. & Baldini, A. 2007. Genetic pathways to mammalian heart development: Recent progress from manipulation of the mouse genome. Semin Cell Dev Biol, 18, 77-83.

Yalcin, H. C., Shekhar, A., Nishimura, N., Rane, A. A., Schaffer, C. B. & Butcher, J. T. 2010. Two-photon microscopy-guided femtosecond-laser photoablation of avian cardiogenesis: noninvasive creation of localized heart defects. Am J Physiol Heart Circ Physiol, 299, H1728-35.

Yamada, T., Yamaguchi, Y., Inukai, N., Okamoto, S., Mura, T. & Handa, H. 2006. P-TEFb-mediated phosphorylation of hSpt5 C-terminal repeats is critical for processive transcription elongation. Mol Cell, 21, 227-37.

Yamaguchi, Y., Takagi, T., Wada, T., Yano, K., Furuya, A., Sugimoto, S., Hasegawa, J. & Handa, H. 1999. NELF, a multisubunit complex containing RD, cooperates with DSIF to repress RNA polymerase II elongation. Cell, 97, 41-51.

Yan, Y. T., Gritsman, K., Ding, J., Burdine, R. D., Corrales, J. D., Price, S. M., Talbot, W. S., Schier, A. F. & Shen, M. M. 1999. Conserved requirement for EGF-CFC genes in vertebrate left-right axis formation. Genes Dev, 13, 2527-37.

Yang, Z., Yik, J. H., Chen, R., He, N., Jang, M. K., Ozato, K. & Zhou, Q. 2005. Recruitment of P-TEFb for stimulation of transcriptional elongation by the bromodomain protein Brd4. Mol Cell, 19, 535-45.

Yang, Z., Zhu, Q., Luo, K. & Zhou, Q. 2001. The 7SK small nuclear RNA inhibits the CDK9/cyclin T1 kinase to control transcription. Nature, 414, 317-22.

Yelon, D., Horne, S. A. & Stainier, D. Y. 1999. Restricted expression of cardiac myosin genes reveals regulated aspects of heart tube assembly in zebrafish. Dev Biol, 214, 23-37.

Yelon, D., Ticho, B., Halpern, M. E., Ruvinsky, I., Ho, R. K., Silver, L. M. & Stainier, D. Y. 2000. The bHLH transcription factor hand2 plays parallel roles in zebrafish heart and pectoral fin development. Development, 127, 2573-82.

Yelon, D., Weinstein, B. M. & Fishman, M. C. 2002. Cardiovascular system. Results Probl Cell Differ, 40, 298-321.

Yik, J. H., Chen, R., Nishimura, R., Jennings, J. L., Link, A. J. & Zhou, Q. 2003. Inhibition of P-TEFb (CDK9/Cyclin T) kinase and RNA polymerase II transcription by the coordinated actions of HEXIM1 and 7SK snRNA. Mol Cell, 12, 971-82.

Yost, H. J. 1999. Diverse initiation in a conserved left-right pathway? Curr Opin Genet Dev, 9, 422-6.

Zak, R. 1974. Development and proliferative capacity of cardiac muscle cells. Circ Res, 35, suppl II:17-26.

Zeisberg, E. M., Ma, Q., Juraszek, A. L., Moses, K., Schwartz, R. J., Izumo, S. & Pu, W. T. 2005. Morphogenesis of the right ventricle requires myocardial expression of Gata4. J Clin Invest, 115, 1522-31.

Zhang, J., Cicero, S. A., Wang, L., Romito-Digiacomo, R. R., Yang, Y. & Herrup, K. 2008. Nuclear localization of Cdk5 is a key determinant in the postmitotic state of neurons. Proc Natl Acad Sci U S A, 105, 8772-7.

Zhou, B., Honor, L. B., He, H., Ma, Q., Oh, J. H., Butterfield, C., Lin, R. Z., Melero-Martin, J. M., Dolmatova, E., Duffy, H. S., Gise, A., Zhou, P., Hu, Y. W., Wang, G., Zhang, B., Wang, L., Hall, J. L., Moses, M. A., Mcgowan, F. X. & Pu, W. T. 2011. Adult mouse epicardium modulates myocardial injury by secreting paracrine factors. J Clin Invest, 121, 1894-904.

Zhou, M., Lu, H., Park, H., Wilson-Chiru, J., Linton, R. & Brady, J. N. 2006. Tax interacts with P-TEFb in a novel manner to stimulate human T-lymphotropic virus type 1 transcription. J Virol, 80, 4781-91.

Zhou, P., He, A. & Pu, W. T. 2012. Regulation of GATA4 transcriptional activity in cardiovascular development and disease. Curr Top Dev Biol, 100, 143-69.

Zhou, Q. & Yik, J. H. 2006. The Yin and Yang of P-TEFb regulation: implications for human immunodeficiency virus gene expression and global control of cell growth and differentiation. Microbiol Mol Biol Rev, 70, 646-59.

Zhu, H., Doherty, J. R., Kuliyev, E. & Mead, P. E. 2009. CDK9/cyclin complexes modulate endoderm induction by direct interaction with Mix.3/mixer. Dev Dyn, 238, 1346-57.

Zhu, Y., Pe'ery, T., Peng, J., Ramanathan, Y., Marshall, N., Marshall, T., Amendt, B., Mathews, M. B. & Price, D. H. 1997. Transcription elongation factor P-TEFb is required for HIV-1 tat transactivation in vitro. Genes Dev, 11, 2622-32.